



University of  
**Nottingham**

UK | CHINA | MALAYSIA

**EXPERIMENTAL AND  
COMPUTATIONAL STUDY  
OF LATEX CLEARING PROTEIN  
LcpK30 FOR RUBBER DEGRADATION**

**Aziana Abu Hassan**

Thesis submitted to the  
University of Nottingham  
for the degree of  
Doctor of Philosophy

August 2023



## **ACKNOWLEDGEMENTS**

All praise is to ALLAH, The Most Gracious and The Most Merciful.

Firstly, I would like to express my deepest gratitude to my principal supervisor, Dr Anca Pordea, for her patience, guidance, ideas, knowledge, moral support and encouragement. Her understanding has kept me strong and determined to the final level of my project. I also adore her commitment to ensuring her students strive for excellent achievements on finishing the project and in future undertakings. My heartfelt thanks to the members of the supervisory committee, Prof Derek Irvine and Dr Cordula Hege. Their contribution and valuable suggestions guided me to complete this project.

I also would like to thank all the members of the SPT group, past and present. Special thanks to Steve, Rachael, Li Fang and Amy for their excellent technical assistance.

I would like to acknowledge and extend my heartfelt gratitude to the Director of the Malaysian Rubber Board (MRB), Dato' Dr Zairossani Mohd Noor, for his support and approval for a scholarship from MRB and necessary financial support to complete this project.

My warmest and deepest thanks go to my parents, families and friends, and most importantly, to my husband, Azral and our children Azimah, Azwani, Azmuna, Azhar and Azira for their love, understanding, encouragement and never-ending support from the initial to the final level of my PhD.

Last but not least, I offer my regards and blessing to all who have supported me by sharing their thoughts and ideas or in any way during these years of carrying out this project.

## ABSTRACT

The demand for rubber products grows exponentially. This condition results in significant amounts of rubber waste in the environment. Most of the rubber waste would come from synthetic rubber. Rubber waste management without a sustainable strategy will harm the environment and the general public's health. This work aims to introduce a sustainable approach to degrading rubber using enzymes. Latex-clearing protein K30 (LcpK30) catalyses the oxidative cleavage of the C=C bond in *cis*-1,4-polyisoprene natural rubber (NR). This enzyme can degrade synthetic polyisoprene, but the degradation rate is still low, and its potential to degrade other diene rubbers remains poorly understood. The ability of LcpK30 to interact with a sizeable hydrophobic substrate is interesting. It thus raises the question of how the substrates can access the catalytic site that is buried inside the protein cavity.

The work presented in this thesis explores ways to increase the applicability of LcpK30 to rubber degradation and provides a further understanding of how LcpK30 interacts with the polyisoprene substrate. Optimum production of the oligomers is essential to materialise the utilisation of the products from enzymatic degradation of NR for high-value applications. The optimum yield of oligomer at 65 % was obtained when the NR degradation was performed with 20 mg mL<sup>-1</sup> NR emulsion at 30 °C and 6 µM LcpK30 added in three batches over 24 hours.

Degradation of other diene rubbers with varied molecular weights, chemical structure and morphology catalysed by LcpK30 was assisted by pre-treating the rubber into film, particles and co-solvent emulsion. The degradability was evaluated based on the production of oligomers with carbonyl end-group. The oligomers were analysed using high performance liquid chromatography (HPLC), <sup>1</sup>H Nuclear Magnetic Resonance (NMR) and gel permeation

chromatography (GPC). It was found that the catalytic ability of LcpK30 to degrade other rubbers depended on the chemical structure and physical morphology of the rubber during the degradation. LcpK30 could degrade epoxidised NR with a low epoxide level (25 %), and the pretreatment improved LcpK30's contact with synthetic isoprene rubber (IR) molecules. The presence of other structural units (e.g. vinyl) in polybutadiene rubber or stereostructural changes (*trans*- polyisoprene) inhibits its catalytic activity.

Protein tunnel identification using CAVER-Pymol plugin 3.0.3 revealed two dominant tunnels that could offer access to the substrate from the surface to the buried active site. Computational modelling of protein (LcpK30) and ligand (*cis*-1,4-polyisoprene with ten C=C bonds) interaction using GOLD molecular docking showed two potential binding modes for the substrate, which are in extended and folded conformation that mostly interacted with LcpK30 through hydrophobic contact. Intriguingly, this study provided insight into interactions taking place further away from the active site, which a short substrate model cannot fully explain. The potential site for introducing mutation that no studies have yet reported was identified, which were Ala159, Ile396, and Leu171. In this study, the Leu171Phe mutant was prepared and showed an improved heme occupancy with similar activity to the wild type.

Findings from this study have enhanced the fundamental understanding needed to advance the research of LcpK30 to increase its potential as a biocatalyst for the environmentally friendly treatment of rubber waste. The application of LcpK30 can also be expanded as a tool for NR modification to develop new speciality rubber.

## TABLE OF CONTENTS

<b>ACKNOWLEDGEMENTS</b> .....	<b>i</b>
<b>ABSTRACT</b> .....	<b>ii</b>
<b>LIST OF ABBREVIATIONS, SYMBOLS AND ACRONYMS</b> .....	<b>xiii</b>
<b>CHAPTER 1</b> .....	<b>1</b>
<b>INTRODUCTION AND LITERATURE REVIEW</b> .....	<b>1</b>
Background and motivation .....	1
1.1 Introduction to different types of rubbers .....	3
1.1.1 Natural <i>cis</i> -1,4-polyisoprene rubber .....	3
1.1.2 Synthetic <i>cis</i> -1,4-polyisoprene rubber .....	5
1.1.3 Vulcanised rubber .....	6
1.1.4 Epoxidised natural rubber .....	7
1.1.5 Polybutadiene rubbers .....	9
1.2 Rubber degradation.....	12
1.2.1 Rubber degradation and waste treatment .....	12
1.2.2 Rubber degradation and chemical structure modification.....	15
1.2.2.1 Modification of epoxidised natural rubber using chemical and oxidative degradation .....	16
1.2.2.2 Cross-metathesis on vulcanised polybutadiene rubber.....	16
1.2.2.3 Alkene cleavage via ozonolysis .....	18
1.2.3. Biodegradation of rubber .....	19
1.2.4 Enzymatic biodegradation of polymers .....	20
1.3 Latex clearing protein .....	23
1.3.1 Structure of latex clearing protein .....	27
1.3.2 Cleavage mechanisms of latex clearing protein .....	28
1.3.3 Production of latex clearing protein .....	32
1.3.4 Rubber degradation catalysed by latex clearing protein.....	35

1.4 Molecular tools for protein engineering.....	39
1.4.1 Tunnel engineering.....	41
1.4.2 Molecular docking.....	43
1.5 Aim and Objectives .....	45
<b>CHAPTER 2 .....</b>	<b>48</b>
<b>MATERIALS AND METHODS.....</b>	<b>48</b>
2.1 Materials .....	48
2.1.1 Chemicals.....	48
2.1.2 Reagents .....	48
2.1.3 Polymer .....	48
2.1.4 Enzymes.....	49
2.1.5 Plasmids and strains.....	49
2.2 Methods .....	49
2.2.1 Solution and stocks preparation.....	49
2.2.1.1 Hemin solution .....	49
2.2.1.2 Glycerol stocks.....	49
2.2.1.3 Potassium phosphate buffer .....	50
2.2.2 Microbiological methods .....	50
2.2.2.1 Media preparation .....	50
2.2.2.2 Strains growth .....	50
2.2.3 Molecular biology methods .....	51
2.2.3.1 Gene synthesis .....	51
2.2.3.2 Preparation of LcpK30 mutants .....	51
2.2.3.3 Bacterial transformation.....	51
2.2.3.4 DNA extraction .....	52
2.2.3.5 DNA Analysis .....	53
2.2.3.6 Agarose gel electrophoresis .....	53
2.2.4 Protein expression.....	53
2.2.5 Protein purification .....	54

2.2.6 SDS-PAGE analysis .....	55
2.2.7 Quantification of protein concentration .....	56
2.2.8 Screening for enzyme activity .....	58
2.2.8.1 Colorimetric assay .....	58
2.2.8.2 Dissolved oxygen consumption assay .....	58
2.2.9 Polymer or substrate preparation .....	59
2.2.9.1 Natural rubber and epoxidised natural rubber .....	59
2.2.9.2 Synthetic cis- and trans-1,4-polyisoprene .....	60
2.2.9.3 Polybutadienes .....	60
2.2.9.4 Droplets size .....	60
2.2.9.5 Zeta potential .....	61
2.2.9.6 Microscopy .....	61
2.2.10 Enzymatic degradation of rubbers .....	61
2.2.11 Characterisation of the degradation products .....	62
2.2.11.1 High-Performance Liquid Chromatography .....	62
2.2.11.2 Nuclear Magnetic Resonance ( <sup>1</sup> H) .....	63
2.2.11.3 Gel Permeation Chromatography .....	63
2.2.12 Computational techniques .....	64
2.2.12.1 Protein structure preparation .....	64
2.2.12.2 Protein tunnel calculations .....	64
2.2.12.3 Protein-ligand molecular docking .....	64
<b>CHAPTER 3 .....</b>	<b>66</b>
<b>PRODUCTION AND CHARACTERISATION OF LcpK30 AND NATURAL RUBBER DEGRADATION CATALYSED BY THE ENZYME .....</b>	<b>66</b>
Background .....	66
3.1 Expression and purification of LcpK30 .....	67
3.1.1 Expression of LcpK30 in <i>Escherichia coli</i> BL21(DE3) .....	68
3.1.2 Expression of LcpK30 in <i>Escherichia coli</i> C41(DE3) .....	72
3.1.3 Purification of LcpK30 .....	75
3.1.4 Optimisation of LcpK30 expression .....	77

3.1.5 Spectroscopic characterisation of LcpK30 .....	79
3.1.6 Stability of LcpK30 upon storage .....	80
3.2 Enzymatic degradation of natural rubber catalysed by LcpK30 .....	81
3.2.1 Effect of enzyme concentration.....	82
3.2.2 Effect of temperature .....	83
3.2.3 Effect of substrate loading .....	84
3.2.4 Effect of solvent .....	86
3.2.5 Optimisation of oligo-isoprenoid production .....	89
3.2.6 Characterisation of the oligo-isoprenoids .....	92
3.3 Development of quantitative colourimetric screening assay for LcpK30 enzymatic activity.....	97
3.4 Discussion.....	102
3.5 Summary and Conclusions.....	105
<b>CHAPTER 4 .....</b>	<b>107</b>
<b>ENZYMATIC DEGRADATION OF MODIFIED NATURAL RUBBER AND SYNTHETIC RUBBER CATALYSED BY LcpK30.....</b>	<b>107</b>
Background.....	107
4.1 The substrates for enzymatic degradation.....	109
4.2 Substrates preparation and characterisation .....	114
4.2.1 Preparation of solid substrate .....	115
4.2.2 Preparation of co-solvent emulsion with <i>I</i> -IR-38K.....	116
4.2.3 Characterisation of the co-solvent emulsions.....	119
4.3 Enzymatic degradation of modified and synthetic rubbers .....	124
4.3.1 Epoxidised natural rubber .....	124



4.3.2 High molecular weight synthetic <i>cis</i> -1,4-polyisoprene rubber ( <i>h</i> -IR-100K).....	132
4.3.3 Low molecular weight synthetic <i>cis</i> -1,4-polyisoprene rubber made from synthetic rubber ( <i>l</i> -IR-35K).....	137
4.3.4 Low molecular weight synthetic <i>cis</i> -1,4-polyisoprene rubber made from natural rubber ( <i>l</i> -IR-38K).....	141
4.3.5 Polybutadiene rubber.....	145
4.4 Discussion.....	147
4.5 Summary and Conclusions.....	152
<b>CHAPTER 5 .....</b>	<b>155</b>
<b>CHARACTERISATION OF LcpK30-SUBSTRATE INTERACTIONS AND DESIGN OF A MUTANT WITH EXPANDED SUBSTRATE SCOPE .....</b>	<b>155</b>
Background.....	155
5. 1 Computational modelling of molecular interaction between LcpK30 and <i>cis</i> -1,4-polyisoprene.....	157
5.1.1 Identification of tunnels in LcpK30.....	157
5.1.2 Molecular docking of the <i>cis</i> -1,4-polyisoprene substrate into LcpK30 .....	160
5.2 Modification of LcpK30.....	170
5.2.1 Mutant design .....	170
5.2.2 Tunnel identification in LcpK30 mutants.....	171
5.2.3 Molecular docking of <i>cis</i> - and <i>trans</i> - 1,4-polyisoprene ligands to wild-type LcpK30 and the mutants .....	174
5.2.4 Expression and purification of LcpK30 mutants.....	176
5.2.5 Degradation of <i>cis</i> -1,4-polyisoprene catalysed with LcpK30 wild type and mutants.....	181

5.2.6 Degradations of <i>trans</i> -1,4-polyisoprene catalysed with LcpK30 wild type and the mutants .....	185
5.3 Discussion.....	188
5.4 Summary and Conclusions.....	191
<b>CHAPTER 6 .....</b>	<b>195</b>
<b>OVERALL DISCUSSION, CONCLUSION AND FUTURE WORKS .....</b>	<b>195</b>
6.1 Overall discussion .....	195
6.2 Conclusions and future work .....	199
<b>APPENDICES .....</b>	<b>202</b>
Appendix 1: COVID-19 Impact statement.....	202
Appendix C2.1: Plasmid map of pET-21a(+) .....	206
Appendix C2.2: Gene and amino acid sequences of the wild-type LcpK30 .....	207
Appendix C2.3: Gene and amino acid sequences of the mutated LcpK30 (Leu171Ala) .....	208
Appendix C2.4: Gene and amino acid sequences of the mutated LcpK30 (Leu171Phe) .....	209
Appendix C3.1: Oxygen consumption assay of purified LcpK30.....	210
Appendix C3.2: Sum of HPLC chromatogram peak area of oligomer derived from reactions with different enzyme concentration.....	211
Appendix C3.3: Sum of HPLC chromatogram peak area of oligomer derived from reactions with different temperature .....	212
Appendix C3.4: Sum of HPLC chromatogram peak area of oligomer derived from reactions with different substrate loading .....	213
Appendix C3.5: HPLC chromatogram of oligomer peaks from reaction in the presence of solvents .....	214

Appendix C3.6: HPLC chromatogram of oligomers from Reaction A and Reaction B: Calculation of the peak area percentage difference .....	215
Appendix C3.7: HPLC chromatogram of oligomers from Reaction A and Reaction B: Calculation of the molecular weight based on area (%).....	216
Appendix C3.8: Schiff's reagent reaction on butyraldehyde.....	218
Appendix C4.1: Size distribution intensity of emulsion droplets in the co-solvent emulsion .....	219
Appendix C4.2: Estimation of the number of repeating units based on <sup>1</sup> H NMR spectrum of products from enzymatic degradation of ENR.....	221
Appendix C4.3: Colourimetric assay of the reaction suspension of NR degradation in solid-film form. ....	222
Appendix C4.4: Molecular weight size distribution of oligo-isoprenoids ....	222
Appendix C4.5: HPLC chromatogram and 1H NMR spectra of oligomers from the degradation of <i>h</i> -IR-100K in 600 μM particles .....	224
Appendix C4.6: HPLC Chromatogram of dried residual extract from <i>l</i> -IR-35K and <i>l</i> -IR-38K degradation with and without LcpK30. ....	225
Appendix C4.7: HPLC chromatogram of dried residual extract from a reaction with PB-5000.....	226
Appendix C4.8: HPLC chromatogram of dried residual extract from a reaction with PB-2200.....	226
Appendix C4.9: HPLC chromatogram of dried residual extract from a reaction with PB-5000S .....	227
Appendix C4.10: HPLC chromatogram of dried residual extract from a reaction with PB-1300 .....	227

Appendix C4.11: HPLC chromatogram of dried residual extract from a reaction with PB-1500 .....	228
Appendix C4.12: <sup>1</sup> H NMR spectrum of dried residual extract from a reaction with PB-5000.....	229
Appendix C4.13: <sup>1</sup> H NMR spectrum of dried residual extract from a reaction with PB-1300.....	230
Appendix C4.14: <sup>1</sup> H NMR spectrum of dried residual extract from a reaction with PB-5000S .....	231
Appendix C4.15: <sup>1</sup> H NMR spectrum of dried residual extract from a reaction with PB-1500.....	232
Appendix C5.1a: Superimposed of ten docking poses result from rigid docking of <i>cis</i> -1,4-polyisoprene C <sub>50</sub> H <sub>82</sub> within LcpK30 .....	233
Appendix C5.1b: Docking solutions obtained from rigid docking within GOLD software .....	233
Appendix C5.2a: List of residues interacting with the docked <i>cis</i> -1,4-polyisoprene.....	234
Appendix C5.2b: List of residues interacting with the docked <i>cis</i> -1,4-polyisoprene.....	235
Appendix C5.3: Protein sequences alignment of LcpK30 and LcpSH22a.	237
Appendix C5.4: Docking conformation of (a) <i>cis</i> -1,4-polyisoprene and (b) <i>trans</i> -1,4-polyisoprene on wild-type LcpK30.....	238
Appendix C5.5: Docking conformation of (a) <i>cis</i> -1,4-polyisoprene and (b) <i>trans</i> -1,4-polyisoprene on Leu143Ala mutant.....	239
Appendix C5.6: Docking conformation of (a) <i>cis</i> -1,4-polyisoprene and (b) <i>trans</i> -1,4-polyisoprene on Leu143Phe mutant.....	240

Appendix C5.7: Docking conformation of (a) <i>cis</i> -1,4-polyisoprene and (b) <i>trans</i> -1,4-polyisoprene on Leu143Trp mutant.....	241
Appendix C5.8: Structural features of the <i>cis</i> -1,4-polyisoprene docking poses .....	242
Appendix C5.9: Structural features of the <i>trans</i> -1,4-polyisoprene docking poses .....	244
Appendix C5.10: Primers used for site-directed mutagenesis.....	246
Appendix C5.11: SDS-PAGE analysis of purified proteins (1) wild-type LcpK30 (2) Leu171Phe mutant and (c) Leu171Ala mutant .....	246
Appendix C5.12: HPLC Chromatogram of oligomers from NR degradation catalysed by LcpK30 variants.....	247
Appendix C5.13: <sup>1</sup> H NMR spectra of oligomers from NR degradation catalysed by (a) LcpK30 wild type (b) LcpK30 Leu171Ala and (c) LcpK30 Leu171Phe.....	249
<b>REFERENCES .....</b>	<b>251</b>

## LIST OF ABBREVIATIONS, SYMBOLS AND ACRONYMS

Cp	Centripoise
d	Day
DMSO	Dimethyl sulphoxide
DNA	Deoxyribonucleic acid
DRC	Dry rubber content
ENR	Epoxidised natural rubber
g L <sup>-1</sup>	Gram per litre
g mol <sup>-1</sup>	Gram per mol
IR	Isoprene rubber
KPi	Potassium phosphate buffer
Lcp	Latex clearing protein
min	Minutes
mRNA	Messenger ribonucleic acid
NC	Negative control
NMR	Nuclear magnetic resonance
NR	Natural Rubber
OD (OD600)	Optical density (measured at 600 nm)
P	Poise
PC	Positive control
PCR	Polymerase chain reaction
phr	<i>Parts per hundred</i>
ppm	Parts per million
rpm	Revolution per minit
Rox	Rubber oxygenase
SDS-PAGE	Sodium dodecyl sulfate-polyacrylamide gel electrophoresis
sp.	Species
T <sub>g</sub>	Transition glass temperature
UV-vis	Ultraviolet and visible light
v/v	Volume /volume ratio

w/v	Weight/volume ratio
wt %	Weight percent
ZDEC	Zinc diethyldithiocarbamate

## **CHAPTER 1**

### **INTRODUCTION AND LITERATURE REVIEW**

#### **Background and motivation**

Since Charles Goodyear introduced the vulcanisation process of natural rubber (NR) in 1839, rubber has been an essential material for transportation and everything related to everyday life, from healthcare to household and personal products. As time evolves, the rubber industry also experiences a revolution. In the 1950s, an alternative rubber synthetically made by isoprene polymerisation entered the market as a more superior and uniform material than NR and less laborious. Moreover, in the late 1980s, there was an upsurge in the number of immediate-type I allergy cases towards the protein that constitutes NR-based products, particularly the surgical and medical examination NR gloves. This incident has triggered worldwide awareness, increasing the production of synthetic rubber gloves. As a result, the consumption of synthetic rubber has surpassed its natural counterpart, the NR. Rubber products continue to increase yearly with the innovation of other elastomers and new speciality rubbers. Without proper management, this situation leads to higher amounts of rubber waste in the environment. Commonly, disposal of rubber waste, including crushing and grinding, burning at extreme temperatures, treating it with hazardous chemicals, or merely piling it up in landfills, could trigger massive toxic fires and cause environmental pollution.

The degradability of a material refers to how easily it can be disintegrated and assimilated into the environment after reaching the end of its life cycle. However, this is not always relevant to the waste of higher molecular weight polymers, such as rubber. Over the years, extremely high temperatures and harsh chemicals were used to dispose of these materials, but most also ended up in landfills. Rubber-based materials exposed to an open environment could



trigger cross-degradation and 'self-disintegration', influenced by several external factors such as humidity, heat, and light.<sup>1</sup> Harmful chemicals, or hazardous materials, are products derived from uncontrollable degradation processes that could endanger the ecosystem and disrupt the habitat of various biota and humans.<sup>2,3</sup>

In most circumstances, rubber waste is transformed into reclaimed rubber, typically by grinding and involving technologies that require extreme heat, high energy consumption, and chemicals, which can trigger severe environmental pollution and health hazards.<sup>4,5</sup> Another technology that enables a higher recovery of rubber waste is pyrolysis. This process could cause a profound ecological impact by emitting CO<sub>2</sub> and ashes that could threaten public health.<sup>6,7</sup> All these technologies require certain chemicals added to the rubber waste during mixing processing, such as desulphurising agent, devulcanising agent and regeneration agent.<sup>8,9</sup> Consequently, it leads to the generation of scheduled chemical waste that requires higher handling costs with restricted regulation.

The degradation of rubber is not only crucial for waste disposal but also for the synthesis of new materials. For example, the degradation of the long-chain NR polymer leads to end-functionalised rubbers such as liquid NR (LNR) with hydroxyl or carbonyl terminal group that can be repurposed for other uses such as adhesive, coating and reactive plasticiser.<sup>10</sup> However, obtaining a homogenous low molecular weight telechelic rubber is not always possible and controlling the product's molecular weight and functionality is also challenging. Moreover, the isolation and purification of the products are laborious and can form hazardous waste. Additionally, most previously described procedures need specific chemical reagents, extensive reaction times, and high temperatures. Therefore, biotechnology-based solutions utilising enzyme technology might offer a better alternative for developing a sustainable method

of processing rubber waste and making or regenerating functional polymers through rubber degradation.

## **1.1 Introduction to different types of rubbers**

Natural, synthetic and modified rubbers have a significant influence on human life. The utilisation and creation of these materials have led to the innovation of more sophisticated technology beneficial for transportation, medical, food, agriculture, and other diversified applications. The following section discusses the characteristics of several examples of synthetic and modified rubber, including NR derived from a rubber tree, *Hevea brasiliensis*. Modification of NR includes polymer blending or chemical structure modification. These types of rubber are widely used to produce rubber-based products and thus mainly contribute to the amount of rubber waste. According to the World Bank Group analysis, global annual waste generation is predicted to increase by 70% from 2016 to 3.4 billion tonnes by 2050.<sup>11</sup> From the 3.4 billion tons, approximately 68 million tons are made of rubber.

### **1.1.1 Natural *cis*-1,4-polyisoprene rubber**

Natural rubber (NR) latex is a whitish milky emulsion derived from latex ducts in a layer outside the cambium (located between the xylem and phloem layer of a tree trunk) of most lactiferous trees such as the rubber tree (*Hevea brasiliensis*).<sup>12</sup> The *cis*-1,4-polyisoprene rubber produced by *Hevea brasiliensis* is one of the major rubber sources for manufacturing rubber-based products. The NR emulsion is a stable dispersion of *cis*-1,4-polyisoprene encapsulated in spherical particles with diameters ranging from ~0.1 µm to ~1 µm in an aqueous phase.<sup>13</sup> The interfacial layer of NR particles comprises a monolayer of proteins and phospholipids with a thickness of ~3.5 nm.<sup>14,15</sup> Meanwhile, the core of the NR particles contains the hydrophobic rubber hydrocarbon that is linked with the phospholipid and the protein at the monolayer of the particles during

polyisoprene chain biosynthesis.<sup>16,17</sup> The chemical structure of NR comprises more than 5000 isoprene units in *cis*- configuration connected with two *trans*-isoprene units (Figure 1.1).<sup>18-20</sup> Besides the isoprene units that contribute to 35 % of total latex content by weight, the NR latex also includes non-rubber components such as proteinaceous substances (1 %), resinous substances (1-2.5 %), ash and sugar (2 %) and 60% water.<sup>21</sup>

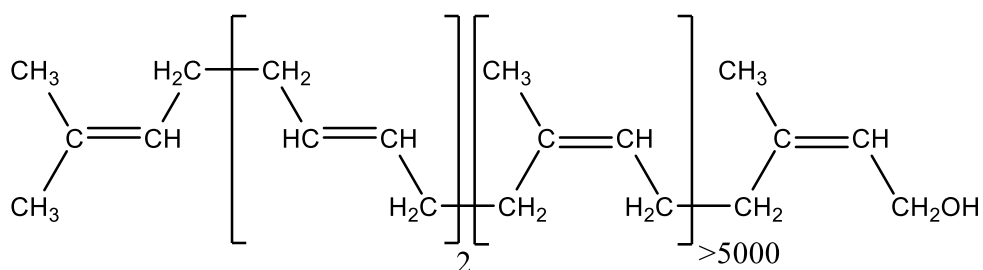


**Figure 1.1.** Structure of natural rubber adapted from Amerik *et al.* (2018).<sup>20</sup>

The distinctive physiochemical behaviour of NR is attributed to the non-rubber components that significantly contribute to its strong mechanical properties (e.g. modulus, tensile strength, and tear strength).<sup>14</sup> The mechanical properties of rubber are also determined by its molecular weight characteristics, including the number average ( $M_n$ ), weight average ( $M_w$ ), and polydispersity ( $M_w/M_n$ ) values. A higher  $M_w$  results in better mechanical properties of the rubber.<sup>22,23</sup> The  $M_w$  of NR is highly varied, ranging from  $1.1 \times 10^5$  to  $1.3 \times 10^6$  g mol<sup>-1</sup> and influenced by types of different rubber tree clones (e.g. RRIM 600, SK1, SK2, etc.), the age of the rubber trees, and soil and climate conditions of the plantation that contribute to NR's peculiar architecture.<sup>24,25</sup> Generally, the  $M_w/M_n$  of freshly tapped NR latex was  $\sim 3$  and shown to be in a bimodal distribution.<sup>26</sup> The chemical structure of NR also influences the final mechanical properties of the rubber. The linear arrangement of NR polymer chains with a double bond (C=C) within the repeating unit of *cis*-1,4-polyisoprene gives the NR molecule a high structural regularity, allowing the polymer chains to pack and crystallise

spontaneously at low temperatures.<sup>27</sup> Although NR has excellent mechanical properties, utilising NR for manufacturing rubber-based products requires chemical modifications to enhance its properties, increase shelf life and improve its resistance towards decomposition.

Natural rubber is a material of choice in many specialised applications due to its specific chemical characteristics and biodegradability.<sup>28,29</sup> According to Expert Market Research, the demand for natural rubber on the world market was 15.2 million metric tonnes in 2020 and is projected to increase further at a CAGR of 4.8% in the forecast period of 2023-2028.<sup>30</sup> However, the sustainable production of NR can be impacted by climate changes, the susceptibility of the rubber trees against pests and diseases and high price volatility due to an upsurge in demand from emerging countries and manufacturer preferences for synthetic rubber.<sup>31</sup>

### **1.1.2 Synthetic *cis*-1,4-polyisoprene rubber**

Contrary to NR, which is biosynthesised in a particle surrounded by a monolayer of protein and lipid, synthetic isoprene rubber (IR) is chemically synthesised by solution polymerisation of the isoprene monomer (2-methyl-1,3-butadiene). The isoprene monomers can be polymerised in four isomeric configurations: *trans*-1,4-addition, *cis*-1,4-addition, 1,2-addition and 3,4-addition with a molecular weight ranging from  $10^5$  to  $10^6$ , similar to NR (Figure 1.2).<sup>32</sup>

The polydispersity or molecular weight distribution ( $M_w/M_n$ ) of IR is usually unimodal and lower compared to NR due to the absence of non-rubber compounds such as protein and lipids. Because of the lack of non-rubber compounds, especially proteins, synthetic rubber is frequently used for manufacturing medical rubber products, including surgical gloves, catheters, dental dams and breathing bags. There have been prolonged issues regarding allergies to proteins in NR.<sup>33</sup> The creation of IR has helped to reduce protein

allergy incidents among patients and healthcare workers.<sup>34</sup> The rubber particles in IR were stabilised by surfactant and more uniform in size and shape, thus contributing to its mechanical properties, including high tensile strength, low hysteresis that give low heat build-up during flexing and higher resistance in extreme conditions.<sup>35</sup> Although IR and NR have similar mechanical properties, NR nonetheless exhibits better stress-strain behaviour.<sup>36</sup>

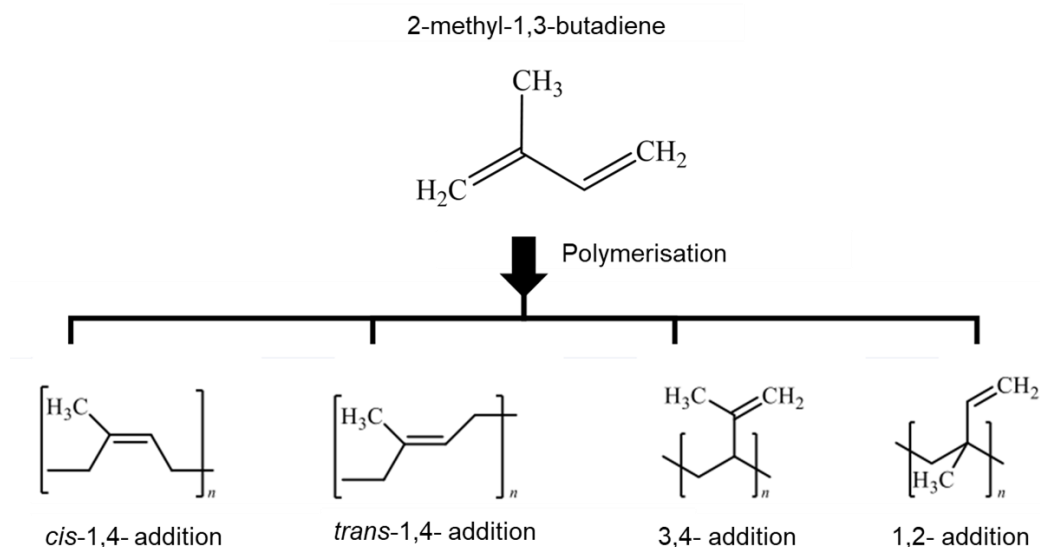


**Figure 1.2.** Isoprene unit (top) and isomeric configurations of synthetic polyisoprene ( $n > 400$ ) (bottom).

### 1.1.3 Vulcanised rubber

Rubber vulcanisation is a process of heating rubber with sulphur to develop chemical cross-links.<sup>37</sup> The process improves the physical properties of NR or IR by forming an intermolecular bonding between the unsaturated rubber molecules, leading to a three-dimensional network (Figure 1.3).<sup>38</sup> The three-dimensional network increases elasticity and flexibility and induces rubber strength and resistance to cutting, tearing and abrasion.<sup>39</sup> Most rubber-based products are made from vulcanised rubber to meet the standards for strength, extended design life, and preservation of high product quality.

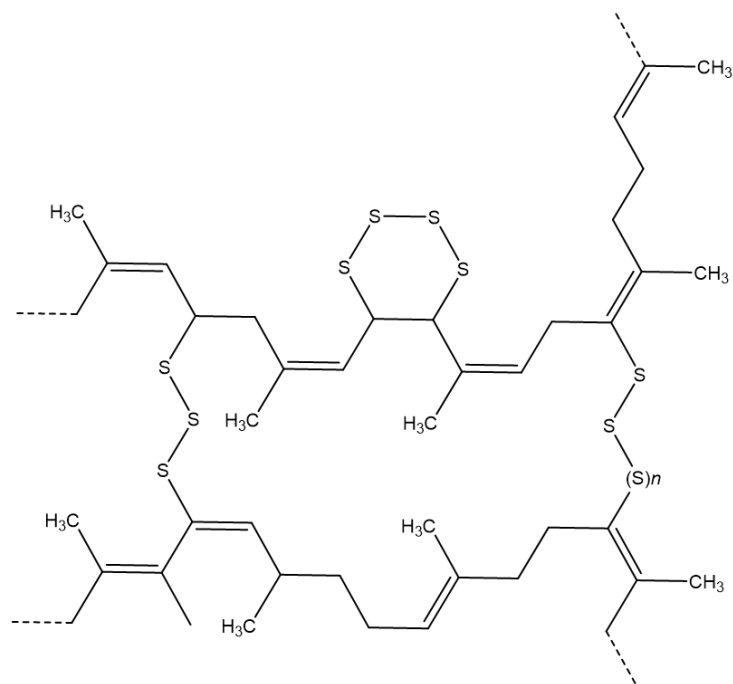


**Figure 1.3.** The three-dimensional network of sulphur vulcanised rubber reproduced from Chauhan *et al.* (2015).<sup>40</sup>

#### 1.1.4 Epoxidised natural rubber

There are numerous methods to modify the NR chemically, and the most notable methods are cyclisation, chlorination, and epoxidation. Among these three methods, epoxidation of NR is widely used to produce epoxidised NR (ENR). Chemical modification of NR polymer chains through epoxidation creates a molecular structure with the epoxide group that randomly replaces the double bonds in the NR polymer backbone.<sup>41</sup> The random distribution of the epoxidised and non-epoxidised isoprene unit gives rise to several probable sequences and makes the characterisation of the structure *via* NMR techniques quite challenging. Bradbury and Perera established a procedure of grouping the randomly located monomer units into a triad sequence comprising three possible monomer units to predict the neighbouring units (Figure 1.4). Their study denoted the epoxidised and non-epoxidised isoprene units as E and C, respectively.

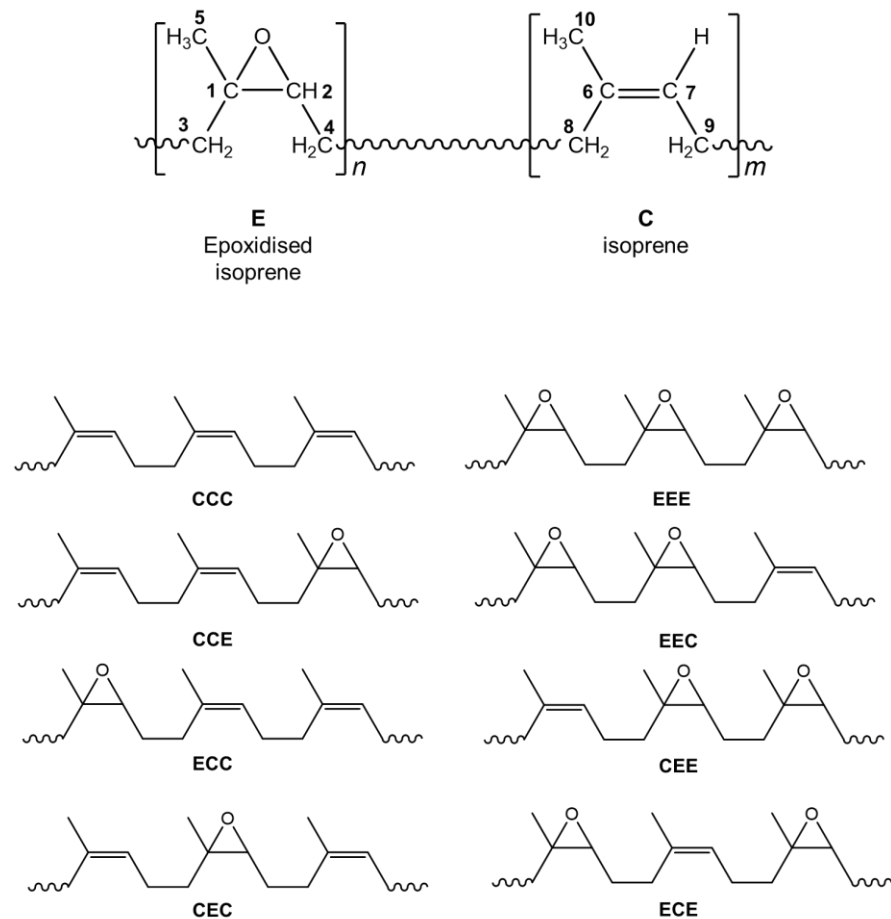
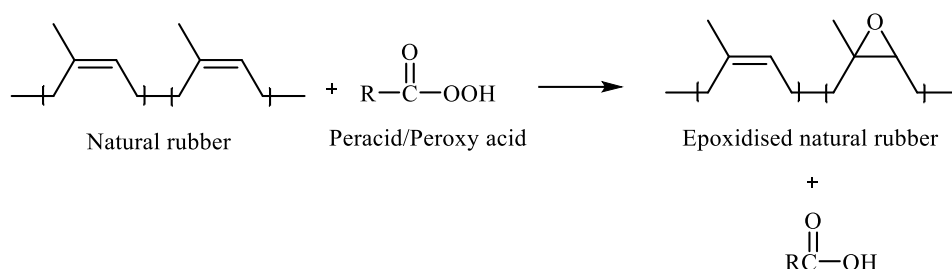


**Figure 1.4.** The general structure includes the numbering of carbon atoms in ENR (top) and possible triad sequence of ENR (bottom).

The epoxidation of NR can be carried out in an organic solvent or aqueous media under one of the following routes: (1) adding the preformed peracid into the reaction, (2) *in-situ* synthesis that generates performic acid by the reaction of hydrogen peroxide ( $\text{H}_2\text{O}_2$ ) and formic acid ( $\text{HCOOH}$ ) in the reaction with the presence of NR latex (the aqueous media) as shown in Scheme 1.1.<sup>42</sup> Currently, the commercially available ENR is produced using peracid with different epoxidation levels: 25 mol% and 50 mol%, known as ENR25 and ENR50, respectively. The properties of ENR depend on the degree of epoxidation level, which is controlled by the type and content of peracid, reaction temperature and reaction time.<sup>43</sup> Due to the high polarity of epoxide groups, ENR has high damping at room temperature, low air permeability and good resistance to oils

and non-polar solvents. Compared to NR, ENR has a higher glass transition temperature ( $T_g$ ) by approximately 1 °C for every mol% epoxidation.<sup>44</sup>



**Scheme 1.1.** Epoxidation of natural rubber using peracid ( $\text{RCO}_3\text{H}$ ). The epoxidation can also be performed using *in-situ* performic acid generated from the reaction of formic acid ( $\text{HCOOH}$ ) and hydrogen peroxide ( $\text{H}_2\text{O}_2$ ). Adapted from Phinyocheep (2014).<sup>42</sup>

### 1.1.5 Polybutadiene rubbers

Polybutadiene rubber (PBR) is a synthetic rubber produced from monomers derived from petroleum (1,3-butadiene).<sup>35</sup> The monomers are combined by three geometric isomers: the *cis*-1,4, *trans*-1,4 and 1,2-vinyl structural units that comprise the PBR chain (Figure 1.5). The polymerisation method applied to synthesise PBR determines the microstructure of the polymer chain. The anionic coordination polymerisation is carried out using Ziegler–Natta-type catalyst systems consisting of either titanium, cobalt or nickel salt or organic compounds of these metals with an alkyl aluminium halide to produce PBR with high *cis* content (> 90 %).<sup>45</sup> The PBR with low *cis* content (< 40 %) is produced by anionic polymerisation in the presence of an alkyl lithium initiator.<sup>35</sup>

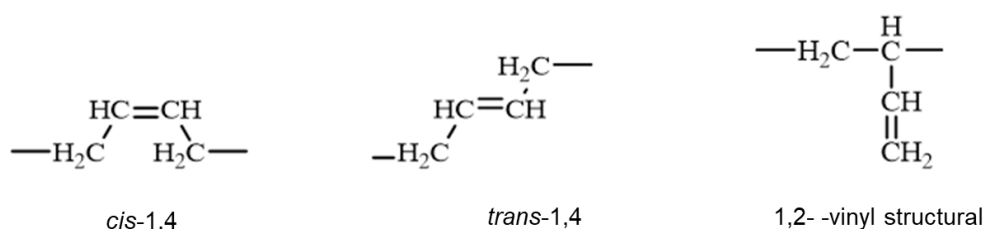


**Figure 1.5.** Isomeric configurations of butadiene rubber.



High-quality PBR was produced by developing new catalyst systems with enhanced catalytic activity and high stereoselectivity.<sup>46</sup> Table 1.1 shows the general characteristics of PBR produced with different transition metal catalysts. The low *cis*-content PBR is frequently used as a co-polymer to form composite blending for tire manufacturing, thermoplastics such as high-impact polystyrene and acrylonitrile butadiene styrene terpolymer (ABS) and other commercial products such as shoe soles and golf balls.<sup>47,48</sup> The PBR with high vinyl content (70 %) is usually used to produce a polymer with an excellent balance of low rolling resistance and high wet grip suitable for tire production as it can result in reduced fuel consumption.<sup>49</sup> Different vinyl content contributes to specific thermal and mechanical properties of PBR, such as transition glass temperature ( $T_g$ ) and storage and loss modulus.<sup>50</sup>

**Table 1.1.** Properties of different types of polybutadiene rubbers (PBR) with their catalyst. Source: Dinsmore (2007), Chandrasekaran (2017) and Kumar *et al.* (2021).

BR Type	Ti-BR	Co-BR	Ni-BR	Li-BR	Alfin-BR	Peroxide-BR
Catalyst	Titanium	Co-bis(octanoate) and diethyl aluminum chloride	Naphthenate/boron trifluoride/ethylene oxide/aluminum trialkyl	Alkyl lithium	Sodium salts of organic alkoxides with sodium chloride	
<i>cis</i> -1,4 content (%)	93	96	97	35	5	15
<i>trans</i> -1,4 content (%)	3	2	2	55	70	70
1,2 content (%)	6	2	1	10	25	15
Glass transition temperature (T <sub>g</sub> ) <sup>a</sup>		Below -100 °C		-15 °C	n.a	n.a
Elasticity	High	High	High	Absent	Absent	Absent
Molecular weight			250 000 – 300 000 g mol <sup>-1</sup>			
Tensile strength			Low			

<sup>a</sup> temperature region where the polymer transitions from hard, glassy material to a soft, rubbery material

n.a. not available

## **1.2 Rubber degradation**

The significance of rubber degrading research includes two primary areas of focus: (1) managing rubber waste and (2) enhancing rubber processability and features through structural modification. When rubber degrades, the polyisoprene chains disintegrate at the C=C double bond. Thus, structural modifications occur at the C=C bonds, resulting in oligomers of isoprene containing carbonyl, hydroxyl or other functional groups depending on the catalyst or reaction involved. The following sections review the current management of rubber waste and the degradation methods for structural modification.

### **1.2.1 Rubber degradation and waste treatment**

The life cycle of rubber products consists of three main stages: the upstream, the middle stream and the downstream. Activities involved in the upstream stage are mainly on a rubber plantation and NR latex harvesting. Rubber processing is categorised under the middle stream stage, which starts with the preservation of the NR latex from the plantation field with ammonia or other chemicals, such as tetramethylthiuramdisulphite (TMTD) and zinc oxide (ZnO), before being transferred to rubber processing factories.<sup>52</sup> The preserved NR latex is treated with formic acid in the rubber processing factory to produce solid/coagulated rubber. The NR latex can be concentrated by centrifugation, creaming with sodium alginate, or evaporation.<sup>51</sup> More than 90% of commercial latex concentrates are produced by centrifugation.<sup>52</sup> The downstream stage involves producing and commercialising end-products. Solid rubbers are commonly used for making tires, tubing, hoses, footwear and automotive components.<sup>53</sup> Meanwhile, latex concentrates are mainly used for making latex-dipped products such as gloves and condoms.

Due to the escalating amount of rubber waste, there is a need for a post-downstream stage to monitor and prevent waste disposal activities that could cause environmental pollution. Conventional approaches to dealing with rubber waste would be reclaiming and recycling. Reclaiming is a process that turns the rubber into small granules called crumb rubber (Figure 1.6), achieved by chemical and physical treatments (e.g., grinding, extruding or milling).<sup>54</sup> The resulting products are applied as a filler for rubberised composite, as an additive in cement concrete or processed into new products such as flooring and playground mats.<sup>55</sup>



**Figure 1.6.** Crumb rubber made from tire waste.<sup>56,57</sup>

Another industrially implemented method for rubber waste management is a process called pyrolysis. Pyrolysis is a technology that can convert solid rubber scraps into liquid fuel. The process is performed in an enclosed environment. Thermal decomposition is induced at elevated temperatures in an inert atmosphere.<sup>6,58</sup> Medical waste, such as surgical gloves and catheters, is disposed of through incineration. On the other hand, waste from single-use, non-hazardous examination gloves will either end up in the landfill or undergo physical reshaping to be further utilised as a secondary compound in plastic products or used as a filler in a composite material.<sup>55,59,60</sup>

However, it is undeniable that improper waste management has led to most of these wastes ending up in landfills. Degradation of the material in an open area,

such as a landfill, is a process that takes place over an extended period and is highly influenced by environmental conditions. Most synthetic rubbers would take 50 - 80 years to disintegrate, and for tyres, it could be up to 2000 years.<sup>61</sup> Tyres consists of a 40 to 50 % mixture of vulcanised natural (NR) and synthetic rubber (styrene-butadiene and butyl rubber) that provide traction and tread wear. The vulcanisation process, toxic additives, and zinc in tyre tread formulation generally hinder tyre degradation.<sup>62</sup> Although some of these materials would eventually be disposed of and assimilated into landfills, studies have revealed that the products from the degradation process can be dangerous to the environment.<sup>63</sup> The production of micro-size polymer fragments could invade the water supply system and disrupt aquatic habitation. The soil could be polluted by harmful chemicals resulting from the disintegration of the chemical-containing materials.<sup>1</sup>

The degradation process impacts both the macro- and the micro-structure of material. The degradation process could macroscopically affect a material through bulk degradation or surface erosion. Bulk degradation refers to a significant deterioration in the interior and surface of a substance that results in a substantial loss of material weight and a decrease in mechanical strength over a while. Surface erosion mainly occurs at the surface of a material, resulting in a shrinking sample size, with no changes to the sample geometric shape and predictable mass loss profiles.<sup>64</sup> While microscopically at the molecular level, degradation involves a chain scission process that transforms the polymer chains into smaller fragments of oligomers or even monomers. Therefore, research was geared to discover the factors that influenced the degradation process and ultimately utilise the degradation products for other purposes instead of being released to the environment. Hence, a controlled degradation

process has also brought forth the advancement of rubber degradation as a tool for rubber modification. Table 1.2 briefly describes some of the factors that trigger the degradation process.

**Table 1.2.** Different types of degradation processes and the causing factors.

<b>Degradation Process</b>	<b>Definition</b>
Biodegradation	Mediated with at least one step by biological agents or microorganisms
Photo-degradation	Occurs upon ultraviolet (UV) radiation in the environment.
Thermal degradation	Caused by heat and temperature
Chemical degradation	Occur either in aqueous solution with water-soluble compounds of acids, alkalis and salts or in organic-solvents
Ultrasonic degradation	Occurs through ultrasonic sound.
High energy degradation	Caused by high energy radiation such as X-rays, $\alpha$ , $\beta$ and $\gamma$ rays.

### 1.2.2 Rubber degradation and chemical structure modification

Rubber modification is a process that alters the chemical structure of rubber molecules into a material with different purposes. This process enhances rubber quality, especially NR, for numerous other applications. The principle of rubber modification is to reduce the molar mass of high molecular weight rubber into a soluble low molecular weight compound through C=C bond scission. Breakages of the C=C bonds can be achieved by employing a catalytic chemical process, which includes chemical, ozonolysis, photochemical, biodegradation, ultrasound irradiation, and cross-metathesis reactions.<sup>65</sup> Furthermore, the modification can also be performed through devulcanisation, which refers to the scission of the cross-linking bonds, mainly the C–S and S–S bonds in vulcanised rubber. However, most rubber modification methods involve chemicals that could be harsh to the environment or laborious during post-reaction management. The following sections give some examples of rubber modification via the chemical method for characteristic improvement (Section

1.2.2.1), pre-treating rubber via devulcanisation (Section 1.2.2.2) and modification of rubber into telechelic compounds (Section 1.2.2.3).

#### *1.2.2.1 Modification of epoxidised natural rubber using chemical and oxidative degradation*

Further modification of ENR was developed that introduces a derivative of ENR known as liquid ENR (LENR). Chemical degradation of ENR in the latex form and the presence of surfactant is based on the reaction with peroxy nitrite ions, formed from the reaction of sodium nitrite and hydrogen peroxide, and produces smaller polymer chains with either hydroxyl or carbonyl telechelic functional groups with  $\pm 10\,000\text{ g mol}^{-1}$  of number average molecular weight ( $M_n$ ) and with similar epoxidation level to the parent ENR.<sup>66,67</sup> Hydroxyl-terminated liquid epoxidised natural rubber (HTLENR) with lower  $M_n$  ( $3233\text{ g mol}^{-1}$ ) could be produced by the oxidation method of LENR in the presence of ethanol, sodium borohydride ( $\text{NaBH}_4$ ) as a reducing agent to introduce the hydroxyl functional groups, and cobalt acetyl-acetonate (CAA) as the oxidising agent at  $80\text{ }^\circ\text{C}$ .<sup>68</sup> Synthesis of HTLENR from ENR50 was successfully achieved with  $M_n$  of  $5163\text{ g mol}^{-1}$  using similar oxidation conditions at  $60\text{ }^\circ\text{C}$ .<sup>69</sup>

#### *1.2.2.2 Cross-metathesis on vulcanised polybutadiene rubber*

Cross-linked polybutadiene rubber (cPBR) has been reported to be broken down using cross-metathesis (CM) by soaking into the Grubbs' catalysts solution (1 mol % ) without the presence of low molecular weight chains transfer agent such as diester.<sup>70</sup> Pendant  $-\text{CH}=\text{CH}_2$  that are derived from 1,2 enchainment of cPBR were postulated to be involved in the CM reaction with a  $-\text{CH}=\text{CH}-$  backbone, resulting in lasso-like (tangling) and linear polymer chains. Furthermore, CM degradation of styrene-butadiene (SBR) sheet under the same condition but at a higher temperature ( $40\text{ }^\circ\text{C}$ ) resulted in the formation

of 95.6% vinyl contents of the BR in the generated products after CM degradation.

Latent metathesis catalysis has brought up a new field of research for CM chemistry. The latent catalyst needs a stimulus such as light, heat or ultrasound to initiate the metathesis reaction. Herman and co-workers performed CM depolymerisation of cPBR using a commercially available thermally latent Ru catalyst (dichloro(1,3-bis(2,4,6-trimethylphenyl)imidazolidin-2-ylidene){2-[(ethoxy-2 oxoethylidene)amino]benzylidene}ruthenium(II)) called HeatMet (Figure 1.7a).<sup>71</sup> The reaction performed on urethane-linked hydroxy-terminated polybutadiene (HTBR) containing HeatMet at 0.004 mol % demonstrated a balance transition from cross-linking (liquid-solid) to depolymerisation (solid-liquid) upon high temperature. Analysis using <sup>1</sup>H NMR detected oligomers with vinyl and cyclopentene chain ends with molecular weight less than 400 g mol<sup>-1</sup> as the depolymerisation products and significant *cis-to-trans* isomerisation of 1,4 units (Figure 1.7b). However, due to heat sensitivity, the cross-linking of the polymer chains in the presence of the catalyst has to be carried out at moderate to low temperatures to avoid premature activation.

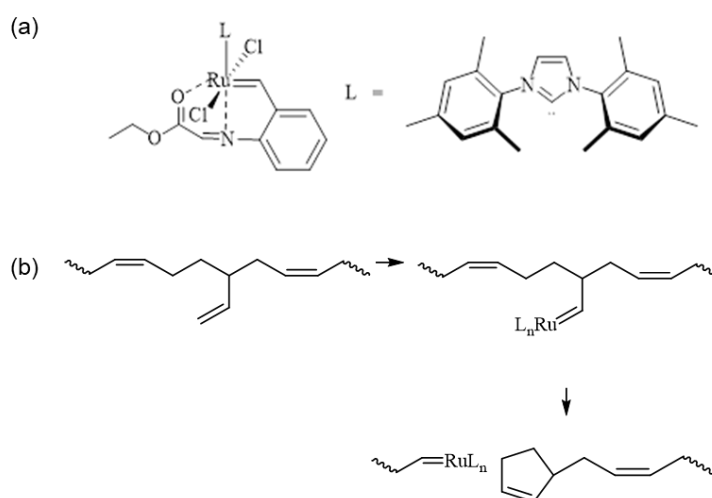


**Figure 1.7.** (a) Chemical structures of latent metathesis catalysts HeatMet and (b) Depolymerisation of butadiene rubber into vinyl and cyclopentene chain ends.

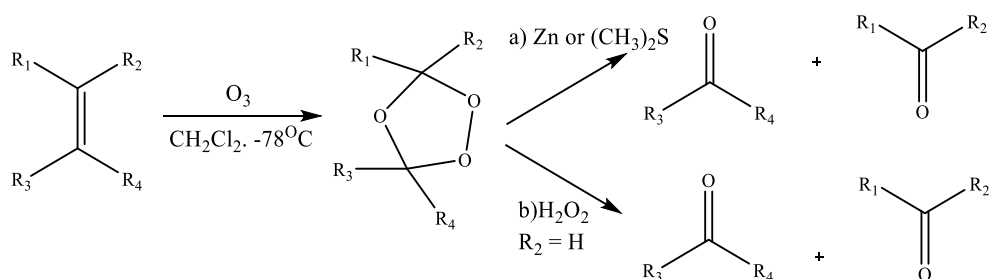


### 1.2.2.3 Alkene cleavage via ozonolysis

Diene rubbers, such as those described in the previous sections, are made from polymerised dienes and contain either *cis*- or *trans*-alkene bonds in the backbone. Alkenes can undergo a wide range of reactions, including electrophilic addition of acids, rearrangements of carbocations, hydrogenation and oxidation.<sup>72</sup> Cleavage of the alkene bonds through oxidation results in molecules containing oxygen functionalities in the form of carbonyl functional groups (aldehydes or ketones). Moreover, the oxidative cleavage of alkenes is also useful in protecting group removal and large molecule degradation.<sup>73</sup> This could be achieved by chemical methods that include ozonolysis, chemical oxidants (KMnO<sub>4</sub>, OsO<sub>4</sub>, RuO<sub>4</sub>), electrochemical alternatives, singlet oxygen, hypervalent iodine and organic catalysts in combination with oxygen.<sup>74</sup> The most commonly employed approach is the ozonolysis of the C=C double bonds, allowing access to aldehyde or ketones.<sup>75,76</sup>

Ozone is a highly reactive oxidant and adds as an electrophile to an alkene that generates ozonides and other peroxidic ozonolysis products.<sup>74</sup> In a separate step, the ozonides will be cleaved to carbonyl products in the presence of a reducing or oxidising agent. For example, in the presence of zinc or dimethyl sulphide, as shown in Scheme 1.2 (pathway a), it will lead to the formation of ketones and/or aldehydes.<sup>77</sup> On the other hand, an oxidising agent such as hydrogen peroxide cleaved the ozonides into ketones and/or carboxylic acids (Scheme 1.2, pathway b).<sup>78</sup> Alternatively, in situ, carbonyl oxide reduction was performed in a rotating zigzag bed (RZB) high-gravity unit. Water was used as a zwitterion in a mixture of acetone to produce the corresponding aldehyde (main product) between 72.3% and 95.8%, with a small amount of acids as the by-product.<sup>79</sup> However, the chemical ozonolysis has been reported to cause

explosive accidents, thus complicating this reaction to be performed on a large scale.<sup>80</sup> Furthermore, the reaction requires extremely low temperatures and high concentrations of reducing agents. Ozonolysis by the metal-based method also has several drawbacks. Most metals used, such as Chromium, Osmium, or Ruthenium, are less abundant, expensive and poisonous heavy metals.<sup>81</sup>



**Scheme 1.2.** Ozonolysis of alkenes followed by work-up with reducing or oxidising agents.

### 1.2.3. Biodegradation of rubber

Biodegradation is a process where the initial disintegration of material is caused by contact with specific groups of microorganisms or other biological and abiotic agents in particular surroundings. Subsequently, changes at the molecular level of the polymeric substances occur due to a chemical reaction catalysed by the microbial enzyme (hydrolytic or oxidative enzyme) and other catalytic agents (free radicals). Thus, biodegradation reduces the molecular weight of polymeric materials, which are further processed in the environment during the mineralisation process.<sup>64</sup>

Numerous investigations were conducted to identify the microorganisms, such as bacteria and fungi, that can degrade rubber. Initially, most studies of rubber biodegradation used a population of microorganisms to disintegrate rubber products.<sup>82,83</sup> The objective was to determine the time required for complete

disintegration. Observation of the physical changes to the rubber, such as weight, surface and shape, was performed. Rubber-degrading microorganisms use rubber as a carbon source by synthesising an enzyme that can break the C=C bond in the polyisoprene chain to produce a compound that can be consumed by the cells. There are two mechanisms of rubber degradation via the microbial attack: (1) the enzymatic reaction and (2) the surface colonisation in which the microorganisms must be attached to the rubber surface to initiate the degradation.<sup>84,85</sup> Growing the microbes on a latex overlay agar plate was used to distinguish rubber degrader microorganisms between the two mechanisms. Those microorganisms that degrade the rubber through the enzymatic reaction produce a translucent opaque on the agar plate. In contrast, this reaction is absent in the plate with microorganisms that degrade rubber via surface colonisation. Thus, these microorganisms were then classified as clearing-forming zones and the latter as non-clearing-forming zone rubber degraders. Nevertheless, research has proven that enzymes are responsible for both mechanisms.<sup>86</sup> The ultimate advantages of biodegradation were highlighted in recent years when specific microbial enzymes that can degrade rubber were isolated and characterised.<sup>84,87,88</sup>

#### **1.2.4 Enzymatic biodegradation of polymers**

The biodegradability of polymers and their cleavage mechanisms mainly depends on the type of backbone that links the monomers. Polymers have two major linkage types: the C-C bond and the hydrolysable bond.<sup>89</sup> Synthetic polymers containing C-C bonds backbone are more resistant to biodegradation than hydrolysable bond polymers. Nevertheless, the similarity of the chemical bonds between synthetic and natural polymers opens the possibility of using enzymes for synthetic polymer biodegradation.

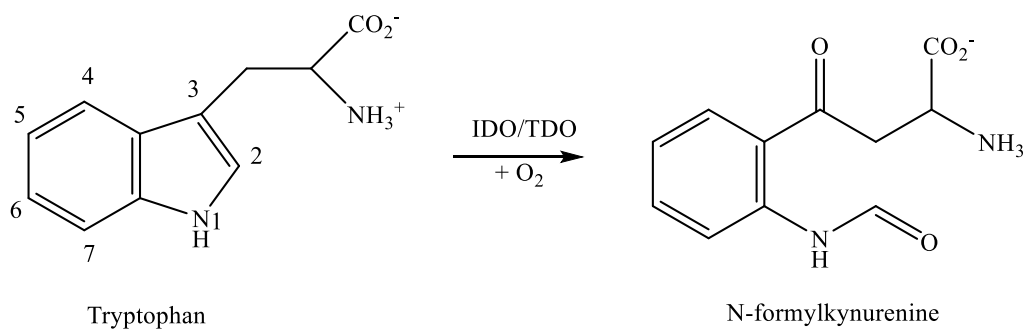
Azevedo and Reis (2005) suggested that highly crystalline and hydrophobic homopolymers might undergo enzyme-catalysed degradation based on the surface erosion mechanism.<sup>90</sup> Some polymer molecules are arranged in a tightly packed structure or encapsulated in a particle with a relatively large size compared to the enzyme molecules. Therefore, the enzymatic degradation occurs only at the polymer–enzyme interface and causes an increased surface area due to morphological changes (increased roughness and fragmentation) on the polymer surface, further enhancing the enzymatic catalysis at the molecular level.

Hydrolytic and oxidative enzymes are microbial enzymes commonly involved in biodegradation. The hydrolytic enzymes catalyse the breakdown of polymers with hydrolysable bonds in the presence of water.<sup>91</sup> These enzymes are ubiquitous and essential in facilitating nutrient and solute absorption. The oxidative enzymes degrade a substrate in the presence of oxidants, such as oxygen, peroxides, or free radicals.<sup>92</sup> Most synthetic polymers are water-insoluble, thus making them resistant to physical, chemical, and biological deterioration, which causes a significant hurdle to degrade these materials. Numerous studies have been reported on the application of hydrolytic enzymes on synthetic polymers with hydrolysable bonds, such as ester (polyethylene terephthalate (PET)) and urethane backbones (polyurethane (PUR)).<sup>93,94</sup> Non-hydrolysable synthetic polymers such as polyethylene (PE) and polystyrene (PS) are more resistant to enzymatic degradation, thus requiring a further understanding of the enzyme-polymer interaction or modification to the enzyme (enzyme engineering).

Meanwhile, enzymes catalysing the alkene cleavage can be divided into heme and non-heme iron-dependent. The heme enzymes are either peroxidases or

oxygenases, requiring either hydrogen peroxide or molecular oxygen as an oxidant, whilst non-heme iron-dependent enzymes only require molecular oxygen for alkene cleavage.<sup>73</sup> The cleavage mechanisms differ depending on whether the substrate is an aromatic C=C or an aliphatic C=C alkene.<sup>74</sup> Enzymes containing heme and non-heme iron play an important role in substrate oxidation via the activation of dioxygen. These enzymes employ different methods of dioxygen activation that are influenced by the ligand environment and the redox properties of the metal.<sup>95</sup> Heme co-factors consist of four pyrrole subunits connected by methine bridges as the basis of the co-factors aromatic structure. They exhibit intense spectral features, distinguishing them from the non-heme enzyme.<sup>96</sup> The iron metal of a heme iron-dependent enzyme is coordinated at the centre of the organic porphyrin framework in a tetradentate fashion. It occupies an entire plane of the octahedron. Perpendicular to the equatorial plane, additional axial ligands can occupy one or both coordination sites, which could be amino acid side chains in the active site of an enzyme.<sup>97</sup>

The enzymatic cleavage of C=C bonds is a complex process, and only a few heme iron-dependent enzymes have been reported for this purpose. The most frequently studied until recently is tryptophan 2,3-dioxygenase (TDO) and its isozyme, indoleamine 2,3- dioxygenase (IDO). These enzymes are heme-dependent dioxygenase that employs a *b*-type ferrous heme to catalyse the oxidative C=C bond cleavage of the indole ring of L-tryptophan (L-Trp), converting it to *N*-formylkynurenine (NFK) (Scheme 1.3).<sup>98,99</sup>



**Scheme 1.3.** Alkene cleavage reaction catalysed by heme dioxygenase enzymes.

Another type of interesting heme iron-dependent dioxygenases is the family of rubber-degrading enzymes. These enzymes catalyse the oxidative cleavage of the C=C in NR polyisoprene backbone, resulting in low-molecular-weight oligo-isoprenoids, which feature oxidised functional groups at their termini.<sup>84,100,101</sup> The oligo-isoprenoids' size distribution ranges from two to twelve repetitive isoprene with decreased concentrations for smaller and larger products. The most extensively studied rubber degrading enzymes are rubber oxygenase A (RoxA), RoxB, and latex clearing protein (Lcp).

### 1.3 Latex clearing protein

Enzymes degrading the rubber by catalysing the C=C bond cleavage are known as rubber oxygenases (RoxA, RoxB) and latex clearing protein (Lcp). The RoxA and RoxB are mainly produced by Gram-negative rubber-degrading bacteria known as *Xanthomonas*.<sup>102,103</sup> Meanwhile, the Lcp is mainly produced by Gram-positive rubber-degrading bacteria. The first microorganism that can produce Lcp was isolated from soil near a city highway in Germany and later was identified as *Streptomyces* sp. strain K30 (LcpK30).<sup>84</sup> The Roxs and Lcp enzymes harbour different characteristics, reaction mechanisms and types of degradation products.

Based on the National Centre for Biotechnology Information (NCBI) on August 2023, there are 19964 latex-clearing protein (Lcp) protein sequences in Protein databases from four taxonomic groups: bacteria, eucaryotes, viruses, and archaea (<https://www.ncbi.nlm.nih.gov/protein/>). Most of the characterised Lcp protein sequences were isolated from actinobacteria, including *Gordonia polyisoprenivorans*, *Streptomyces*, *Rhodococcus*, *Nocardia*, *Mycobacterium* and many others. The first Lcp, known as LcpK30 with heme co-factor containing iron, was isolated from *Streptomyces* sp. strains K30 and has been well characterised by its crystal structure, sequences and other biochemical properties.

In 2014, biochemical information was published on the rubber degradation pathway for Lcp1VH2, isolated from *Gordonia polyisoprenivorans* strain VH2.<sup>104</sup> According to the author, two Cu(II)- dependent *lcp*-encoding genes were detected, namely *lcp1VH2* and *lcp2VH2*. Further research has concluded that Lcp1VH2 is an iron (Fe<sup>3+</sup>) dependent Lcp and does not contain Cu.<sup>105</sup> Isolation, and identification of Lcps from *G. polyisoprenivorans* was an interesting finding, as very few non-clearing-zone-forming rubber degrader strains encoded for the *lcp* gene was identified. Another strain from the genus *Gordonia* that also encodes an *lcp* gene was isolated from a composting operation in São Paulo Zoo, Brazil. The strain, later known as *G. paraffinivorans* MTZ041, was able to form a biofilm on the rubber surface and used rubber as the sole carbon source.<sup>106</sup>

In 2016, Watcharakul and co-workers isolated LcpRr from the *Rhodococcus rhodochrous* strain RPK1 culture, which was enriched with rubber.<sup>107</sup> An actinobacterium identified as *Nocardia nova* SH22a was found able to degrade poly(*cis*-1,4-isoprene) and poly(*trans*-1,4-isoprene) also encoded *lcp* gene,

which was later named as LcpSH22a.<sup>108,109</sup> For the first time, *Solimonas fluminis* HR-BB has been reported to have an active rubber oxygenase of the Lcp type, which is not commonly identified in Gram-negative bacteria.<sup>110</sup> Table 1.3 lists some of the most studied Lcps with their characteristics.

Extensive research relating to these enzymes has been continuously reported until this date due to their high potential to be applied for developing biotechnological rubber treatments. Nevertheless, LcpK30 is the only rubber-degrading enzyme with a well-characterised and documented crystal structure, which makes the enzyme a potential biocatalyst for further exploration. Furthermore, until recently, most research on synthetic polymer biodegradation use Lcp to investigate its potential to degrade synthetic polymers, such as UV-treated polyolefins and synthetic isoprene rubber.<sup>111,112</sup> A study conducted to upscale the production of Lcps also indicates that this enzyme will be the future biocatalyst potentially applied for environmental remediation.<sup>113</sup> Moreover, Lcps can be easily produced through heterologous expression in *E.coli*, thus increasing its potential to be utilised in biotechnology applications. Another advantage of using Lcps is that the products produced after rubber degradation can be easily recovered and used to synthesise value-added compounds.



**Table 1.3.** List of Lcps with their characteristics.

Lcp notation	K30	VH2	RPK1	SH22a	HR-BB
<b>Microorganism</b>	<i>Streptomyces</i> sp. K30	<i>Gordonia polyisoprenivorans</i>	<i>Rhodococcus rhodochrous</i> strain RPK1	<i>Nocardia nova</i>	<i>Solimonas fluminis</i>
<b>Molecular weight (kDa)</b>	48 kDa corresponded to theoretical value of 43.3 kDa for a Strep-tagged version of LcpK30	~ 38	42.2	≈ 40	44
<b>Enzyme activity (U mg<sup>-1</sup>)</b>					
<b>23 °C</b>	1.5	1.3	0.9	n.d	1.5
<b>30 °C</b>	n.d	n.d	3.1	0.03	n.d
<b>37 °C</b>	4.7	n.d	n.d	n.d	n.d
<b>Metal</b>	Fe <sup>3+</sup>	Fe <sup>3+</sup>	Fe <sup>3+</sup>	Fe <sup>3+</sup>	Fe <sup>3+</sup>
<b>Gene sequence similarity</b>		K30 vs VH2 (50%)	K30 vs RPK1 (57%)	n/a	RPK1 vs HR-BB (73%)
<b>Degradation products</b>	Mixture of C <sub>20</sub> and higher oligo-isoprenoids	Mixture of C <sub>20</sub> and higher oligo-isoprenoids	Mixture of C <sub>20</sub> and higher oligo-isoprenoids	Oligo-isoprenoid molecules with carbonyl groups (cis-oligo-isoprenoid molecules (n= 20 - 185) and oligo(trans-1,4-isoprenes) with n = 10-20	Mixture of C <sub>20</sub> and higher oligo-isoprenoids

n.d: not determined

### 1.3.1 Structure of latex clearing protein

The Lcps have a relative molecular mass ( $M_r$ ) of 40 to 46 kDa.<sup>114</sup> More than 63 % of the enzyme structure is alpha-helical, and another 37 % consists of connecting loops.<sup>101</sup> Disulphide bridge between cysteine residues contributes to the building blocks of molecular architecture in most enzymes.<sup>115,116</sup> However, disulphide bridges are not detected in the LcpK30 structure due to the absence of cysteines. Thus, the LcpK30 structure is stabilised by several internal salt bridges and hydrogen bonds.<sup>117</sup> The *b*-type heme-containing iron serves as a co-factor in LcpK30. It is not covalently bound to the polypeptide but stabilised through interactions with neighbouring residues such as histidine (His198) and lysine (Lys167).<sup>105,117,118</sup> The active site of LcpK30 is represented by the heme, with several residues, including Lys167, arginine (Arg164) and threonine (Thr168) located at the distal heme site.<sup>105,117</sup>

Structural and spectroscopic analysis of LcpK30 suggested the existence of two conformational states, closed and open states. The iron at the centre of the heme is directly attached to His198, which is the proximal axial ligand that assists in upholding the iron position during the close and open state of the enzyme. The open structure of the enzyme provides the catalytic relevant state, allowing the substrate to reach the heme moiety via a hydrophobic channel (Figure 1.8). In the closed state, the channel is blocked by coordination of the heme to Lys167, which functions as the distal axial ligand and locks the enzyme into its closed structure, thus effectively preventing access for the  $O_2$  (Figure 1.9).<sup>117</sup>

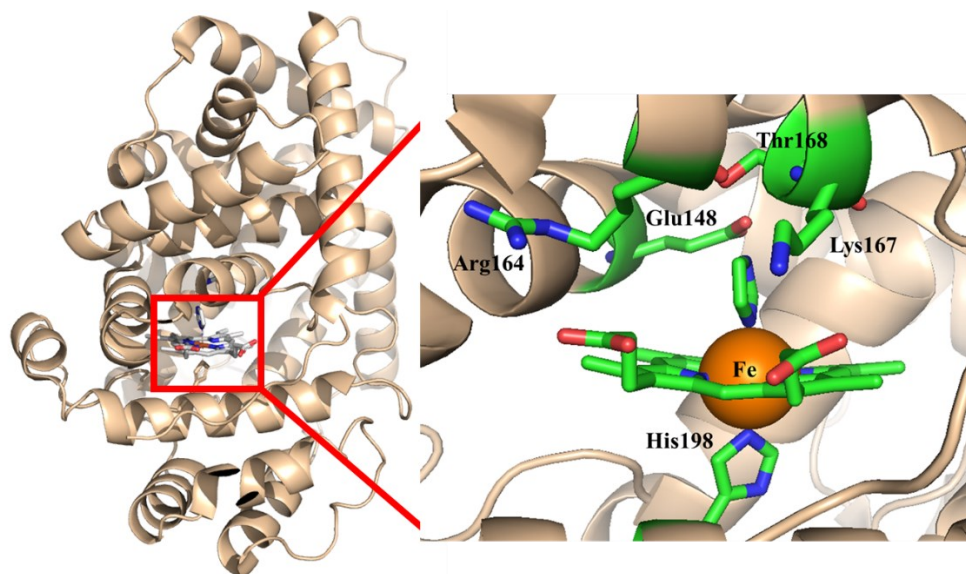


**Figure 1.8.** Structure of LcpK30 in the open state (PDB: 5O1L) with bound imidazole shows the enzyme active site lined by hydrophobic residues.

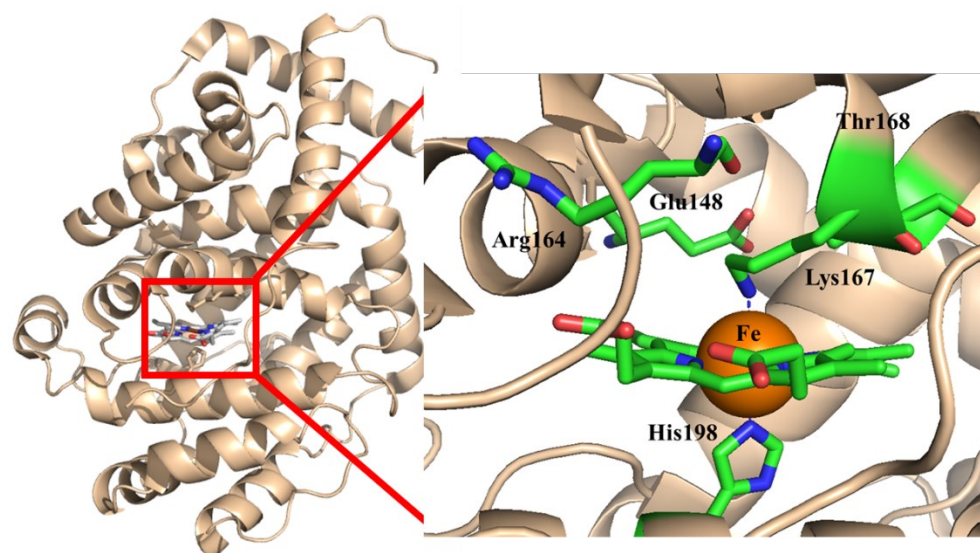


**Figure 1.9.** Structure of LcpK30 in the closed state (PDB:5O1M) shows that the ligation of the iron ion by residue Lys167 effectively blocks the entrance through the hydrophobic channel of the enzyme active site.

### 1.3.2 Cleavage mechanisms of latex clearing protein

Lcps catalyse the oxidative cleavage of *cis*-1,4-polyisoprene at the C=C bonds in an endo-cleavage manner, which produces a mixture of cleavage products (oligo-isoprenoids) with different lengths ( $C_{20}$ ,  $C_{25}$ ,  $C_{30}$  and higher). The oligo-isoprenoids possess keto or aldehyde end groups (Figure 1.10).<sup>119</sup>

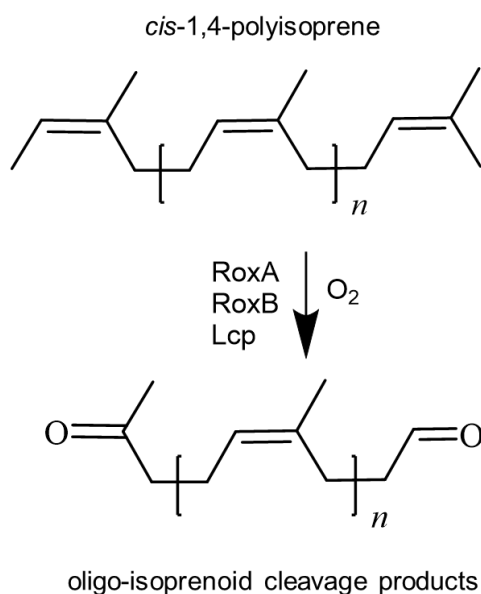
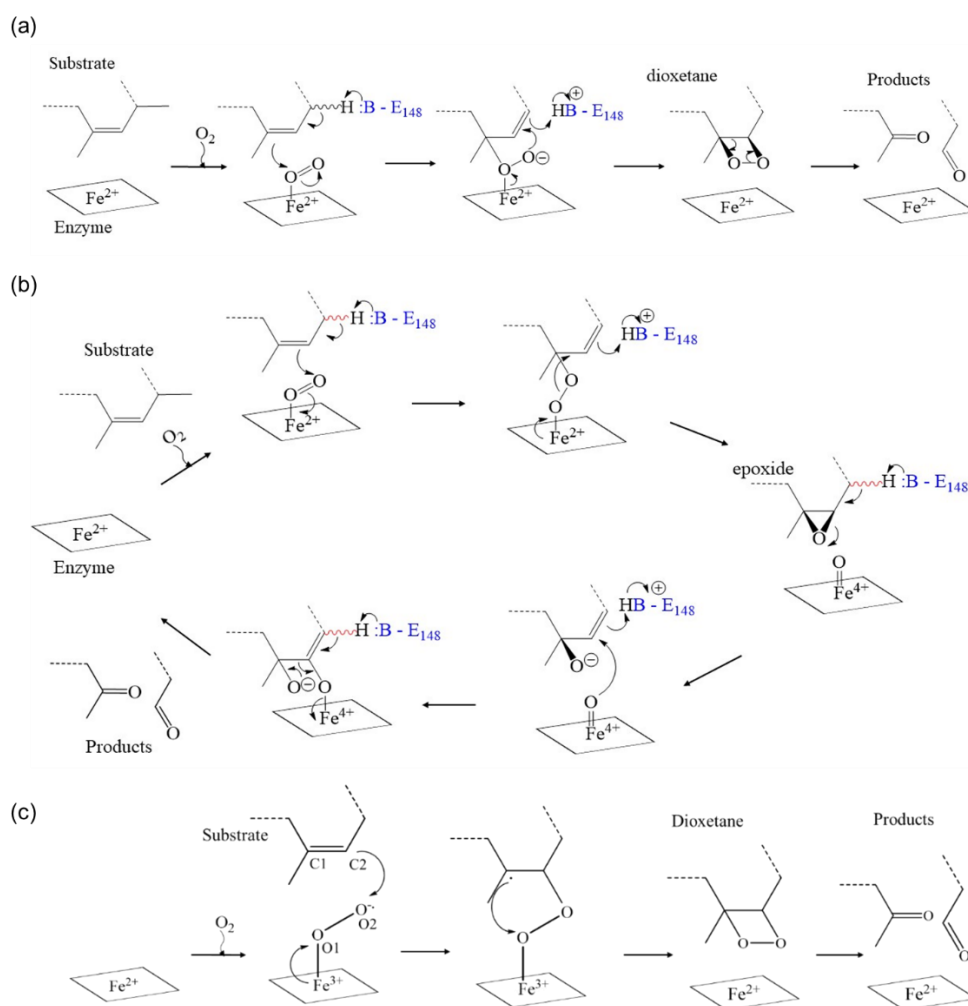


**Figure 1.10.** Oxidative cleavage of rubber produces a mixture of oligo-isoprenoids with different chain lengths ( $n$  represents the number of isoprenes). Reproduced from R other *et al.* (2017).<sup>114</sup>

The catalytic activity of Lcps is activated when dioxygen ( $O_2$ ) binds to the central iron atom of the heme. The activation occurs when the  $O_2$  is directly bound to the divalent cation ( $Fe^{2+}$ ) iron or as a superoxide molecule bound to the iron in a trivalent oxidation state ( $Fe^{3+}$ ). Both attachments result in the formation of a heme-bound  $Fe^{2+}-O_2$  species. According to Ilcu *et al.* (2017), there are two hypothesised mechanisms to activate the cleavage of the  $C=C$ . In both mechanisms, the absence of water in the enzyme's active site during the open state allows the  $O_2$  binding. The hydrophobic channel crossing from the enzyme surface through to the heme moiety is disrupted by a glutamate residue (Glu148). The Glu148 is a polar residue serving as a base and initiates the polyisoprene cleavage by abstracting a proton from the allylic hydrogen positions that show elevated acidity. Proton abstraction from the isoprene by the Glu148 results in bond formation between one carbon atom of the  $C=C$  bond and one oxygen atom of the  $O_2$  molecule. In the first mechanism (Scheme 1.4a),

the oxygen atom that initiates the cleavage is the one bound to the iron (proximal oxygen), and the remaining carbon atom from the former C=C bond, which is now positively charged, will be attacked by the other oxygen atom leading to the formation of a cyclic dioxetane intermediate. Eventually, spontaneous cleavage of the isoprene polymer into keto and aldehyde oligomers will occur.<sup>120</sup> In the second mechanism, the C=C oxidation is initiated by the oxygen atom further from the iron (distal oxygen). The heme-bound dioxygen is eventually cleaved into epoxide and oxo-ferryl intermediate. The oxo-ferryl intermediate will then transfer its oxygen atom and open the epoxide bond, forming the iron-oxygen bond and substrate complex. Due to the deprotonation of the allylic hydrogen from the isoprene, the iron-oxygen bond will be broken, releasing the polyisoprene's degradation products and reserving the enzyme's initial state (Scheme 1.4b).<sup>121–123</sup>

Recent investigation on the cleavage mechanism of the C=C bond in *cis*-1,4-polyisoprene catalysed by LcpK30 has reported some different views from the previous research. The study's motivation was based on several observations of the catalytic mechanisms of other heme and non-heme dioxygenases. Based on the well-studied heme-dioxygenase, the tryptophan dioxygenase (TDO) and indoleamine 2,3-dioxygenase (IDO) showed unfavourability towards the base-triggered reaction mechanism.<sup>124</sup>



**Scheme 1.4.** Hypothetical pathways of the oxidative C=C bond cleavage mechanisms catalysed by LcpK30 (a and b) adapted from Ilcu *et al.* (2017)<sup>117</sup> (b) The possible pathways investigated by quantum mechanical and molecular mechanical (QM/MM) simulations adapted from Zhang and Liu (2020).<sup>125</sup>

Most of the heme-dioxygenase reactions generally accept that both atoms of the dioxygen are incorporated into the substrate.<sup>126</sup> Reactions catalysed by several non-heme dioxygenases, such as stilbene cleavage oxygenase (SCO) NOV1, generate a similar intermediate: the dioxetane intermediate instead of the epoxide intermediate.<sup>127</sup> Thus, the initiators of the reaction and the formation of intermediates are still under debate.

Aided by computational methodology, the LcpK30 cleavage mechanism was scrutinised by quantum mechanical and molecular mechanical (QM/MM)

simulations. The study outlined that the mechanism followed a direct addition of heme-bound dioxygen to the C=C bond. In the beginning, the dioxygen binds to the Fe<sup>2+</sup> and triggers oxidation of Fe<sup>2+</sup> to Fe<sup>3+</sup> by electron transfer from the Fe centre to the dioxygen moiety, forming the ferric-superoxide complex (Fe(III)-O-O·-). In the situation where the position of the dioxygen (O1-O2) is parallel with the C=C bond of the substrate (C1=C2), the distal oxygen of the Fe-bound dioxygen (O2) will attack the C2 atom to form the heme-bound alkyl peroxide in which one β-electron from the double bond of the substrate is pairing with the α-electron of Fe(III)-O-O·- to form the C-O covalent bond (C2-O2). The C=C bond will cleave in the following reaction and form a carbon radical (C1·). The other oxygen atom (O1) coordinated with the iron will attack the C1· to form the dioxetane intermediate. At this stage, the central Fe accepts the α-electron of the substrate to form the O1-C1 bond, and the ferric iron will be reduced to Fe(II). Thus, the Fe-O coordinate bond will be cleaved. The dioxetane intermediate is an unstable intermediate, which collapses to generate the final carbonyl products by the homolytic O1-O2 and C1-C2 bond scission. The study also shows that Glu148 does not serve as a catalytic base to deprotonate the substrate to initiate the reaction as previously proposed but could be involved in accommodating the substrate at the active site. Scheme 1.4c summarised the recent oxidative cleavage mechanism of the C=C bond by LcpK30, as reported by Zhang and Liu (2020).<sup>125</sup>

### 1.3.3 Production of latex clearing protein

Extensive research on Lcp's production through heterologous expression and purification started after the identification of the enzyme because of its high potential for biotechnology application. Lcp is expressed and secreted *via* the twin-arginine translocation (Tat) pathway into the extracellular medium.<sup>88</sup> Earlier

studies on the heterologous expression of LcpK30 were performed using pET23a and pET19b recombinant plasmids. In an earlier study, *Escherichia coli* (*E.coli*) strain C41(DE3) and C43(DE3), which are mutants of BL21(DE3) harbouring plasmid pET23a::*hyaA**lcpK30* containing the twin-arginine motif as a signal peptide (*hyaA*, hydrogenase 1 small subunit) was cultivated in Luria Bertani (LB) medium with addition of 1 mM IPTG.<sup>88</sup> Following from that, *E.coli* BL21(DE3) harbouring plasmid pET- 23a::*lcpHis* was cultivated in similar conditions.<sup>128</sup> In both attempts, inclusion bodies (IB) were formed.

Additionally, Lcp was also subcloned into plasmids pUC19 and pET19b and other strains such as *Pseudomonas putida*, which results in non-active Lcp protein despite several attempts of expression with different types of culture medium, variable incubation temperature, and high or low agitation rates.<sup>128</sup> Nevertheless, expression of Lcp in homologous strains such as *Streptomyces lividans* and *Streptomyces erythraea* was successful. The ability of the transformed strains to produce Lcp was evaluated by growing the culture on a latex overlay agar plate to observe for clearing-zone formation. Further screening confirmation was performed by staining the medium with Schiff's reagent. Schiff's reagent gives an indication of the presence of aldehyde at the end-terminal of the oligo-isoprenoid produced. The colourless reagent develops into purple upon adding to the assay mixture.<sup>120</sup> The molecular mass of LcpK30 was determined at approximately 43-kDa using Western Blot employing anti-Lcp-IgGs.<sup>128</sup> However, the amount of Lcp was low and insufficient for purification.

In another attempt, the gene for LcpK30 with the signal sequence for TAT-dependent secretion was cloned into the pNH1 plasmid, resulting in pNH1::*lcp* plasmid. The plasmid was transformed into a *Xanthomonas* sp. Strain 35Y is a



strain that secretes rubber oxygenase (RoxA). The recombinant cells were grown in a modified LB-rhamnose medium, and the functional native LcpK30 with molecular mass corresponding to the theoretical value for mature Lcp (41 kDa) was successfully expressed, which was further purified to yield 1.5 mg Lcp from a 12-litre culture volume.<sup>120</sup> The purified Lcp appeared colourless, although the specific activity was slightly higher than the RoxA, 0.70 and 0.48 U mg<sup>-1</sup>, respectively.

Further improvement in LcpK30 production was carried out by substituting the Lcp TAT-dependent signal sequence with Strep-tag. The modified LcpK30 was constructed into p4782.1 (SN3513) plasmid and transformed into the expression strain *E. coli* JM109. Expression of Strep-tagged LcpK30 was a success in which the enzyme was managed to be purified from the soluble cell extracts with 5.4 mg of Lcp per litre culture, and specific activity of 1.5 U mg<sup>-1</sup> was determined for freshly purified LcpK30 at 23 °C using an oxygen consumption assay.<sup>118</sup> The specific activity was increased to 4.6 U mg<sup>-1</sup> at temperatures of 37 °C. SDS-PAGE analysis of the purified Strep-tagged version of LcpK30 showed an intense band at an apparent molecular mass of approximately 48kDa that nearly matched the theoretical value of 43.3 kDa for an LcpK30. Ultimately, this study has proven that LcpK30 is an iron-containing *b*-type cytochrome. In a study conducted by Röther *et al.* (2017), the production of the Strap-tagged version of LcpK30 was increased to 15 mg per litre culture. However, the over-expression of heme-containing Lcp could be challenging due to the co-factor's intercellular availability.<sup>129</sup>

Despite LcpK30 being well-characterised, more advanced studies were performed on another *lcp*-encoded gene, which is *lcp1VH2*. The Lcp1VH2 enzyme with a molecular mass of approximately ~38 kDa was isolated from

*Gordonia polyisoprenivorans* VH2 is known as one of the most potent rubber degraders and could be easily synthesised by a recombinant *E. coli* strain C41(DE3). Several studies were geared to increase the enzyme production yield with minimal cost by designing a more efficient fermentation system using an auto-induction medium (AIM) to promote high cell density and avoid using IPTG, thus preventing IB formation.<sup>113,130–134</sup> A final enzyme concentration of 60 mg L<sup>-1</sup> was achieved by the cultivation of *E. coli* C41(DE3) harbouring pET23a::*lcp1VH2* in AIM and using salting out precipitation for purification.<sup>130</sup> Introduction to complex media components, including hemins precursor of the essential heme *b* co-factor, has further improved the soluble and active Lcp1VH2 yield from 60 mg L<sup>-1</sup> to 223 mg L<sup>-1</sup>.

#### **1.3.4 Rubber degradation catalysed by latex clearing protein**

The oxidative cleavage of the C=C in NR latex catalysed by Lcps produces a mixture of oligomers (oligo-isoprenoids) with terminal keto and aldehyde groups.<sup>135</sup> A defined distribution of oligomers is observed, with a preference for 5-6 (for Lcp1VH2) or 5-8 (for LcpK30) isoprene repetitive units and a decrease in the concentrations for smaller and larger products (Figure 1.11)<sup>136,137</sup>. In a recent study, LcpK30 was found able to catalyse the degradation of low molecular weight synthetic rubber of 3000 to 15000 g mol<sup>-1</sup> with different compositions of monomers in the *cis*- and *trans*-configuration and pure synthetic *cis*-1,4-polyisoprene with a molecular weight of 7000 g mol<sup>-1</sup>.<sup>111</sup> In the study, enzymatically catalysed degradation was performed in a surfactant-free emulsion with *n*-hexadecane used as the stabilising solvent that assists in dispersing the rubber in the aqueous medium. This approach has been proven to improve the enzymatic degradation of synthetically derived polyisoprene with

low molecular weight. However, it was not known whether the *trans*-isoprene part was degraded.<sup>111</sup>

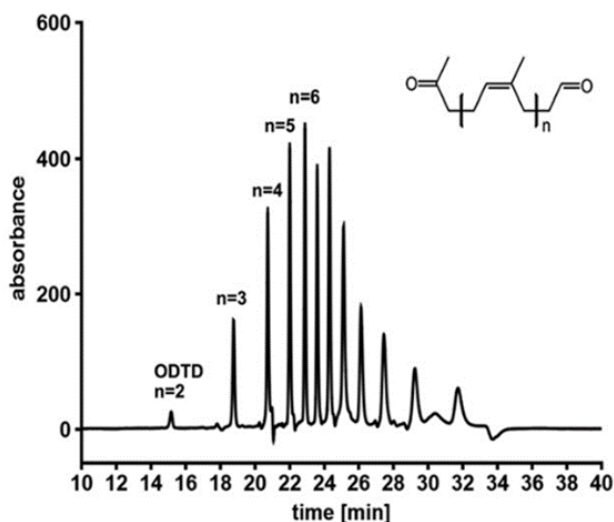


**Figure 1.11.** HPLC chromatogram of cleavage products derived from NRL degradation catalysed by Lcp. The formula of generated oligo-isoprenoid products is shown at the top right. The number of isoprene units in the cleavage products is indicated by n above the identified peaks. The chromatogram was extracted from Birke *et al.* (2015).<sup>118</sup>

The Lcp homolog known as Lcp1VH2 has shown some potential to degrade higher molecular weight synthetic *cis*-1,4-polyisoprene rubber (*cis*-IR); however, the efficiencies remained low.<sup>134,137</sup> Synthetic *cis*-IR has a molecular weight of more than  $10^5$  g mol<sup>-1</sup>. Enzymatic degradation on carbon black-filled vulcanised rubber (CFVR) was performed by incubation with Lcp1VH2. The CFVR was cryo-ground into particles in several sizes (e.g., < 250  $\mu$ m, 250 – 700  $\mu$ m and 700 -1000  $\mu$ m) and pre-treated with acetone and cyclohexane. An analysis of the impact of particle size showed that reduced particle diameter to less than 250  $\mu$ m increases the particles' surface area, thus allowing better contact between Lcp1VH2 and the C=C bonds.<sup>137</sup>

The oligomers produced from rubber degradation can be used as building blocks for value-added compounds due to the presence of aldehyde and ketone as functional groups at the terminal end. The reactivity of the aldehydes can

undergo additional reactions to form covalent bonds with other molecules, such as amine, to build Schiff bases with alcohols in aldol reactions.<sup>138</sup> Meanwhile, the ketone group can undergo addition, reduction, enol and enolate reactions.<sup>119,139</sup> The bifunctional oligo-isoprenoid that resembles the concept of telechelic polymers has the potential to undergo post-polymerisation functionalisation by combined enzymatic and chemical modifications.<sup>139</sup> However, the range of oligo-isoprenoid products is too heterogeneous to be convenient for applications as materials. Nevertheless, Röther and colleagues have shown that degradation of NR in combination with LcpK30, RoxA and RoxB has resulted in upscale production of oligo-isoprenoid with C<sub>15</sub> (two isoprene units) to C<sub>65</sub> (twelve isoprene units) that can be separated and purified according to its structure and size. Their study also hypothesised that the bifunctional oligomers could also be applied for the production of fragrances, hormones and pharmaceuticals.<sup>119</sup> Table 1.4 summarises the previous finding of rubber degradation catalysed by Lcps and the produced oligomer mass.

**Table 1.4.** Enzymatic degradation of natural and synthetic rubber catalysed by Lcps

Lcp type	Substrate	Initial substrate mass (g)	Enzyme concentration ( $\mu\text{g mL}^{-1}$ )	Reaction volume (mL)	Reaction conditions (e.g., buffer, temperature, incubation time, stirring speed)	Extraction solvent	Oligomer's mass (g)	Oligomer's molecular weight ( $\text{g mol}^{-1}$ )	Enzyme activity	Reference
LcpK30	Natural rubber latex (emulsion)	0.002	5	1	100 mM potassium phosphate buffer, pH 7; 2 hours; 22 °C	ethyl acetate	nd	nd	0.7 U $\text{mg}^{-1}$ at 22°C	Birke <i>et al.</i> (2014)
LcpK30	Natural rubber latex (emulsion)	50	4	1000	100 mM potassium phosphate buffer, pH 7; room temperature; 24 hours; 200 rpm	ethyl acetate	$\approx 0.1$	nd	6.2 U $\text{mg}^{-1}$ at 37°C	Röther <i>et al.</i> (2017)
Lcp1VH2	Synthetic <i>cis</i> -1,4-polyisoprene in particles	0.4	50 (enzymes were added every 24 hours)	200	0.2 M Tris-buffer, pH 7; 30 °C; 5 days in a 500 mL bottle	Pentane	$\approx 0.3$	885	not mentioned	Andler <i>et al.</i> (2018)
Lcp1VH2	Synthetic <i>cis</i> -1,4-polyisoprene in particles	4	50 (enzymes were added every 24 hours)	200	0.2 M Tris-buffer, pH 7; 30 °C; 5 days in a multiphase reactor	Continuous extraction with 40 mL ethyl acetate	$\approx 2.1$	550	4.66 U $\text{mg}^{-1}$ at 30 °C	Andler <i>et al.</i> (2020)

#### **1.4 Molecular tools for protein engineering**

Traditionally, natural enzymes have been the most commonly used biocatalysts for producing various natural products, ranging from industrial chemicals to pharmaceuticals.<sup>140</sup> They are proficient macromolecular biological catalysts that are extremely versatile with high catalytic efficiency and stereoselectivity under mild conditions that can perform 'molecular editing'.<sup>141</sup> These enzymes are responsible for synthesising biological building blocks from available elemental resources essential to produce biomolecules, complex natural products, and macromolecular materials. These materials could even be broken down into reusable fragments by an enzyme.

Hence, biocatalysts are in great demand in the current era of synthetic biology and green chemical synthesis to replace or complement conventional manufacturing processes. However, there are several drawbacks with native enzymes, such as thermal stability, pH stability, organic solvent tolerance and expression patterns. Thus, enzymes must be modified for desired physical and catalytic properties to meet the needs of industrial applications.<sup>142–144</sup> Protein engineering has emerged as a powerful biotechnological toolbox to increase the yield of isolated enzymes and to improve biocatalytic activity, stability, enzyme-substrate affinity and substrate specificity or stereoselectivity. To a greater extent, protein engineering allows the manipulation of enzymes for reactions beyond the biological spectrum.

The evolution of protein engineering technologies is shown in Figure 1.12. Provided that the advancement in protein engineering technologies is so rapid, it is crucial to determine which strategies are suitable based on the optimisation target.

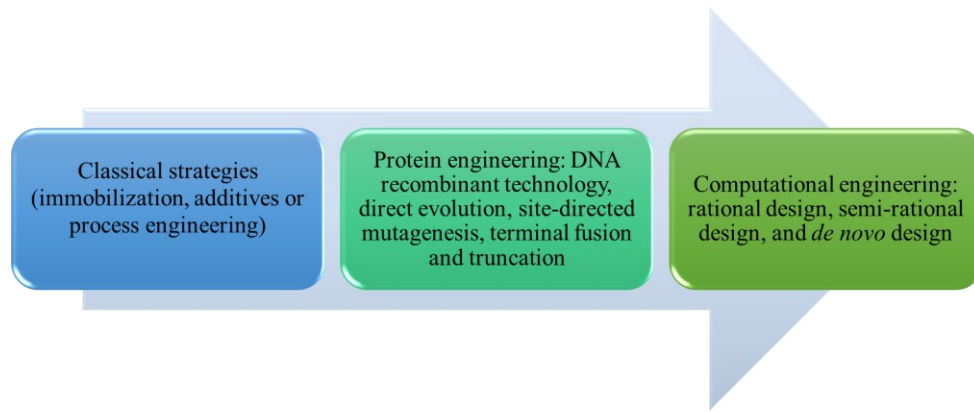


**Figure 1.12.** The evolution of protein engineering strategies.

The exploitation of an enzyme requires an understanding of the structural characteristics and their influence on the function of the enzyme. A structural analysis is typically conducted by studying the enzyme's crystal structure, which enables the recognition of residues interacting with the substrate and/or lining the enzyme's active site. The specific residues are then selected as the target for mutagenesis, in which further characterisation and analysis are performed.<sup>143</sup> <sup>145</sup>Sequence analysis by multiple sequence alignment assists in identifying essential residues that should be avoided from mutation because those residues are highly conserved and necessary for the structure and function of the enzyme.

Computational engineering has improved our understanding of protein function and provided new insights for efficient enzyme design. Advancements in computational software have made biomolecular simulations an efficient tool for understanding enzyme mechanisms.<sup>145</sup> Table 1.5 lists some of the computer-integrated analysing tools that are available to use.

**Table 1.5.** List of examples of computational software

<b>Software programme</b>	<b>Purposes</b>	<b>References</b>
<b>Caver</b>	Identification and analysis of transport pathways in macromolecules	Pavelka <i>et al.</i> (2016) <sup>146</sup>
<b>Mdpocket</b>	An open-source tool for tracking small molecule binding sites and gas migration pathways on molecular dynamics (MDs) trajectories or other conformational ensembles	Schmidtke <i>et al.</i> (2011) <sup>147</sup>
<b>AutoDock Vina</b> <b>GOLD</b>	Understanding the molecular interactions between two molecules	Mohanty and Mohanty (2023) <sup>148</sup>
<b>Swiss-Model</b>		Schwede <i>et al.</i> (2003) <sup>149</sup>
<b>AlphaFold</b>	Modelling and prediction of protein structure	Jumper <i>et al.</i> (2021) <sup>150</sup>
<b>Rosetta</b>		Kaufmann <i>et al.</i> (2010) <sup>151</sup>
<b>IntFold</b>	Protein folding recognition, 3D model quality assessment, intrinsic disorder prediction, domain prediction and ligand binding site prediction	McGuffin <i>et al.</i> (2023) <sup>152</sup>

### 1.4.1 Tunnel engineering

Conventional protein engineering mainly targets the buried active site where the chemical reaction occurs. Exploring tunnels and channels connecting the bulk solvent environment with the active site is crucial for enzymes' catalytic properties. Enzyme engineering through the access tunnel has enabled the modification of enzyme access tunnels and channels precisely tailored for a specific reaction. Pathways represented structurally by channels and tunnels in protein are a vital transportation medium of substrates, cofactors, solvents, and products to and from the active site.<sup>153</sup> They have crucial roles in the biological function and structural stability of an enzyme.<sup>154</sup> More than 60% of enzymes



have active sites deep in the protein's core.<sup>155</sup> Thus, it is important to explore the protein-substrate (ligand) interaction inside the tunnels that will influence enzyme activity, specificity, promiscuity, enantioselectivity and stability. Protein tunnels and channels link to the function of the protein differently. Tunnels of a protein are responsible for linking the inner protein cavity to the protein surface. On the other hand, the movement of solvents, water or other compounds throughout the inner and outer protein structure without blocking by the internal cavity is facilitated by a channel with both sides exposed to the external solvent.<sup>156</sup> CAVER is a software tool widely used to identify and characterise transport pathways in static and dynamic macromolecular structures.<sup>156</sup>

Engineering of enzyme access tunnel could be achieved through several approaches: (i) single-point mutations in a tunnel-lining residue, (ii) blocking of transport tunnels by bulky residues, (iii) widening the tunnel bottleneck area by substituting the bottleneck residues with shorter and hydrophobic residues, and (iv) opening an auxiliary access tunnel.<sup>154,157</sup> Lu *et al.* (2019) have used structure-guided multi-site saturation mutagenesis to shorten the tunnel-like structure in xylanase S7-xyl.<sup>157</sup> Xylanase S7-xyl belongs to glycoside hydrolase family 10 (GH10) catalyse biopolymer degradation. It catalyses the hydrolysis of glycosidic bonds in carbohydrates such as soluble starch, avicel cellulose and polygalacturonic acid and produces reducing sugars or galacturonic acid. In the study, three tunnels in S7-xyl were simultaneously reshaped (Val207Asp/Glu238Ser/Try241Arg), resulting in a variant called 254RL1. This mutant that exhibited a 340% increase in specific activity confers an insignificant difference in bottleneck radii size but a shorter tunnel length than wild-type xylanase. Due to minor changes in substrate binding and structural stability of

S7-xyl and 254RL1, the improved activity was suggested to be caused by the acceleration in the product release by the tunnel with the shortest length.

An example of single-point mutations in a tunnel-lining residue was on haloalkane dehalogenase (HLD DhaA31). A bottleneck residue (Tyr176) was selected to improve DhaA31 catalytic activity by modulating the tunnel properties.<sup>158</sup> The Tyr176 single-point mutants comprise five variants: Tyr 176Cys, Tyr 176Leu, Tyr 176Ser, Tyr 176Ala, and Tyr 176Val. These variants showed varied thermostability and tolerance to organic co-solvents. A study on the binding kinetics of two substrates in DhaA31 by the different mutants revealed that the tunnel engineering effects are strictly ligand specific. Alteration to the bottleneck radii affects the catalytic efficiencies toward a specific ligand, although the two ligands are chemically similar.

Another example of single point mutation was shown on a carbonyl reductase mutant (LsCRM3) that was developed by protein engineering of NADPH-dependent short-chain dehydrogenase/reductase from *Levilactobacillus suantsaii*.<sup>159</sup> The mutant had an increase in activity but poor thermostability. Single point mutation on the mutant at the site Glu145 into Glu145Ala has resulted in a robust mutant (LsCRM4) that displays excellent thermostability and strong organic solvent tolerance.<sup>160</sup> Additionally, via the substrate-binding pocket and substrate access tunnel analysis, the Glu145 was found to be located at the entrance of the substrate with a larger channel radius than the initial mutant (LsCRM3).

#### **1.4.2 Molecular docking**

Computational protein–ligand docking analysis is used to model the interactions between a protein (receptor) and small molecules (ligands) at the atomic level by predicting their stable complex virtually to complement the experimental

method.<sup>161,162</sup> The stable complex of both molecules mainly involves non-covalent interaction forces such as torsional, hydrophilic, hydrophobic, van der Waals, electrostatic, hydrogen-bonding, and desolvation.<sup>148</sup> The computational protein-ligand docking analysis generally starts with a protein with a known crystallographic structure. Thus, it is essential to determine the target position (e.g. the active site, binding site or binding pocket) before performing the docking. Protein-ligand docking offers crucial insights into the effect of a chemical structure and the chemical nature of non-covalent interactions generated between proteins and ligands, particularly at the active site of a protein.<sup>163,164</sup>

Numerous docking software programs have recently been developed for academic and commercial uses. These programs can be broadly categorized based on several algorithm strategies, which include incremental construction approaches (FlexX), shape-based algorithms (DOCK), genetic algorithms (GOLD), systematic search techniques (Glide) and Monte Carlo simulations (LigandFit).<sup>165</sup> The docking technique for protein-ligand can be categorised into three: rigid receptor–rigid ligand, rigid receptor–flexible ligand, and flexible receptor–flexible ligand.<sup>166</sup> DynaDock, GLIDE, AutoDock Vina, GOLD, CABS-dock, FlexPepDock, and pepATTRACT, are among the docking tools that provide flexibility in both receptor and ligand. During the rigid docking process, the protein-ligand complex was bound proportional to a geometric fit between their shapes. Meanwhile, the flexible docking process, or induced fit docking, involves backbone movement that affects multiple side chains and allows a higher order of magnitude in terms of the number of degrees of freedom, thus giving a more accurate binding mode and binding affinity.<sup>167</sup> The preferred protein and ligand conformation is ranked and grouped using scoring functions.

Different molecular docking software uses four types of scoring functions: force-field-based, empirical, knowledge-based, and machine-learning-based. The primary objective was identifying the most stable receptor-ligand complex with ideal geometry and minimum binding energy or fitness score.<sup>148</sup>

Computational modelling has been used to identify the ligand for enzyme binding, explain the enzyme catalytic mechanisms from experimental results, and determine potential targets for mutagenesis.<sup>168</sup> Enzyme degrading poly(ethylene terephthalate) (PET) known as Is-PETase from *Ideonella sakaiensis* poses the ability to catalyse the hydrolysis of PET, converting it to mono(2-hydroxyethyl) terephthalic acid (MHET), bis(2-hydroxyethyl)-TPA (BHET), and terephthalic acid (TPA).<sup>169</sup> Catalytic mechanisms of Is-PETase have been explained by performing hybrid quantum mechanics and molecular mechanics (QM/MM). This study used molecular docking to generate relevant starting structures of the Is-PETase enzyme with various lengths of PET chain (3PET, 2PET and HEMT). These complexes were used for subsequent molecular dynamic simulations and QM/MM calculations.<sup>170</sup> In another study, da Costa *et al.* (2021) used AutoDock Vina and Molecular Dynamic simulations to analyse the protein conformational changes and residue fluctuations to find potential regions of Is-PETase for mutagenesis.<sup>171</sup>

### **1.5 Aim and Objectives**

The vision of the research discussed in this thesis was to develop a biotechnology-based approach for rubber degradation that could ultimately be applied to treating rubber waste more sustainably. Following previous research on the degradation of natural and synthetic *cis*-1,4-polyisoprene rubber by Lcps, this study aims to enhance the catalytic activity of LcpK30 towards *cis*-IR and explore its broader substrate scope. The approaches involve the optimisation

of reaction conditions to facilitate substrate-protein contact, as well as the use of protein engineering strategies. This study employed LcpK30 because it is the only Lcp with a well-characterised and documented crystal structure necessary for protein engineering analysis. To accomplish these aims, the work was structured into three main objectives:

### **1. Production and characterisation of LcpK30 and evaluation of the degradation reaction of NR catalysed by LcpK30.**

The initial work is the implementation of a methodology to produce and characterise LcpK30 in our lab, as well as to assess the application scope of the enzyme. Enzyme expression and purification methods to produce LcpK30 have previously been reported.<sup>113,118,130,131</sup> However, a systematic procedure to increase LcpK30 production is missing. Therefore, the initial task is to find an optimal procedure for producing an active LcpK30, increase its production compared to the currently stated in the literature, and characterise its ability to degrade NR. The following task is to study the impact of reaction conditions on oligo-isoprenoid production by varying parameters such as substrate and enzyme concentration, temperature and routine of enzyme addition into the reaction. Finally, another task is to develop a quick quantitative screening assay for LcpK30 activity based on a colourimetric assay, which could be used to screen for active mutants during protein engineering.

### **2. Diversifying the activity of LcpK30 to catalyse the degradation of other C=C bond polymers.**

The LcpK30's ability to cleave C=C bonds opens the opportunity to use this enzyme for alkene cleavage on other synthetic diene rubbers. The primary objective of this work is to assess how the chemical structure and physical

properties of the rubber will influence the degradation outcome. The potential for enzymatically catalysed degradation of synthetic *cis*-polyisoprene, epoxidised rubber, and polybutadiene rubber with a variety of molecular weights (1300 to more than  $10^5$  g mol<sup>-1</sup>) and morphologies (solid elastic, viscous liquid) will be assessed. These polymers will be pre-treated to improve substrate accessibility to LcpK30. The pretreatment methods will be adapted from previous studies, which include cryo-grinding into particles, casting as a film and dispersing in oil-in-water surfactant-free emulsion stabilised with a solvent.<sup>111,172,173</sup>

### **3. Characterisation of protein-substrate interactions and design of a mutant with expanded substrate scope.**

The primary objective of this work is to introduce mutations via a rational design strategy that can extend the substrate scope of LcpK30 to accept other substrates with different stereochemistry, such as *trans*-isoprene. Computational tools on tunnel identification and molecular docking will be applied to identify the substrate access to the active site and to understand the interaction of the substrate with the protein. Additionally, potential mutation sites will be determined by comparing the sequence of LcpK30 with LcpSH22a, which can degrade *trans*-polyisoprene rubber. Thus, a mutant will be designed and experimentally tested to evaluate the effect of the mutation on the enzyme activity and acceptance of *trans*-isoprene as a substrate.

## **CHAPTER 2**

### **MATERIALS AND METHODS**

#### **2.1 Materials**

##### **2.1.1 Chemicals**

All chemicals such as the following, unless otherwise stated were purchased from Sigma-Aldrich: glucose, agar, carbenicillin, ethanol (EtOH), isopropanol, glycerol, isopropyl  $\beta$ -D-1-thiogalactopyranoside (IPTG),  $\beta$ -mercaptoethanol, sodium dodecyl sulphate (SDS), dimethyl sulfoxide (DMSO), 48thylenediaminetetraacetic acid (EDTA), deuterated chloroform ( $\text{CDCl}_3$ ), chloroform ( $\text{CHCl}_3$ ), sodium chloride (NaCl), potassium chloride (KCl), sodium hydroxide (NaOH), ethyl acetate ( $\text{C}_4\text{H}_8\text{O}_2$ ), alpha-tocopherol, 1,2-dimyristoyl-sn-glycero-3- phosphocholine (DMPC). The purity of all chemicals was within analytical standards. Poloxamer 188 was provided by Access to Advanced Health Institute (AAHI) USA.

##### **2.1.2 Reagents**

EZBlue Stain solution, TAE buffer, Precision Plus Protein™ All Blue Prestained Protein Standards and Laemmli Sample Buffer were purchased from Bio-Rad. PageRuler™ Unstained Protein Ladder was purchased from Thermo Scientific. DNA Loading Dye and Gene Ruler™ 1 Kb Plus DNA Ladder Fermentas. BugBuster Reagent™ was purchased from Merck-Millipore. SOC medium and cComplete EDTA-Free Protease Inhibitor were purchased from Novagen and Roche, respectively. Bradford Reagent was purchased from Sigma-Aldrich.

##### **2.1.3 Polymer**

Natural rubber (NR) latex and epoxidised natural rubber latex (ENR 25 and ENR 50) were provided by the Malaysian Rubber Board (MRB). Liquid polybutadiene was provided by Synthomer. All the following polymers were purchased from

Sigma-Aldrich: *cis*-1,4-polyisoprene average  $M_w$  ~38,000 by GPC, made from NR (Catalog No.: 431257), *cis*-1,4-polyisoprene average  $M_w$  ~35,000 by GPC, made from synthetic rubber (Catalog No.: 431265), synthetic 97 % *cis*-1,4-polyisoprene (Catalog No.: 182141), synthetic 99+ % *trans*-1,4-polyisoprene (Catalog No.: 182168), and Polybutadiene average  $M_n$  ~5,000 (Catalog No.: 383694).

#### **2.1.4 Enzymes**

Restriction enzymes (FastDigest®) were purchased from Thermo Scientific. Benzonase® nuclease was purchased from Sigma-Aldrich.

#### **2.1.5 Plasmids and strains**

Plasmid pET-21a(+) was obtained from Biomatik as a carrier of the synthesised gene (refer to Appendix C3.1 for the plasmid map). *Escherichia coli* BL21(DE3) and DH5α Competent Cells were purchased from New England Biolabs (NEB Inc.). OverExpress™ C41(DE3) Chemically Competent Cells was purchased from Lucigen, US.

### **2.2 Methods**

#### **2.2.1 Solution and stocks preparation**

##### *2.2.1.1 Hemin solution*

A hemin solution was prepared by combining 60 mg Hemin (Sigma Aldrich, UK), 1.74 g potassium phosphate dibasic (K<sub>2</sub>HPO<sub>4</sub>), and 100 mL of distilled water. The solution was heated to boil and stored at -20 °C in 10 mL aliquots.

##### *2.2.1.2 Glycerol stocks*

Strains of *E.coli* were routinely stored as glycerol stocks at -80 °C. Glycerol stocks were prepared by picking a single colony of the strain and culturing it overnight in LB supplemented with an appropriate antibiotic. Cultures were



mixed with sterile 80% aqueous glycerol solution to a final glycerol concentration of 20 % (vol) glycerol, and the cryotubes were stored at -80 °C.

#### *2.2.1.3 Potassium phosphate buffer*

To prepare 1 L of 100 mM potassium phosphate buffer (KPi buffer) at pH 7; 38.5 mL of 1 M potassium monobasic (13.6 g / 100 mL) and 61.5 mL of 1 M potassium dibasic (17.4 g / 100 mL) was mixed together and added with 900 mL distilled water (dH<sub>2</sub>O).

### **2.2.2 Microbiological methods**

#### *2.2.2.1 Media preparation*

All media used were sterilised by autoclaving (121 °C, 1 atm for 20 min or as stated in the text) using a Prestige Classic 2100 benchtop autoclave (Medstore Medical). Antibiotics stocks were prepared at 100 mg/mL in nuclease-free water, filter sterilised (0.2 µm), stored at -20 °C and mixed into the media when cooled. Media solutions were dissolved in distilled water (dH<sub>2</sub>O). For the preparation of agar plates, agar (Melford, 15 g L<sup>-1</sup>) was added to the medium before autoclaving. Agar media were then cooled to ~ 50 °C and poured manually into Petri dishes. Glucose stock was prepared at 2M concentration, heated to 30 °C to assist solubilisation and filtered sterilised using a 0.2 µm filter.

#### *2.2.2.2 Strains growth*

Except otherwise stated, *Escherichia coli* C41(DE3) and BL21(DE3) were grown in Luria–Bertani (LB) medium (10 g L<sup>-1</sup> tryptone, 5 g L<sup>-1</sup> yeast extract and 5 g L<sup>-1</sup> sodium chloride) supplemented with 100 µg mL<sup>-1</sup> carbenicillin for selection purposes.<sup>113</sup> The strains were generally grown overnight (16-18 h) at 250 rpm and 37 °C.

## 2.2.3 Molecular biology methods

### 2.2.3.1 Gene synthesis

The gene sequence for latex clearing protein from *Streptomyces* sp. Strain K30 (LcpK30) was adapted from the GenBank Accession Number AAR25849.1 (Appendix C2.2). The gene was synthesised by BioMatik, optimised for overexpression in *E. coli* with the addition of NdeI and HindIII restriction sites and contained an *N*-terminal Strep-tag® system followed by TEV protease cleavage site to assist during protein purification by affinity chromatography. The genes were delivered in lyophilised form as inserts in the pET-21a(+) plasmid, providing carbenicillin resistance. Plasmids were reconstituted in nuclease-free and filtered dH<sub>2</sub>O and used for further procedures.

### 2.2.3.2 Preparation of LcpK30 mutants

Mutants were prepared using the QuikChange II XL Site-Directed Mutagenesis Kit (Agilent Technologies, USA). PCR was performed on a Mastercycler® personal (Eppendorf) under the following conditions: 1 cycle at 98 °C for 1 min followed by 29 cycles of 98 °C for 30 s, 61 °C for 20 s and 72 °C for 30 s, finishing with a cycle at 72 °C for 2 min. Following successful mutagenesis, the mutated plasmids were then transformed into C41 (DE3) cells and glycerol stock was prepared and stored at -80 °C. The DNA sequences for all mutants were confirmed by sequencing performed by Source BioScience. All *lcps* gene sequences used in this study can be found in the Appendices (C3.3-C3.4).

### 2.2.3.3 Bacterial transformation

The bacterial transformation was performed by following the manufacturer's protocol (New England Biolabs Inc.). Transformation of *E. coli* BL21(DE3) and *E. coli* C41 (DE3) with pET-21a(+):*strep-lcpK30* was performed by standard heat shock. The purchased competent cells were conserved in aliquots (20 –

50 µL) at – 80 °C. The required amount of aliquots to be used was thawed on ice for 2 – 5 min, and the plasmids (10 ng) were directly added into the tubes. The tube containing the mixture was gently mixed by flicking the bottom of the tube with a finger a few times before proceeding to the heat shock step. Table 2.1 shows the heat shock protocol and different growth mediums based on strains used in this study.

**Table 2.1.** Heat shock protocols

<b>Strains</b>	<b>BL21(DE3)</b>	<b>C41(DE3)</b>	<b>DH5α</b>
<b>Incubation time on ice before heat shock (min)</b>	5	30	5
<b>Heat shock time and temperature</b>	30 s; 42 °C	45 s; 42 °C	30 s; 42 °C
<b>Growth medium</b>	SOC Medium	Expression Recovery Medium	SOC Medium

After the heat shock, the tube was immediately returned to the ice for 2 min. Room temperature growth medium was then added, and the cells were incubated at 37 °C for 60 min with 250 rpm shaking. Transformants were selected by plating the culture (10 – 50 µL) on pre-warmed LB agar plates containing appropriate antibiotics and incubated overnight at 37 °C in an incubator.

#### *2.2.3.4 DNA extraction*

The recombinant gene was extracted and purified by transferring one colony of the transformed cell into an LB liquid media with an appropriate antibiotic and growing it overnight at 37 °C at 250 rpm. The cells were pelleted at 14000 x g at 4 °C, and the supernatant was discarded. The DNA was extracted using QIAprep Spin MiniPrep (Qiagen) or Monarch<sup>®</sup> Plasmid Miniprep purchased from New England Biolabs (NEB Inc.) by following the manufacturer's

instructions.  $\mu$ LITE+ (BioDrop) was used to determine DNA concentration after extraction. DNA sequencing was performed by Source BioScience.

#### 2.2.3.5 DNA Analysis

Digestions on the purified plasmid were performed with the following restriction enzymes: (NdeI, HindIII for pET-21a(+)) with 1  $\mu$ L of the enzyme for 1.5  $\mu$ g of DNA and FastDigest Green Buffer at a dilution of 1/10 in 20  $\mu$ L reaction. Reactions were incubated at 37 °C for one hour. The digested plasmids were analysed by agarose gel electrophoresis.

#### 2.2.3.6 Agarose gel electrophoresis

Agarose gel electrophoresis was performed using a Green Range™ Horizontal Gel Electrophoresis Unit (Scie-Plas). The agarose gel (1 % w/v) was prepared with Tris-acetate EDTA (TAE) buffer (Bio-Rad) containing agarose. TAE buffer was prepared from a 50x concentrate by diluting in dH<sub>2</sub>O. After dissolving the agarose by microwaving (800 W, 2.5 min), the solution, ethidium bromide (EtBr) (1% w/v), was added to the cooled agar, mixed by swirling, and the solution was poured into the pre-assembled electrophoresis gel mould. The comb was inserted immediately. When solidification was completed, the comb was removed, and the DNA samples were loaded into the wells. Before loading, DNA samples were pre-mixed with 6X blue gel loading dye (New England Biolabs). GeneRuler™ 1 Kb Plus DNA Ladder was added as standard for each analysis. The agarose gel electrophoresis analyses were performed at 50 - 80 mV for 40-60 min using TAE buffer. Pictures of the gels were obtained using uGenius<sup>3</sup> Gel Documentation System (Syngene).

#### 2.2.4 Protein expression

Experimental cultures were derived from glycerol stocks of transformed *E.coli* C41(DE3) harbouring the plasmid pET21a(+):*strep-lcpK30*. The strains were

grown overnight (16-18 hours) on LB agar supplemented with carbenicillin at 37 °C. Single colonies from the plates were used to inoculate precultures (100 mL LB medium containing 100 µg mL<sup>-1</sup> carbenicillin) and incubated at 37 °C overnight in a shaking incubator at 250 rpm. From this preculture, an appropriate volume was transferred to the expression culture (800 – 1000 mL LB medium supplemented with 5 g of yeast extract, 8 µM hemin, and 100 µg mL<sup>-1</sup> carbenicillin in a 2 L flask) to obtain a starting optical density of 0.1 at 600 nm (OD<sub>600</sub> = 0.1). All cultivations were performed in baffled Erlenmeyer flasks, with nominal volumes five times the culture volume, unless when 1 L expression was performed, the total volume of the flask was double (2 L). The expression culture was further incubated at 37 °C and agitated at 250 rpm until the OD<sub>600</sub> reached 0.6 to 1.0. Protein expression was induced by the addition of filter-sterilised IPTG to a final concentration of 1 mM (or otherwise stated in the text), followed by incubation at 20 °C overnight at 100 rpm shaking. The cells were collected by centrifugation at 18600 x g (4 °C, 15 min) (Avanti J-26 XP centrifuge, Beckman Coulter), the supernatant was discarded, and the cell pellet was stored at - 80 °C for further assay. Protein expression for all mutants prepared in this study was performed similarly to the wild-type LcpK30 or otherwise stated in the text.

### **2.2.5 Protein purification**

The cell pellet was resuspended with binding buffer (100 mM potassium phosphate buffer, pH 7, containing 150 mM sodium chloride) supplemented with lysozyme (0.2 - 1 mg mL<sup>-1</sup>), cOmplete 47 EDTA-Free Protease inhibitor (0.1 µL mL<sup>-1</sup>; 1 tablet every 50 mL) and Benzonase® Nuclease (0.1 µL mL<sup>-1</sup>). The tube was left on ice for 1 hour and gently shaken from time to time, after which the cell pellet was physically lysed using a sonicator (Model 120 Sonic

Dismembrator, Fisherbrand). The sonication was carried out on the ice for 5 minutes with a 30 s pulse 'on' and a 30 s pulse 'off' at 35 % amplitude power. The cell debris was removed by centrifugation at 48000 x g (4°C, 30 mins) (Avanti J-26 XP centrifuge, Beckman Coulter) to yield the cell-free extract (soluble fraction), which then was filtered sterilised with a 0.45 µm filter.

The AKTA Fast Liquid Protein Chromatography System (GE Healthcare, UK) was used to purify the protein. The filtered soluble fraction was applied on a 5 mL StrepTrap™ HP Prepacked Columns (GE Healthcare, UK) pre-equilibrated with five column volumes (CV) of the binding buffer. The LcpK30 protein was eluted with five CV of an elution buffer containing 100 mM Tris/HCl, pH 7, 150 mM NaCl, 1 mM EDTA and 2.5 mM desthiobiotin. The LcpK30-containing fractions were identified by SDS-PAGE, combined and dialysed with 20 mM potassium phosphate buffer, pH 7 overnight. The dialysis buffer was replaced overnight and further dialysed for two hours. Subsequently, the combined LcpK30-containing fractions were concentrated using a 10 kDa cutoff value concentrator tube (Sartorius™ Vivaspin™, UK) at 6000 x g centrifugation (4 °C, 1 hour), and the purified protein was stored at - 80 °C.

#### **2.2.6 SDS-PAGE analysis**

For protein expression analysis, samples (5 mL) were centrifuged (Eppendorf centrifuge 5810R) at 8000 x g for 10 min. The supernatant was discarded, and the cell pellets were resuspended in an appropriate buffer (as described in the text), lysozyme (0.2 mg mL<sup>-1</sup>), cOmplete 47 EDTA-Free Protease inhibitor (0.1 µL mL<sup>-1</sup>; 1 tablet every 50 mL) and Benzonase® Nuclease (0.1 µL mL<sup>-1</sup>). The tube was left on ice for 1 hour and gently shaken from time to time, after which the cell pellet was physically lysed using a sonicator (Model 120 Sonic Dismembrator, Fisherbrand). The sonication was carried out on the ice for 5 min

with a 30 s pulse 'on' and a 30 s pulse 'off' at 35 % amplitude power. The cell debris was removed by centrifugation at 8000 x *g* for 10 min. The cleared lysate was used as the soluble fraction sample. The remaining pellet was resuspended into the same buffer used for the cell lysis in the same volume as the sample volume before centrifugation and used as the insoluble fraction sample. A sample (20  $\mu$ L) was transferred to a fresh tube containing 20  $\mu$ L sample buffer. The sample buffer was prepared by mixing 950  $\mu$ L of pre-made loading 2x Laemmli Sample Buffer (Bio-Rad) with 50  $\mu$ L of  $\beta$ -mercaptoethanol. The samples were heated at 95 °C for 5 minutes, short-spinned, and stored on ice until required. A Pre-made kD™ Mini-PROTEAN® TGX™ (Bio-Rad) gel was used, and wells were loaded with 15  $\mu$ L of the samples. The electrophoresis was carried out generally at 200 mV for 35 min. Thereafter, the gel was washed with distilled water three times and stained overnight with EZBlue Stain (Bio-Rad). The enzyme's presence was checked by visual inspection according to the fraction (soluble or insoluble) in which the protein band corresponding to the size of the enzyme was thickest. Pictures of the gels were obtained from a Gel uGenius<sup>3</sup> Gel Documentation System (Syngene).

### **2.2.7 Quantification of protein concentration**

Protein concentration was determined according to the method outlined by Bradford (1976).<sup>174</sup> A standard curve was plotted from the absorbance reading at 595 nm wavelength ( $A_{595}$ ) of bovine serum albumin (BSA) with a range of concentration from 0.125 mg mL<sup>-1</sup> to 2 mg mL<sup>-1</sup>. The protein concentration was calculated using the equation generated from the standard curve. A typical calibration curve for the Bradford assay is shown in Figure 2.1.

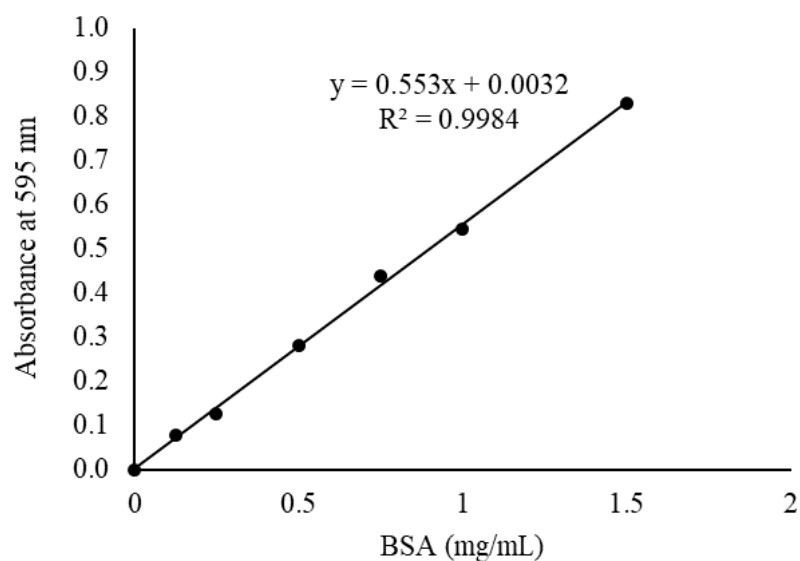


**Figure 2. 1:** Calibration curve for the Bradford assay

A typical calculation of the protein concentration of a sample is given below.

Sample : 10x dilution

Sample absorbance:  $A_{595} = 0.70$  (within calibration range)

Calibration equation:  $A_{595} = 0.553 \times [\text{conc. (mg mL}^{-1})] + 0.0032$

$0.7 = 0.553 \times [\text{conc. (mg mL}^{-1})] + 0.0032$

$\text{conc. (mg mL}^{-1}) = (0.7 - 0.0032) / 0.553$

$= 1.26 \text{ mg mL}^{-1}$

Thus, non-diluted sample conc.  $= 1.26 \times 10$

$= \mathbf{12.6 \text{ mg mL}^{-1}}$

The UV-visible spectrum of the purified protein at a concentration of  $1 \text{ mg mL}^{-1}$  was recorded from 200 nm to 800 nm wavelength using a UV mini-1240 UV-vis spectrophotometer (Shimadzu, UK) to detect a strong absorbance at 412 nm that indicated the presence of heme.



## **2.2.8 Screening for enzyme activity**

### *2.2.8.1 Colorimetric assay*

A qualitative assay for an active enzyme was performed using the colourimetric method using Schiff's reagent (Sigma Aldrich, UK). Enzymatic degradation reaction mixture was prepared by diluting the washed NR emulsion to 0.2 % (wt/vol) with 100 mM KPi buffer (pH 7), and 4  $\mu\text{g ml}^{-1}$  of purified LcpK30 was added. The mixture was kept in a 30 °C incubator shaker at 250 rpm for 2 hours. After that time, Schiff's reagent was added to the reaction mixture to a final concentration of 400 mM and the development of purple or magenta colour was monitored.

### *2.2.8.2 Dissolved oxygen consumption assay*

The specific activity of the enzyme was measured by dissolved oxygen consumption assay using Oxygraph+ System with an S1 Clark type O<sub>2</sub> electrode disc (Hansatech Instruments, UK). The instrument reaction chamber was fitted with a small magnetic stirrer and coupled to a heated circulating water bath (Grant TC120) to regulate the reaction temperature. The instrument was set to default atmospheric pressure at 30 °C and calibrated by automated two-step calibration with air-saturated and deoxygenated water to derive an Offset and Calibration Factor. Calibration was performed to enable the electrical signal received from the electrode disc to be presented as actual calibrated units (nmol mL<sup>-1</sup>). Potassium phosphate buffer (100 mM, pH 7) supplemented with 0.2% (wt/vol) washed NR emulsion was added into the reaction chamber. The oxygen content in the chamber was homogeneously distributed by mixing with a magnetic micro-stirring bar. The baseline was measured for up to 5 minutes until the linearity of the oxygen saturation was reached. The reaction was started by adding Lcp at final concentration of 4  $\mu\text{g mL}^{-1}$ . The rate of O<sub>2</sub>

utilisation was determined by measuring the slope of a tangent drawn to the  $O_2$  concentration ( $\text{nmol mL}^{-1}$ ) versus the time (s) curve during the first 60 s of the reaction. The enzyme activity ( $\text{U mL}^{-1}$ ) was measured by the difference between the slope of a tangent from the reaction in the presence of the enzyme and the slope of a tangent from the control (no enzyme). The specific activity ( $\text{U mg}^{-1}$ ) was calculated by dividing the enzyme activity in  $\text{U mL}^{-1}$  by the amount of protein in the assay ( $\text{mg mL}^{-1}$ ). The samples were prepared in triplicates.

## 2.2.9 Polymer or substrate preparation

### 2.2.9.1 Natural rubber and epoxidised natural rubber

NR was stabilised by 0.7 wt % ammonia. The stabilising compound was removed by washing the NR emulsion with 0.1 % (wt/vol) Nonidet-P40. The washing was performed three times. Nonidet solution was mixed into the emulsion in a 1:1 ratio and slowly inverted ten times, followed by centrifugation at  $9000 \times g$  ( $4^\circ\text{C}$ , 30 min) (Centrifuge 5810R, Eppendorf) to separate the rubber phase (Figure 2.2). The white rubber layer at the top was transferred into a new tube and resuspended with the same volume of Nonidet. After the last centrifugation, the remaining rubber was resuspended with distilled water to 60 % (wt/vol) or  $600 \text{ mg mL}^{-1}$  concentration.

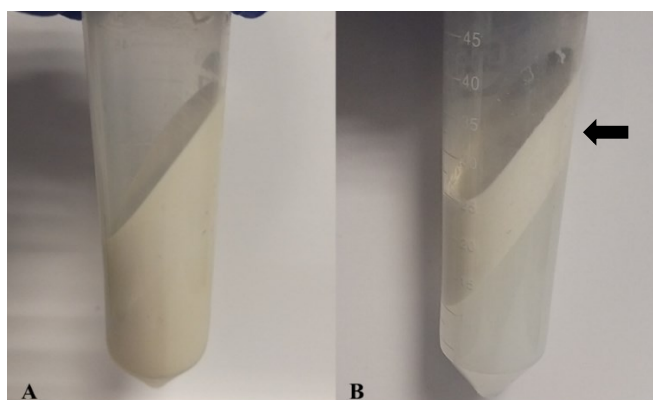


**Figure 2. 2.** Rubber phase separation. (A) After first washing with 0.1% (wt/vol) Nonidet-P40. (B) After the third washing step, the rubber phase was separated at the top layer (black arrow).

### 2.2.9.2 Synthetic *cis-* and *trans*-1,4-polyisoprene

The high molecular weight of synthetic *cis-* and *trans*-1,4-polyisoprene ( $10^5$ - $10^6$  g mol<sup>-1</sup>) were dissolved in CHCl<sub>3</sub> (3 % wt/vol). Once the polymer was completely dissolved, the mixture was precipitated in ethanol as a droplet on a glass petri dish using a syringe and dried under the fume hood, resulting in macroparticles with a diameter of  $\pm 2$  mm measured using the Vernier scale. The resulting macroparticles were further ground in a cryo-mill (6875 Freezer/Mill, SPEC®SamplePrep, USA) for 2 min for each cycle (total of 3 cycles at 15 cps (cycles per second) rate), and the particles were sieved at 600  $\mu$ m and 250  $\mu$ m size. The high molecular weight of synthetic *cis*-1,4-polyisoprene was also prepared into a thin film by weighing the macroparticles at a desired weight (10 mg mL<sup>-1</sup>) and redissolved with chloroform in a vial. After the polymer was completely dissolved, the mixture was spread to cover the inside bottom surface of the vial and dried under the fume hood. Meanwhile, the low molecular weight synthetic *cis*-1,4-polyisoprene (35 000 and 38 000 g mol<sup>-1</sup>) was prepared by dissolving the commercial polymer within *n*-tetradecane in a concentration of 100 mg mL<sup>-1</sup>. After that, the solution was dispersed in 5 mM potassium phosphate buffer at 1 % (wt/vol) concentration by sonication at 50 % amplitude with 30 s pulses on and 10 s pulses off for 5 minutes before adding the enzyme for degradation reaction.

### 2.2.9.3 Polybutadienes

The polybutadienes were prepared similarly to low molecular weight synthetic *cis*-1,4-polyisoprene (Section 2.2.9.2).

### 2.2.9.4 Droplets size

The size distributions of the emulsions were determined on Malvern Zetasizer – Nano ZS/Ultra (Malvern Instrument, UK). Samples were measured using

dynamic light scattering with non-invasive backscatter (NIBS) optics at an angle of 173°. A series of 3 measurement runs with a disposable cuvette at 25 °C temperature was evaluated. A refractive index of 1.33 for the utilised dispersant was applied. The samples were prepared in triplicates.

#### *2.2.9.5 Zeta potential*

Zeta potential measurements were performed on the Malvern Zetasizer – Nano ZS/Ultra (Malvern Instrument, UK). Laser Doppler Micro-electrophoresis is used to measure zeta potential. An electric field is applied (up to 150V, less than 200mS/cm) to a solution of molecules or a dispersion of particles, which then move with a velocity related to their zeta potential. This velocity is measured using a patented laser interferometric technique called M3-PALS (Phase Analysis Light Scattering). Standard values supplied by the instrument software were used for the viscosity and refractive index of water. Three measurements were made at 25°C using an automatic software determination of the measurement duration between 10 and 100 runs. The samples were prepared in triplicates.

#### *2.2.9.6 Microscopy*

Microscopic examination of the co-solvent emulsion droplets was carried out using a Leica DM2500 P Reflected and Transmitted Polarizing Light Microscope (Leica Microsystems, Germany). The emulsion was diluted to 1:100, and 100 µL of the sample was dropped on a grease-free glass slide. The slides were observed under x50 resolution, and microscopic images were taken using a built-in camera.

### **2.2.10 Enzymatic degradation of rubbers**

The enzymatic degradation set-up system was carried out based on the physical morphology of the polymer, which included (i) an aqueous emulsion for

NR and ENR, (ii) a co-solvent emulsion for low molecular weight *cis*-1,4-polyisoprene and polybutadiene rubber, and (iii) solid substrate for high molecular weight *cis*- and *trans*-1,4-polyisoprene. This is a general set-up for the enzymatically catalysed rubber degradation; otherwise, the method is explained in the text; the rubber was added into KPi buffer (5 mM, pH 7) to a final concentration of 100 mg mL<sup>-1</sup> in a round bottom flask. LcpK30 was added thrice to a final concentration of 750 µg mL<sup>-1</sup> (18 µM), and the reaction was stirred at 450 rpm, at 30 °C for overnight (24 hours). A control reaction was also set up, where no enzyme was added. After this time, the reaction was washed three times with ethyl acetate in the same volume as the reaction volume. The mixture was vigorously shaken and centrifuged at 7871 x g for 1 min. The upper layer, which was the organic phase, was removed into a new round-bottom flask. This washing step was repeated thrice. The ethyl acetate was evaporated completely using a rotary evaporator set at 40 °C with appropriate pressure. The extracted products were further dried under the vacuum pump.

## **2.2.11 Characterisation of the degradation products**

### *2.2.11.1 High-Performance Liquid Chromatography*

In general, the dried extracted degradation products were resuspended in methanol with concentration at 1 mg mL<sup>-1</sup> and analysed by High-Performance Liquid Chromatography (HPLC) using Agilent Technologies 1200 series (Agilent Technologies, USA) on a LiChrospher® 100 RP-8 end-capped column (4 mm × 125 mm, particle size 5 µm, Merck KGaA, Darmstadt, Germany). In the case for small scale reaction (1 mL), the dried products were dissolved with 200 µL of methanol. The injection volume was 40 µL, and sample components were detected using a photometric UV/VIS detector at 210 nm. A water/methanol mixture in gradient elution mode was used as the eluent at a

0.7 mL/min flow rate. The gradient used was 50 % of water and methanol at zero time and 100 % of methanol at 5 min. The percentage of water/methanol was kept constant at 50 % / 50 % after 35 min.

#### *2.2.11.2 Nuclear Magnetic Resonance (<sup>1</sup>H)*

The dried extracted degradation products were dissolved in deuterated chloroform (CDCl<sub>3</sub>) to a final concentration of a maximum of 10 mg mL<sup>-1</sup> for proton nuclear magnetic resonance (<sup>1</sup>H NMR). The NMR spectra of the samples were obtained at 298 K using a Bruker AV(III)400 (400 MHz <sup>1</sup>H frequency) (Bruker, USA). Chemical shifts are reported in parts per million (ppm), with the residual deuterated solvent mentioned in the text as an internal standard. The coupling constants J are given in Hz. The multiplicity of each signal is denoted by the abbreviations: s, for singlet; d, for doublet; t, for triplet; q, for quartet; m, for multiplet; app, for apparent; br, for broad.

#### *2.2.11.3 Gel Permeation Chromatography*

Gel Permeation Chromatography (GPC) was performed using an Agilent 1260 Infinity instrument (Agilent Technologies, USA) equipped with a double detector with a light scattering configuration. Two mixed C columns at 35 °C were employed, using THF as the mobile phase with a 1 mL min<sup>-1</sup> flow rate. GPC samples were prepared in HPLC-grade THF and filtered before injection. Analysis was carried out using Astra software. The number and weight average molecular weight ( $M_n$  and  $M_w$ ) and polydispersity ( $\mathcal{D}$ ) were calculated using narrow standards of poly (methyl methacrylate) (PMMA) for the calibration curve.

## **2.2.12 Computational techniques**

### *2.2.12.1 Protein structure preparation*

The high-resolution crystal structure of the LcpK30 enzyme in the open conformation was obtained from the RCSB Protein Data Bank (PDB ID: 5O1L).<sup>117</sup> Although the LcpK30 is a biologically active dimer, only one monomer (chain A) was retained for all calculations and modelling because the interface between the two monomers is relatively far from the active site. The corresponding heme cofactor was also retained, while all other co-crystallised species, including imidazole, 2,3-butanediol and 1,2-ethanediol molecules and waters, were removed prior to all calculations.

### *2.2.12.2 Protein tunnel calculations*

Putative tunnels were calculated with the CAVER-Pymol plugin 3.0.3.<sup>175</sup> The hydrogen atoms were added to the protein structure using Chimera 1.16, considering the H-bonds network.<sup>176</sup> The initial starting point for the tunnel search was specified by the central iron atom of the heme prosthetic group. The search was performed using a minimum probe radius of 0.9 Å. Default parameters for the maximum distance of 3 Å, desired radius of 5 Å, shell depth of 4 Å, and shell radius of 3 Å were used. The clustering of tunnels was performed by the average-link hierarchical Murtagh algorithm based on the calculated matrix of pairwise tunnel distances. The clustering threshold was set to a default value of 3.5. Each atom of the protein was approximated by 12 spheres.

### *2.2.12.3 Protein-ligand molecular docking*

The GOLD program (version 2022.2.0) was used for the molecular docking protocols, with the default parameters as defined within the program.<sup>177</sup> The protonation states of the titratable residues were assigned using the H++

server.<sup>178</sup> To simulate the catalytically active state of the protein, the imidazole molecule coordinated on the iron of heme was replaced with O<sub>2</sub>, which was manually added. The 2D structure of the C50 *cis*-1,4-polyisoprene ligand model was constructed using ChemDraw 18.2 (Perkin Elmer, MA, USA) and the 3D structure with all hydrogen atoms included was obtained using Chem3D 18.2 (Perkin Elmer, MA, USA).

The ChemPLP and ChemScore fitness functions available in GOLD were used.<sup>179</sup> The binding site was defined as all protein residues whose atoms are within 10 Å or 15 Å from the central iron of heme. All docking runs were performed with default parameters using rigid and flexible (induced fit) docking. Ligand flexibility was enabled during all docking runs. Flexible docking was carried out, where the side chains of all residues that have been identified as important to the catalytic activity of LcpK30 (Glu148, Arg164, Lys167, Thr168) were specified as fully flexible.<sup>135</sup> Several other residues which were found in the pathway identified from the static tunnel calculations using CAVER (Ser142, Ile145, Val152, Leu171, Thr230 and Leu234) were also defined as flexible. These side chains were allowed to rotate freely during docking to vary over the range of -180 to +180 rotatable torsion degrees. The protein-ligand interaction was analysed using the Protein-Ligand Interaction Profiler (PLIP) program.<sup>180</sup>



## CHAPTER 3

### PRODUCTION AND CHARACTERISATION OF LcpK30 AND NATURAL RUBBER DEGRADATION CATALYSED BY THE ENZYME

#### Background

In this chapter, the experimental works were performed to achieve the first objective which is to produce and characterise the LcpK30 and evaluate the degradation reaction of NR catalysed by LcpK30. Initially, LcpK30 has been reported to be inactive when heterologously expressed in *Escherichia coli* strain BL21(DE3), resulting in inclusion bodies (IBs).<sup>88,100,128</sup> Eventually, LcpK30 was successfully expressed in *E. coli* JM109, harbouring a LcpK30 gene constructed with Strep-tagged to facilitate enzyme purification.<sup>118</sup> As reported by Röther and his colleagues, the production of soluble LcpK30 was  $\approx 15 \text{ mg L}^{-1}$ .<sup>119</sup> Further optimised production of Lcp was performed using Lcp1VH2 in a fed-batch fermentation process with a modified defined mineral salt medium supplemented with hemin.<sup>132</sup>

This is the first report on the production of Strep-tagged version LcpK30 in the Sustainable Process Technology Research Group (SPT) laboratory at the University of Nottingham. Thus, the methods to express and purify LcpK30 were adapted from several published studies on Lcps. Through systematic trials and some modifications, the yields of soluble LcpK30 were improved. Comprehensive analyses were conducted to examine the impact of substrate concentration, reaction temperature, and enzyme concentration on the activity of LcpK30 in order to ascertain the limitations of the reaction system. The findings correlate with a theory regarding the surface area-to-volume ratio of NR particles to the reaction volume, which has not been previously discussed in any prior research.

Protein engineering of LcpK30 can potentially improve the enzyme's ability to catalyse the degradation of different rubbers. This approach would rely on a quick screening assay to identify potential variants for further investigation. A colourimetric assay using Schiff's reagent provides a qualitative method to detect the presence of aldehyde, the terminal groups of oligo-isoprenoid.<sup>118</sup> An assay that could give a quick and quantitative measurement of enzyme activity would be more informative. Given that the current screening test depends on qualitative evaluation based on Schiff's reagent colour changes, the final experiment in this chapter is the most intriguing part.

This chapter also discusses an attempt to develop a quantitative Schiff's colourimetric assay based on spectrophotometry. The optimal absorbance for Schiff's-aldehyde-coloured products was determined using butyraldehyde (C<sub>4</sub>H<sub>8</sub>O) as the aldehyde model. Staining was performed on the reaction mixture and solvent-soluble fraction. The suitability of these staining approaches for spectrophotometry measurement was tested and discussed through a systematic study. Overall, the work presented in this chapter aims to provide valuable information and knowledge that can be referred to for further research on LcpK30 engineering and application.

### **3.1 Expression and purification of LcpK30**

Expression of LcpK30 was performed using two competent cells. The recombinant plasmid containing the synthetic LcpK30 gene with N-terminal Strep-tag (pET21a(+)::*strep-lcpK30*) was transformed into *E. coli* BL21(DE3) and *E. coli* C41(DE3). The expression in *E. coli* was chosen due to the simplicity of using the *lac* operon system to express a foreign gene. The expression condition, including the medium, inducing agent and temperature, was adjusted according to previous studies. All purification of LcpK30 discussed in this study was performed using the StrepTrap™ HP Prepacked Columns affinity

chromatography (see Chapter 2.2.5). The LcpK30 protein was eluted with a buffer containing desthiobiotin. Qualitative screening using Schiff's reagent was performed before determining the enzyme's specific activity. The efficiency of the expression method was evaluated by the yield of purified protein and the specific activity of the enzyme. The specific activity of the purified LcpK30 was measured using a dissolved oxygen assay, as previously reported.<sup>119</sup> Dissolved oxygen assay is a direct indicator that the enzyme consumes oxygen.

### **3.1.1 Expression of LcpK30 in *Escherichia coli* BL21(DE3)**

The Strep-tagged version of LcpK30 was first constructed in p47182.1 plasmid and was expressed in *E.coli* JM109.<sup>4</sup> This version of LcpK30 was recently reported and successfully expressed in *E. coli* BL21(DE3) by Binder and his team.<sup>111,118</sup> Moreover, the expression of a foreign gene of interest in *E. coli* BL21(DE3) is more common. Therefore, the first attempt to produce Lcp in this study was by using this strain.

The expression culture of *E.coli* BL21(DE3) was grown in Luria–Bertani (LB) medium supplemented with 100 µg mL<sup>-1</sup> carbenicillin at 37 °C and 250 rpm agitation. The protein expression was induced with 1 mM isopropyl-β-D-1-thiogalactopyranoside (IPTG) after the cell culture reached an optical density of 0.6 at 600 nm (OD<sub>600</sub> = 0.6). The induction of LcpK30 expression was carried out overnight at a lower temperature (20 °C) and 200 rpm speed by referring to a published work of the first Strep-tagged LcpK30 expression.<sup>118</sup> Analysis of SDS-PAGE confirmed the presence of LcpK30 after overnight induction (Figure 3.1). The LcpK30 band was visible at approximately 40 kDa, which agrees well with the 41.8 kDa molecular weight calculated by ExPASy ([https://web.expasy.org/compute\\_pi/](https://web.expasy.org/compute_pi/)) based on the LcpK30 protein sequence (Appendix C2.2). However, a protein band was also observed in the insoluble fraction.

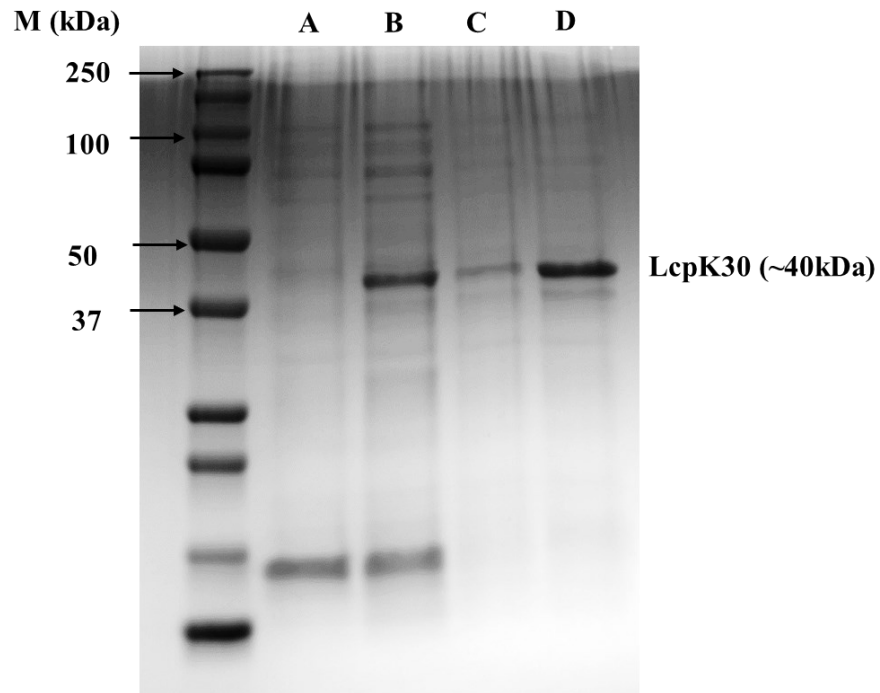


**Figure 3.1.** SDS-PAGE analysis of first LcpK30 (41.8 kDa) expression attempt in *E. coli* BL21(DE3). The *E. coli* strain harbouring plasmid pET21a(+):*strep-lcpK30*. M: Marker; A and B: soluble fractions after two hours and overnight induction; C and D: insoluble fractions after two hours and overnight induction.

A small volume (1 mL) of NR degradation reaction mixture containing 100 mM potassium phosphate (KPi) buffer (pH 7), 2 mg mL<sup>-1</sup> NR and 100 µL cell-free crude extract was prepared. The reaction was incubated at 30 °C and 250 rpm agitation for two hours. Unfortunately, qualitative screening with Schiff's reagent did not produce the Schiff's – aldehyde adduct magenta colour products. The reagent could not identify any aldehyde compound because the degradation of NR did not occur, indicating that the protein was inactive (Figure 3.2).

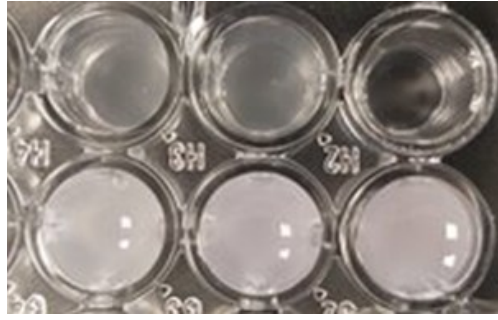


**Figure 3.2.** Colourimetric assay on the reaction mixture of NR with the cell-free crude extract of LcpK30 expressed in *E.coli* BL21(DE3). The reagent was added to the reaction mixture in a 1:1 ratio. Above is the negative control, and below are the testing samples.

Another attempt of LcpK30 expression in *E.coli* BL21(DE3) was carried out under similar conditions to check for the reproducibility of the expression method. However, as shown in Figure 3.3, the LcpK30 was mainly present in the insoluble fraction known as inclusion bodies (IBs). The formation of IBs from the expression of LcpK30 in *E. coli* BL21(DE3) could be due to insufficient providence of the cofactor.<sup>129</sup> Additionally, the turbidity of the expression culture remained unchanged following post-induction and overnight incubation (data not measured), indicating the cells were not propagating well, which might be due to physiological instability such as cellular stress.<sup>181</sup> Expression of heterologous protein could lead to a high degree accumulation of the soluble or insoluble product in the host cell, which would subsequently trigger the cellular stress response and lead to an incompetent metabolic system of the host cell.<sup>182</sup>

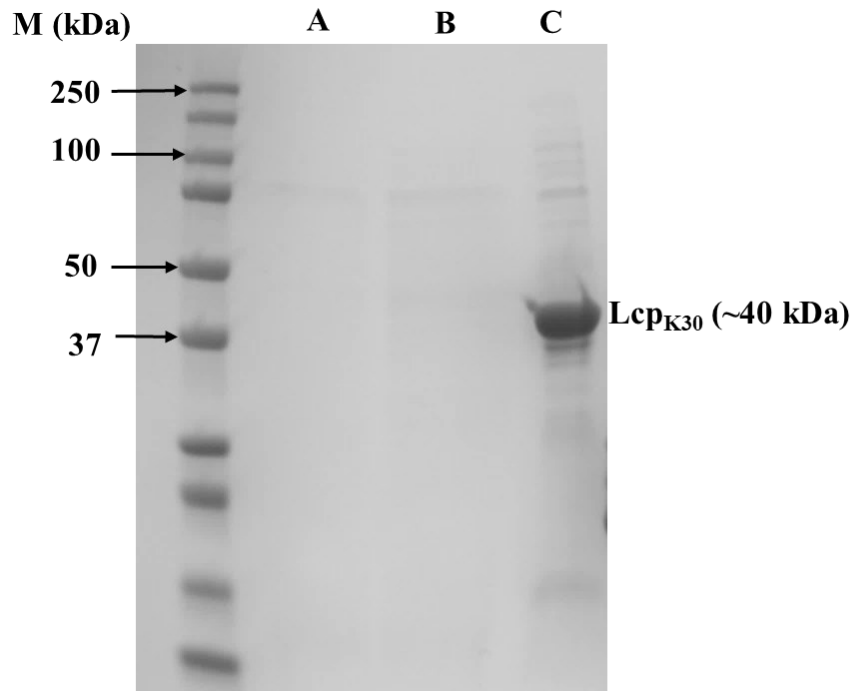


**Figure 3.3.** SDS-PAGE analysis of the second attempt of LcpK30 (41.8 kDa) expression in *E. coli* BL21(DE3). The *E. coli* strain harbouring plasmid pET21a(+):*strep-lcpK30*. M: Marker; Lanes A: soluble fraction after two hours of induction; Lane B: soluble fraction after overnight induction; Lanes C: insoluble fraction after overnight induction.

Due to an unsuccessful attempt to produce active LcpK30, a new expression approach was planned, and three strategies were adopted:

(1) Using a different strain of *E. coli*. such as C41(DE3), which is more stable for expressing toxic or difficult proteins. The strain C41(DE3) is a mutant of BL21(DE3), which has been phenotypically selected to withstand the lethal effect of toxic proteins and thus can grow to high saturation density with the ability to continue producing the proteins.<sup>183</sup> Interestingly, the production of Lcp1VH2, isolated from *Gordonia polyisoprenivorans* VH2 was optimised using a similar strain.<sup>130,131</sup>

(2) Supplementing the expression medium with hemin. The incorporation of hemin into the expression medium was performed by taking into account the suggestion by Rother et al. (2017) that the lack of a source of cofactor might impact the expression of heme-containing protein.<sup>119</sup> A specific cofactor in the

culture media is important to assist in proper protein folding to the exact construction that allows compatible activity at the active site, thus increasing the yield of soluble proteins.<sup>182,184,185</sup> Steinbüchel and his team adopted this suggestion and successfully increased Lcp1VH2 production by adding hemin as the essential heme *b* cofactor source into the expression culture.<sup>113</sup>

(3) Supplementing the expression medium with nutritional additives such as yeast extract to increase the recombinant *E. coli* growth. Introducing yeast extract as the nitrogen source for cell culture has been proven to significantly increase the growth of recombinant *E. coli* in protein production.<sup>185–188</sup>

### **3.1.2 Expression of LcpK30 in *Escherichia coli* C41(DE3)**

Next, the aim was to increase the production of an active and soluble LcpK30 by implementing the strategies explained in the previous section. Additionally, several protein expression studies have reported that using IPTG as an inducing agent could decrease the amount of soluble recombinant protein and exacerbate substrate toxicity.<sup>189,190</sup> On the other hand, lactose is a much cheaper, safer and equally effective expression inducer compared to IPTG. Lactose and IPTG are the common inducing agents used for recombinant protein expression. Hence, the basic protein expression mechanisms induced by lactose and IPTG are quite similar.<sup>191</sup> Therefore, in this study, the impact of IPTG and lactose on cell growth and protein yield was also observed.

The *E. coli* C41(DE3) cells harbouring pET21a(+):*strep-lcpK30* were grown in three different flasks with 100 mL LB-medium, supplemented with 5 g L<sup>-1</sup> of yeast extract, 8 µM hemin and 100 µg mL<sup>-1</sup> carbenicillin. The first flask was induced by IPTG (1 mM), and 3 mM lactose<sup>113</sup> was used as the expression-inducing agent in the second flask. The third flask was set up as a control without the inducing agent. The expression was performed under similar conditions as previously described in Section 3.1.1. After overnight induction,

the cell mass from each flask was measured, and the total protein concentration was determined using the protein Bradford assay (Table 3.1). Quantification of total protein concentration showed that the lactose-induced LcpK30 expression results in higher total protein concentration than IPTG-induced.

**Table 3.1.** Cell mass and total protein concentration were obtained after overnight expression of LcpK30 using *E.coli* C41(DE3) in a supplemented LB medium.

<b>Inducing agent</b>	<b>Cell mass (g)</b>	<b>Protein (mg mL<sup>-1</sup>)</b>
None	0.23 ± 0.03	1.2 ± 0.1
1 mM IPTG	0.97 ± 0.02	2.7 ± 0.1
3 mM Lactose	1.1 ± 0.2	5.5 ± 1.3

<sup>a</sup> The experiments were performed as two replicates

The cell mass of *E. coli* in the presence of lactose could be influenced by the host cell consuming some of the molecules for a carbon source when glucose is unavailable.<sup>192,193</sup> Unconsumed lactose molecules will be converted to allolactose (an isomer of lactose) inside the host cell and bind to the lac repressor. When excess lactose is available, the lac repressor will be dissociated from the T7 promoter, allowing the T7 RNA Polymerase to transcribe the gene of interest.

However, the lower cell mass obtained from the non-induced culture was unexpected. The addition of yeast extract should support cell growth. Furthermore, analysis of the crude cell extracts by SDS-PAGE shows that LcpK30 was expressed in all conditions, including the culture without the inducing agent, with a small protein appearance in a non-soluble fraction (Figure 3.4;1b). This observation is quite peculiar because the formation of IBs was still observed even after the medium was supplemented with hemin. Moreover, in the absence of an inducing agent, the formation of IBs cannot be correlated to metabolic burden due to the overexpression of the recombinant protein. Nevertheless, low cell mass and formation of IBs in the uninduced culture could be explained by several potential causes: (1) the cells grow at different rates



upon dilution into fresh media due to different metabolic states <sup>194</sup> (2) leakage expression of T7 RNA polymerase caused the target protein to be expressed pre-maturely under uninduced state, eventually leads to loss of the expression plasmid and adverse effects on the growth of the cells <sup>129,195</sup> (3) the pre-matured expression of LcpK30 might have improper protein folding that results into the exposure of the hydrophobic surfaces lead to accumulation as IBs <sup>196,197</sup>.

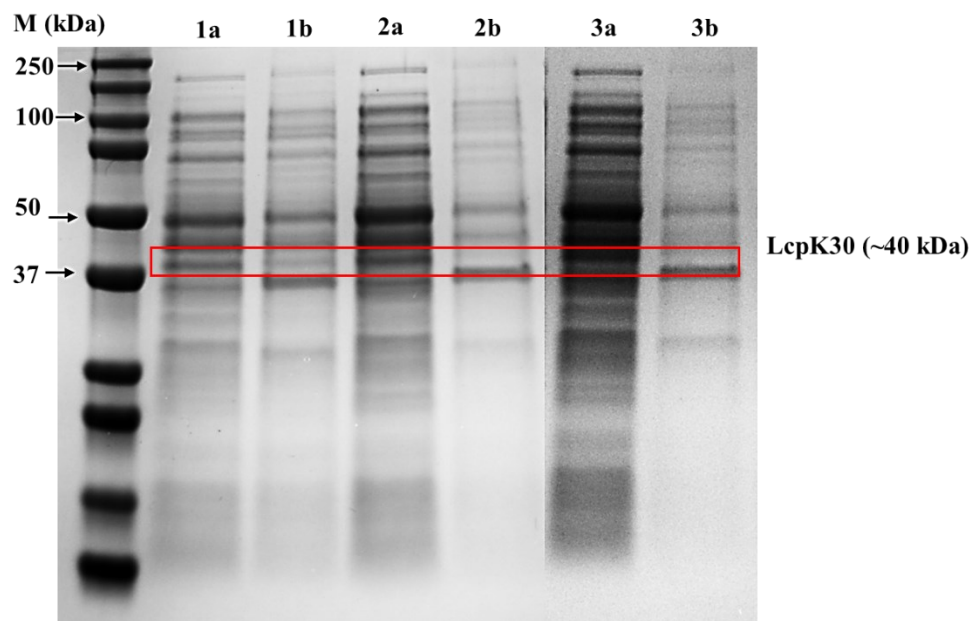


**Figure 3.4.** SDS-PAGE analysis of LcpK30 (41.8 kDa) expression by *E. coli* strain C41(DE3) harbouring plasmid pET21a(+):*strep-lcpK30* (indicated by the red box). Expression conditions were LB medium supplemented with (5 g L<sup>-1</sup>) and hemin (8 μM), with different inducing agents, incubated at 20 °C and agitated at 200 rpm. M: Marker; 1a and 1b: soluble and insoluble fractions after lysis from non-induced expression; 2a and 2b: soluble and insoluble fractions after lysis from 1 mM IPTG induced expression; 3a and 3b soluble and insoluble fractions after lysis from 3 mM lactose induced expression.

IPTG has frequently been used instead of lactose in experimental studies of recombinant protein expression because of its stability in the growth medium. However, previous studies on IPTG-induced Lcp expression have been reported on low bacterial growth, protein yield, and the formation of IBs.<sup>88,100,105</sup> Nevertheless, this study shows that the IPTG does not have significant adverse effects on the cells' growth but results in lower protein yield compared to lactose-

induced LcpK30. Production of LcpK30 in this study was continued by using lactose as the inducing agent.

### 3.1.3 Purification of LcpK30

LcpK30 derived from expression in *E. coli* C41(DE3) in 800 mL LB-medium, supplemented with 5 g L<sup>-1</sup> of yeast extract, 8 μM hemin, 100 μg mL<sup>-1</sup> carbenicillin, and induced with 3 mM lactose was successfully purified by affinity chromatography, as shown by the sharp peak of absorbance at 280 nm eluted at maximum of 70 % concentration of 2.5 mM desthiobiotin buffer (Figure 3.5).

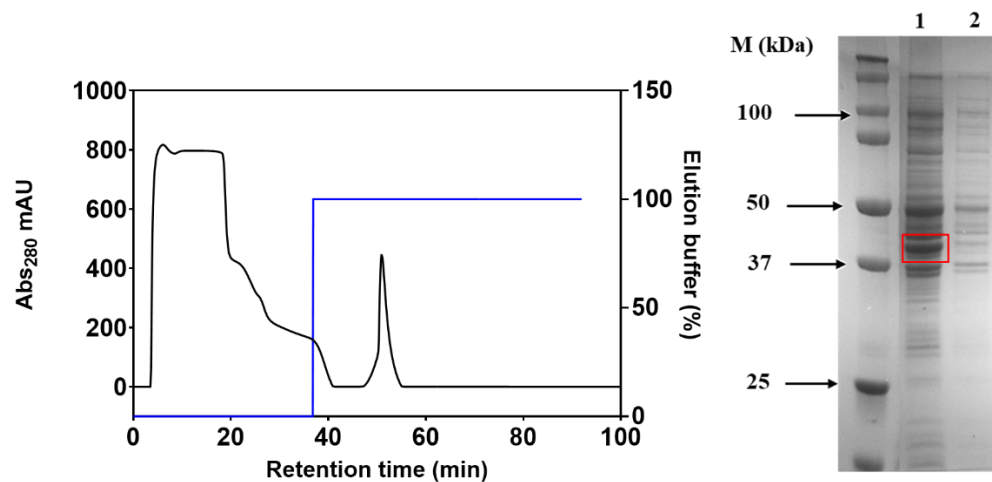


**Figure 3.5.** Purification of LcpK30 expressed by *E.coli* C41(DE3) using AKTA-Fast Protein Liquid Chromatography (FPLC). The black line of the chromatogram represents the absorbance for protein at 280 nm wavelength obtained from the AKTA-FPLC chromatogram. The blue line represents the concentration of elution buffer. The image to the right shows the SDS-PAGE analysis of the crude cell extract: 1- soluble cell extract, obtained after cell lysis and centrifugation, and 2- insoluble cell extract. The red box indicates the LcpK30 protein band.

The SDS-PAGE analysis of the purified LcpK30 is shown in Figure 3.6, indicating a protein band at ~41.8 kDa representing the molecular mass of LcpK30. The fractions containing LcpK30 were concentrated using a 10 kDa cutoff value concentrator tube, and the purified protein was stored at - 80 °C.

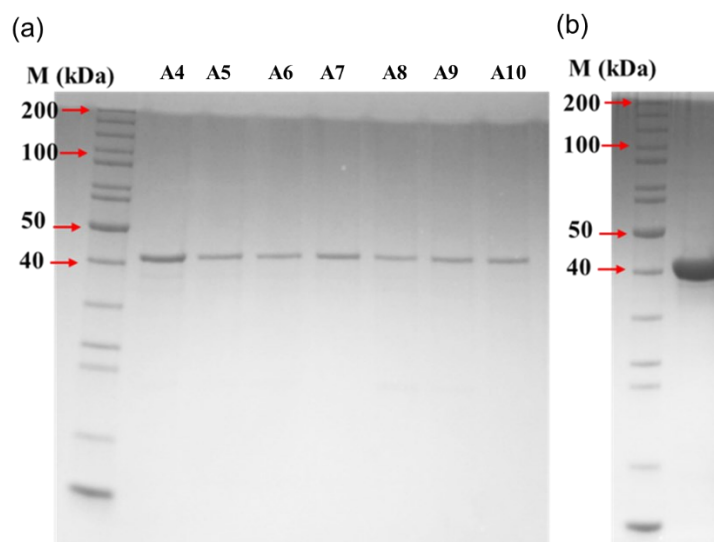


**Figure 3.6.** Purified LcpK30. (a) fractions containing purified LcpK30 (c) concentrated purified LcpK30.

A red-coloured LcpK30 with a concentration of  $3.7 \text{ mg mL}^{-1}$  was obtained. A colourimetric assay was performed to screen an active LcpK30. The development of a magenta colour in the reaction mixture staining with Schiff's reagent confirmed the presence of aldehyde, indicating that the enzyme was active (Figure 3.7).



**Figure 3.7.** LcpK30 colourimetric analysis. After incubating with Schiff's reagent, the natural rubber degradation products with aldehyde terminal ends reacted with Schiff's reagent to give a magenta colour. The reagent was added to the reaction mixture in a 1:1 ratio.

The enzymatic activity of the purified Strep-tagged LcpK30 was quantitatively measured using a dissolved oxygen detection system. This assay directly indicates that the enzyme can reduce oxygen by measuring the dissolved

oxygen concentration reduction rate. The specific activity ( $\text{U mg}^{-1}$ ) was calculated by dividing the enzyme activity in  $\text{U mL}^{-1}$  by the amount of protein in the assay ( $\text{mg mL}^{-1}$ ). The specific activity of  $4 \mu\text{g}$  purified LcpK30 derived from *E.coli* C41(DE3) expression at  $30^\circ\text{C}$  was recorded at  $4.5 \text{ U mg}^{-1}$  (Appendix C3.1). This value was almost identical to the activity of Lcp1VH2 reported by Andler *et al.* (2020).<sup>134</sup> Adding hemin in the culture medium thus assists the intracellular heme cooperation. Table 3.2 shows details of the total protein concentration, expression yield and enzyme activity of the purified LcpK30.

**Table 3.2.** Protein concentration of LcpK30 expressed by *E.coli* C41(DE3) in supplemented LB-medium and induced by 3 mM lactose.

	<sup>a</sup> Protein concentration ( $\text{mg mL}^{-1}$ )	Enzyme activity ( $\text{U mL}^{-1}$ )	<sup>b</sup> Specific activity ( $\text{U mg}^{-1}$ )
Cell-free extract	12.1	$0.006 \pm 0.003$	$1.5 \pm 0.8$
Concentrated protein	3.7	$0.018 \pm 0.000$	$4.5 \pm 0.1$
<b>Purification yield (mg) per 800 mL culture</b>		<b>1.1</b>	

<sup>a</sup> The protein concentration was determined from a 800 mL expression culture

<sup>b</sup> Measurement was performed in triplicates to determine the standard deviation

However, the production of LcpK30 in a quantity suitable for subsequent experiments was still lower than the last work reported on LcpK30 production by Rother *et al.* (2017), which was  $\approx 15 \text{ mg L}^{-1}$ .<sup>119</sup> Thus, further work to increase LcpK30 expression was performed.

### 3.1.4 Optimisation of LcpK30 expression

The addition of glucose in the *E.coli* growth medium is able to eliminate leaky expression from uninduced gene expression.<sup>198</sup> An attempt was made to optimise LcpK30 expression by adding 0.2 M glucose in the *E.coli* C41(DE3) pre-culture. Expression was carried out similarly to the method described in Section 3.1.2 by using 3 mM lactose as the inducing agent.

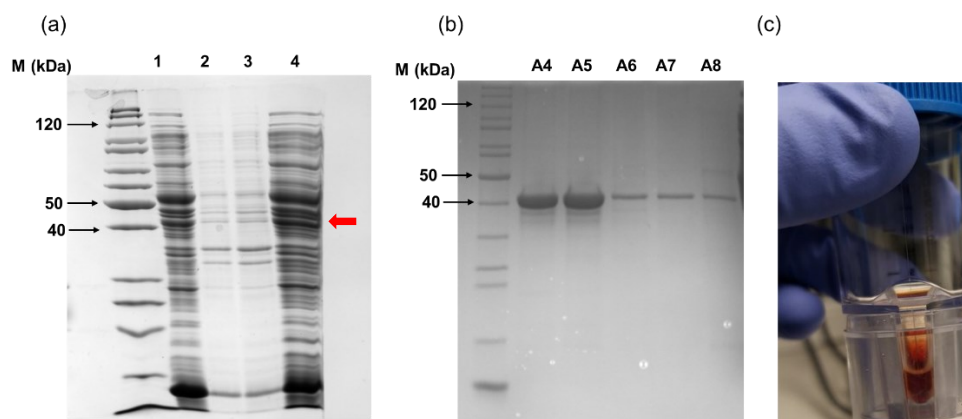


**Figure 3.8.** Purification of LcpK30 by AKTA Fast Liquid Protein Liquid Chromatography. (a) SDS-PAGE analysis of LcpK30 expression. 1 and 4: soluble cell extract, 2 and 3: insoluble cell extract. The red arrow shows the position of the LcpK30 protein band, (b) fractions containing purified LcpK30, and (c) concentrated purified LcpK30 appearing in a red-coloured solution.

As shown in Figure 3.8, the LcpK30 was successfully expressed with minimal formation of IBs. Upon concentration, a red-coloured LcpK30 was obtained, indicating the presence of heme. Moreover, the presence of hemin and yeast extract in the cultivation medium improved the heme uptakes and growth of the recombinant *E. coli*. The purification yield of LcpK30 was increased from 1 mg to 11.2 mg per 800 mL culture (Table 3.3), therefore improving the production of Strep-tagged LcpK30.

**Table 3.3.** Protein concentration of LcpK30 expressed by *E.coli* C41(DE3) in supplemented LB-medium and induced by 3 mM lactose. The pre-culture growth of *E.coli* C41(DE3) was enriched with 0.2 M glucose.

	<b>Protein concentration (mg mL<sup>-1</sup>)</b>	<b>Enzyme activity (U mL<sup>-1</sup>)</b>	<b>Specific activity (U mg<sup>-1</sup>)</b>
Cell-free extract	50 ± 0.003	0.023 ± 0.002	0.005 ± 0.000
Concentrated protein	18.7 ± 0.039	0.011 ± 0.002	3.048 ± 0.408
<b>Purification yield (mg) per 800 mL culture</b>		<b>11.2 ± 1.78</b>	

The experiments were performed in triplicate to determine the standard deviation

However, given that the amount of LcpK30 produced was still comparatively low compared to 15 mg obtained in the study by Rother *et al.* (2007), the expression was carried out in a larger volume using multiple 2 L flasks in an incubator

shaker to allow the production of enough mass of LcpK30 for further experiments.

### 3.1.5 Spectroscopic characterisation of LcpK30

The UV-visible spectrum of the purified LcpK30 was recorded from 200 nm to 800 nm wavelength to check for the presence of the heme cofactor. The appearance of a strong absorption band at 412 nm (Soret,  $\gamma$ -band) and an additional band at 544 nm ( $\beta$ -band) confirmed the presence of heme in the purified LcpK30. These signals are typical for heme-containing proteins and indicate the protein was in an oxidised form containing the low-spin ferric ( $\text{Fe}^{3+}$ ) state (resting state).<sup>107</sup> Absorption at these wavelengths showed the successful incorporation of the heme cofactor in the LcpK30 structure.<sup>135</sup> Heme occupancy was quantified using the Reinheitszahl value ( $R_z$  value), representing the ratio between the Soret band ( $A_{412}$ ) over  $A_{280}$  (indicating protein concentration).<sup>199,200</sup> The  $R_z$  value of LcpK30 expressed in *E. coli* BL21(DE3) without hemin in the culture media was compared with LcpK30 expressed in *E. coli* C41(DE3) with the hemin. The heme occupancy difference was 85 %, from 0.48 to 3.23 (Figure 3.9).

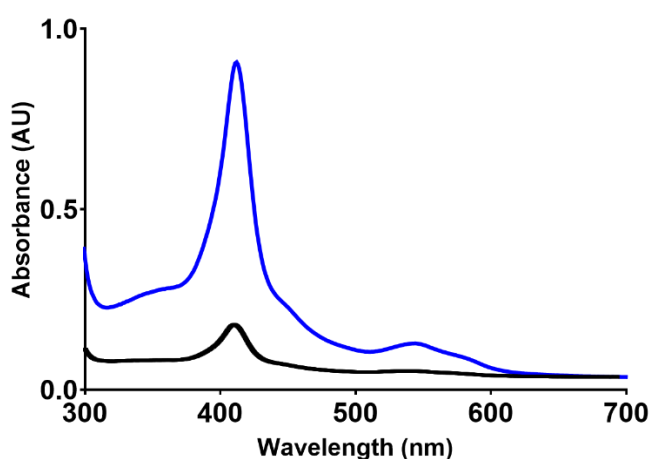


**Figure 3.9.** UV-visible spectrum of 0.5 mg mL<sup>-1</sup> purified LcpK30. The blue line represents the LcpK30 produced in *E.coli* C41(DE3), and the black line represents LcpK30 produced in *E. coli* BL21(DE3).

### 3.1.6 Stability of LcpK30 upon storage

This experiment aims to test the stability of LcpK30 when stored in concentrated stock with a concentration of 10 mg mL<sup>-1</sup>. Based on previous studies, the presence of glycerol assists in maintaining the activity of LcpK30 when stored at – 60 °C.<sup>130</sup> In this study, the purified LcpK30 was stored at – 80 °C and at – 20 °C in the presence and absence of 50 % glycerol and the activity was monitored for five weeks (Figure 3.10).

Figure 3.10a shows that the LcpK30 activity was reduced by less than 50 % when stored in 50 % glycerol and further to more than 50 % when stored without the same glycerol concentration (Figure 3.10b). Moreover, there were no significant differences when stored in both temperatures for up to a month. Thus, it was a standard practice in the lab to store the purified LcpK30 at -20 °C with 50% glycerol for short-term storage and preferably at -80 °C for up to a month storage.

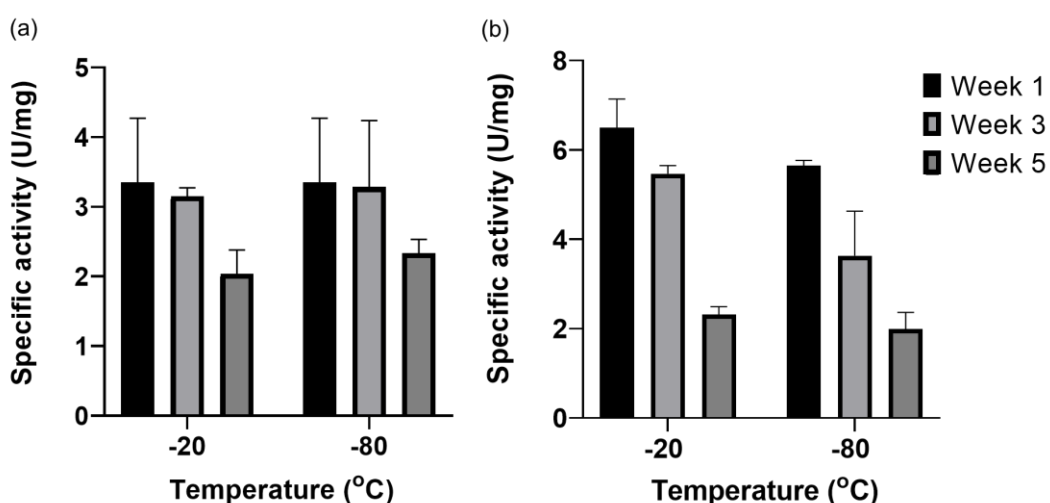


**Figure 3.10.** The specific activity of LcpK30 after one month of storage. The specific activity of purified LcpK30 stored at -20 °C and -80 °C (a) with 50 % glycerol and (b) without 50 % glycerol. The samples were prepared in triplicate to determine the standard error.

### 3.2 Enzymatic degradation of natural rubber catalysed by LcpK30

This work aimed to determine the ideal enzymatic reaction conditions to produce a substantial amount of degradation products that could be utilised in subsequent experiments. In earlier published work to increase the production of oligomers, the degradation of NR was carried out at low temperature (room temperature: 22 °C) using 4 mg of LcpK30 in a 1 L reaction with 100 mM KPi buffer (pH 7) that produced about 100 mg of oligo-isoprenoids.<sup>119</sup> Optimised conditions for oligomer production were also achieved by using Lcp1VH2 as the catalyst in a multiphase reactor at 30 °C with 0.2 M Tris-buffer (pH 7) as the aqueous phase.<sup>134</sup> In a recent study involving LcpK30, the enzyme showed better degradation activity at 5 µM with no significant effect on a temperature higher than room temperature (above 25 °C).<sup>111</sup> Considering the method used in previous studies, the ability of LcpK30 to catalyse the oxidative cleavage of C=C of NR in this study was evaluated under different conditions, as summarised in Table 3.4. The sum of the integrated area of the oligomer peaks from the high performance liquid chromatography (HPLC) chromatogram was used to compare the degradability of NR under different conditions.

**Table 3.4.** Variable conditions are used during the enzymatic degradation of NR.

Substrate loading (mg mL <sup>-1</sup> )	Enzyme concentration		Temperature
	mg mL <sup>-1</sup>	µM	
100	0.25	6	30
100	0.5	12	30
100	0.75	18	30
100	1	24	30
100	0.25	6	37
100	0.25	6	30
100	0.25	6	23
10	0.25	6	30
40	0.25	6	30
60	0.25	6	30
100	0.25	6	30

Reactions were performed in triplicates in 1 mL reaction volume, incubated for 2 hours at 30 °C with 250 rpm agitation.



### 3.2.1 Effect of enzyme concentration

This experiment aimed to estimate the minimum enzyme concentration for enzymatic degradation. In this study, purified LcpK30 was added to the reaction mixture in a concentration range from 6  $\mu\text{M}$  ( $0.25 \text{ mg mL}^{-1}$ ) to 24  $\mu\text{M}$  ( $1 \text{ mg mL}^{-1}$ ). The NR emulsion with an initial rubber content of 60 % (wt/vol) ( $600 \text{ mg mL}^{-1}$ ) was added into 1 mL KPi buffer (100 mM, pH 7) at  $100 \text{ mg mL}^{-1}$ , and the reaction was incubated at 30 °C for 2 hours.

The solvent-soluble organic phase was dried and redissolved in methanol for HPLC analysis. As predicted, the integrated area of the oligomer peaks from the HPLC chromatogram increased with enzyme concentration (Figure 3.11 and Appendix C3.2). The oligomers' size distribution patterns, as shown in Figure 3.12, were comparable with chromatogram data presented in previous literature (Chapter 1, Section 1.3.4).

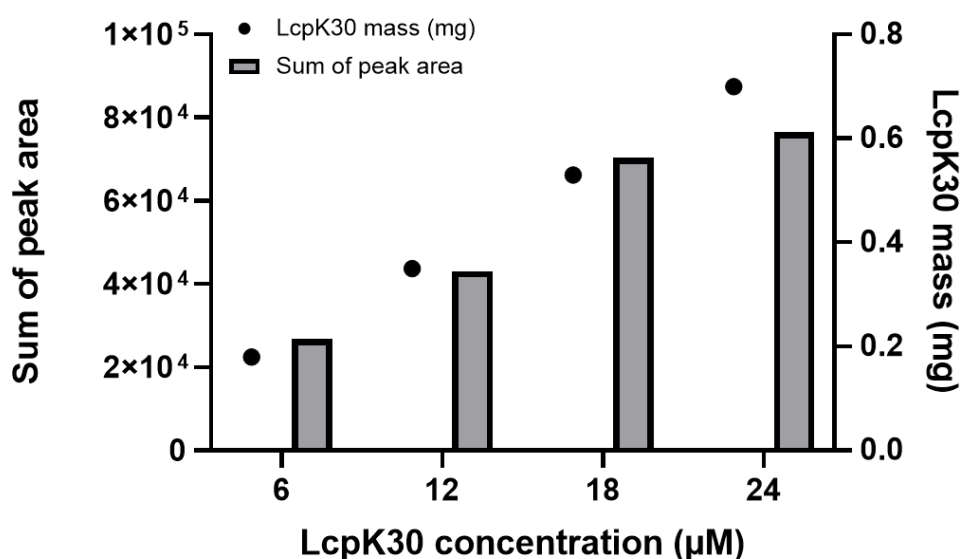


**Figure 3.11.** The graph shows the mass of LcpK30 added into the reaction with the estimated amount of the oligomers produced. The amount of oligomers was estimated based on the sum of the integrated area of the oligomer peaks from the HPLC chromatogram. The experiments were performed in triplicates. However due to insufficient amount of samples, the sum of the integrated area was determined from a single replicate.

Therefore, a minimum concentration of LcpK30 used in this study was determined at 6  $\mu\text{M}$  and not more than 18  $\mu\text{M}$ . Compared to previous literature, Adjedje *et al.* (2021) performed degradation of low molecular weight synthetic polyisoprene with 5  $\mu\text{M}$  of purified LcpK30.<sup>111</sup> Another reaction using Lcp1VH2 as the catalyst used a total of 0.25 mg mL<sup>-1</sup> purified enzyme to degrade higher molecular weight IR.<sup>137</sup> An efficient biocatalyst would require low concentration to achieve a higher product conversion rate. Moreover, using higher concentrations of enzymes would not be economically practical.

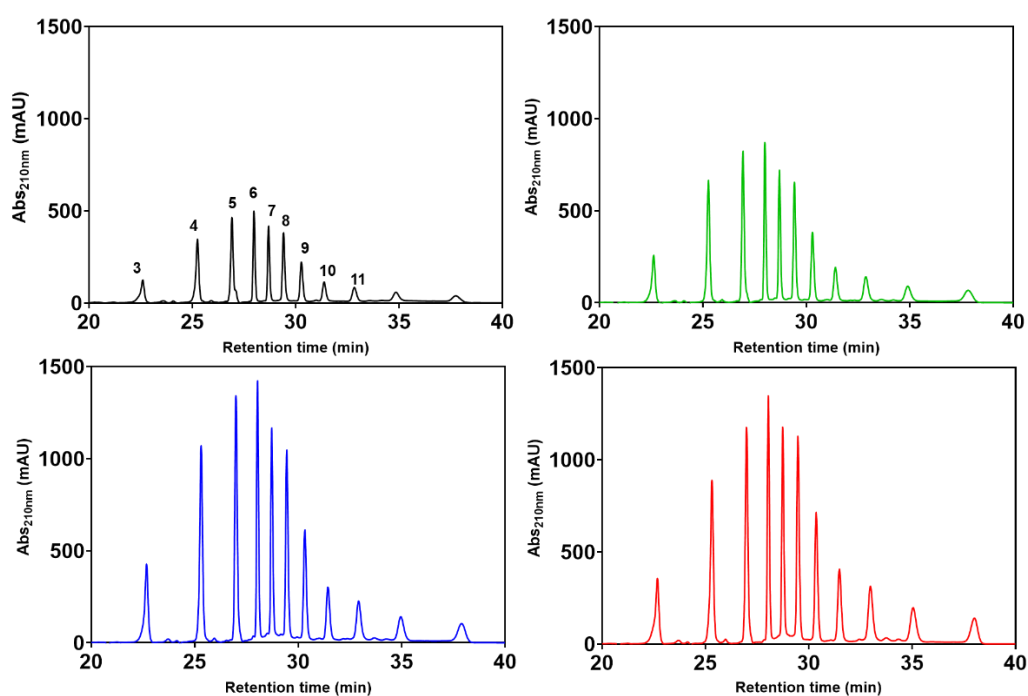


**Figure 3.12.** HPLC chromatogram of oligomers produced from NR degradation with different enzyme concentrations. The black line represents the oligomers retrieved from a reaction with 6  $\mu\text{M}$  purified LcpK30; green line (12  $\mu\text{M}$ ), blue line (18  $\mu\text{M}$ ) and red line (24  $\mu\text{M}$ ). The number on top of the peak represents the repetitive isoprene unit number.

### 3.2.2 Effect of temperature

Degradation of NR using LcpK30 was previously reported to be performed at room temperature between 22 °C to 25 °C with minimal degradation rate improvement above that temperature.<sup>111,120,135</sup> Nonetheless, previous studies have shown an increase in LcpK30's specific activity from 1.5 U mg<sup>-1</sup> at 23 °C

to  $4.6 \text{ U mg}^{-1}$  at  $37 \text{ }^\circ\text{C}$ .<sup>118</sup> Therefore, the following reaction was performed to observe the degradation outcome at temperatures lower and higher than  $30 \text{ }^\circ\text{C}$ . For this purpose, a reaction consisting of  $100 \text{ mg mL}^{-1}$  NR content with a similar amount of purified LcpK30 ( $6 \text{ } \mu\text{M}$ ) in  $100 \text{ mM}$  KPi buffer was incubated at  $23 \text{ }^\circ\text{C}$ ,  $30 \text{ }^\circ\text{C}$  and  $37 \text{ }^\circ\text{C}$  for two hours. The HPLC chromatogram in Figure 3.13 shows the oligomer's size distribution from the reaction performed at  $23 \text{ }^\circ\text{C}$  and  $30 \text{ }^\circ\text{C}$ , respectively. Due to low oligomer mass, the HPLC analysis of the products that result from the reaction at  $37 \text{ }^\circ\text{C}$  was not carried out. The sum of the integrated area of product peaks derived from the reaction at  $30 \text{ }^\circ\text{C}$  was higher by 67 % than the products from reactions performed at  $23 \text{ }^\circ\text{C}$  (Appendix C3.3). Therefore, all enzymatic degradation carried out in this study was incubated at  $30 \text{ }^\circ\text{C}$ .

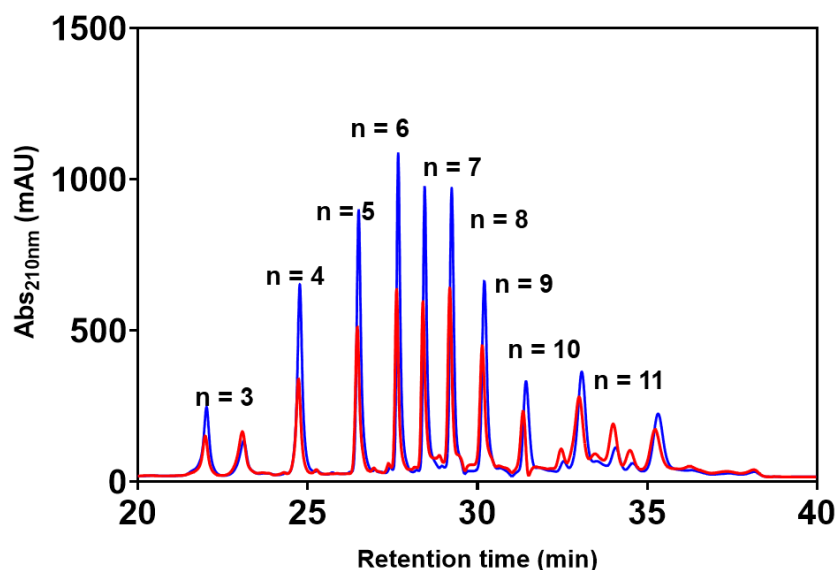


**Figure 3.13.** HPLC chromatogram of oligomers produced from NR degradation reaction catalysed by LcpK30 at different temperatures. The blue and red lines represent the oligomers retrieved from a reaction incubated at  $30 \text{ }^\circ\text{C}$  and  $23 \text{ }^\circ\text{C}$ , respectively. Alphabet n is corresponding to the isoprene unit number.

### 3.2.3 Effect of substrate loading

The enzymatic degradation was performed with different substrate loading of NR. The NR emulsion with an initial rubber content of 60 % (wt/vol) ( $600 \text{ mg}$

mL<sup>-1</sup>) was added into 1 mL KPi buffer (100 mM, pH 7) in different loading ranges from 10 to 100 mg mL<sup>-1</sup>. To this milky suspension, LcpK30 was added to a final concentration of 6 μM and the suspension was incubated at 30 °C for 2 hours. The reaction with NR content at 40 mg mL<sup>-1</sup> appeared to have a slightly higher overall area of product peaks (Appendix C3.4 and Figure 3.14). Increasing the concentration of NR to 60 and 100 mg mL<sup>-1</sup> seemed to have a negative effect on the oligomer production. This was hypothesised to occur due to the aggregation of solid particles at a higher concentration.

NR latex is a natural emulsion of particles containing rubber molecules encapsulated by a monolayer of proteins and phospholipids.<sup>14</sup> The release of polyisoprene chains through the protein and phospholipid monolayer of the rubber particles might impact the accessibility of NR to LcpK30. The polyisoprene chains could have been released into the aqueous environment due to several conditions, including the following: (1) the rubber particle monolayer is permeable, allowing the low molecular weight enzyme to penetrate, and (2) charge neutralisation occurs on the rubber particle surface, causing the monolayer to rupture and release the polyisoprene chains into the aqueous medium.

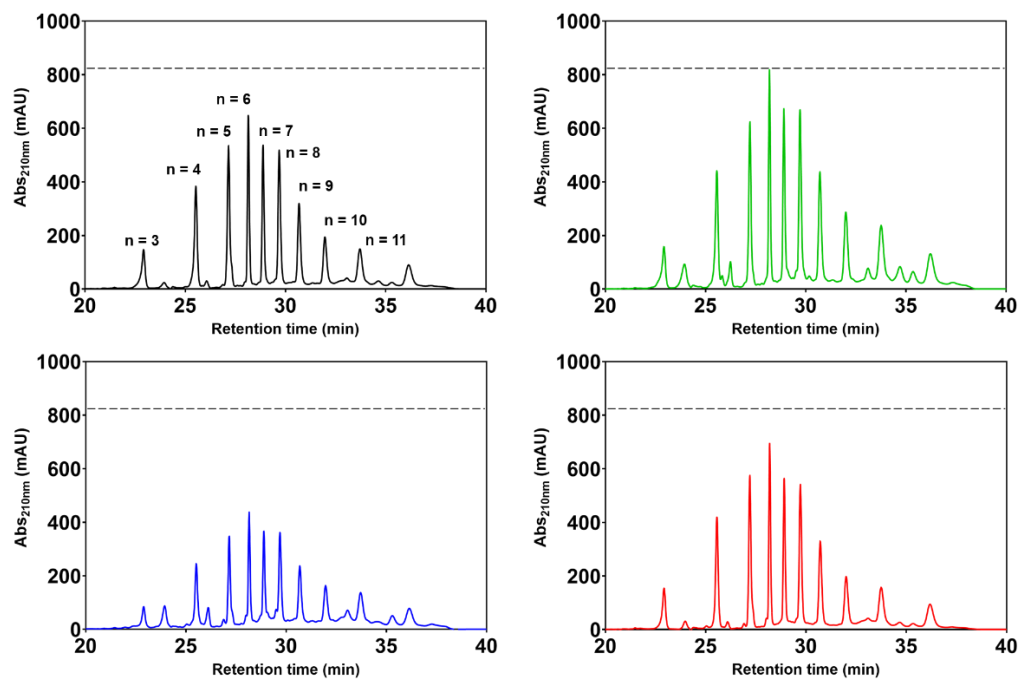


**Figure 3.14.** HPLC chromatogram of oligomers produced from NR degradation reaction with different substrate content (NR) loading. The black line represents the oligomers retrieved from a reaction with NR loading at  $10 \text{ mg mL}^{-1}$ ; green line ( $40 \text{ mg mL}^{-1}$ ), blue line ( $60 \text{ mg mL}^{-1}$ ) and red line ( $100 \text{ mg mL}^{-1}$ ). The dotted line represent the maximum absorption of oligo-isoprenoid with six isoprene unit retrieved from the reaction with  $40 \text{ mg mL}^{-1}$ . Alphabet n is corresponding to the isoprene unit number.

While continuous agitation ensures the hydrophobic NR chain is dispersed in the aqueous medium, aggregation of the rubber molecule into particles up to 40 % larger than the initial diameter of rubber particles might still occur.<sup>201</sup> The aggregation effect of the particles might limit the availability of polyisoprene chains that can make contact with the enzyme and thread into the active site, thus influencing the cleavage site of the C=C bonds.

### 3.2.4 Effect of solvent

This section discussed the effect of several hydrocarbon solvents on LcpK30 activity. The efficiency of an enzyme to reach the substrates can influence the rate of the enzymatic reactions. In most cases, enzymatic reactions occur in aqueous media. *In vitro*, enzymatic reactions would require additional components such as buffer and salt reagents to maintain the pH of the solution and structures of the proteins.<sup>202</sup> Pretreatment of highly hydrophobic materials

such as rubber before the enzymatic reaction could improve the reaction rate.<sup>137,203</sup> The substrate pretreatment can be either grinding or solvent extraction and devulcanisation. Solvent extraction usually uses a hydrocarbon solvent that could solubilise the rubber or extract any additives incorporated with the rubber.<sup>143</sup> In this study, several alkane hydrocarbon solvents that could potentially be utilised as substrate pretreatment agents, such as *n*-hexadecane, *n*-tetradecane, *n*-dodecane and *n*-hexane, were chosen, and their effect on LcpK30 was evaluated.

The effect of hydrophobic solvents on LcpK30 activity was studied in a biphasic mixture at different volumetric ratios of 0.2 %, 0.5 % and 1 % (vol/vol) in 100 mM KPi buffer (pH 7) and incubated at 30 °C with 250 rpm agitation for 2 hours. After ethyl acetate extraction, the HPLC analysis of the dried residuals showed that the absorbance peaks representing the oligomers decreased as the solvent concentration increased (Appendix C3.5). The result indicates that fewer oligomeric products were made as more solvent was used. LcpK30 activity was completely inhibited when 1 % (vol/vol) of dodecane was present in the reaction mixture. The reduction in enzyme activity in the presence of solvents can be attributed to the constrained interaction between the substrate and enzymes due to the propensity of the substrates to remain in the organic solvents.<sup>204</sup> Nevertheless, the most common factor that contributes to enzyme activity loss is enzyme denaturation by the organic solvents.<sup>205</sup>

The effect of *n*-hexadecane, *n*-tetradecane and *n*-hexane on LcpK30 was estimated based on the relative yield for oligomers derived from the enzymatic degradation of NR with the solvents at volumetric ratios of 0.2 %, 0.5 % and 1 % (vol/vol). The relative yields were compared with a control reaction of NR without the solvents (Figure 3.15). The inhibitory effect of the solvents on the enzymatic activity increased to above 70% when a higher volumetric ratio (1%

vol/vol) was introduced, followed by more than 50 % yield reduction at 0.5 % concentration. At a lower volumetric ratio (0.2 % vol/vol), *n*-hexadecane shows the least inhibition effect on the LcpK30 activity by showing less than 40 % reduction compared to oligomers produced from the non-solvent reaction. The result was consistent with earlier research that demonstrated a 1:1 ratio of *n*-hexadecane to the substrate was preferable to prevent an utterly inhibitory impact at higher solvent concentrations.<sup>111,206</sup> Findings from this work provide preliminary information on the effect of these solvents on LcpK30.

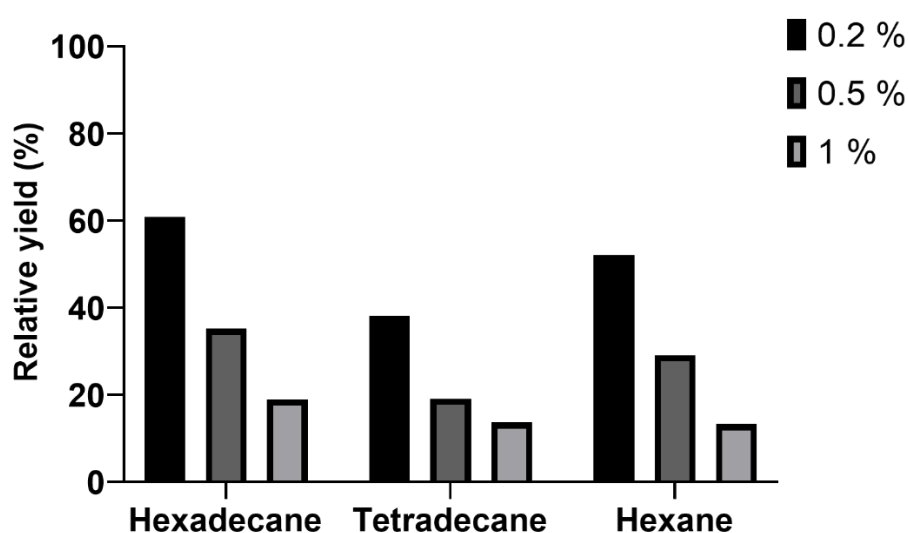


**Figure 3.15.** Relative yield of oligomers. The relative yield was based on the integrated peak area of the oligomers from the HPLC chromatogram. Oligomers derived from NR degradation with solvents were compared to the 100 % relative yield of oligomers produced from NR degradation without solvent. The concentration of the solvent is reflected as a volumetric ratio vol/vol. The experiments were performed in triplicates. However due to insufficient amount of samples, the sum of the integrated area was determined from a single replicate.

It is suggested that *n*-tetradecane and *n*-hexane could potentially be tested as pretreatment agents of a hydrophobic substrate (e.g. rubber) before being used for enzymatic degradation. Moreover, *n*-tetradecane has been previously reported to be used as an oil to create an interfacial layer in microemulsion preparation.<sup>207</sup> Hexane is a versatile extraction solvent that has been employed in various industries, including biorefineries, the food industry, and most

recently, as a chemical treatment for contaminated disposable rubber gloves and the recycling of rubber scrap tyres.<sup>208–210</sup>

### 3.2.5 Optimisation of oligo-isoprenoid production

The next part of the work was to extract the degradation products and obtain enough oligo-isoprenoid for further characterisation and application. In this attempt, the addition of enzyme into the reaction mixture was performed in two different routines: (1) one-time addition of 18  $\mu\text{M}$  (Reaction A) and (2) three-time addition of 6  $\mu\text{M}$  each (Reaction B, a total of 18  $\mu\text{M}$  final concentration). The reaction was stirred at 450 rpm in a round bottom flask at 30 °C. The incubation time was extended to 24 hours, with a total volume of reaction set up at 5 mL. The enzyme addition routine was the only variable for these reactions, whereas the specific activity of LcpK30 for each reaction was determined at 6 U mg<sup>-1</sup>.

After 24 hours, the ethyl acetate used to extract the oligomers was removed using a rotary evaporator, followed by drying under the vacuum pump. After drying, a light brownish precipitate of the degradation products was obtained and weighted (Figure 3.16).

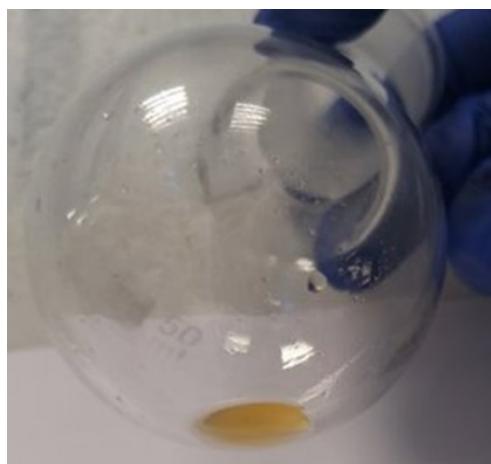


**Figure 3.16.** The oligo-isoprenoid with carbonyl-ends derived from NR degradation after ethyl acetate extraction and drying.



The extracted products were confirmed as a mixture of oligomers in different sizes, as shown in the HPLC chromatogram (Figure 3.17). The percentage difference of the sum peak area (at 20 to 33 min retention time) between Reaction A and Reaction B is 15% (calculation is included in Appendix C3.6).

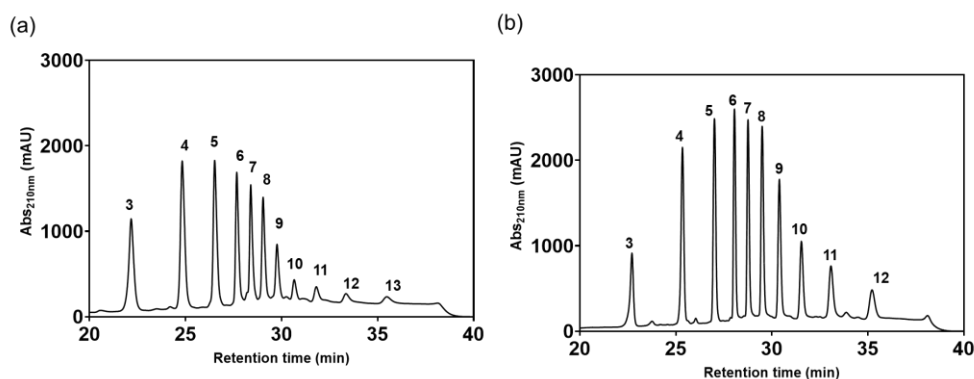


**Figure 3.17.** HPLC chromatogram of oligomers. (a) Oligomers produced from Reaction A and (b) Oligomers produced from Reaction B. The concentration of oligomers analysed for HPLC was at 1 mg mL<sup>-1</sup>. The number on top of the peak represents the repetitive isoprene unit number.

Table 3.5 summarises the reaction conditions and the weight balance between the oligomers and the coagulated rubber retrieved after extraction with ethyl acetate. The weight balance appeared less than the initial rubber concentration (500 mg), which could be due to several causes: (1) Some remaining coagulated rubber still adhered to the reaction flask (2) On another note, the accurate volume of NR added into the reaction buffer could be influenced by the aspiration and dispensing during pipetting due to the hydrophobic attraction between rubber molecules and the hydrophobic surface of the tips (3) Additionally, the working concentration of NR might also contribute to the inconsistency of the initial substrate loading. The working concentration of NR was prepared at approximately 600 mg mL<sup>-1</sup> by resuspending the rubber with water after washing it with a surfactant (Nonidet), as described in Chapter 2, section 2.2.9.1.

**Table 3.5.** The mass balance of the oligomers and remaining rubber retrieved after solvent extraction.

Reaction	Initial substrate mass (mg)	Final enzyme concentration ( $\mu\text{M}$ ); Addition regime	Reaction volume (L)	Reaction duration (hr)	Oligomers dry mass (mg)	Recovered rubber mass (mg)
A	500	18; Once	0.005	24	20	nd
B	500	18; Thrice (6 $\mu\text{M}$ at each addition)	0.005	24	54	226

The percentage difference between the oligomer mass extracted from Reaction A and Reaction B is 92 %. Availability of oxygen could influence the efficiency of LcpK30 in catalysing the C=C cleavage in Reactions A and B. Given that the reaction was conducted in a flask with a lid, there might be limited air in the flask headspace, which probably could halt the catalytic activity due to the reduced oxygen concentration. However, by adding the enzyme to the reaction mixture at regular intervals, the available oxygen was replenished indirectly. Therefore, it improved the NR polyisoprene chain cleavage into oligomers. These observations correspond to the previous study by Andler *et al.* (2018) comparing the oxygen consumption between once and pulse addition of enzymes.<sup>137</sup>

The amount of pure LcpK30 used in this experiment to produce 54 mg of oligomers from 0.5 g initial NR mass was  $0.75 \text{ mg mL}^{-1}$ . As a comparison, a study by Rother *et al.* (2017) used  $0.004 \text{ mg mL}^{-1}$  of pure enzyme to obtain about 100 mg of products after degradation of 50 g NR.<sup>119</sup> The specific activity of LcpK30 used in the study by Rother and the team was  $6.2 \text{ U mg}^{-1}$ , which was nearly similar to the specific activity of LcpK30 in this study ( $6.0 \text{ U mg}^{-1}$ ). Besides different concentrations being used, the other difference between Reaction B and the reaction performed by Rother *et al.* (2017) was the amount of substrate loading (mass per volume). The mass per volume in Reaction B was two times

higher (100 mg per 1 mL) than in the published study (50 mg per 1 mL). The yield obtained in this study was higher than the referred study, probably because of better mixing achieved at a lower scale. To summarise, a comparison of the two reactions was outlined in Table 3.6.

**Table 3.6.** Comparison between Reaction B (this study) and an up-scale reaction to increase oligomer production published by Rother *et al.* (2017).

	<b>This study</b>	<b>Rother <i>et al.</i> (2007)</b>
Mass/volume (mg mL <sup>-1</sup> )	100	50
Reaction volume (L)	0.005	1
Reaction time (hr)	24	24
Enzyme concentration (mg mL <sup>-1</sup> )	0.75	0.004
Enzyme specific activity ( U mg <sup>-1</sup> )	6	6.2
Oligomer yield (%)	10	0.2

### 3.2.6 Characterisation of the oligo-isoprenoids

In addition to HPLC analysis, the oligo-isoprenoids were also characterised using Gel Permeation Chromatography (GPC) and <sup>1</sup>H Nuclear Magnetic Resonance (<sup>1</sup>H NMR). These analyses were performed to obtain a general idea of the molecular characteristics of the oligo-isoprenoid molecules.

The HPLC chromatogram showed a clear separation of products of oligomers with three up to 14 isoprene units under the conditions used. GPC was used to determine the number average molecular weight ( $M_n$ ), weight average molecular weight ( $M_w$ ) and size distribution or polydispersity ( $M_w/M_n$ ;  $\mathcal{D}$ ). Measurement of molecular weight by GPC gives the statistical  $M_n$  of all oligomer chains. The  $M_w$  indicates the size of an oligomer chain that contributes to the average weight. Therefore, theoretically, longer oligomers will give higher  $M_w$ . A lower size distribution (near 1) would indicate that the oligomers' lengths are more or less similar.

In contrast, higher size distribution shows higher variations of short and long oligomers. The  $^1\text{H}$  NMR spectrum was used to confirm the presence of the oligo-isoprenoids' aldehyde (-C-CHO) and ketone (-C-COC') terminal groups by the appearance of signals at 9.8 ppm and 2.1 ppm. Methyl proton (-C=C-CH<sub>3</sub>) with chemical shift ( $\delta$ ) at 1.68 ppm, olefinic proton (-C=CH-CH<sub>2</sub>-)  $\delta$  = 5.12 ppm, and methylene proton (-CH<sub>2</sub>-CH<sub>2</sub>-)  $\delta$  = 2.05 ppm were representing the isoprene unit. Based on the  $^1\text{H}$  NMR spectrum, the average chain length of the oligomers was determined by integrating the methyl, olefinic and aldehyde proton peaks. The average chain length was calculated based on an equation published by Izunobi and Higginbotham (2011)<sup>211</sup>, who described that the repeating unit of a moiety could be calculated by,

$$n_x = \frac{a_x m_y n_y}{a_y m_x}$$

Equation 3.1

Where,

$a_x$  = peak area of moiety x

$n_x$  = no. of repeating units of moiety x

$m_x$  = no. of protons of moiety x

$a_y$  = peak area of moiety y

$n_y$  = no. of repeating units of moiety y

and  $m_y$  = no. of protons of moiety y

By determining the average chain length, the average molecular weight can be estimated by multiplying the repeating isoprene number with isoprene molecular weight (68.1 g mol<sup>-1</sup>) with an addition of 102.1 g mol<sup>-1</sup> representing the molecular weight of the carbonyl group.

The  $M_n$ ,  $M_w$ , and polydispersity indexes of oligomers from Reactions A and B are shown in Table 3.7. The population of the oligomers produced was estimated to be dominated mainly by either shorter oligomers or longer

oligomers with  $n$  less or more than 14 isoprene units. These results were compared to the GPC results published by Andler *et al.* (2018), who performed synthetic isoprene rubber (IR) degradation catalysed by Lcp1VH2 as summarised in Table 1.4 (Chapter 1, Section 1.3.4). In their report, the  $M_n$  of oligomers extracted with ethyl acetate was  $550 \text{ g mol}^{-1}$  and a  $\mathcal{D}$  of 1.20 from the initial  $M_n$  of IR of  $405000 \text{ g mol}^{-1}$  with a  $\mathcal{D}$  of 2.58. There was a 53 % reduction in the  $\mathcal{D}$ , whereas, in this study, the reduction was smaller, less than 10 %. This result could be attributed to the different behaviour of molecular characteristics of NR and its synthetic counterpart part, IR, in which the molecular size of IR is much more uniform than NR, thus resulting in a narrower  $\mathcal{D}$  after being degraded.

**Table 3.7.** The molecular weight of the initial substrate (natural rubber before degradation) and oligomers from reactions A and B were measured by GPC.

Sample	$M_n \text{ (g mol}^{-1}\text{)}$	$M_w \text{ (g mol}^{-1}\text{)}$	$\mathcal{D}$
Natural rubber before degradation	193600	706640	3.65
Oligomers -Reaction A	667	2243	3.36
Oligomer - Reaction B	907	3512	3.51

Further characterisation of the oligomers using  $^1\text{H}$  NMR was performed on the degradation products from Reaction B. The number of repeating units ( $n$ ) in the oligomer chain was estimated based on the peak areas of the olefinic proton ( $-\text{C}=\text{CH}-\text{CH}_2-$ ), methyl proton ( $-\text{C}=\text{C}-\text{CH}_3$ ) aldehyde ( $-\text{C}-\text{CHO}$ ) obtained from the  $^1\text{H}$  NMR spectrum (Figure 3.18 and Table 3.8) and appropriately substituted into Eq.3.1.

$$n_{-\text{CH}_3} = \frac{3.01 \times 1 \times 1}{0.08 \times 3} = 12.54 \approx 13$$

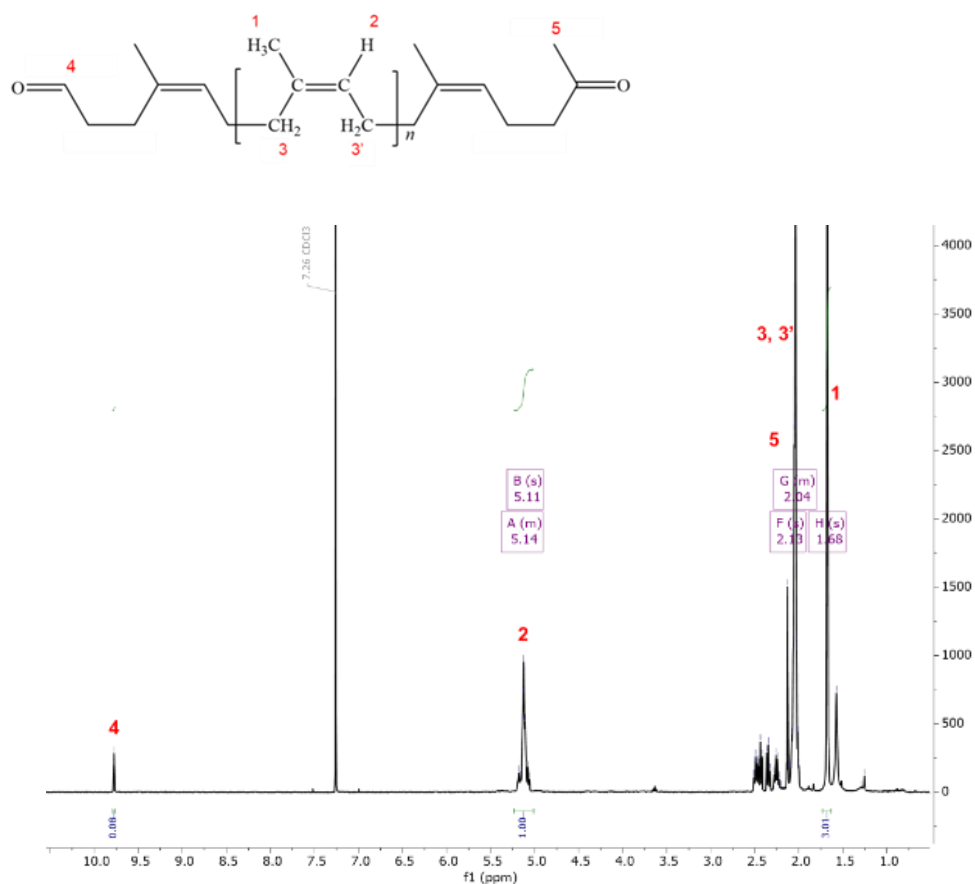


**Figure 3.18.**  $^1\text{H}$  NMR spectrum of the oligo-isoprenoid extracted using ethyl acetate from NR degradation catalysed by LcpK30 analysed in  $\text{CDCl}_3$  with the formula of generated oligo-isoprenoid products is shown at the top.  $n$  = the number of isoprene units. The resonance at 7.26 ppm is from  $\text{CDCl}_3$ , which was used as a reference solvent.

On average, the oligo-isoprenoid obtained from enzymatic degradation in this work consisted of 13 repeating isoprene units. Thus, the molecular weight is estimated at  $987 \text{ g mol}^{-1}$ . This estimation is near the  $M_n$  measured by GPC ( $907 \text{ g mol}^{-1}$ ).

**Table 3.8.** Extracted values of the salient peak areas from the  $^1\text{H}$  NMR spectrum of oligomers extracted from Reaction B.

Moiety	Chemical shift ( $\delta$ ) ppm	Peak area	No. of protons	No. of repeating units
$-\text{C}=\text{CH}-\text{CH}_2-$	5.12	1	1	N/A (Reference peak)
$-\text{C}=\text{C}-\text{CH}_3$	1.68	3.01	3	13
$-\text{C}-\text{CHO}$	9.8	0.08	1	1

The estimated molecular weight of the oligomer from Reaction B, obtained from HPLC, GPC and NMR, was compared and outlined in Table 3.9. The estimation from HPLC was calculated based on the peak area percentage (Appendix C3.7).

**Table 3.9.** Oligomer molecular weight determination with different analytical approaches.

	HPLC (g mol <sup>-1</sup> )	GPC (g mol <sup>-1</sup> )	<sup>1</sup> H NMR (g mol <sup>-1</sup> )
This study	566	907	~987 (13 isoprene units)
Andler <i>et al.</i> (2018) <sup>137</sup>	-	885	-
Andler <i>et al.</i> (2018) <sup>212</sup>		550 1030	
Hiessl <i>et al.</i> (2014) <sup>132</sup>	-	-	~783 (10 isoprene units) ~1328 (18 isoprene units)

-: not mentioned

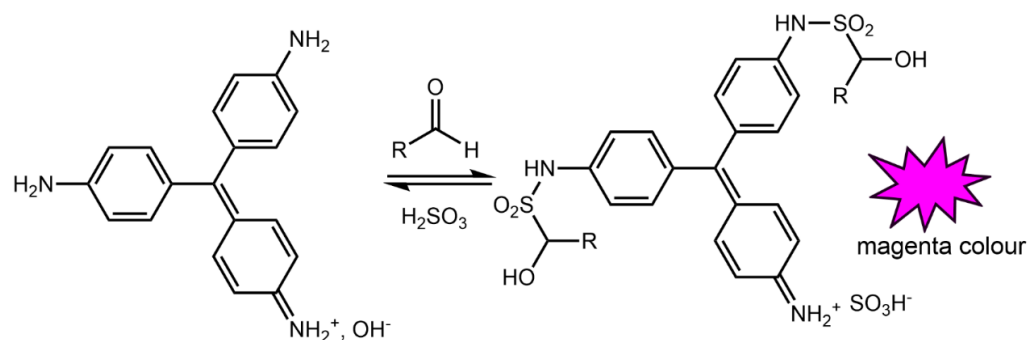
A slightly higher molecular weight measured by GPC could be influenced by the presence of oligomers with higher isoprene unit numbers. Estimation of the average chain length of oligomer based on <sup>1</sup>H NMR integral peak area was performed by Hiessl *et al.* (2014)<sup>132</sup> before the HPLC measurement was introduced by Rother *et al.* (2017)<sup>213</sup>. In the study by Hiessl and his team, they discovered degradation products with 10 and 18 isoprene repeating units. In conclusion, the estimated molecular weight of oligomers in this study obtained from different analytical methods are comparable and within the range of data published by previous literature. HPLC estimated a slightly lower M<sub>n</sub> compared to <sup>1</sup>H NMR and GPC, possibly because higher molecular weight peaks may not elute from the column under the conditions used, and/or they may have been too dilute to be detected. However, although they were individually diluted, their total concentration contributed to a higher M<sub>n</sub>. This was also suggested by the higher M<sub>w</sub> observed by GPC.

### **3.3 Development of quantitative colourimetric screening assay for LcpK30 enzymatic activity**

The performance of LcpK30 as a biocatalyst could be improved by enhancing the enzyme catalytic activity, improving the substrate specificity and selectivity or developing LcpK30 variants resistant to extreme conditions (e.g., solvents or high temperature). By understanding the interaction between substrate and protein through protein engineering, several mutants can be created to achieve the desired results. Development of a mutant's library would require a quick assay to screen for an active mutant. Thus, this section discusses the attempt to transform Schiff's colourimetric assay from a qualitative observation into a quantitative spectrophotometry measurement for quick screening and estimation of enzyme activity.

An active LcpK30 can be screened by staining the reaction mixture with Schiff's reagent. A qualitative colourimetric indicator was formed by the reagent's reaction with the oligo-isoprenoid's aldehyde group, which changed the colour of the colourless solution into purple or magenta. Schiff's reagent is a pararosaniline hydrochloride solution decolourised with sulphurous acid.<sup>214</sup> The three aromatic rings of pararosaniline with bisulfite group attached to a sulfonated central carbon, thus forming a tetrahedral structure (no conjugation among the rings). In the presence of aldehyde, it will react with uncharged amine groups from the aromatic ring to create an aldimine group. It also triggers the elimination of the sulfur group at the central carbon and becomes trigonal (conjugated). The electrophile aldamine group undergoes further reaction with the bisulfite ion to form a bisulfite conjugated adduct, which is magenta (Scheme 3.1).





**Scheme 3.1.** The mechanisms of aldehyde detection using Schiff's reagent. The left structure is a pararosaniline compound before reacting with the bisulfite group ( $\text{H}_2\text{SO}_3$ ) to form a non-conjugated adduct of colourless Schiff's reagent with tetrahedral sulfonated central carbon. The maximum spectrophotometric absorbance for Schiff's reagent mixture (magenta colour) is between 535 and 574 nm.<sup>215</sup>

Initially, the colourimetric assay was carried out by mixing equal amounts of Schiff's reagent and a reaction mixture of NR after degradation. This resulted in a final concentration of 1.5 M of Schiff's reagent, which produced immediate colour changes when aldehyde compounds were present (see Figure 3.7 in Section 3.1.3). This approach was not ideal for spectrophotometric measurement due to the turbidity of the NR-containing mixture and the saturated colour development. Further investigation was carried out to determine a suitable staining method for quantifying the colour development based on the absorbance of the Schiff's – aldehyde conjugated coloured compounds.

Another approach for preparing the staining assay on the reaction mixture was performed. In this approach, the assay was performed using a lower concentration of Schiff's reagent (0.4 M) over different loading of the reaction mixture (10, 50 and 100  $\mu\text{L}$ ) to observe the intensity of colour developed based on aldehyde concentration. The resulting colour changes were less intense, and a consistent increasing intensity of colour change was observed according to the increased loading of the reaction mixture (Figure 3.19). Nevertheless, the homogeneity of the assay mixture was still persistent, thus measuring the

absorbance over a spectrum of wavelength by a UV-spectrophotometer practically unstable.

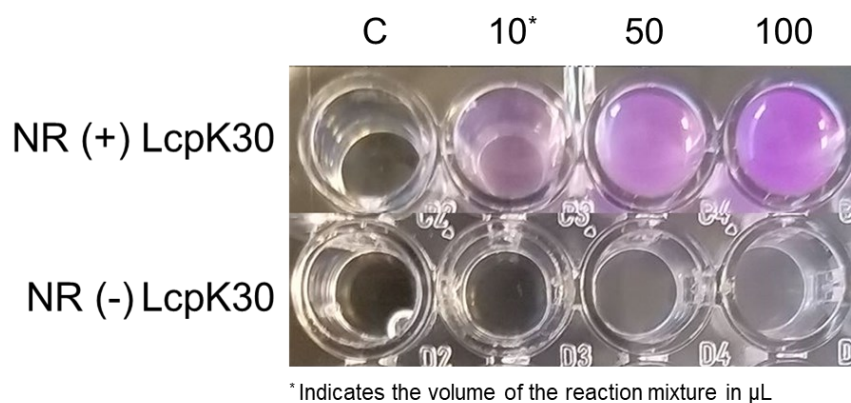


**Figure 3.19.** Colourimetric assays on the reaction mixture with 0.4 M Schiff's reagent concentrations. The volume ( $\mu\text{L}$ ) added into the microwell was indicated by the number across the column.

Another attempt to obtain quantitative spectrophotometry measurement from the colourimetric assay was performed by staining the oligomer fraction that was extracted into ethyl acetate. Staining the solvent-soluble fraction perhaps would avoid the influence of NR latex turbidity. However, Schiff's reagent is immiscible in ethyl acetate. Thus, mixing the reagent into the ethyl acetate-soluble fraction containing the oligomers was impossible. A modification was made by adding ethanol as a co-solvent to solubilise the mixture.<sup>216</sup> The three components (ethyl acetate-soluble fraction: Schiff's reagent: ethanol) were mixed in a 1:1:1 ratio with a final concentration of Schiff's reagent at 1 M. The staining assay was performed on the oligomers that were extracted from a series of NR degradation reactions catalysed with different purified LcpK30 concentrations (6 – 24  $\mu\text{M}$ ). After one hour of staining at room temperature, the intensity of the resulting colour change was similar in all samples. Before the assay mixture was measured using a spectrophotometer, the ideal absorbance wavelength was established through a series of Schiff's reagent reactions with a known aldehyde compound at different concentrations. A series of butyraldehyde

(C<sub>4</sub>H<sub>8</sub>O) concentrations in a range from 1 mM to 70 mM was prepared in ethanol.

Similarly, ethyl acetate and Schiff's reagent were added for the staining assay in a 1:1:1 ratio. The intensity of colour development increased with aldehyde concentration. An absorbance spectrum from 350 to 1000 nm wavelength was acquired, and the C<sub>4</sub>H<sub>8</sub>O – Schiff's reagent complex showed optimal absorbance at 560 nm. The mixture of ethyl acetate, ethanol, and the reagent was used as the reference blank. However, above 10 mM of C<sub>4</sub>H<sub>8</sub>O, the intensity of colour changes became saturated. Thus, it is impossible to measure the absorbance. Therefore, a linear relationship between the absorbance measurement and aldehyde concentration was possible only over a small concentration range (1 to 10 mM) (Appendix C3.8).

The conversion of non-conjugated Schiff's reagent into conjugated Schiff's adducts after coupling with aldehyde depends on the equilibrium constant of the reactants and products. The equilibrium constant of the reaction is influenced by the concentration of Schiff's reagent and aldehyde. The equilibrium constant of the reaction will shift when the aldehyde concentration increases, producing more conjugated Schiff's adduct. Subsequently, a more intense colour change develops, thus making the staining mixture cannot be quantified with a spectrophotometer. Therefore, Schiff's reagent concentration must be in excess to ensure complete conversion of the aldehyde and the colour development end-point proportional to the amount of aldehyde, which explains the linearity of the above experiment was only possible over a small range of aldehyde concentration.

Following this experiment, the absorbance of the staining assay of oligomers extracted from a series of NR degradation reactions catalysed with different purified LcpK30 concentrations (6 – 24 μM) was measured at 560 nm. All

samples show absorbance above 1 ( $A_{560}$ ) with no significant difference between each sample (Figure 3.20).

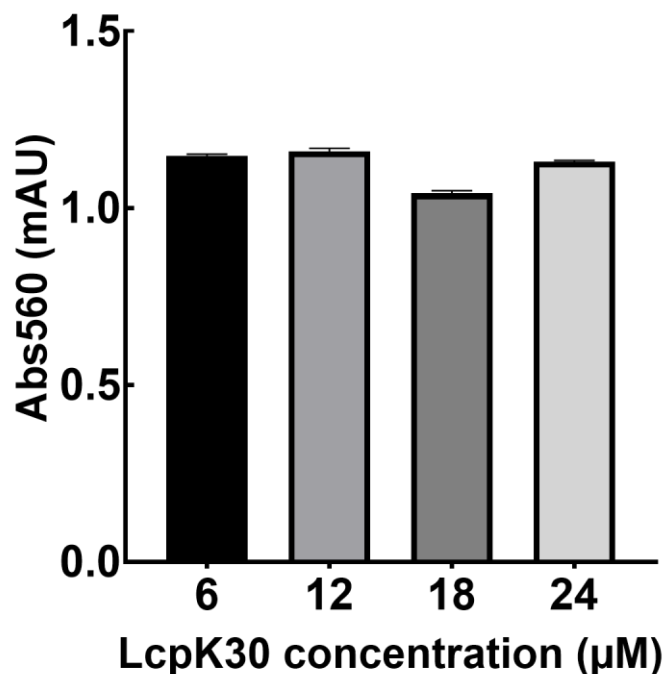


**Figure 3.20.** Absorbance measurement of the colourimetric assay on solvent-soluble fractions derived from degradation reaction catalysed by higher LcpK30 concentration. Samples were prepared in triplicates to determine the standard error.

Accordingly, it was assumed that catalysing the NR degradation with a higher concentration of LcpK30 resulted in an excess of oligomers with terminal aldehyde groups relative to the amount of Schiff's reagent. Another experiment was performed to justify this assumption by measuring the absorbance of the colourimetric assay with samples derived from NR degradation catalysed using lower concentrations of LcpK30 (0.1  $\mu\text{M}$ , 0.2  $\mu\text{M}$  and 2  $\mu\text{M}$ ). The colour intensity changes after one hour upon staining are proportional to the increasing enzyme concentration, and the absorbance measurement was in agreement with the intensity of the colour change (Figure 3.21). Therefore, quantitative spectrophotometric measurement of Schiff's reagent colourimetric assay on the ethyl acetate-soluble fractions with ethanol as co-solubiliser seems promising.

Nevertheless, certain limitation has been encountered, such as (1) the presence of ethyl acetate in the mixture might affect Schiff's reagent molarity due to evaporation of the solvent, (2) the absorbance in the reference blank was inconsistent and considered high (>0.2) (3) the ethyl acetate-soluble fraction must be sure to be free from contaminants such as traces of coagulated rubber.

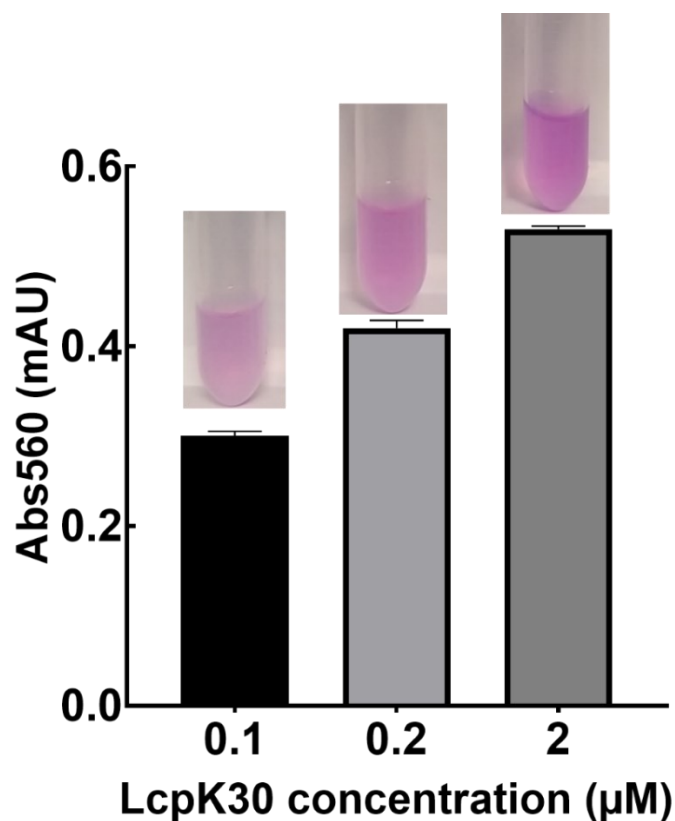


**Figure 3.21.** Absorbance measurement of the colourimetric assay on solvent-soluble fractions derived from degradation reaction catalysed by lower LcpK30 concentration. Samples were prepared in triplicates to determine the standard error.

### 3.4 Discussion

In this study, the production of pure LcpK30 has been successfully obtained by determining the expression method based on several studies on Lcps. One of the challenges in heme-protein expression is the ability of the *E.coli* cells to uptake heme. The bacteria are able to directly uptake heme by heme-specific periplasmic transport protein receptors (ChuT) on the bacterial surface and then transport it into the cell through ATP-binding cassette (ABC) transporters.<sup>217</sup>

Nevertheless, it has been reported that the ability of a standard *E.coli* laboratory strain to uptake heme is still limited due to the lack of a high-affinity heme transport system.<sup>129,218</sup> One of the approaches to increase heme uptake for the expression of heme proteins is by co-expression of the gene of interest with high-affinity heme from pathogenic bacteria such as *Plesiomonas shigelloides*.<sup>218</sup> A study by Fiege *et al.* (2018) has reported on using non-pathogenic *E.coli* strains Nissle 1917 that possesses a chromosomal copy of the gene encoding heme receptor ChuA. The cell has been used as the host for recombinant production of heme protein that could take up heme from the culture medium more efficiently.<sup>200</sup> More recently, an intracellular heme protein production has been developed using *E.coli* chassis known as Ec-M13 strain, harbouring a set combination of heme synthesis genes constructed to produce high intracellular heme without significant formation of intermediates.<sup>219</sup>

The correlation between the degradation products and the substrate loading can be related to the surface area-to-volume ratio. The biodegradation of lignocellulosic biomass is a good example of the impact of the surface area to volume ratio in enzymatic reaction. The biodegradability of this biomass is greatly influenced by the accessibility surface area (ASA) and specific surface area (SSA).<sup>220</sup> These factors determine (1) ASA - the surface area the enzyme can contact the substrate and (2) SSA - the total surface area per unit of solid or bulk volume. Both factors are influenced by the particle size, porosity and pore volume of the substrate.<sup>221</sup> In general, ASA is increased with SSA, but not all of the entire surface is effective for the enzyme to react with the substrate. As in the case of lignocellulosic biodegradation, cellulose hydrolysis by cellulase is increased with lower average fibre size, smaller particle size of microcrystalline cellulose and pore size larger than the rate-limiting pore size.<sup>222,223</sup> Meanwhile, as for NR, the particle size of NR is already convenient

enough for enzymatic degradation. However, when NR is added into the aqueous medium for *in vitro* biodegradation, the available polyisoprene chains on the NR particle's surfaces and exposed to the aqueous medium determine its SSA and ASA. Therefore, it is important to ensure that the loading of the substrate is suitable to ensure the NR particles are well dispersed and eventually increase the ASA. This theory also applies when dealing with other hydrophobic rubber as a substrate.

The HPLC chromatogram gave a good indication of the length differences of the oligomers. In this study, the average molecular weight of oligomers from NR estimated using different analytical approaches of HPLC, GPC and <sup>1</sup>H NMR were compared. From the comparison, data from GPC would give the average molecular weight between the other two calculated methods from the area percentage of HPLC peak and the integral peak area of <sup>1</sup>H NMR. Thus, the GPC measurement would be more representative of the average molecular weight ( $M_n$ ). In comparison to the literature, Andler *et al.* (2018) also reported the  $M_n$  from GPC measurement.<sup>134,137</sup>

Several studies have reported on the low reproducibility and instability of the colour development from analysis using the Schiff's reagent.<sup>224–226</sup> A study by Robins *et al.* (1980) also quoted that rigorous calibration is necessary to obtain quantitative results since the formation of Schiff's reagent aldehyde adducts was dependent on the amounts of dye, sulphur dioxide, and aldehyde in a complex pattern.<sup>214</sup> Although the commercially available Schiff's reagents are more stable<sup>227</sup>, the approach used in this study to develop a quantitative colourimetric assay based on the spectrophotometric method would require extensive validation to acquire the desired analytical requirements such as high sensitivity, freedom from interference, good colour stability, and ease of operation.

### 3.5 Summary and Conclusions

Expression and purification of LcpK30 performed in this study were modified and referred to various previously described methods. Most optimised expression and purification of Lcp were performed on Lcp derived from *G. polyisoprenivorans* (LcpVH2). Therefore, finding the most suitable approach to produce higher LcpK30 than previously reported ( $\sim 15 \text{ mg L}^{-1}$ ) was challenging. This obstacle was resolved by systematic trials and modifications of the expression method. Performing the LcpK30 protein expression in larger volumes and stored as cell pellets at  $-80 \text{ }^{\circ}\text{C}$  also ensures the enzyme's availability for future experiments. The activity of the purified LcpK30 in this study was found to be comparable to the previously reported results. Therefore, no evidence indicates that the activity is superior to the earlier findings. The purified enzyme activity was reduced by less than  $\sim 50 \%$  after one month of storage at  $-80 \text{ }^{\circ}\text{C}$  in 50% glycerol. These results are specific to the initial evidence of LcpK30 production in the SPT lab, which could provide further insights for enhancing LcpK30 production and activity.

The effect of substrate loading and enzyme concentration on the degradation of NR catalysed by LcpK30 was determined. The produced oligomers were found to be linearly related to the enzyme concentrations. However, different reaction conditions could promote variation in the concentration of the most abundant oligomer that was produced. Comparison of relatively most abundant oligomers based on the peak percentage area of the corresponding HPLC chromatogram shows that the products might have higher concentrations of oligomers with four, five, seven or eight isoprene units. This study is the first to explain and discuss the importance of determining a suitable substrate loading and reaction volume. It was suggested that there was a possibility that substrate-related factors might have an effect and thus influence the cleaving



site of the polyisoprene chains. This work also highlighted the influence of other factors, such as enzyme concentration, reaction temperature and enzyme addition regime, on LcpK30 catalysing activity. The findings provide insightful information to plan for the subsequent experimental work discussed in Chapter 4. A comprehensive comparison of three analytical methods (HPLC, GPC and  $^1\text{H}$  NMR) to determine which approaches best represent the average molecular weight ( $M_n$ ) contributes to a deeper understanding of the product size distribution.

The potential of LcpK30 to be manipulated using protein engineering has initiated the idea of developing a quantitative colourimetric assay based on spectrophotometry for quick active enzyme screening. The discussion from this study elucidates the various variables that impact the sensitivity of Schiff's reagent and lead to the lack of consistency in absorbance measurement. Hence, a thorough validation process was necessary to attain a high level of accuracy in the analytical test.

## **CHAPTER 4**

### **ENZYMATIC DEGRADATION OF MODIFIED NATURAL RUBBER AND SYNTHETIC RUBBER CATALYSED BY LcpK30**

#### **Background**

In the rubber industry, two important research areas are related to rubber degradation: (1) rubber waste management - aiming to recycle, reclaim, or dispose of rubber waste and (2) rubber modification - aiming to improve natural rubber (NR) quality through structural modifications by introducing functional groups at the C=C bonds or by cleaving the bond to produce telechelic oligomers. Modifying the chemical structure of NR to improve its processability and properties is commonly performed using chemical additives, resulting in rubber derivatives that cannot be recycled easily and are challenging to decompose.<sup>42,228</sup> Eventually, this contributes to more hassle in rubber waste management.

Conventional approaches to dealing with rubber waste would be recycling and reclaiming.<sup>3</sup> However, the enormous waste produced is too much to be processed by recycling and reclaiming. Due to its difficulties in reshaping, not all rubber waste can be reclaimed, and none can be transformed into the same initial monomer.<sup>89</sup> Some common rubber-based waste materials include non-surgical nitrile gloves, tyres made of either polybutadiene rubber (PBR) or styrene-polybutadiene rubber (SBR), toys (vulcanised NR or its synthetic counterpart), rubber hoses (butyl rubber), household and automotive products and modified rubber such as epoxidised natural rubber (ENR).<sup>3,54</sup> The synthetic and modified rubber are mostly water-insoluble and resistant to physical, chemical, and biological deterioration, which caused a major hurdle in degrading these materials.

It was suggested that an enzyme-based biotechnological solution is an option for managing issues related to rubber waste management that can degrade the rubber in a more environmentally friendly approach.<sup>133</sup> However, enzymatic degradation is limited to *cis*-1,4-polyisoprene rubber, whilst the degradation of other diene rubbers remains largely underexplored. Moreover, the efficiency of the enzyme to catalyse rubber degradation remains low due to the hydrophobicity of the polymer preventing interaction with enzymes in an aqueous environment.<sup>229</sup>

The work presented here was to investigate the ability of LcpK30 to catalyse the C=C bond cleavage of other diene rubber and to identify optimum conditions that allow the enzyme to access the C=C bonds. Synthetic and modified rubbers of various molecular weights, chemical structures, and morphology, such as synthetic isoprene rubber (IR), ENR and PBR, were chosen as the test substrate. The test substrates were prepared in film, with different sizes of particles and a surfactant-free oil in water emulsion co-stabilised with a solvent based on the method previously published.<sup>111,137</sup> The effect of different substrate morphology and chemical structure on LcpK30 catalytic activity was evaluated. The work presented in this chapter is also useful as it provides information on the alternative approach to improving enzymatic reactions on hydrophobic polymers without modifying the enzyme structure for activity improvement.

#### 4.1 The substrates for enzymatic degradation

An introduction to all rubber used in this work is described and listed in Table 4.1.

**Table 4.1.** List of rubbers that were used as a substrate in this study.

No	Type of rubber	Sample name used in this study
1	Epoxidised natural rubber 25 %	ENR25
2	Epoxidised natural rubber 50 %	ENR50
3	High molecular weight <i>cis</i> -1,4-polyisoprene	<i>h</i> -IR-100K
4	Low molecular weight <i>cis</i> -1,4-isoprene rubber made from synthetic rubber	<i>l</i> -IR-35
5	Low molecular weight <i>cis</i> -1,4-isoprene rubber made from natural rubber	<i>l</i> -IR-38K
6	Polybutadiene rubber Vinyl -1,2: 45-55 %	PB-1300
7	Polybutadiene rubber Vinyl -1,2: 15-25 %	PB-1500
8	Polybutadiene rubber Vinyl -1,2: 15-25 %	PB-2200
9	Polybutadiene rubber Vinyl-1,2: 10-20 %	PB-5000
10	Polybutadiene rubber <i>cis</i> - and <i>trans</i> - 1,4 80 % vinyl- 20 %	PB-5000S

Chemical modification of NR polymer chains by epoxidation produces an NR polymer backbone with the epoxide group randomly replacing the C=C double bonds known as ENR (Figure 4.1).<sup>41</sup> Currently, the commercially available ENR is produced using peracid in different epoxidation levels: 25 mol and 50 mol (%), known as ENR25 and ENR50, respectively. The degree of epoxidation is influenced by the type and amount of peracid, reaction temperature and duration, which determines the properties of ENR.<sup>43</sup>

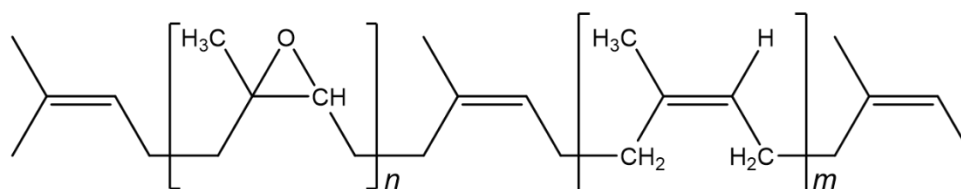


**Figure 4.1.** ENR chemical structure and physical form of ENR latex emulsion.

ENR has several better properties than NR, such as higher oil resistance, lower gas permeability, better wet grip, higher damping characteristics, and higher  $T_g$  and polarity.<sup>44</sup> However, the processing of ENR is still challenging due to its low solubility in organic solvents caused by its higher molecular weight. Thus, the degradation of ENR into shorter chain lengths to form liquid epoxidised natural rubber (LENR) becomes essential. Different degradation methods of ENR have been reported, such as chemical degradation and UV-irradiation methods.<sup>230,231</sup> ENR is commercially produced as a block or sheet rubber and has been widely applied for dry rubber products such as green tyres and shoe soles.<sup>232,233</sup> ENR is also a potential substance in a composite blend to reinforce the physical properties and to improve the biodegradability of other polymeric materials due to its similarity to NR, which is prone to be biodegraded specifically by an enzyme.<sup>234–236</sup> However, there is a limited study on the *in vitro* enzymatic degradation of ENR and the products produced from the degradation.

The Malaysian Rubber Board (MRB) has recently initiated research to utilise ENR latex to produce latex-dipped products such as gloves.<sup>237</sup> It was evident that ENR-latex dipped film has good mechanical properties that meet the

requirements specified by a quality standard with additional properties such as oil and chemical resistance, hydrophilicity effect, and improved wettability effect for donning and coating application. The ENR latex used in this study was supplied by the MRB in a stabilised emulsion, and the properties are outlined in Table 4.2.

Isoprene rubber (IR) is a synthetic analogue of NR. Synthetic petroleum-based isoprene monomer (2-methyl-1,3-butadiene) is an important feedstock to produce commercially available IR by solution polymerisation using anionic and Ziegler-Natta catalysts.<sup>238</sup> The level of linearity and branching properties of its structure can be controlled using different catalysts. In an aqueous serum phase, NR contains non-rubber components such as carbohydrates, proteins, lipids, minerals, and salt content.<sup>239</sup> Unlike NR, IR has a very low level of non-rubber constituents. Synthesis of IR by polymerisation ensured its chemical specificity (stereoregularity, linear or branching structure). NR and IR exhibit good mechanical properties, although several have reported that NR has better modulus, tensile strength and tear resistance than IR.<sup>240</sup> Nevertheless, IR is much easier to process due to its purity.<sup>241</sup> A well-blended IR with ethylene propylene diene monomer increased its resistance to reaction with oxygen and ozone, which could cause degradation and loss of physical and mechanical properties.<sup>238</sup>

This study employed three types of commercially available IR with different molecular weights, types of monomers and morphology, as shown in Figure 4.2. The high molecular weight IR is in solid-elastic form. In contrast, the low molecular weight IR is produced from synthetic (*I*-IR-35K) or natural (*I*-IR-38K) isoprene monomers that appeared as viscous liquids. Detailed characteristics of these polymers are outlined in Table 4.2.

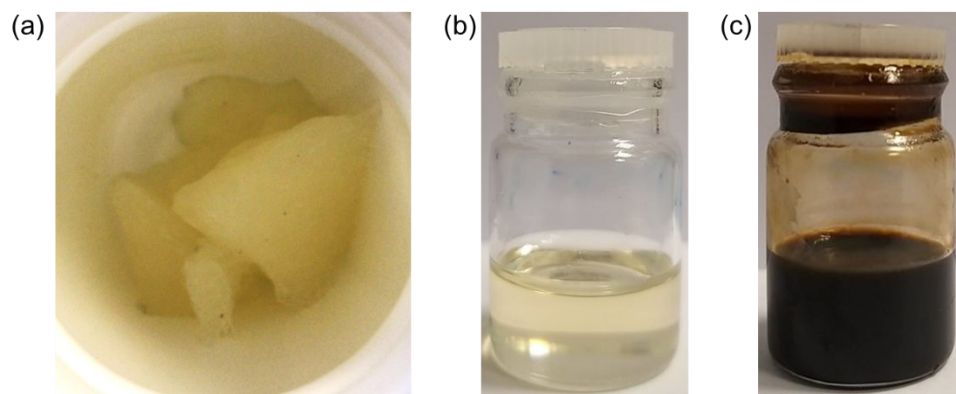


**Figure 4.2.** Physical form of synthetic *cis*-polyisoprene rubber. (a) Higher molecular weight synthetic *cis*-polyisoprene rubber ( $>10^5 - 10^6 \text{ g mol}^{-1}$ ), (b) Lower molecular weight synthetic *cis*-polyisoprene rubber made from synthetic rubber, (c) Lower molecular weight synthetic *cis*-polyisoprene rubber made from natural rubber.

Polybutadiene rubber (PBR) is a synthetic rubber produced by the coordination polymerisation of 1,3-butadiene monomers.<sup>27</sup> Polybutadiene rubber is a non-polar and highly unsaturated synthetic rubber comprising a mixture of structural units of *cis*-1,4 and *trans*-1,4 configurations, with 1,2-vinyl in the main backbone (Figure 4.3).<sup>242</sup> The microstructure of PBR polymeric chains depends on the catalyst system and initiator used during polymerisation and eventually influences the basic mechanical properties of PBR.<sup>27,35</sup>

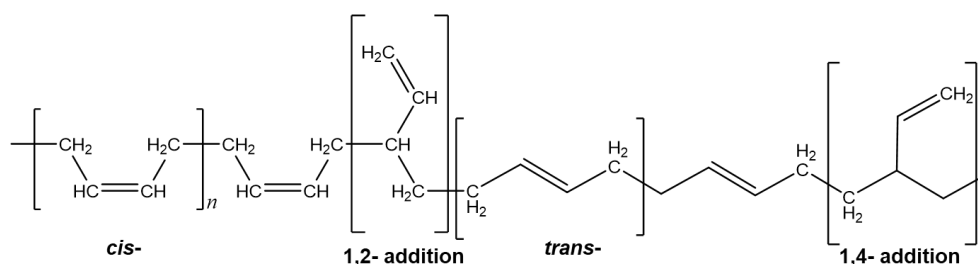


**Figure 4.3.** Molecule structure of polybutadiene rubbers.

**Table 4.2.** Characteristics of epoxidised and synthetic *cis*-polyisoprene rubber.

	<b>Epoxidised natural rubber</b>	<b>High molecular weight <i>cis</i>-polyisoprene rubber: 97% <i>cis</i>-1,4</b>	<b>Low molecular weight <i>cis</i>-polyisoprene rubber made from synthetic rubber</b>	<b>Low molecular weight <i>cis</i>-polyisoprene rubber made from natural rubber</b>
	<b>(ENR)</b>	<b>(<i>h</i>-IR-100K)</b>	<b>(<i>l</i>-IR-35K)</b>	<b>(<i>l</i>-IR-38K)</b>
<b>Stereochemistry</b>	<i>cis</i> with an epoxide group	<i>cis</i>	<i>cis</i>	<i>cis</i>
<b>n (number of monomers)</b>	>10,000	>10,000	>350	>380
<b>Average molecular weight <math>M_w</math> (g mol<sup>-1</sup>)</b>	10 <sup>5</sup> -10 <sup>6</sup>	10 <sup>5</sup> -10 <sup>6</sup>	35,000	38,000
<b>Physical morphology</b>	Stable emulsion	Solid-elastic	Viscous liquid (360-550 P at 37 °C) *	Viscous liquid (360-550 P at 37 °C) *

P = poise (measuring unit for viscosity). Data were obtained from the specification sheet provided by the manufacturer (Sigma Aldrich, USA).



PBR is commonly used as a copolymer in the dry rubber compound to produce tyres, an intermediate in acrylonitrile–butadiene–styrene (ABS) resins and as an impact modifier for plastics.<sup>243</sup> Recently, a derivative of PBR, known as liquid PBR (L-PBR), has been widely used as an important compound in rubber composites to improve the mechanical properties of various rubber-based products, especially in automotive industries.<sup>2,244</sup> In this study, various L-PBRs, as listed in Table 4.3, were used as the substrate for enzymatic degradation.

**Table 4.3.** Characteristics of polybutadiene rubber.

	<b>PB-1300</b>	<b>PB-1500</b>	<b>PB-2200</b>	<b>PB-5000</b>	<b>PB-5000S</b>
<b>Stereochemistry</b>	Vinyl -1,2: 45-55 %	Vinyl -1,2: 15-25 %	Vinyl -1,2: 15-25 %	Vinyl -1,2: 10-20 %	<i>cis</i> - and <i>trans</i> - 1,4 80 % vinyl- 20 %
<b>Average molecular weight <math>M_w</math> (<math>g\ mol^{-1}</math>)</b>	1300	1500	2200	5000	5000
<b>Physical morphology</b>	Viscous liquid				

#### 4.2 Substrates preparation and characterisation

This section discussed the preparation of the substrates for enzymatic degradation. The substrates were prepared as film, particles or surfactant-free emulsions based on their initial morphology. The ENRs supplied by MRB were in stabilised emulsion form. Samples were prepared similarly to NR, as described in section 2.2.9.1. After the final washing cycle with Nonidet, the rubber phase of ENR was redispersed in water at 60 % dry rubber content (600 mg mL<sup>-1</sup>). Therefore, the degradation study of ENR was prepared as an emulsion in an aqueous system similar to NR.

#### 4.2.1 Preparation of solid substrate

The high molecular weight synthetic IR (*h*-IR-100K) was prepared in macroparticles ( $\pm 2$  mm) and microparticles (600  $\mu\text{m}$ ). Additionally, the *h*-IR-100K was also prepared as a thin film. The method of preparing *h*-IR-100K in a thin film was inspired by a previous study by Sato *et al.* (2003), who successfully demonstrated that the proposed enzymatic systems with laccase/linoleic acid and manganese peroxidase/linoleic acid can degrade non-vulcanised IR cast as a film.<sup>173</sup> These approaches were taken to increase the contact area between rubber and aqueous solution containing enzyme and to evaluate the degradation activity of LcpK30 towards different substrate shapes. The substrate preparation was illustrated in Figure 4.4, and the details were described in Chapter 2.2.9.2.

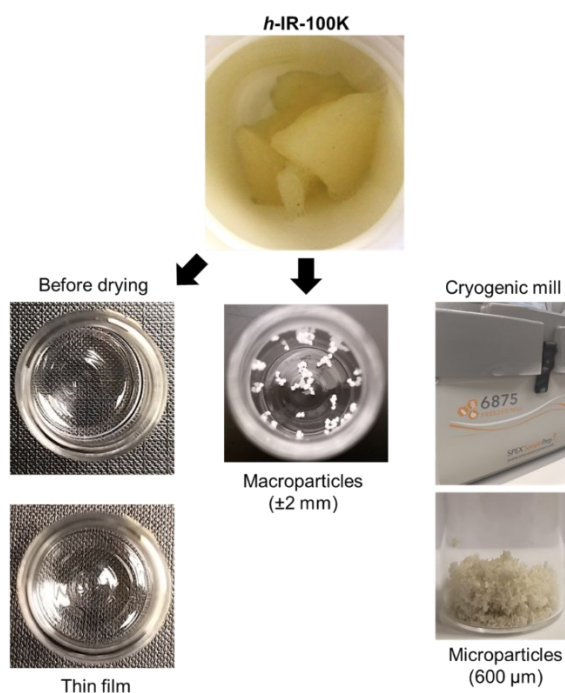


**Figure 4.4.** Morphology transformation of higher molecular weight synthetic rubber (*h*-IR-100K). The thin film was prepared by drying a thin layer of *h*-IR-100K dispersed in chloroform at the bottom of a glass vial. The macroparticles were prepared by solvent precipitation with a diameter of  $\pm 2$  mm measured using the Vernier scale. The microparticles were prepared by cryogenic milling and were sieved at 600  $\mu\text{m}$ .

#### 4.2.2 Preparation of co-solvent emulsion with *I*-IR-38K

Viscous liquid rubber was prepared as a co-solvent emulsion without surfactant based on a previously reported method with some modifications.<sup>111</sup> The rubber was dissolved in a suitable solvent to make a hydrophobic mixture (the dispersed phase). The hydrophobic mixture was dispersed in an aqueous medium by acoustic approach. This section assessed the preparation of low molecular weight synthetic IR made from NR (*I*-IR-38K) into a co-solvent emulsion to determine the suitable method for this study to prepare substrate in a co-solvent emulsion.

The *I*-IR-38K and other viscous liquid rubbers could be dissolved in *n*-hexadecane and *n*-tetradecane. The effect of these solvents on LcpK30 activity has been described in Chapter 3, Section 3.2.4 and has the potential to be used as a co-solvent to prepare the hydrophobic mixture. The hydrophobic mixture was added to potassium phosphate buffer (KPi buffer; 5 mM, pH 7) as the dispersion medium. The molarity of the KPi buffer was determined based on the study by Adjedje *et al.* (2021), who reported lower buffer molarity results in better enzyme stability in the presence of hydrocarbon solvent.<sup>111</sup> The hydrophobic mixture was dispersed by sonication under different conditions, and the resulting emulsion was analysed by visual appearance. The sonication helps to disperse the hydrophobic mixture as small droplets in the buffer to mimic the colloidal suspension of NR latex. After sonication, the mixture was expected to have a homogeneous milky-white visual appearance as a visual indication of emulsion formation.

It was found that the hydrophobic mixture made using *n*-hexadecane was not suitable for making the emulsion. The sonication was carried out in an ice bath to avoid heat build-up. The ice-bath temperature was below the *n*-hexadecane melting point (18.1 °C)<sup>245</sup> and caused the solvent to solidify, and the rubber was attached to the sonicator probe. Thus, the preparation of the *I*-IR-38K was continued with *n*-tetradecane, which has a lower melting point at 5.8 °C<sup>245</sup>.

The *I*-IR-38K was dissolved in *n*-tetradecane at 600 mg mL<sup>-1</sup> concentration. The hydrophobic mixture was then transferred into 5 mM KPi buffer (pH 7) at 0.2 % and 1 % (v/v) final ratio, followed by sonication to disperse the hydrophobic phase into the aqueous phase evenly. Sonication was performed at 20 % and 50 % amplitude for 5 minutes with pulsing intervals of 30 s on and 10 s off in an ice bath to observe the effect of mixing efficiency. Non-uniform mixtures were obtained in all cases (Figure 4.5), with the hydrophobic phase still visible on the top layer after sonication at different amplitudes. Nevertheless, a more turbid solution was obtained at the bottom layer when subjected to 50 % sonication amplitude, thus indicating that the higher amplitude might assist in getting better dispersion of the hydrophobic phase.

Based on an experiment of preparing a surfactant-free emulsion by Kamogawa *et al.* (2003), their research team found that the colloidal stability of hydrophobic polystyrene with benzene in water was enhanced at a 1:10 mixture ratio.<sup>246</sup> Therefore, the following attempt was carried out by reducing the *I*-IR-38K load to 100 mg mL<sup>-1</sup> into *n*-tetradecane for the hydrophobic phase. Next, the hydrophobic phase was added into the KPi buffer at 1 % (vol/vol), which would contain a 1:1 ratio of the rubber with the *n*-tetradecane, the ratio similarly used in the study by Adjedje *et al.* (2021) to prepare the surfactant-free emulsion of low molecular weight synthetic polyisoprene with different stereochemistry.<sup>111</sup>

The sonication was performed at 50 % amplitude for 5 mins with pulsing intervals of 30 s on and 10 s off.

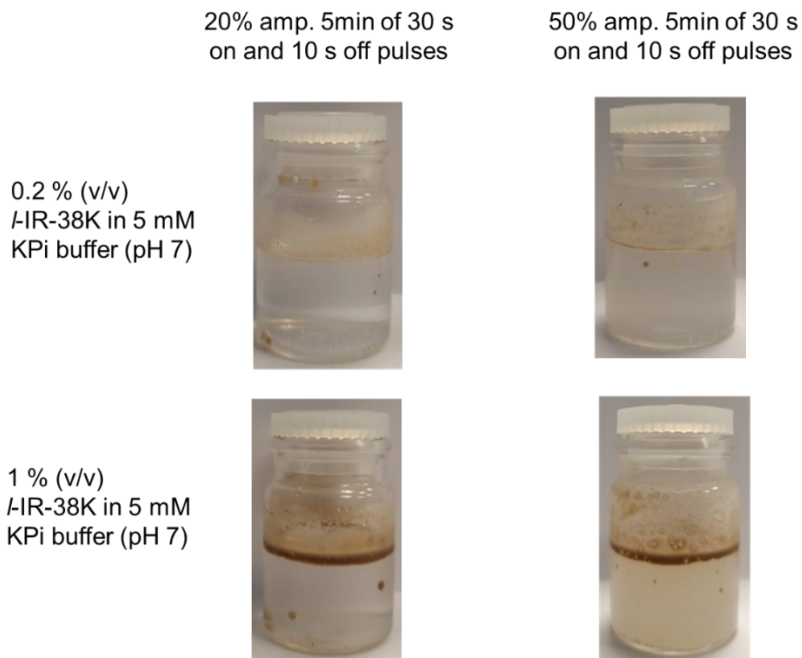


**Figure 4.5.** The appearance of *I*-IR-38K hydrophobic mixture dispersed in a buffer. The top figure represents the mixture of the concentrated hydrophobic mixture ( $600 \text{ mg mL}^{-1}$ ) in KPi buffer at a final concentration of 0.2 % (v/v) followed by sonication at 20 % amplitude (left) and 50 % amplitude (right) with a pulsing interval of 30 s on and 10 s off for 5 mins. The bottom figures show the mixture of the concentrated hydrophobic mixture ( $600 \text{ mg mL}^{-1}$ ) at a final concentration of 1 % (v/v) after sonication at 20 % amplitude (left) and 50 % amplitude (right) with a similar pulsing interval.

The homogeneous milky-white visual appearance showed better dispersion of the hydrophobic phase in the aqueous phase (Figure 5.5). It was concluded that the best approach to prepare the co-solvent stabilised emulsions was using the following method (1) preparing the hydrophobic phase in *n*-tetradecane at  $100 \text{ mg mL}^{-1}$  (2) setting the concentration of the hydrophobic phase in the emulsion is at 1 % (vol/vol) (3) performing the sonication at 50 % amplitude for 5 mins with pulsing intervals of 30 s on and 10 s off in ice bath. Therefore, all the viscous liquid rubbers used in this study were prepared according to this approach.

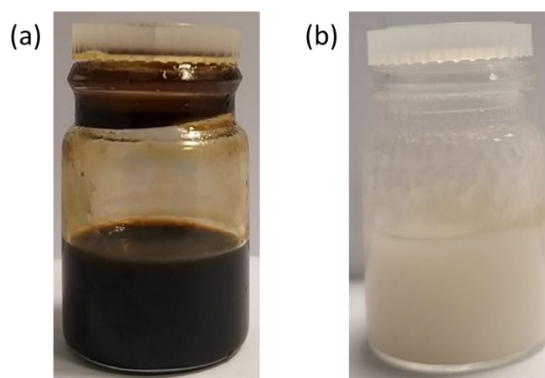


**Figure 4.6.** Morphology transformation of *I*-IR-38K. (a) The appearance of *I*-IR-38K before being dissolved in *n*-tetradecane (b) Homogeneous milky-white suspension of *I*-IR-38K consists of 1 % (vol/vol) hydrophobic phase in 5 mM KPi buffer (pH 7) after sonication at 50 % amplitude, 5 min of 30 s on and 10 s off pulses.

#### 4.2.3 Characterisation of the co-solvent emulsions

The following work was to prepare the co-solvent emulsion off all viscous liquid rubber using the method described in the previous section. The emulsions were characterised based on visual appearance, the emulsion droplets were viewed using optical microscopy and the diameter was measured using dynamic light scattering (DLS). The droplet diameter of the emulsion was compared to the NR particle size. A small droplet diameter was hypothesised to increase the surface area exposed to the aqueous phase containing the enzyme, thus increasing the C=C bonds cleavage activity.

All viscous liquid rubbers described in section 4.1 were dissolved in *n*-tetradecane (100 mg mL<sup>-1</sup>). From there, 1 % vol/vol was dispersed in an aqueous solution (5 mM KPi buffer, pH 7) followed by sonication at 50 % amplitude, 5 min of 30 s on and 10 s off pulses. The resulting mixture appeared as a homogenous milky-white emulsion except for emulsified PB-5000S, which appeared more translucent (Figure 4.7).

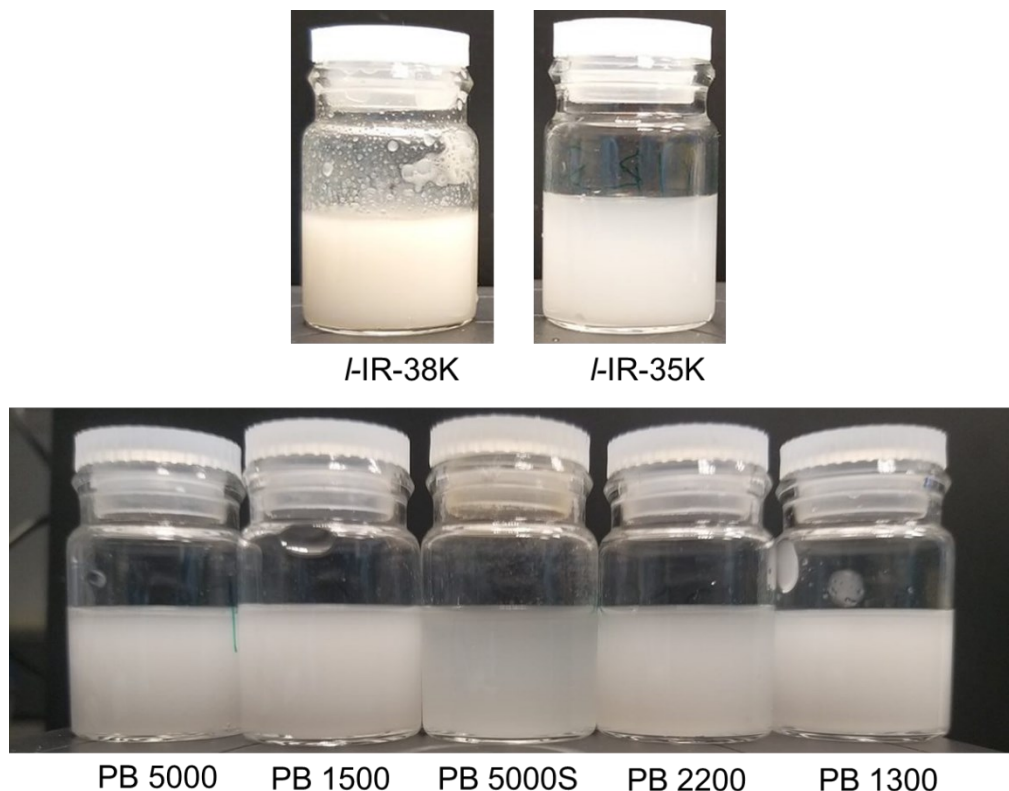


**Figure 4.7.** The physical appearance of viscous liquid rubbers in a co-solvent solution mimics the natural rubber emulsion. The solution is a mixture of the hydrophobic phase consisting of the rubber dissolved in *n*-tetradecane and the aqueous phase of 5 mM KPi buffer, pH 7 followed by sonication at 50 % amplitude with a pulsing interval at 30 s on and 10 s off for 5 mins.

The emulsified rubbers resulted in an average droplet size range between 300 nm and 1900 nm with a polydispersity index (PDI) higher than NR. (Figure 4.8). Theoretically, a colloidal suspension with smaller droplet diameters will increase the surface area, thus exposing the polymer chains to the aqueous mixture and resulting in improved accessibility of the enzyme to the C=C bonds. Among all rubbers, /-IR-35K had the largest emulsion droplet size at an average of 1900 nm with 0.2 polydispersity (PDI). Nevertheless, the size distribution of the droplets was unimodal, which indicated that the emulsion consisted of a uniform size of larger droplets (Appendix C4.1c). The higher diameter might be attributed to the entanglement of long polymeric chains of *cis*-polyisoprene that densely surrounded the surface of the solvent droplet, which appeared as a droplet with a darker circle, as shown in Figure 4.9b.

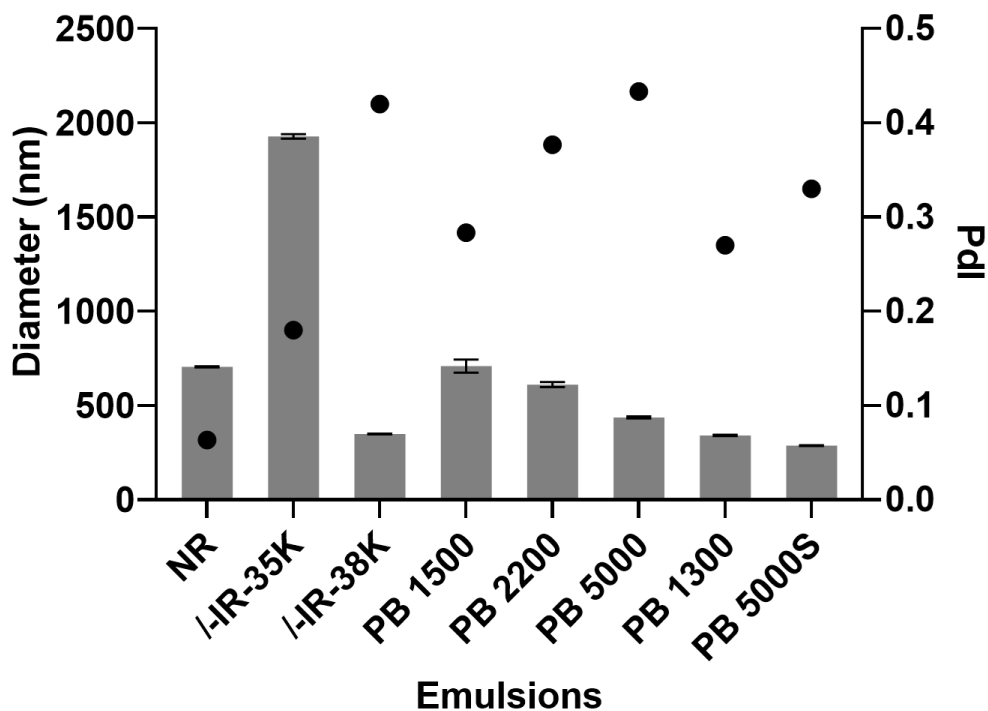
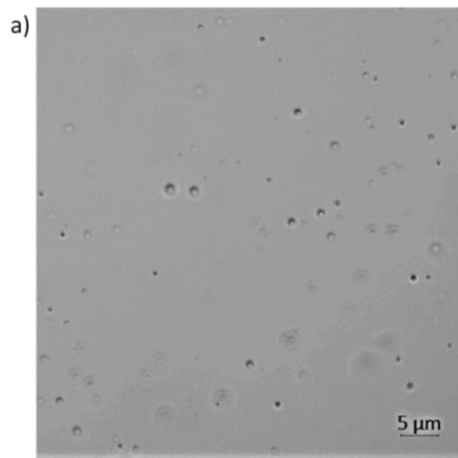


**Figure 4.8.** The diameter and particle size distribution of the emulsion droplet. The droplet diameter was measured in nanometers (nm), represented by the grey bar. Black points represented the polydispersity index (Pdl). The sample containing 1 % (vol/vol) of the hydrophobic phase (100 mg mL<sup>-1</sup> rubber dissolved in *n*-tetradecane) dispersed in the aqueous phase (5 mM KPi buffer, pH 7) was taken immediately after sonication and diluted with water at 1:100 dilution prior to analysis. The samples were prepared in triplicate to determine the standard error.

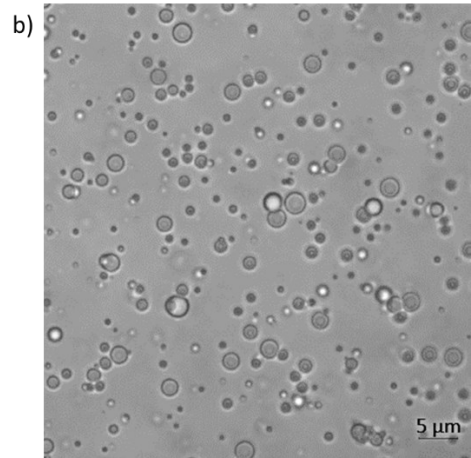
The emulsion droplet size in emulsified *I*-IR-38K was, on average, smaller than NR particles (349 nm) but with a broader bimodal size distribution (Appendix C4.1b). The microscopic image of emulsified *I*-IR-38K showed that the polymer was dispersed mainly by small droplets, with a few larger droplets (Figure 4.9c) corresponding to the higher Pdl. The diameter of the droplets in the emulsified L-PBRs (PB-1300, PB-5000 and PB-5000S), as determined by DLS, appeared smaller than those observed using the microscope (Figure 4.9f-h). The larger size compared to the DLS could result from water evaporating before the observation, which would cause the droplets to aggregate.<sup>111</sup> This also might indicate the formation of droplets with the PBR was influenced by the molecular



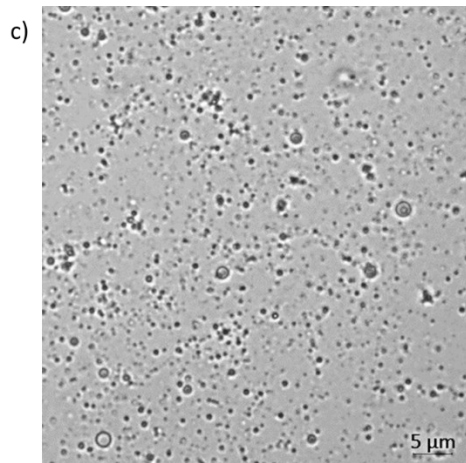
structure of the rubber chains. The PB-1300 contains more than 50 % vinyl content.



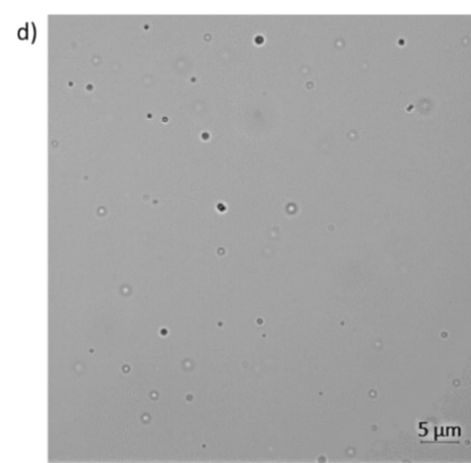
NR



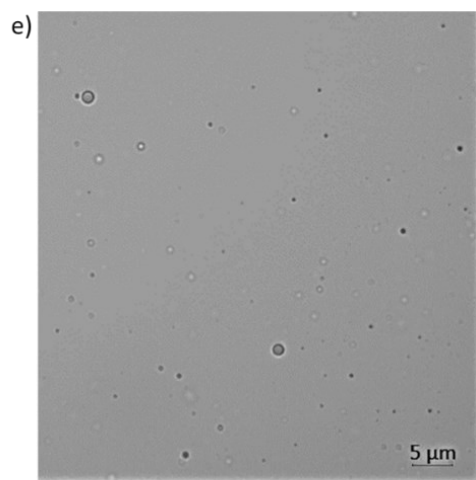
IIR-35K



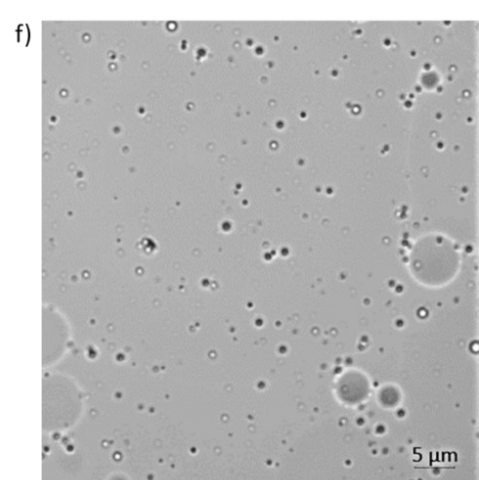
IIR-38K



PB 1500



PB 2200



PB 5000

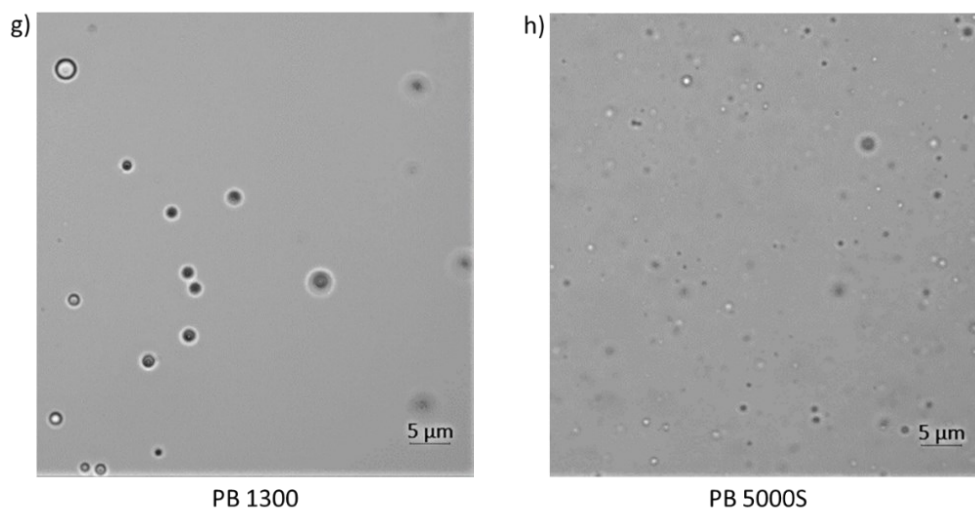


**Figure 4.9.** Microscopic images of the emulsion droplets from a colloidal suspension after sonication containing 1 % (vol/vol) of the hydrophobic phase (consists of 100 mg mL<sup>-1</sup> rubber dissolved in *n*-tetradecane) in 5 mM KPi buffer, pH 7 (aqueous phase) diluted with water at 1:100 dilution prior viewing.

Although none of the co-solvent emulsified prepared in this study could resemble NR, the finding has shown that by dissolving the rubber in *n*-tetradecane, the solvent could assist in dispersing the hydrophobic rubber in the aqueous system by forming variations sizes of droplets. The arrangement of the rubber microstructure on the solvent droplet surface potentially influenced the size of the droplets. The preparation of emulsified rubber in this study was referred to a published work that prepared the co-solvent emulsion using lower molecular weight rubber of 3000 and 15000 g mol<sup>-1</sup> that consist of different *cis*- and *trans*-configuration ratios. The efficiency of LcpK30, as measured by the integration area of UHPLC-UV chromatograms, exhibited insignificant rubber degradation at higher molecular weight, indicating a weaker stabilising effect due to the rubber molecular size.<sup>111</sup> However, the stability study of the prepared emulsified rubber was not quantitatively analysed in this current study. Therefore, to avoid any major destabilisation effect, the stirring during the reaction was set at 1000 rpm for 5 mins before adding the enzyme and continued at 450 rpm. A similar stirring condition was performed during the next enzyme loading.

### 4.3 Enzymatic degradation of modified and synthetic rubbers

This section presents the ability of LcpK30 to catalyse C=C double bond cleavage of various rubbers (ENR, *h*-IR-100K, *l*-IR-35K, *l*-IR-38K, and L-PBRs). The degradation reaction was performed in the following conditions: purified LcpK30 was added three times until reaching a final concentration of 18  $\mu\text{M}$  ( $0.75 \text{ mg mL}^{-1}$ ); NR and ENR were added at  $100 \text{ mg mL}^{-1}$ ; solid rubber (particles and film) was added at  $10 \text{ mg mL}^{-1}$ ; co-solvent emulsified rubber was added at  $1.3 \text{ mg mL}^{-1}$ ; stirring at 450 rpm and incubation at 30 °C. The molarity of the KPi buffer used in this experiment was at 5 mM, pH 7 as referred to Adjedje *et al.* (2021) who reported that the stability of LcpK30 was better preserved at 5 mM KPi buffer compared to a higher concentration of buffer (100 mM).

Oligomeric products produced from the degradation were weighed and analysed using GPC to determine the number of average molecular weights ( $M_n$ ), weight average molecular weights ( $M_w$ ), and size distributions ( $M_w/M_n$ ). Integration of the  $^1\text{H}$  NMR peaks representing the aldehyde proton and three prominent functional groups for polyisoprene structure (methyl, methylene and olefinic) were extracted to estimate the oligomers' average number of isoprene units using the Equation 3.1 as described in Chapter 3 section 3.2.6.

#### 4.3.1 Epoxidised natural rubber

Preliminary screening of the ability of LcpK30 to catalyse the degradation of ENR50 and ENR25 was performed using the colourimetric assay of the reaction suspension after two hours of incubation at 30 °C with 250 rpm agitation. The results showed that the aldehyde compound was only detected in the reaction with ENR25 (Figure 4.10). This observation suggested that the epoxide content affected the ability of LcpK30 to cleave the C=C bonds in ENR and that a low epoxide content is preferable.

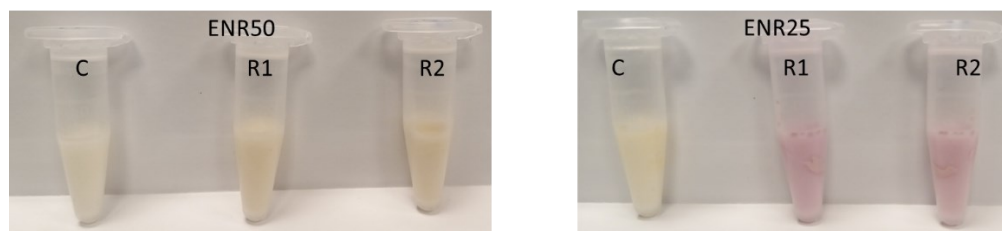


**Figure 4.10.** A colourimetric assay using Schiff's reagent to detect aldehyde compound in ENR degradation catalysed by LcpK30.

The degradation reaction of ENR25 was repeated, and the colourimetric assay of the reaction suspension with Schiff's reagent confirmed aldehyde formation (Figure 4.11). However, the lower intensity of Schiff's reagent colour indicated that the presence of the aldehyde group was lower compared to the degradation on NR (positive control).

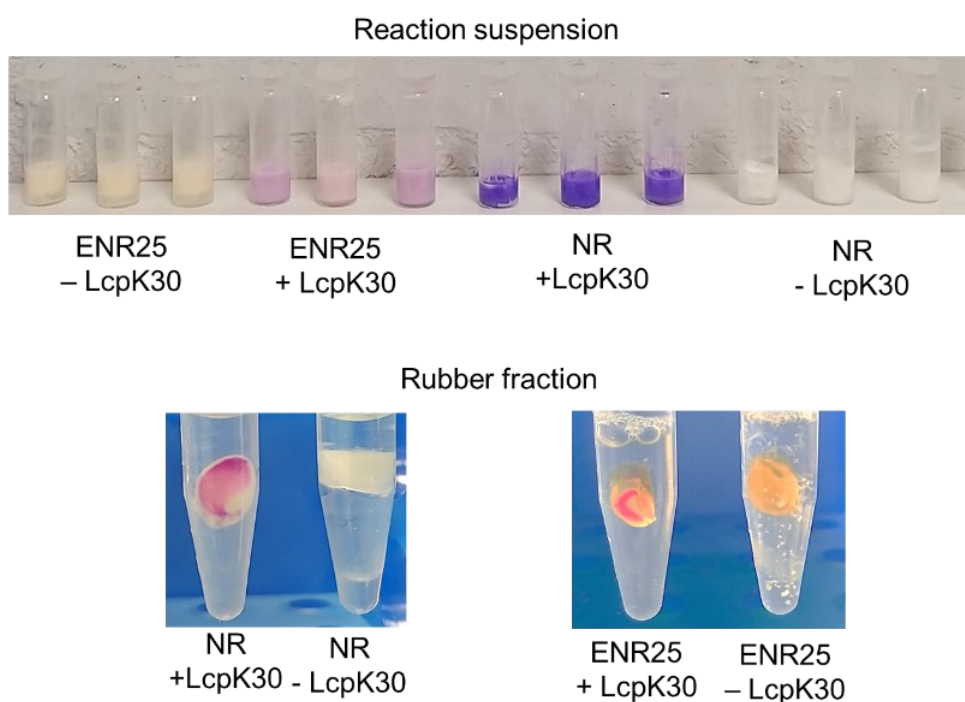


**Figure 4.11.** Colourimetric screening assays of ENR25 and NR. Staining with Schiff's reagent was carried out on the reaction suspension and the rubber fraction after ethyl acetate extraction. The appearance of a magenta colour indicates the presence of aldehyde.

Intriguingly, the staining assay also identified molecular alterations on the surface of the solid rubber fraction, indicating that the carbonyl group is exposed to the surface and thus has the potential to undergo surface modification. On

the other hand, no colour change was detected on the rubber from the control reaction without enzyme. The brownish colour of ENR25 rubber was probably due to the reaction of the non-rubber compound in NR during the epoxidation reaction.<sup>247</sup>

Initially, results obtained from the HPLC analysis were inconclusive as the HPLC chromatogram peaks did not show any evidence of oligo-isoprenoid (Figure 4.12a and b). Moreover, an attempt to use dichloromethane (DCM) to improve the product extraction resulted in similar peaks with no indication of the degradation of the products (Figure 4.12c). All these preliminary reactions were performed on a low scale (1 mL). Hence, the amount of oligo-isoprenoids produced may have been too low for detection.

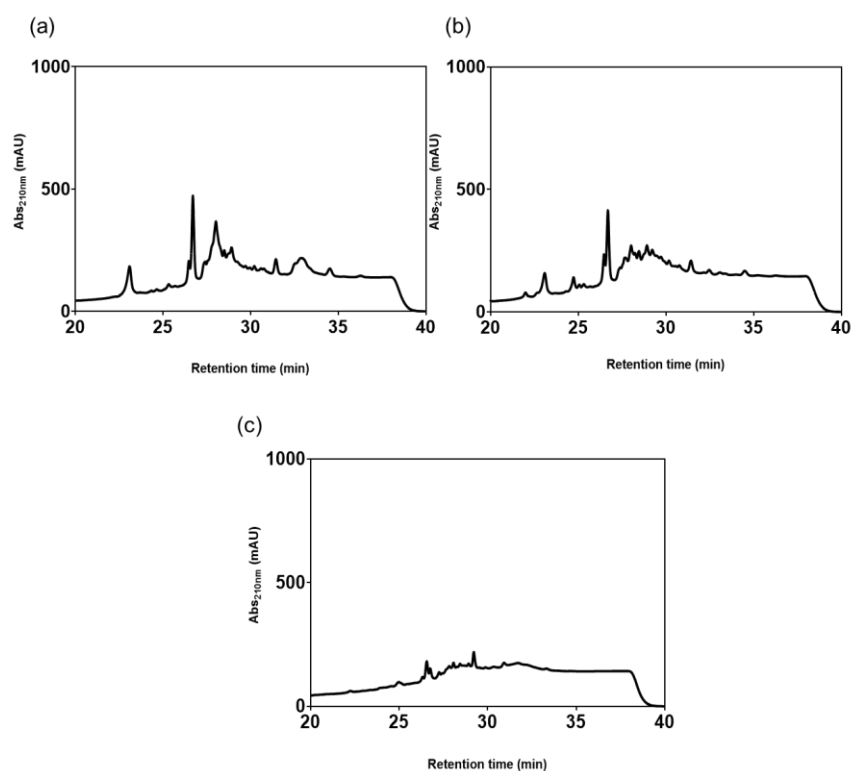


**Figure 4.12.** HPLC chromatogram of samples extracted from ENR25. The preliminary reaction was performed (a) without LcpK30, (b) with LcpK30 followed by extraction using ethyl acetate, and (c) with LcpK30 followed by extraction using dichloromethane (DCM).

In the next attempt, the total reaction volume was increased from 1 mL to 5 mL with an initial concentration of ENR25 emulsion at  $100 \text{ mg mL}^{-1}$ . The oligomer mass produced was weighed at 25 mg. The HPLC chromatogram obtained from ENR25 degradation was compared with NR degradation. The oligo-isoprenoids produced from NR degradation display a separation peak pattern that was separated by a monomer (Figure 4.13a). However, a similar separation peak pattern of oligo-isoprenoid from NR was not observed from the extracted sample of the ENR25 degradation (Figure 4.13b).

The epoxide group in the ENR chain is distributed randomly, and there is a chance that the pattern of the oligo-isoprenoids produced may not be uniformly distributed and thus cannot be separated by one isoprene unit, as in the case of NR. Instead, the oligo-isoprenoids may have different lengths and contain different numbers of epoxidised bonds in various arrangements. Hence, the non-even pattern was obtained.

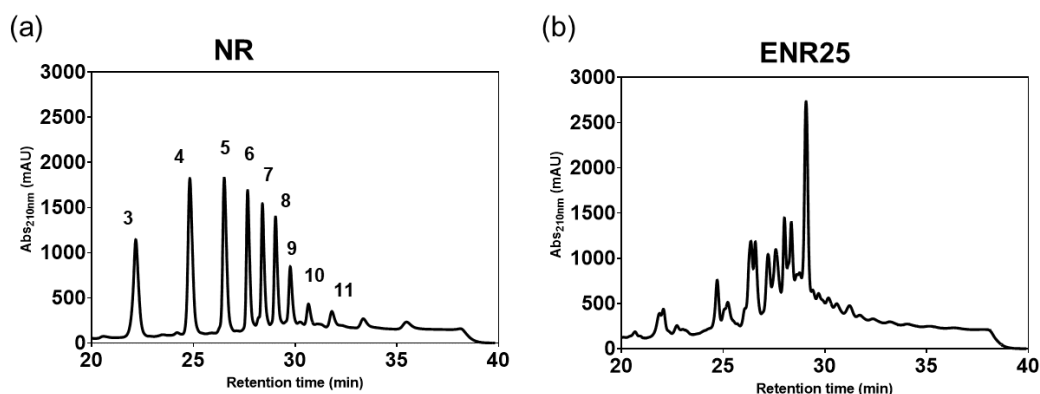


**Figure 4.13.** HPLC chromatogram of degradation products after 24 hr of (a) NR and (b) ENR25 degradation catalysed by LcpK30. The number on top of the peak represents the repetitive number of isoprene.

Based on the GPC measurement, the number average molecular weight ( $M_n$ ) of the oligomer from ENR25 degradation was measured at  $1324 \text{ g mol}^{-1}$ , and the weight average molecular weight ( $M_w$ ) was  $2820 \text{ g mol}^{-1}$  (Table 4.4).

**Table 4.4.** The characterisation of NR and ENR25 and their degradation products were determined by GPC.

Sample name	*M <sub>n</sub> (g mol <sup>-1</sup> )	*M <sub>w</sub> (g mol <sup>-1</sup> )	Đ
NR-original	241.5	837.3	3.47
NR-oligomer	0.897	2.908	3.24
ENR25-original	163.5	676.6	4.09
ENR25-oligomer	1.324	2.82	2.13

\*Multiply the number with 10<sup>3</sup> to get the actual M<sub>n</sub> or M<sub>w</sub> in g mol<sup>-1</sup>  
 The GPC measurement was performed on pooled samples of oligomers retrieved from three experiment replicates

As demonstrated in Figure 4.14, the <sup>1</sup>H NMR spectrum of ENR25 exhibited two additional signals at chemical shift values of 5.1 ppm and 2.7 ppm, which were attributed to olefinic proton (2) and epoxy-methine protons (5), respectively.<sup>248,249</sup>

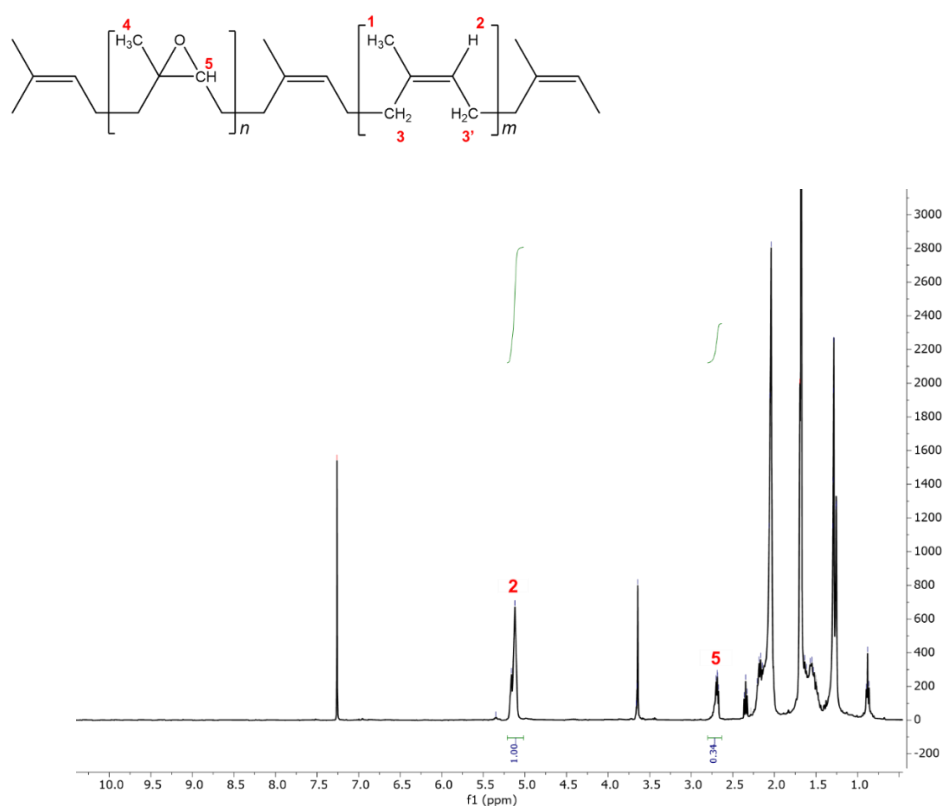


**Figure 4.14.** <sup>1</sup>H NMR spectra of ENR25. The ENR25 was dissolved in deuterated chloroform (CDCl<sub>3</sub>) which use as a reference solvent ( $\delta = 7.26$  ppm).

Further confirmation using  $^1\text{H NMR}$  confirmed the presence of a carbonyl group by the appearance of an aldehyde peak at 9.77 ppm (7) (Figure 4.15). Signals at 2.7 ppm and 1.2 ppm were also present, corresponding to epoxy methine proton (5') and methyl proton (4') of the epoxide group.<sup>248</sup> In addition, the spectra also show peaks at 1.68 ppm, 2.05 ppm and 5.12 ppm, which are attributed to methyl (1'), methylene (3', 3'') and olefinic (2') group of isoprene unit. The signal for methyl ketone that should appear at 2.1 ppm (6) is commonly overlaps with the isoprene methylene group.<sup>250</sup>

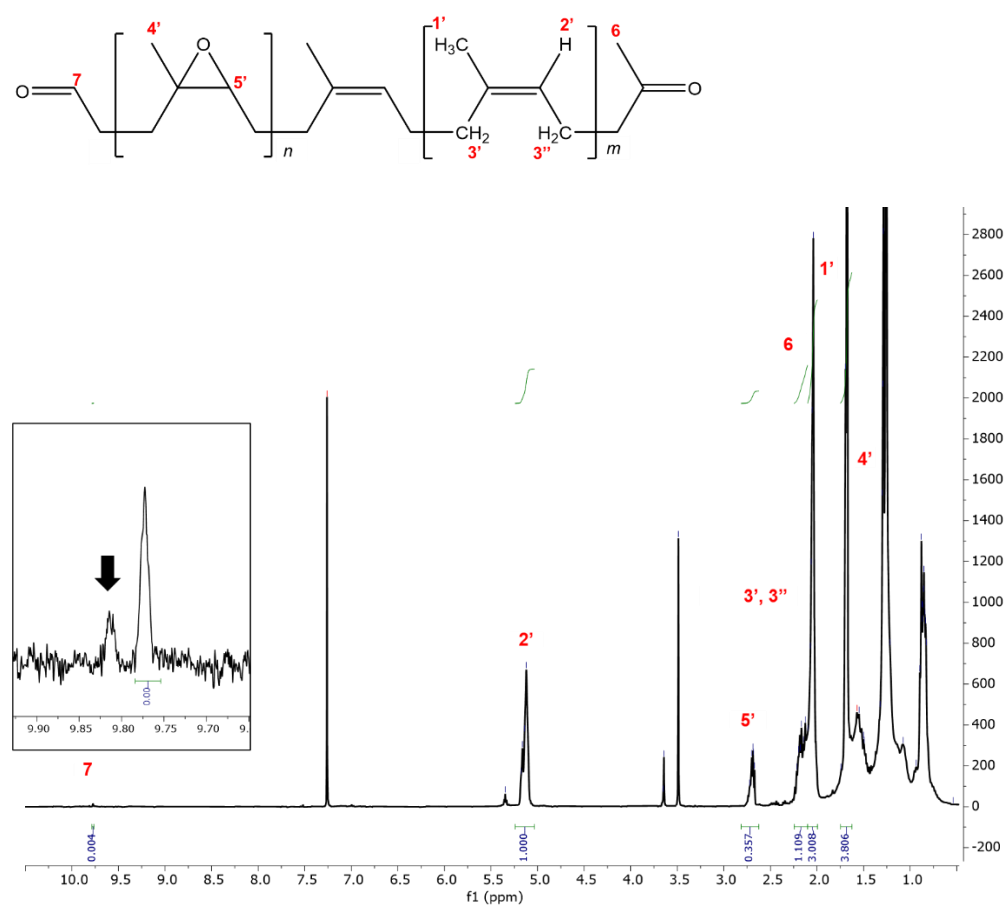


**Figure 4.15.**  $^1\text{H NMR}$  spectra of ENR25 degradation products. After ethyl acetate extraction, the soluble fraction was dried under a rotary evaporator and vacuum pump and solubilised with deuterated chloroform ( $d\text{-CHCl}_3$ ) before being analysed.



Interestingly, an additional peak (pointed by the black arrow in Figure 4.15) shifted downfield from 9.8 ppm, which might indicate the presence of aldehydes of different species. The small aldehyde peak was hypothesised to correspond to an aldehyde proton next to an epoxy-isoprene unit. The presence of other species of aldehyde is not peculiar. Rooshenass *et al.* (2017) reported that the  $^1\text{H}$  NMR spectra of ENR5 after degradation by periodic acid and UV-irradiation method showed an aldehyde peak at 9.78 ppm with an additional peak at 9.5 ppm, which assigned to  $\alpha$ - $\beta$  unsaturated aldehyde.<sup>251</sup>

The epoxidation percentage of ENR25 was calculated using Equation 4.1 based on the  $^1\text{H}$  NMR spectra in which  $I_{2.7}$  and  $I_{5.1}$  represent the integral peak area of the chemical shift of the epoxide group and unsaturated carbon (C=C) proton, respectively.<sup>67,252</sup>

$$\text{Epoxidation level (\%)} = \frac{I_{2.7}}{I_{2.7} + I_{5.1}} \times 100$$

Equation 4.1

The calculated epoxidation percentage in Table 4.5 was coherent with the initial epoxidation level (25 %), with a slight increment observed after the degradation. This increment could be explained by the C=C bonds being cleaved, resulting in an increase in the epoxy-isoprene unit ratio of the ENR backbones.<sup>268</sup> This result was similar to those obtained in the degradation of ENR25 by periodic acid, where a decline in epoxy content was also not observed because the periodic acid tends to oxidise the C=C bonds into vic diol before proceeding with further cleavage.<sup>253</sup>

**Table 4. 5.** Epoxidation level of ENR25 before and after degradation.

	Integration number		Epoxidation level (%)
	Olefinic	Epoxy methine	
<b>ENR25 before degradation</b>	1	0.34	25.4
<b>ENR25 after degradation</b>	1	0.36	26.5

Additionally, the epoxy-isoprene unit ( $\text{CH}_2\text{-C-O}(\text{CH}_3)\text{CH}=\text{CH}_2$ ) and isoprene unit ( $\text{CH}_2=\text{C}(\text{CH}_3)\text{CH}=\text{CH}_2$ ) of the oligo-isoprenoid were estimated by integrating the peaks for aldehyde and aldehyde' proton (7), olefinic proton (2'), methyl proton (1' and 4') and epoxy methine proton (5'). The calculation to obtain the number of repetitive units of epoxy-isoprene and isoprene is shown in Appendix C4.2 and shows an estimated average of 200 isoprene units and 72 epoxy-isoprene units for the oligomers.

Results obtained by  $^1\text{H}$  NMR and GPC analysis were contradictory, which was not observed when the same analysis was performed for oligomers of NR. The  $^1\text{H}$  NMR estimated that the molecular weight of the oligomers derived from ENR25 degradation was approximately  $20000 \text{ g mol}^{-1}$ , which was  $\sim 15$  times higher than the  $M_n$  obtained from GPC analysis (Table 4.4). This result seems to overestimate the average length of the degradation products. Several challenges have been reported regarding analysing the ENR using NMR. According to Hamzah *et al.* (2012), structural interpretation of ENR via the NMR techniques is difficult due to the random arrangement of epoxy-isoprene and isoprene units.<sup>248</sup> In terms of using  $^1\text{H}$  NMR as a tool to estimate the average length of a polymer, several studies have claimed that  $^1\text{H}$  NMR would provide a fast and simple analysis in which the repeating unit can be easily calculated from the peak area of the proton at a particular chemical shift which was being adapted in this study.<sup>211</sup> However, several limitations that could make the determination of  $M_n$  using NMR spectroscopy intractable were also

encountered, such as the integration of the end-group proton and the monomer proton could be inaccurate and different resolution patterns of protons of different segments of a co-polymer is observed.<sup>254</sup> For this reason, further studies are necessary to confirm the molecular weight of ENR oligomers.

#### 4.3.2 High molecular weight synthetic *cis*-1,4-polyisoprene rubber (*h*-IR-100K)

The effect of enzymatic degradation on *h*-IR-100K prepared as a solid substrate (film and particles) was described in this section. The *h*-IR-100K film was evaluated based on physical and chemical changes (HPLC, <sup>1</sup>H NMR, Fourier-transform infrared spectroscopy (FTIR) and GPC). The physical morphology of the film treated with LcpK30 showed distinctive changes compared to the non-treated film (Figure 4.16).



**Figure 4.16.** The physical morphology changes of the treated and non-treated *h*-IR-100K films.

Fourier-transform infrared spectroscopy (FTIR) analysis of the *h*-IR-100K films was performed to support the finding that the film was functionalised, thus leading to the morphology changes observed visually. Detection of the C=O stretching of carbonyl compound at 1736 cm<sup>-1</sup> absorption on the treated *h*-IR-100K film showed evidence of cleavage of C=C bonds producing oligo-isoprenoids chains with aldehyde terminal-end (Figure 4.17).

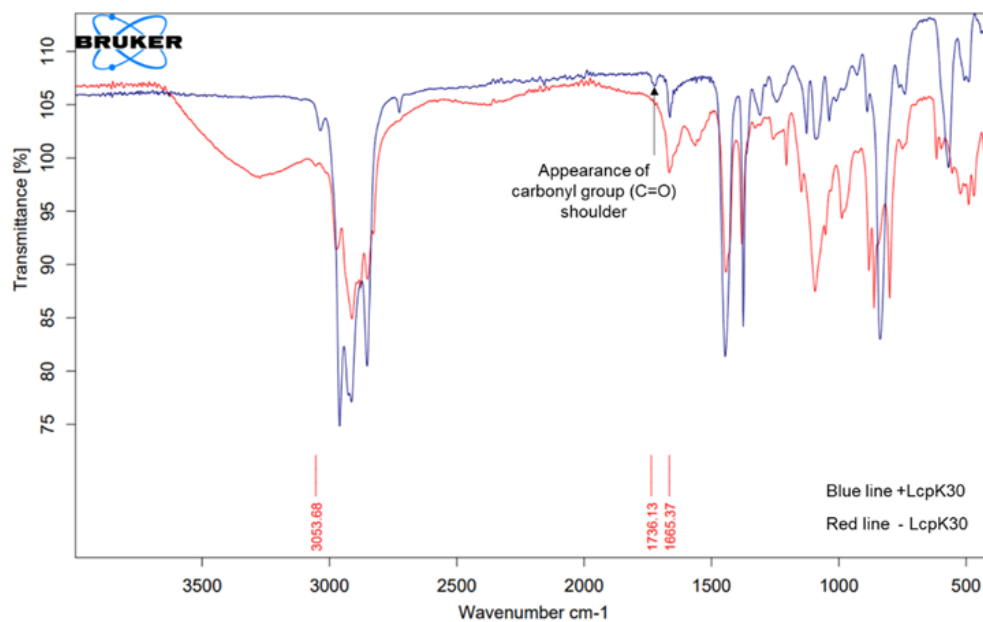


**Figure 4.17.** The FTIR spectra show the presence of a carbonyl group in *h*-IR-100K rubber film after degradation catalysed with LcpK30.

A relatively similar separation pattern of oligomeric products compared to NR was detected by the HPLC (Figure 4.18).

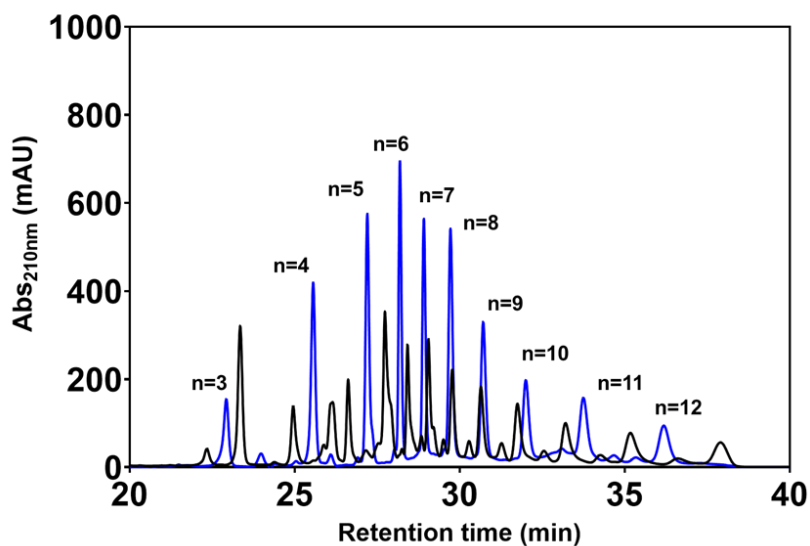


**Figure 4.18.** HPLC chromatogram of oligo-isoprenoids derived from synthetic *cis*-1,4-polyisoprene (*h*-IR-100K) degradation in film formation (black line) and NR (blue line) catalysed with LcpK30.

The HPLC result was further supported by the detection of a single peak at 9.8 ppm and 2.15 ppm on  $^1\text{H}$  NMR spectrum corresponding to the proton of the aldehyde and ketone group (Figure 4.19).

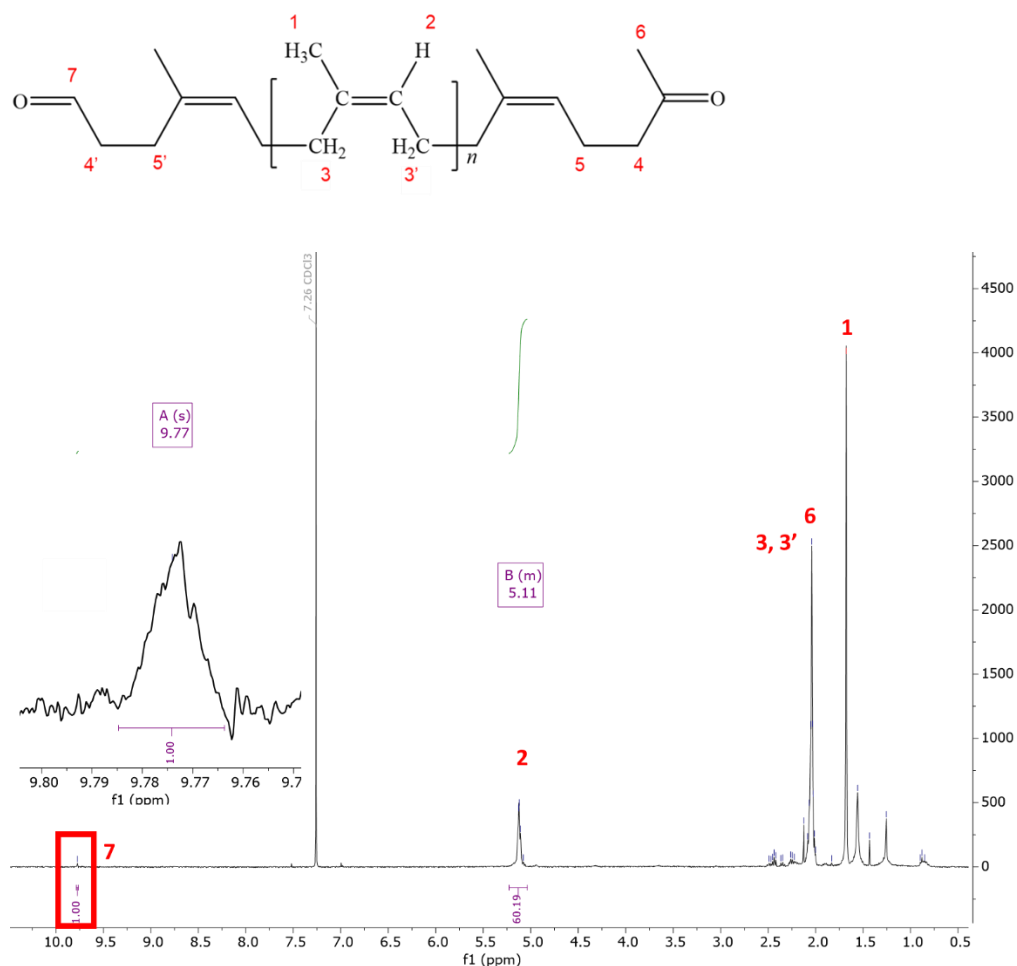


**Figure 4.19.** The  $^1\text{H}$  NMR spectra show the presence of an aldehyde in dried residual extracted from the degradation of synthetic *cis*-1,4-polyisoprene (*h*-IR-100K) in film formation catalysed with LcpK30.

A positive control reaction was also set up using the NR latex prepared into a film. The NR film was prepared in a similar weight with *h*-IR-100K film, as described in Chapter 2, section 2.2.9.2. The NR film is formed by evaporating the water from the aqueous phase. However, enzymatic degradation of NR as a solid substrate could not be observed (Appendix C4.3). Evaporation of water from NR latex could cause changes in the osmotic gradient that would lead to

aggregation of the rubber particles. During the process, the lutoid particles in the B-serum are likely to break and release the destabilising agents (e.g.,  $Mg^{2+}$ ,  $Ca^{2+}$ , acid hydrolases enzymes) into the C-serum. Eventually, the pH becomes acidic and neutralises the negative charges surrounding the rubber particles,<sup>255</sup> causing the rubber molecules to agglomerate, becoming a gel-like structure and eventually hardening over time.<sup>256</sup> This event would result in a solid NR with strong inter-molecular networking or is referred to as premature cross-linking, thus making enzyme penetration impossible. In contrast to the film made of *h*-IR-100K, the absence of the B-serum with the non-rubber compound does not promote inter-molecular networking. Thus, it was assumed that the enzyme could reach the polyisoprene chains that were exposed on the film surfaces.

The experiment on the degradation of *h*-IR-100K catalysed by LcpK30 was continued by performing the degradation on particles in two different sizes: macroparticles ( $\pm 2$  mm) and microparticles (600  $\mu m$ ). The HPLC chromatograms obtained after analysing the dried residual extract from both reactions are shown in Figure 4.20. The intensity of the HPLC chromatogram peaks representing the oligo-isoprenoids with different lengths was far lesser in the dried products retrieved from the reaction with macroparticles than those from the reaction with microparticles.<sup>106,174</sup> The accessibility of the enzyme to the C=C bond was enhanced with the increase of the surface area due to smaller particle size. The amount of oligomer mass produced from the degradation of *h*-IR-100K in 600  $\mu m$  microparticles yields a substantial quantity of oligomers at 33 mg.

The GPC analysis of the oligomer derived from *h*-IR-100K degradation in the microparticle form showed bimodal size distribution, indicating a vast variation in oligomer length (Appendix C4.4d). This observation was supported by a distinctive difference between the  $M_n$  (978 g mol<sup>-1</sup>) and  $M_w$  (4726 g mol<sup>-1</sup>). The

$M_n$  value measured by GPC was coherent with the estimated average number of isoprene repeating units ( $n = 14$ ;  $C_{70}$ ) calculated based on the ratio of integral peak area from  $^1\text{H}$  NMR signals.

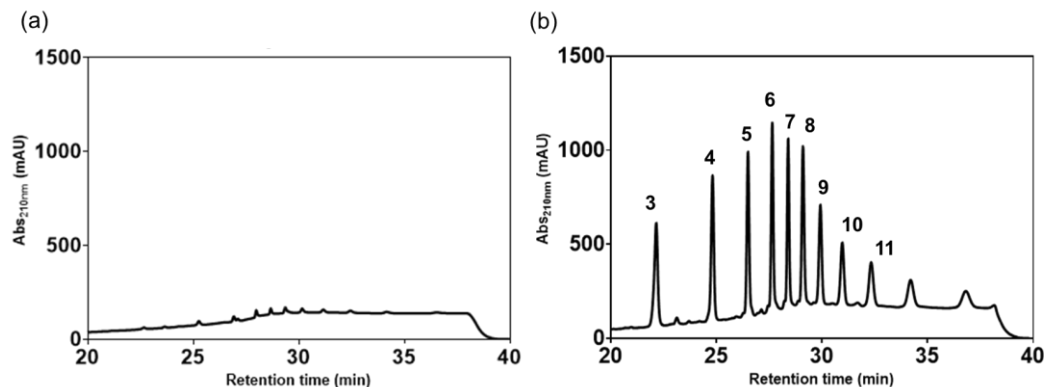


**Figure 4.20.** HPLC chromatogram of oligomeric products derived from degradation reactions of high molecular weight synthetic *cis*-1,4-polyisoprene (*h*-IR-100K) in (a) macroparticles and (b) microparticles substrate form catalysed with LcpK30.

The oligomer size distribution of *h*-IR-100K degradation was comparable with the outcome from NR degradation catalysed with LcpK30. The HPLC chromatogram shown in Figure 4.20b confirmed that the oligomer size distribution was characterised by a preference for five to eight isoprene repeating units with a decreased concentration for shorter and longer oligo-isoprenoids, similar to those reported for NR degradation. Moreover, the molecular weight was relatively similar to other studies that also performed the degradation of *h*-IR-100K but were enzymatically catalysed by Lcp1VH2 as tabulated in Table 4.6.

**Table 4.6.** Molecular weight determination of oligomers derived from *h*-IR-100K with different analytical approaches

	<sup>a</sup> HPLC (g mol <sup>-1</sup> )	GPC (g mol <sup>-1</sup> )	<sup>1</sup> H NMR (g mol <sup>-1</sup> )
This study ( <i>h</i> -IR-100K)	573	978	1056 (14 isoprene units)
Andler <i>et al.</i> (2018)	-	885	-

<sup>a</sup> Calculation for the estimated average  $M_n$  of oligomers from *h*-IR-100K was based on an HPLC chromatogram, and  $^1\text{H}$  NMR spectra are shown in Appendix C4.5.

### 4.3.3 Low molecular weight synthetic *cis*-1,4-polyisoprene rubber made from synthetic rubber (*I*-IR-35K)

The low molecular weight synthetic *cis*-1,4-polyisoprene rubber (*I*-IR-35K) used in this work was purchased with a molecular weight of 35 000 g mol<sup>-1</sup>. The enzymatic reaction was carried out in a co-solvent emulsification system, as described in section 4.2.2, to mimic the well-dispersed polyisoprene system of NR. In the HPLC analysis, 1 mM linalool (C<sub>10</sub>H<sub>18</sub>O) was added into 1 mg mL<sup>-1</sup> samples to estimate the amount of oligomers produced based on the peak area from the corresponding HPLC chromatogram (Figure 4.21). The linalool is a terpenoid with two isoprene units (Appendix C4.6) and was eluted between 16.5 - 16.7 min retention time. The peak area percentage for the oligomers was calculated relative to the peak area (%) of 1 mM linalool.

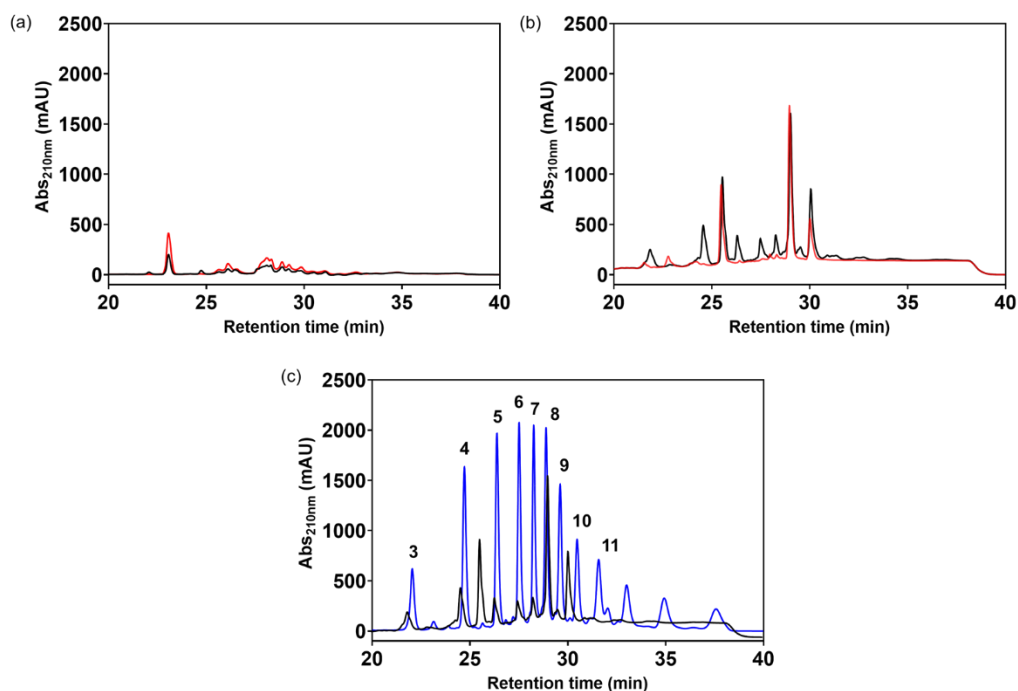


**Figure 4.21.** HPLC chromatogram of dried residual extracts. The sample was extracted using ethyl acetate after 24 hours reaction of (a) non-emulsified *I*-IR-35K with LcpK30 (black line) and without LcpK30 (red line), (b) emulsified *I*-IR-35K with LcpK30 (black line) and without LcpK30 (red line), and (c) emulsified *I*-IR-35K with LcpK30 compared to the positive control of oligomers derived from NR (blue line). The number above the identified peaks indicates the repetitive isoprene units in the cleavage products.



Figures 4.21a and b show the comparison between the HPLC chromatograms from the reactions of non-emulsified *I*-IR-35K and emulsified *I*-IR-35K in the presence and absence of LcpK30. It was evidence that emulsifying the rubber in a co-solvent emulsion increased the chances for LcpK30 to catalyse the cleavage of the C=C bond. Similar peaks that appeared at the retention time of 25.5 min, 29 min, and 30 min in both samples extracted from the reaction of the emulsified *I*-IR-35K with and without LcpK30 might indicate that those compounds were short oligomers resulting from polymerisation during the production of *I*-IR-35K. The relative percentage of these compounds in the reaction of emulsified *I*-IR-35K with and without LcpK30 was relatively similar (Table 4.7).

**Table 4.7.** Oligo-isoprenoids produced by enzymatic cleavage of *I*-IR-35K using purified LcpK30.

Isoprene number (n)	Retention time (min)	Area (A)	Area (%)	$A_{(\text{Oligomer})}/A_{(\text{Linalool})} * 100$
<b>+ LcpK30</b>				
Linalool	16.7	76550.5	56.6	100
3	21.8	4923.3	3.6	6.4
4	24.6	7573.5	5.6	9.9
5'	25.5	10655.8	7.9	13.9
5	26.3	3421.3	2.5	4.5
6	27.5	2798.1	2.1	3.7
7	28.3	2621.1	1.9	3.4
8'	29.0	18341.6	13.6	24.0
9'	30.1	8447.7	6.2	11.0
<b>-LcpK30</b>				
Linalool	16.7	75555.2	70.2	100
5'	25.5	9620.4	8.9	12.7
8'	29.0	17214.6	16.0	22.8
9'	30.0	5233.2	4.9	6.9

The percentage of peak area for the oligomers was calculated relative to the peak area (%) of 1 mM linalool. The highlighted rows are the potential products from *I*-IR-35K degradation catalysed by LcpK30. The HPLC chromatogram, including the linalool peak, is presented in Appendix C4.6. The experiments were performed in triplicates. However due to insufficient amount of samples, the sum of the integrated area was determined from a single replicate.

The HPLC peak pattern of the oligomers derived from *I*-IR-35K differed from those derived from NR (Figure 4.21c). Nevertheless, several separation peaks

were aligned with the NR oligomer peak. Thus, it was concluded that the preference oligomers produced from *I*-IR-35K degradation consist of oligomers with three to seven isoprene units, which is different from previous results with NR when the number of isoprene units obtained was five to eight. Estimation of the compound's relative percentage reveals that the degradation products derived from *I*-IR-35K contained a higher concentration of four isoprene units oligomer.

Further evidence of the ability of LcpK30 to catalyse *I*-IR-35K degradation in a co-solvent emulsion is shown in Figure 4.22. The  $^1\text{H}$  NMR of dried residual extract from emulsified *I*-IR-35K incubated with LcpK30 clearly showed the appearance of aldehyde proton at 9.8 ppm together with methyl proton (1.68 ppm), methylene proton (2 – 2.05 ppm) and olefinic proton at 5.12 ppm which represent the structure of the polyisoprene chain. On the other hand, the peak for aldehyde proton was not detected in the control sample without LcpK30.

The estimated average chain length obtained from the integration of  $^1\text{H}$  NMR proton peaks was equal to 50. The  $M_w$  measured by GPC was  $4026\text{ g mol}^{-1}$  and a broad unimodal size distribution of 2.12 (Appendix C4.4e). Determination of  $M_n$  using GPC ( $1891\text{ g mol}^{-1}$ ) also resulted in a higher molecular weight compared to the ranges of size observed in the HPLC. Nevertheless, considering the results measured by GPC, there would be a possibility that compounds with a length greater than 14 isoprene units ( $>C_{70}$ ) were also present in the products from the degradation of *I*-IR-35K. However, the separation peaks for these compounds were not visible in the HPLC chromatogram, which might be due to very low concentrations or cannot be well separated due to their higher non-polar characteristic, which is contributed by the longer average chain length.

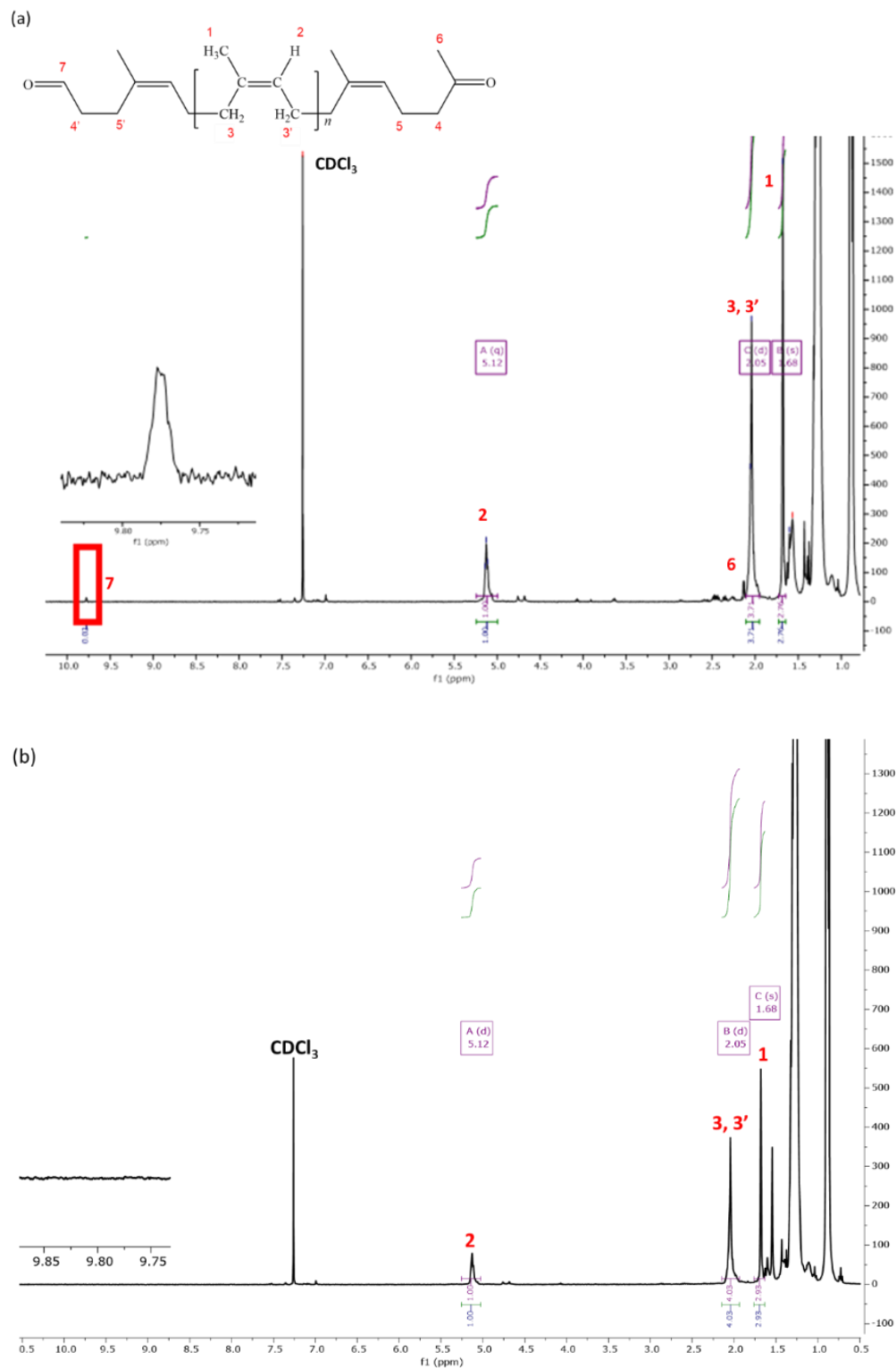


**Figure 4.22.**  $^1\text{H}$  NMR spectrum of (a) LcpK30 catalysed oxidative degradation of emulsified *-IR-35K* and (b) Control setup without enzyme.

#### **4.3.4 Low molecular weight synthetic *cis*-1,4-polyisoprene rubber made from natural rubber (*I*-IR-38K)**

The effect of enzymatic degradation on emulsified *I*-IR-38K was described in this section. Comparison between the HPLC chromatograms from the reactions of non-emulsified *I*-IR-38K and emulsified *I*-IR-38K, in the presence and absence of LcpK30, were shown in Figure 4.23a and b, respectively. Although it indicates that some of the C=C bonds might get cleaved, the chromatogram peak from the non-emulsified *I*-IR-38K degradation sample was inconclusive. Thus, it cannot be compared with a standard oligomer's separation pattern from NR degradation. The chromatogram from HPLC analysis of degradation products derived from emulsified *I*-IR-38K also exhibited different product patterns compared to NR degradation. Interestingly, a more distinctive pattern of separation can be observed. Separation peaks for three until eight isoprene units of NR oligomers were aligned with the oligomer peaks derived from *I*-IR-38K. Weak absorbance peaks were observed for oligomers longer than eight isoprene units (Figure 4.23c).

The absorbance intensity of each peak was much lower than the peak of the NR oligomers, except for the peak at 25 min retention time. An intense peak around retention time at 25 min occurred from both emulsified *I*-IR-38K reactions with and without LcpK30. Given that *I*-IR-38K is a commercial product made by polymerising monomers from NR, this peak could refer to the presence of a shorter polyisoprene chain with four repeating isoprene units that might derive from the polymerisation process.

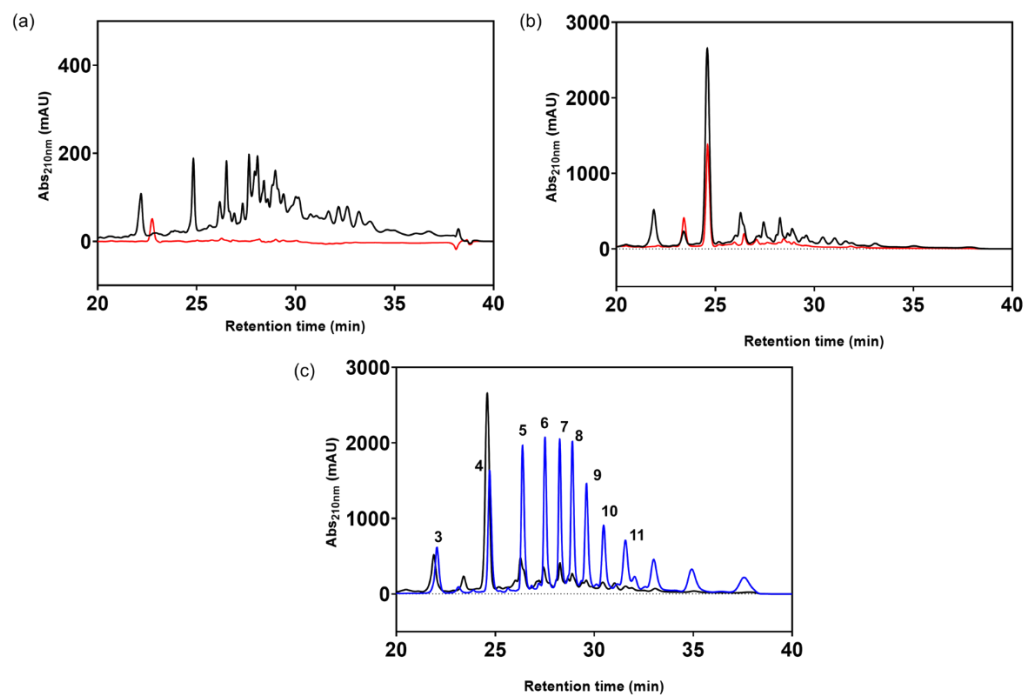


**Figure 4.23.** HPLC chromatogram of dried residual extracts. The sample was extracted using ethyl acetate after 24 hours reaction of (a) non-emulsified *I*-IR-38K with LcpK30 (black line) and without LcpK30 (red line), (b) emulsified *I*-IR-38K with LcpK30 (black line) and without LcpK30 (red line), and (c) emulsified *I*-IR-38K with LcpK30 compared to the positive control of oligomers derived from NR (blue line). The number above the identified peaks indicates the repetitive isoprene units in the cleavage products.

Table 4.8 shows the compound concentrations in the product sample extracted from *I*-IR-38K with and without LcpK30. By comparing the peak area of the oligomer to the peak area of 1 mM linalool, the product with three isoprene units was recognised as the relative abundance of oligomers produced from *I*-IR-38K degradation.

**Table 4.8.** Oligo-isoprenoids produced by enzymatic cleavage of *I*-IR-38K using purified LcpK30.

Isoprene number (n)	Retention time (min)	Area (A)	Area (%)	$A_{(\text{Oligomer})}/A_{(\text{Linalool})} * 100$
<b>+LcpK30</b>				
Linalool	16.71	120065.40	62.97	100
3	21.89	8884.60	4.66	7.40
3'	23.40	3278.70	1.72	2.73
4'	24.59	39601.60	20.77	32.98
5	26.27	6898.20	3.62	5.75
6	27.44	2574.40	1.35	2.14
7	28.26	2931.80	1.54	2.44
8	28.88	2077.40	1.09	1.73
9	29.59	959.30	0.50	0.80
10	30.43	1284.90	0.67	1.07
11	31.03	1285.10	0.67	1.07
12	33.08	818.50	0.43	0.68
<b>-LcpK30</b>				
Linalool	16.62	138267.20	84.79	100
2'	20.24	353.00	0.22	0.25
3'	23.41	5443.60	3.34	3.94
4'	24.60	17473.50	10.72	12.64
5'	26.45	1532.40	0.94	1.11

The percentage of peak area for the oligomers was calculated relative to the peak area (%) of 1 mM linalool. The highlighted rows are the potential products from *I*-IR-35K degradation catalysed by LcpK30. The HPLC chromatogram, including the linalool peak, is presented in Appendix C4.6. The experiments were performed in triplicates. However due to insufficient amount of samples, the sum of the integrated area was determined from a single replicate.

The  $^1\text{H}$  NMR analysis on the dried residual extracted from the degradation of emulsified *I*-IR-38K confirmed the presence of aldehyde, thus supporting that the C=C bond cleavage of *I*-IR-38K has occurred (Figure 4.24). The data obtained from GPC and  $^1\text{H}$  NMR results in overestimating the average molecular weight of the oligomers at  $M_n = 1465 \text{ g mol}^{-1}$  and  $M_w = 3545 \text{ g mol}^{-1}$  with an average length of 30 isoprene units. Similar observations were already encountered and discussed in Section 4.3.3.

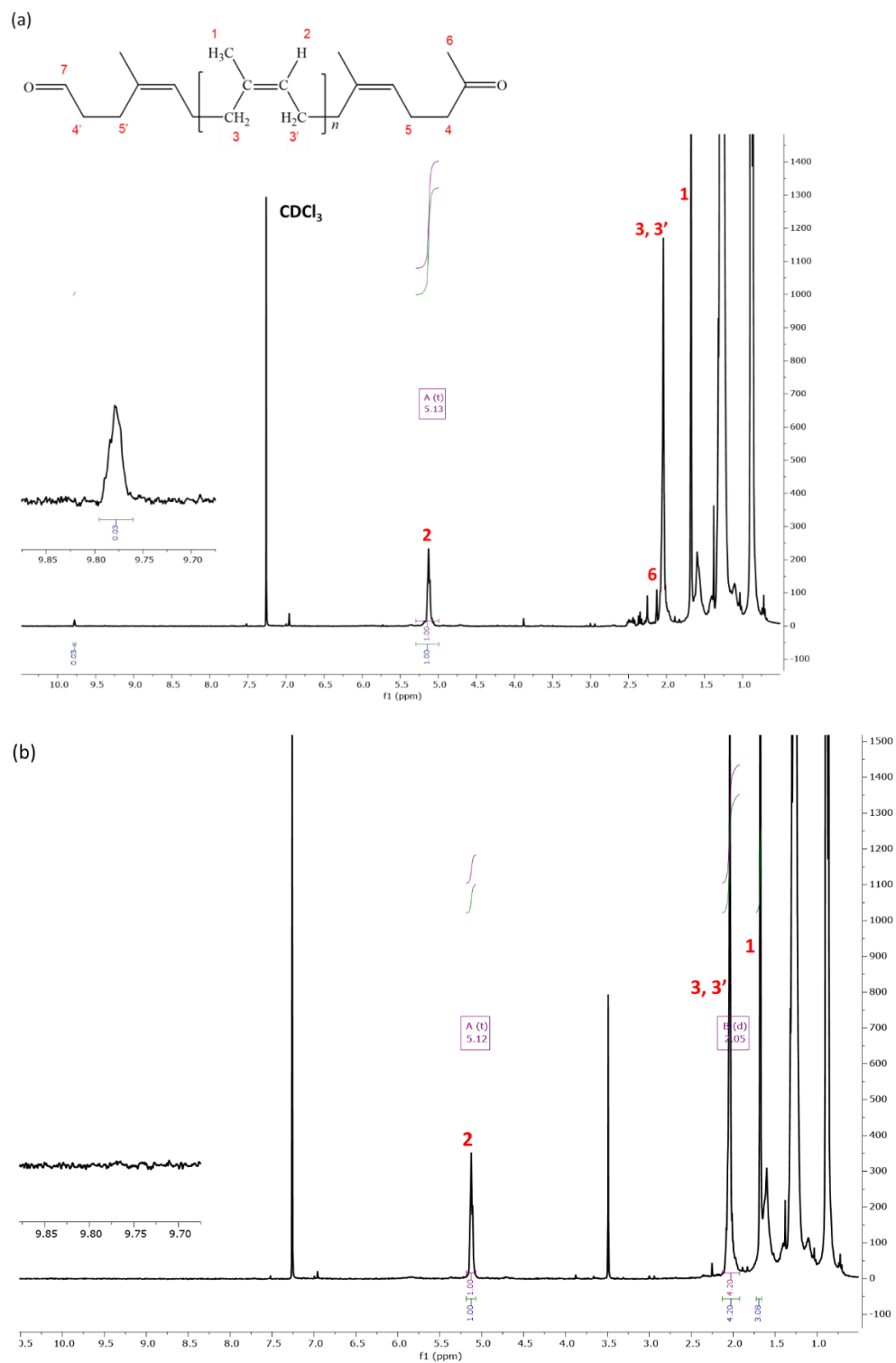


**Figure 4.24.**  $^1\text{H}$  NMR spectrum of (a) LcpK30 catalyzed oxidative degradation of emulsified *I*-IR-38K and (b) Control setup without enzyme.

#### 4.3.5 Polybutadiene rubber

The ability of LcpK30 to catalyse the cleavage of the C=C double bond in the polybutadiene backbone was evaluated. It is hypothesised that the efficiency of LcpK30 activity to catalyse the oxidative cleavage of the C=C bond will be influenced by the ratio of butadiene and vinyl units that might hinder the accessibility of LcpK30 to the C=C bond. This work used several L-PBRs with a molecular weight ranging from 1300 g mol<sup>-1</sup> to 5000 g mol<sup>-1</sup> as the substrates. These polymers exhibit varying degrees of viscosity based on their molecular weight. Thus, the L-PBR was prepared in an emulsion stabilised with *n*-tetradecane before mixing with the enzyme.

HPLC chromatogram of all L-PBRs (PB-5000, PB-2200, PB-1300, PB-1500 and PB-5000S) before and after dissolving in *n*-tetradecane was performed. The results were compared with the extracted samples from L-PBR incubated with and without LcpK30 in an emulsion system (Appendices C4.7 – C4.11). Based on the HPLC chromatogram of the dried residual extract, a firm conclusion on the presence of oligomeric products could not be drawn. The HPLC chromatogram for samples extracted from the reaction without LcpK30 exhibited similar peak patterns to the samples retrieved from the reaction with LcpK30. An intense peak at a retention time of 29 min with a split end was detected in all emulsified L-PBR. Commonly, single peak splitting could be due to two components eluting closer.

Further analysis with <sup>1</sup>H NMR confirmed the absence of oligomeric products with carbonyl ends. There were no significant differences between the <sup>1</sup>H NMR spectra of the untreated L-PBR (L-PBR before dissolving in *n*-tetradecane) with the dried residuals extracted from the emulsified L-PBR incubated with and without LcpK30 as shown in Appendices C4.12 – C4.15. Nevertheless, an additional peak appeared from samples retrieved from the reaction of emulsified



PB-2200 in the presence of LcpK30 at 5.12 ppm (Figures 4.25 and 4.26). The appearance and disappearance of several other small peaks were also observed in the samples extracted from the reaction with and without LcpK30, thus indicating that there might be minor chemical changes to the L-PBR that might be contributed either enzymatically or physically (stirring and ultrasonic vibrating).

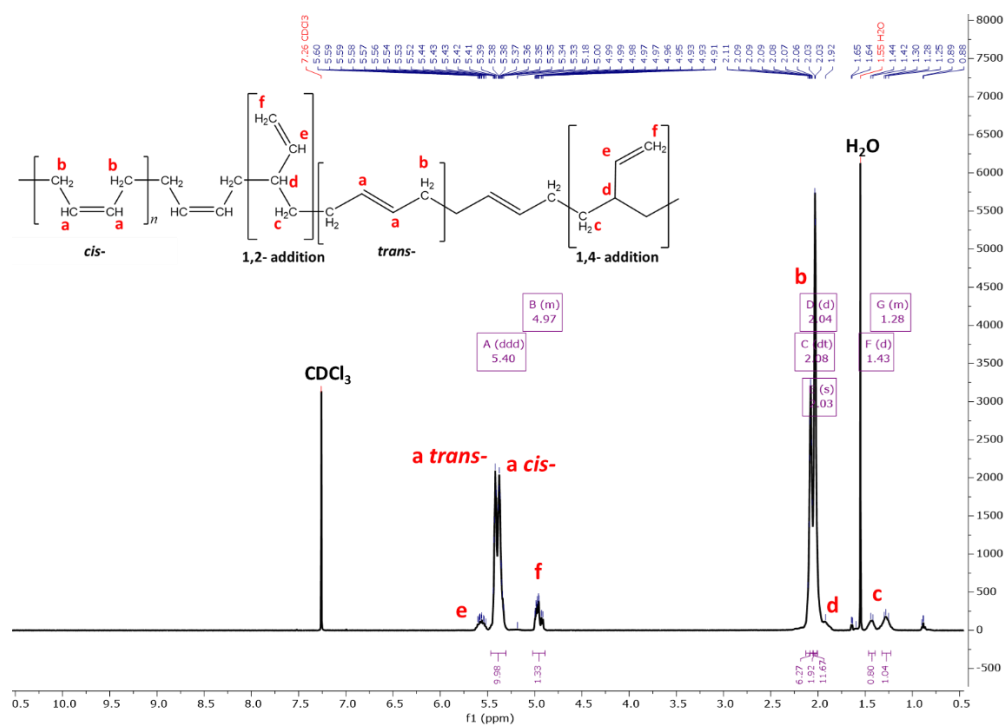


**Figure 4.25.** General chemical structure and <sup>1</sup>H NMR spectra of polybutadiene rubber with *cis*- and *trans*-mixture and vinyl group 1,2- or 1,4- addition.

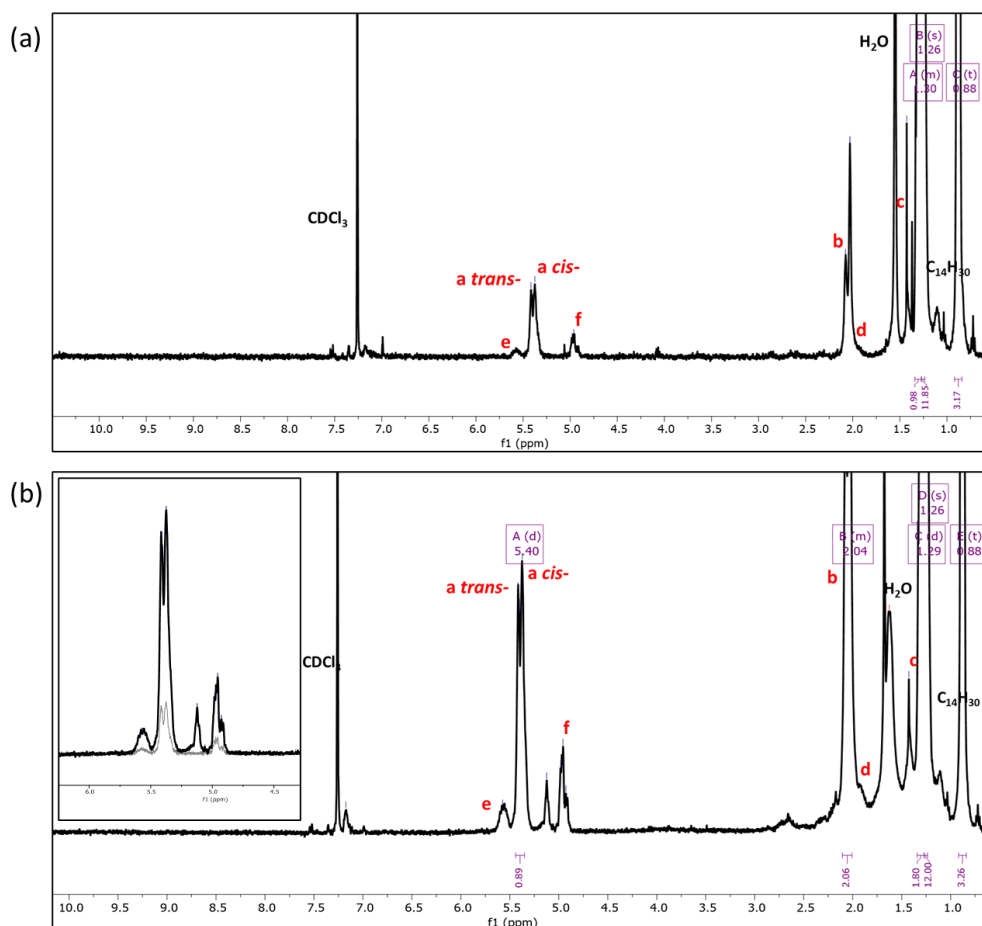


**Figure 4.26.**  $^1\text{H}$  NMR spectrum of dried residues extracted using ethyl acetate. (a) Control setup of emulsified PB-2200 without LcpK30 and (b) emulsified PB-2200 with LcpK30 analysed in  $\text{CDCl}_3$ . Inserts are zoomed sections of superimposed spectrums of emulsified PB-2200 without LcpK30 (grey) and emulsified PB-2200 with LcpK30 (black) that show the appearance of an additional peak between the chemical peak of methyldene proton (f) and 1,4- olefinic proton for *cis*- and *trans*- (a).

#### 4.4 Discussion

In *in vitro* enzymatic reactions, the capacity of the reaction to sustain the stability and activity of the enzyme is crucial. Most of the time, the reaction must be carried out in an aqueous solution using a substrate that is water soluble. However, there is a growing interest in finding more adaptable enzymes that can change their specificity towards larger and more hydrophobic substrates. Altering the substrate's shape is an alternative approach to enhance the enzymatic degradation of large and hydrophobic substrates. Warneke *et al.* (2007) prepared synthetic polyisoprene rubber by cryomilling it as a carbon source for cultivating rubber-degrading bacteria.<sup>172</sup> This approach has been

applied in subsequent studies involving *in vitro* enzymatic catalysed biodegradation of rubber.<sup>134,137,212,229</sup> Altenhoff *et al.* (2019) have introduced an additional pretreatment step.<sup>203</sup> Degradation of carbon black-filled vulcanised rubber (CFVR) was improved by pre-treating the cryo-milled particles of CFVR with organic solvents such as acetone-cyclohexane mixture, cyclohexane or chloroform.

In this study, several examples of modified and synthetic rubber with various physical morphologies, chemical structures, and molecular weights were pre-treated and prepared into different forms, such as film, particles, and co-solvent emulsions. The result proved that the pre-treatment method can assist the contact between the enzyme and the hydrophobic substrates. The impact of different chemical structures and substrate forms was investigated by characterising the degradation products. Combining the findings from analysis with the HPLC, <sup>1</sup>H NMR, and GPC could give a more comprehensive view of the pattern of the products generated. However, GPC and <sup>1</sup>H NMR result in considerable differences in estimating the molecular weight of the oligomers derived from ENR and synthetic IR when compared with the oligomer size that is separated by HPLC.

Nonetheless, these discrepancies were not peculiar as the estimation of NR oligomers by <sup>1</sup>H NMR also results in a higher average chain length with 18 isoprene units.<sup>257</sup> As for GPC, it gives a more representative molecular weight of the overall population of the oligomers. However, the measurement could be influenced by larger molecules that are too low in concentration to be well separated in HPLC. Based on <sup>1</sup>H NMR, characterisation of the compound chemical environment allows confirmation of the presence of aldehyde and other functional units of the rubber chemical structure.

ENR consists of epoxide groups randomly distributed along the polymer chain, either in blocks or scattered among C=C units. The possible arrangement of isoprene and epoxidised isoprene unit in ENR was well described by Bradbury and Perera (1985).<sup>258</sup> The study established a group of eight possible positions of three monomers (triad) representing the structure chain of ENR. Chapter 1, section 1.1.4 illustrates the triad sequences of eight possible positions. Chemical degradation of ENR using sodium nitrite and hydrogen peroxide produced its low molecular weight counterpart called liquid ENR (LENR) with a molecular weight of  $\pm 10\ 000\ \text{g mol}^{-1}$  determined by GPC.<sup>67</sup> Oxidative degradation method on ENR using cobalt acetylacetonate (CAA) as an oxidising agent for chain scission reaction resulted in hydroxyl-terminated liquid epoxidised natural rubber (HTLENR) with an average molecular weight of  $M_n = 5163\ \text{g mol}^{-1}$  and  $M_w = 58\ 087\ \text{g mol}^{-1}$ .<sup>69</sup>

In this study, it has been demonstrated that LcpK30 can catalyse the cleavage of C=C bonds in ENR with a 25 % epoxidation level. The oligomers produced after ENR25 degradation are expected to consist of an inconsistent number of isoprene units with an epoxide ring in addition to the carbonyl groups at both ends. The aldehyde terminal group of the oligomer would probably comprise two species, one next to the isoprene unit and the other next to the epoxy-isoprene unit. However, no further analysis was performed to confirm this observation. Interestingly, the product of ENR25 degradation catalysed by LcpK30 would probably consist of oligomers or partially degraded polymers with molecular weight ranges from  $1000\ \text{g mol}^{-1}$  to  $20\ 000\ \text{g mol}^{-1}$ . These ranges of molecule size have also been obtained from the degradation of ENR into LENR. Nevertheless, results obtained from this work provide a general idea of the degradation product pattern of enzymatically catalysed degradation of ENR.

While working on this project, several studies on Lcp1VH2, a homolog to LcpK30, have been published and shown to be capable of cleaving the polyisoprene chain of synthetic rubber, including the higher molecular weight of IR and vulcanised rubber.<sup>137,203,212</sup> Compared to LcpK30, the Lcp1VH2 was claimed to have a better rubber degradation activity because the enzyme is produced by a non-clearing zone former bacteria that initiates rubber degradation by attaching to the substrate.<sup>85</sup> Nevertheless, in this current work, the result has shown that the LcpK30 also has the capability to degrade the synthetic IR. Degradation of synthetic IR catalysed by LcpK30 results in similar oligomer sizes as produced from the reaction catalysed by Lcp1VH2. Another highlight from this work is the ability of LcpK30 to catalyse the degradation of synthetic IR with low molecular weight (*I*-IR-35K and *I*-IR-38K). Preparation of the *I*-IR-35K and *I*-IR-38K in a co-solvent emulsion system to mimic the stable colloidal emulsion of NR latex has improved the accessibility of the polymer to the enzyme and cleaved the C=C bond, preferably into oligomers with three to five and seven isoprene unit.

A study by Enoki *et al.* (2003) prepared an emulsion of *cis*- and *trans*-1,4-type polybutadiene in a detergent system using Plysurf A210G, widely used to prepare emulsion for plastic degradation.<sup>259,260</sup> However, using surfactants at a certain concentration could denature the enzymes or inhibit the enzyme activity.<sup>260</sup> In a more recent study, the degradation of synthetic rubber with a mixture of *cis*- and *trans*-polyisoprene structures has been well performed and described by Adjedje *et al.* (2021). They suggested that the co-solvent emulsification system can be applied to biodegrade other types of rubber.<sup>111</sup> However, several factors might affect the stability of a surfactant-free oil-in-water emulsion, such as the polymer molecular weight and chemical

structure, types of hydrocarbon solvent and the ability of the polymer that attaches on the solvent droplet surface to create steric repulsion.<sup>261,262</sup>

In this study, the emulsified rubber was prepared using a rather longer hydrocarbon (*n*-tetradecane) with hydrophobic polymers of molecular weight ranging from 1300 g mol<sup>-1</sup> to 38 000 g mol<sup>-1</sup>. Thus, the colloidal stability of the emulsified rubber was governed by the steric repulsion among the polymer chains adsorbed on the *n*-tetradecane droplet surface. The hydrophobic part of the solvents or polymer contributes to the stability of a surfactant-free emulsion. An increase in the hydrocarbon chain length of alkanes (in the order of *n*-hexane, *n*-octane, *n*-decane, *n*-dodecane, *n*-tetradecane and *n*-hexadecane) improved the colloidal stability of surfactant-free oil droplets.<sup>262</sup> Additionally, adding hydrophobic polymers to short-chain hydrocarbons may assist the colloidal stability of oil-in-water emulsions without surfactants.<sup>246</sup>

Enzymatic catalysed degradation of PBR was first reported by Enoki *et al.* (2004). The biodegradation was performed in emulsified *cis*- and *trans*-1,4-polybutadiene by horseradish peroxidase enzyme with a mediator molecule, 1-hydroxybenzotriazole nucleus. The PBR with different stereochemistry of the double bond has an average weight reduction of 38 %, whereas a pure *trans*-1,4-PBR polymer was not affected by the enzymatic treatment.<sup>263</sup> A gram-negative bacterium, the *Moraxella* strain, has been identified as a PBR-degrading bacteria. The bacteria can degrade low molecular weight 1,4-type polybutadiene ( $M_n = 2350 \text{ g mol}^{-1}$ ). However, the bacteria cannot degrade PBR of higher molecular weight ( $M_n = 16\ 100 \text{ g mol}^{-1}$ ) due to the vinyl branching in the polybutadiene that prevents microbial degradation.<sup>264,265</sup> Thus, the inability of LcpK30 to catalyse the degradation of PBR in this study was concluded mainly due to the higher vinyl content and difference in the stereochemistry of the PBR, either a pure *cis*- or *trans*- PBR.

#### 4.5 Summary and Conclusions

A biotechnology-based solution using an enzyme such as LcpK30 is a sustainable approach for rubber degradation. Still, more discoveries about LcpK30's potential to degrade other synthetic diene rubbers are needed. Thus, enzymatic degradation of modified and synthetic rubber with variable morphology and molecular weight was worth investigating. This chapter discussed oxidative enzymatic degradation catalysed by LcpK30 on several rubbers such as ENR, high and low molecular weight synthetic IR and PBR. The aim was to assess the catalysing effect of LcpK30 on the C=C bond cleavage of these substrates with different chemical structures and morphologies. Table 4.9 summarises the finding of the rubber's degradation catalysed by LcpK30.

The epoxidation level influenced the catalytic activity of LcpK30 on ENR. Higher epoxidation levels (> 25 %) reduced the chances for LcpK30 to reach the C=C double bond. Scrutinised analysis based on the  $^1\text{H}$  NMR spectra predicted the chemical structure of the degradation products derived from ENR25 was in an average length of  $\approx 300$  repeating units of isoprene and epoxy-isoprene in a 75 % to 25 % ratio. However, this result was not comparable with GPC measurement. Moreover, structural analysis of ENR using  $^1\text{H}$  NMR is quite challenging due to the randomness of epoxy-isoprene units along the ENR chains. In contrast, much smaller  $M_n$  and  $M_w$  of the oligomers were determined by GPC, which could be a better representative of the average molecular weight. The presence of minor oligomeric products consisting of aldehyde that was predicted to be near the epoxide groups was shown by the appearance of a second aldehyde peak.

The improvement of rubber degradation catalysed by enzymes has been rendered possible by transforming rubber morphology into particles. Evidence

shows that the interface between the enzyme and the polyisoprene chain increased by grinding the rubber into micron-sized particles.<sup>212</sup> Although the degradation of *h*-IR-100K in film and macroparticle form was possible, LcpK30 exhibited better catalytic activity on degradation of *h*-IR-100K in 600  $\mu\text{m}$  particles and produced oligomers similar to those derived from NR.

In this study, *n*-tetradecane has been demonstrated to be able to form droplets with hydrophobic rubber molecules. The droplet-like particles of both molecules were prepared by sonication and vigorous mixing in the aqueous phase. These droplets were stabilised in an aqueous solution by steric repulsion among the polymer chains adsorbed on the droplet surface. As the droplet size decreases, the surface area of the interaction between the enzyme and the polymer chain increases, thus improving the enzyme's catalytic activity. Enzymatic degradation of *h*-IR-35K and *h*-IR-38K with *cis*-1,4 configuration only occurred when the polymers were emulsified with *n*-tetradecane as the co-solvent. The oligo-isoprenoid separation patterns by HPLC were dissimilar to the oligomeric products derived from NR.

The presence of other functional groups due to the rubber chemical structure could impact the frequency and availability of the C=C bond throughout the polymer chain. Eventually, it affected the degree to which LcpK30 could not reach and cleave the C=C bond oxidatively. This statement was supported by the finding on the attempt to degrade PBR in which no evidence of degradation was detected. In conclusion, differences in the enzymatic degradability of LcpK30 were reflected in the changes in the substrate's chemical structure and physical morphology during the degradation.



**Table 4.9.** A summary of the findings from the experiment utilising LcpK30 as the catalyst to oxidatively cleave the C=C bonds in different types of rubber.

No	Type of rubber	Sample name used in this study	Substrate form	Biodegradation catalysed by LcpK30	Oligomers	
					Yield	<sup>a</sup> Molecular weight (g mol <sup>-1</sup> )
1	Epoxidised natural rubber 25 %	ENR25	Emulsion	Yes	5 % (25 mg from 100 mg mL <sup>-1</sup> in a 5 mL reaction)	1324
2	Epoxidised natural rubber 50 %	ENR50	Emulsion	No	-	-
3	High molecular weight <i>cis</i> -1,4-polyisoprene	<i>h</i> -IR-100K	<i>Particles</i>	Yes	66 % (33 mg from 10 mg mL <sup>-1</sup> in a 5 mL reaction)	978
4	Low molecular weight <i>cis</i> -1,4-isoprene rubber made from synthetic rubber	<i>l</i> -IR-35	Co-solvent emulsion	Yes	nd	1891
5	Low molecular weight <i>cis</i> -1,4-isoprene rubber made from natural rubber	<i>l</i> -IR-38K	Co-solvent emulsion	Yes	nd	1465
6	Polybutadiene rubber Vinyl -1,2: 45-55 %	PB-1300	Co-solvent emulsion	No	-	-
7	Polybutadiene rubber Vinyl -1,2: 15-25 %	PB-1500	Co-solvent emulsion	No	-	-
8	Polybutadiene rubber Vinyl -1,2: 15-25 %	PB-2200	Co-solvent emulsion	No	-	-
9	Polybutadiene rubber Vinyl-1,2: 10-20 %	PB-5000	Co-solvent emulsion	No	-	-
10	Polybutadiene rubber <i>cis</i> - and <i>trans</i> - 1,4 80 % vinyl-20 %	PB-5000S	Co-solvent emulsion	No	-	-

<sup>a</sup> Based on the average number molecular weight ( $M_n$ ) determined by Gel Permeation Chromatography

nd : not determine

## CHAPTER 5

### CHARACTERISATION OF LcpK30-SUBSTRATE INTERACTIONS AND DESIGN OF A MUTANT WITH EXPANDED SUBSTRATE SCOPE

#### Background

Despite an increasing understanding of the structure and catalytic function of Lcps, a practical method for rubber degradation and application of the degradation products has not yet been developed. These challenges could be addressed through protein engineering approaches, which require understanding the interaction between substrate and protein.<sup>168</sup> Previous studies have extensively characterised the structure and activity of Lcps by introducing mutations. However, research on protein engineering to address the challenges relating to LcpK30 is still lacking.

A high molecular weight substrate with a long polymeric chain could be highly flexible. It can adopt many conformations that could induce different conformational changes in the protein when accommodated into the protein cavity, especially at the binding sites where hydrophobic interactions between the ligand and the protein are most prominent.<sup>266</sup> Thus, it is essential to investigate the interaction of *cis*-1,4-polyisoprene with the active site of LcpK30 to understand the catalysis, substrate binding and product dissociation. This information is useful for designing mutants at specific amino acid positions of the protein based on rational design protein engineering strategy.

The work in this chapter was divided into two parts (Sections 5.1 and 5.2). The first part is on the computational modelling of molecular interaction between LcpK30 and *cis*-1,4-polyisoprene. The potential access pathways of *cis*-1,4-polyisoprene to the active site of LcpK30 were explored using the CAVER-Pymol plug-in 3.0.3 programme to identify relevant hydrophobic tunnels large enough to accommodate the substrate.<sup>175</sup> Following that, supramolecular

docking of the C<sub>50</sub> substrate model containing ten C=C bonds (10 repeating isoprene units, C<sub>50</sub>H<sub>82</sub>), which was deemed sufficiently large to provide valuable insights into the interaction of the polymer chain with the enzyme, was performed. Protein-ligand docking was used to predict ligands' location, conformations, and interactions inside the active site. Findings from this part of the work were used to predict potential sites to introduce mutation.

The second part of the work discussed in this chapter was on introducing a mutation in LcpK30 to create a mutant with enhanced activity towards its native substrate (*cis*-isoprene) and preferential towards different substrates, particularly *trans*-isoprene. The criteria for choosing the potential site for mutation was based on three approaches. Firstly, an understanding of the structure and catalytic mechanism of Lcps was obtained from previous studies.<sup>117,120,125,135</sup> Secondly, further understanding of the protein-ligand interaction was acquired via computational techniques using a model ligand with ten C=C double bonds. Thirdly, the potential single point mutation was further selected by comparing the protein sequences and structure of LcpK30 with its homolog, LcpSH22a. The mutants were first designed by computational modelling, followed by prediction on the mutants' tunnel pathway and protein-ligand interaction using computational techniques. Subsequently, further experimental investigations were conducted. The mutant's proteins were expressed, characterised and compared to the wild-type LcpK30. Enzymatic degradation of polyisoprene chains with *cis*- or *trans*- configuration was performed to check for any changes in the substrate scope.

To summarise, the work presented here is to improve the understanding of the interaction between LcpK30 and the substrate. It also discusses the findings on mutation through rational design, followed by an introduction to the mutation by site-directed mutagenesis. The expressed protein of a mutated LcpK30 was

characterised, and the catalytic activity and substrate specificity were tested on *cis*- and *trans*- polyisoprene rubber.\*

---

\* Parts of this chapter were included in an article entitled 'Computational investigation of *cis*-1,4-polyisoprene binding to the latex clearing protein LcpK30' that has been sent for publication. The preprint of the article can be accessed via <https://doi.org/10.1101/2023.06.26.546638>.

## **5. 1 Computational modelling of molecular interaction between LcpK30 and *cis*-1,4-polyisoprene**

In this work, the data was gathered based on the analysis using computational tools, including (1) CAVER-Pymol plug-in 3.0.3 to obtain an overview of the substrate and products transport pathway in LcpK30 and (2) GOLD docking to scrutinise the interaction of the protein and ligand complexes by analysing the conformations characteristics. The residues involved in the interaction and the contact between the protein and the ligand were analysed using a Protein-Ligand Interaction Profiler (PLIP).

### **5.1.1 Identification of tunnels in LcpK30**

This work was carried out to identify the overall topology of LcpK30 tunnels, the tunnel size and length, and the residues defining the tunnel bottleneck (the narrowest part of the tunnel). Putative tunnels were identified within the crystal structure of LcpK30 in the open state, using the CAVER-Pymol plug-in 3.0.3 to obtain a general overview of potentially important pathways for substrate access from the surface to the active site. This plug-in provides a graphical interface for setting up the calculation and allows interactive visualisation of tunnels or channels in protein static structures.<sup>285</sup>

Four tunnels were identified, and their average radius, lengths, and bottleneck radius (the narrowest parts of the tunnels) were outlined in Table 5.1. Tunnels 1 and 2 had the highest throughput and thus the highest probability of being used as a substrates transport route. These tunnels are near the heme cofactor in the active site and were lined up by residues of high importance for LcpK30 activity: Glu148, Arg164, Lys167 and Thr168 (Figure 5.1a).<sup>117,135</sup>

**Table 5.1.** The features of dominant tunnels were calculated using the LcpK30 crystal structure in the open state (PDB 5O1L).

Tunnel <sup>a</sup>	Average throughput <sup>b</sup>	Bottleneck radius (Å) <sup>c</sup>	Average radius (Å)	Average length (Å) <sup>d</sup>	Average curvature <sup>e</sup>
1	0.62	0.96	1.73	13.43	1.2
2	0.50	0.96	2.00	25.61	1.24
3	0.46	0.96	1.71	21.83	1.65
4	0.34	0.96	1.64	27.66	2.03

<sup>a</sup> ranking of a given cluster based on the throughput; <sup>b</sup> Probability that the pathway is used as a route for transport of the substances (throughput = e-cost, where cost is calculated by the sum of the cost of the tunnel's Voronoi edges); <sup>c</sup> the narrowest part of the tunnel; <sup>d</sup> length of the tunnel from the starting point to the protein surface; <sup>e</sup> shape of the tunnel as the ratio between the length of the tunnel and the shortest possible distance between the starting point and the tunnel ending point.

The radius of tunnels 1 and 2 ranged from 1 Å to 2.8 Å, with a bottleneck radius of 0.96 Å near the heme (Figure 5.1b). A wider tunnel radius was found towards the outer surface of the protein. There was a significant difference in the length of the tunnels from the central heme to the protein surface, with tunnel 2 being about twice as long as tunnel 1. Whilst a shorter tunnel such as tunnel 1 may generally give quicker access of substrates to the active site, in this case, where the substrate is a long polymer, the longer tunnel 2 may provide more opportunity for interaction with a polymeric substrate.

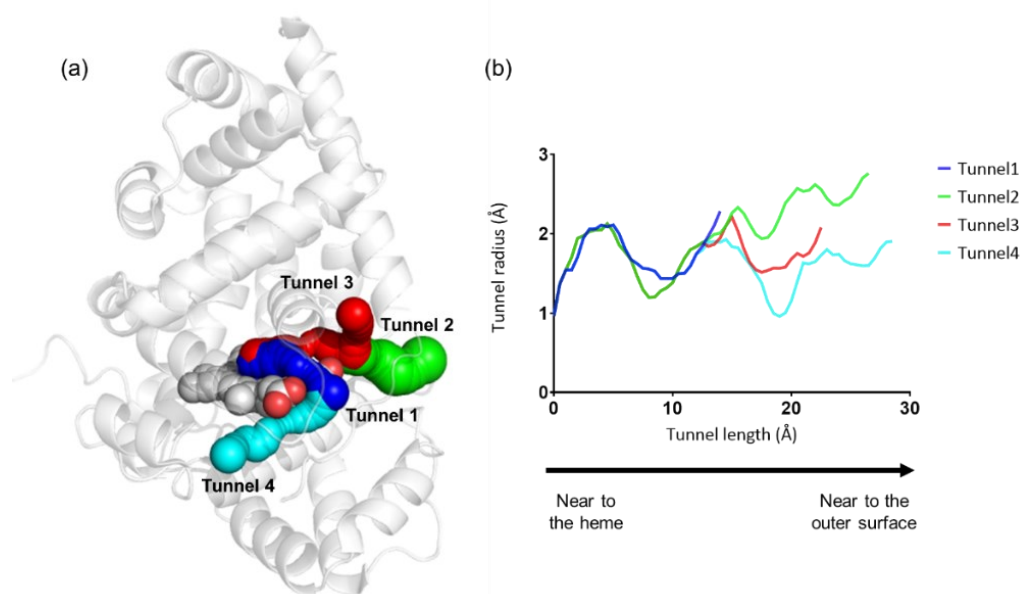


**Figure 5.1.** Tunnel mapping in LcpK30. (a) Four tunnels were identified by CAVER-Pymol plug-in 3.0.3 (tunnel 1 in blue, tunnel 2 in green, tunnel 3 in red and tunnel 4 in cyan). (b) Tunnel profiles for the dominant tunnels (T1-T4) show the variation of tunnel radius with length from the heme towards the opening of the tunnels near the protein's outer surface.

The width of the substrate molecule was determined by measuring the distance between atoms, as indicated in Figure 5.2, to check the suitability of the *cis*-1,4-polyisoprene substrate molecule to accommodate inside the tunnel.

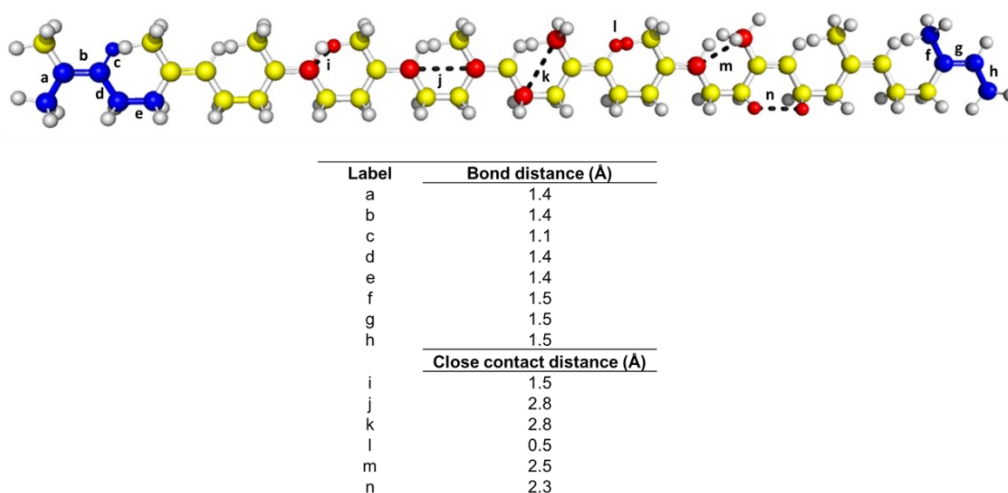


**Figure 5.2.** Distances between different atoms in the *cis*-1,4-polyisoprene chains are used to estimate the maximum width of the chain in an extended conformation. The distances were measured between the indicated carbon atoms that represent the bond length (blue) and close contact atoms (red). The addition of C-H distances is anticipated to add max. 1.1 Å.

The radius of both tunnels at a certain length was smaller than the estimated width of the *cis*-1,4-polyisoprene substrate molecule, which suggested that significant conformational changes of the protein are required to accommodate the hydrophobic chains of the large polymeric substrates through this pathway. Alternatively, these tunnels are also suited for transporting smaller oxygen molecules to the heme. Furthermore, tunnel 2 has a wider opening (2.8 Å) at the protein surface lining up by residues Glu392, Gly393, Arg394, Arg395, and Ile396, which agrees well with the estimated thickness of *cis*-1,4-polyisoprene and which could represent a potential gateway for the substrate access to the active site. The characterisation of these tunnels was further investigated and confirmed using the fpockets program and Molecular Dynamic (MD) simulation. The results obtained from fpockets analysis and MD simulation were discussed in the article entitled 'Computational investigation of *cis*-1,4-polyisoprene binding to the latex clearing protein LcpK30.

### **5.1.2 Molecular docking of the *cis*-1,4-polyisoprene substrate into LcpK30**

The major oligomers produced in the reaction with LcpK30 typically range from C<sub>15</sub> to C<sub>35</sub> (5 to 7 repeating isoprene units). Therefore, a substrate model with ten repeating isoprene units (C<sub>50</sub>H<sub>82</sub>) was considered sufficient to provide valuable insights into the interaction of the polymer substrate with the enzyme. The crystal structure of LcpK30 in its open conformation was used as the protein receptor, where a dioxygen molecule was manually coordinated to the Fe<sup>2+</sup> in heme. The binding site included all atoms within 10 Å of radius from the central iron atom in heme, which also contained the residues reported to be part of the active site of LcpK30 (Arg164, Lys167 and Thr168).<sup>135</sup>

Initially, docking calculations were carried out using three scoring functions in the GOLD software: ChemPLP, Chemscore and Goldscore with different parameter files, either default or p450\_pdb. The p450\_pdb parameter file is

derived from contact statistics from (Protein Data Bank) PDB databases for docking to heme-containing proteins. In this initial standard docking approach, the substrate was fully flexible while the protein was kept rigid (referred to as rigid docking). All protein-ligand conformations obtained using the Goldscore scoring function appeared with extremely low fitness scores (negative value) (Appendix C5.1). The negative binding scores might be contributed by the repulsion outbreak in which the repulsion energy computed between the clashed atom pairs can overwhelm the other terms in the scoring function.<sup>267</sup>

Similar docking solutions were obtained when using Chemscore scoring functions with p450\_pdb parameter files. Thus, ChemPLP and ChemScore with default parameters were selected because they perform well for lipophilic binding sites and accurately model the steric complementarity between protein and ligand, which is interpreted as a fitness score. A higher fitness score indicates a higher probability that a ligand will bind to a protein in the given docking position.<sup>179</sup> However, when using the rigid docking approach, even the highest-ranked poses had a very low fitness score, indicating that significant steric clashes occurred between protein and substrate (Table 5.2 and Figure 5.3). Therefore, this docking approach was unsuitable for accurately describing the interaction between LcpK30 and the polyisoprene substrate.



**Table 5.2.** Docking solutions obtained from rigid docking within GOLD software, ranked based on the fitness score from highest to lowest.

Rank	Fitness Score	<sup>a</sup> C=C unit number closest to Fe-O <sub>2</sub> complex	<sup>b</sup> Distance of C=C to the oxygen atom	
			-H <sub>2</sub> C-C=	=C-CH <sub>3</sub>
<b>ChemPLP docking protocol</b>				
1	21.38	7	4.7	6
2	-11.15	6	5.5	6.2
3	-46.45	7	4.1	5.5
4	-51.25	8	4.7	4.1
5	-53.86	7	4.6	5.2
6	-57.67	4	4.6	5
7	-60.25	4	5.4	6.6
8	-90.1	7	4.7	4.2
9	-103.81	3	2.5	1.4
10	-112.87	3	2.4	3.1
<b>ChemScore docking protocol</b>				
1	25.56	7	4.9	4.6
2	21.11	4	4.8	4.4
3	12.5	7	4.7	3.8
4	6.27	8	5.3	4.2
5	3.4	4	5	4
6	2.7	4	4.4	4
7	2.42	3	2.5	3.3
8	-3.48	4	5	4.5
9	-7.52	7	5.8	4.5
10	-31.98	7	4.7	4.8

<sup>a</sup> the first C=C unit number was counted from the end terminal with two methyl group R-C=C-(CH<sub>3</sub>)<sub>2</sub> – see scheme

<sup>b</sup> the distance was measured from each C atom in the double bond to the distal O atom of the Fe-O<sub>2</sub> complex

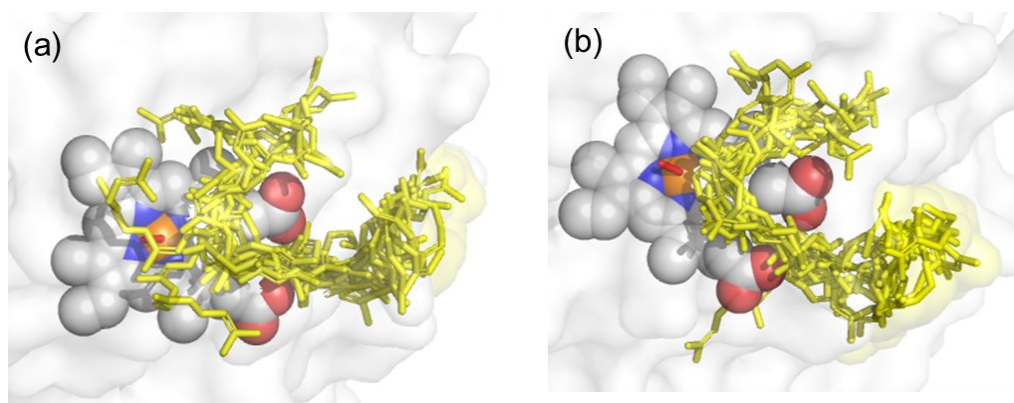


**Figure 5.3.** Superimposed of ten docking poses result from rigid docking of *cis*-1,4-polyisoprene C<sub>50</sub>H<sub>82</sub> within LcpK30. (a) Protein-ligand conformations obtained using the ChemPLP scoring function; (b) Protein-ligand conformations obtained using ChemScore scoring function.

To improve docking quality, induced fit (flexible) docking was carried out, accounting for the flexibility of the receptor by allowing full torsional flexibility of ten amino acid sidechains in the active site of LcpK30 (see Chapter 2.2.12.3). Increasing the defined binding site size from 10 Å to 15 Å was tested but was not suitable. Although higher fitness scores were obtained (Table 5.3), the oligomeric substrate tended to dock preferentially at the surface of the protein without interaction with the heme and the active site of LcpK30 (Figure 5.4).

**Table 5.3.** Impact of the size of the defined protein binding site on the docking results. The ten docking solutions are ranked from highest to lowest based on the fitness score.

Scoring function	ChemPLP	
	Flexible	
Docking protocol	10 Å	15 Å
Radius of the binding site	10 Å	15 Å
Rank	Fitness score	
1	78.94	79.33
2	67.26	75.52
3	64.8	73.59
4	40.51	70.2
5	29.74	69.14
6	21.37	53.44
7	20	53.17
8	-13.14	48.69
9	-42.16	42.23
10	-60.12	38.18

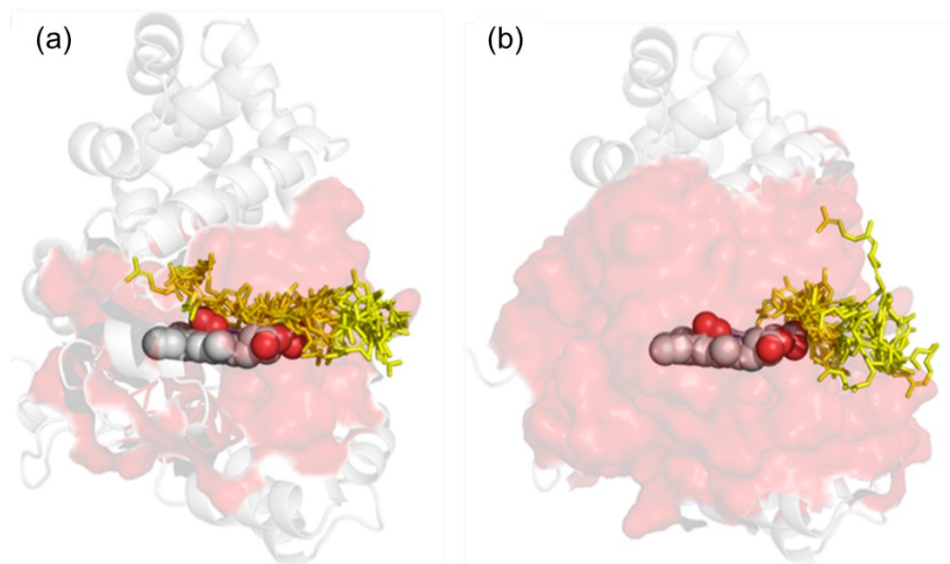
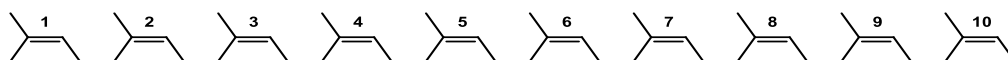


**Figure 5.4.** Superimposed docking conformations results of  $C_{50}H_{82}$  within a defined radius of (a) 10 Å and (b) 15 Å from the central iron atom in heme using ChemPLP flexible docking. Ligand is represented as the yellow stick, and the heme cofactor is represented in spheres (white = C, red = O, blue = N).

The top ten ranked structures obtained using induced fit docking with each ChemPLP and ChemScore protocol were different from those obtained with rigid docking and showed higher fitness scores. The proximity of the C=C bond to the distal oxygen and the polymer conformation based on its span, chain terminus position, and the position of the cleaved double bond were analysed to obtain further information on their orientation during catalysis (Table 5.4). In most docked poses, the distance between the C=C bond and the distal oxygen was below 5 Å, indicating that these structures could represent pre-reactive states.

**Table 5. 4.** Structural features of the best docking poses obtained from induced fit docking within GOLD. Docking solutions are ranked based on the fitness score from highest to lowest.

Oligomeric substrate C<sub>50</sub>H<sub>82</sub>



Rank	Fitness Score	C=C closest to Fe-O <sub>2</sub> complex <sup>a</sup>	Distance of C=C to the oxygen atom (Å) <sup>b</sup>		Ligand conformation
			-H <sub>2</sub> C-C=	=C-CH <sub>3</sub>	
<b>ChemPLP docking protocol</b>					
1	78.94	6	5	5.3	Folded
2	67.25	5	5.2	4	Folded
3	64.80	3	4.3	3.5	Extended
4	40.51	7	5.9	5.1	Folded
5	29.74	9	3.8	2.5	Extended
6	21.37	8	2.2	2.6	Extended
7	19.99	9	5.9	7	Extended
8	-13.14	3	2.6	2.4	Extended
9	-42.16	4	5	5.4	Folded
10	-60.12	5	3.2	2.9	Extended
<b>ChemScore docking protocol</b>					
1	32.65	6	5.8	4.5	Folded
2	29.29	8	3.3	3.8	Extended
3	18.16	4	4	3.1	Extended
4	13.57	3	3	2.9	Extended
5	12.10	3	2.9	2.6	Extended
6	5.80	7	8.3	9	Extended
7	5.44	8	3.4	3.1	Extended
8	-2.20	1	7.8	7.2	Extended
9	-3.92	3	3.7	3.3	Folded
10	-6.98	8	4.1	3.9	Extended

<sup>a</sup> the first C=C unit number was counted from the end terminal with two methyl group R-C=C-(CH<sub>3</sub>)<sub>2</sub> – see scheme

<sup>b</sup> the distance was measured from each C atom in the double bond to the distal O atom of the Fe-O<sub>2</sub> complex

Overall, two prominent docked conformations of the oligomeric substrate were characterised as extended and folded. An extended conformation was defined as a structure in which one terminus of the oligomeric substrate model occupied the hydrophobic cavity within the protein interior near the heme, interacting with the residues above the heme at a distal site, whilst the other terminus was exposed to solvent at the surface of the protein. A folded conformation was defined where both termini were found towards the surface of the protein (Figure 5.5). In both conformations, a C=C double bond was found in the proximity of the distal oxygen, thus increasing the possibility of the reaction. Interestingly, the higher docking scores using both ChemPLP and ChemScore functions were obtained with folded conformations. This result occurred probably due to reduced steric clashes between atoms of neighbouring residues in the protein structure, which increased the fitness scoring function for the folded conformation. In addition, the distance between the C=C double bond to the distal oxygen in folded conformation was almost similar between all docking (with an average of 5 Å), whereas, in an extended conformation, some poses show that the substrate was further away from the heme as shown in ChemPLP docking pose rank 7 (Figure 5.5a) and ChemScore docking poses 6 and 8 (Figure 5.5b).

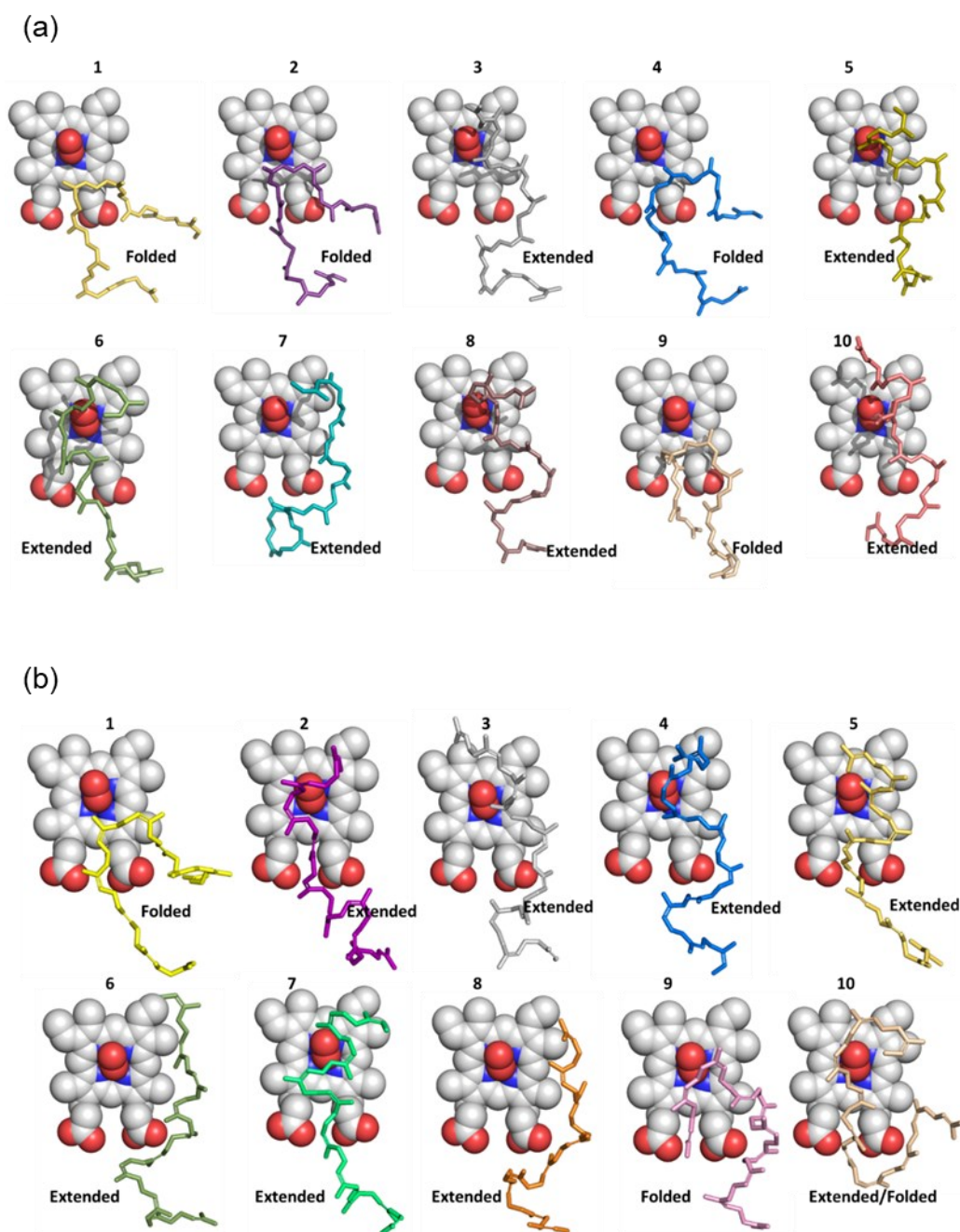


**Figure 5.5.** Docking conformations of *cis*-1,4-polyisoprene ( $C_{50}H_{82}$ ) on LcpK30. (a) Obtained with the ChemPLP scoring function (b) Obtained with the ChemScore scoring function and ranked by the fitness score from highest to lowest. Docking solutions were calculated with induced fit docking using a 10 Å binding site. Enzymes and hydrogens were omitted for the sake of clarity.

The frequency of residues interacting with the docked *cis*-1,4-polyisoprene extracted from PLIP analysis is shown in Appendix C5.2a and C5.2b. PLIP analysis of the substrate-LcpK30 contacts revealed predominantly hydrophobic interactions. Three residues, Lys167, Leu171 and Ile396, were involved in interactions with all docked conformations, while Ala159 engaged in interactions with most docked conformations obtained with both ChemPLP and ChemScore. The interaction of these residues with the *cis*-1,4-polyisoprene ligand in folded (Pose 1) and extended (Pose 3) docking conformation is shown in Figure 5.6. Identification of these residues allowed more options to introduce mutation in LcpK30.

Residue Lys167 has previously been reported to serve as a gating mechanism that opens and closes the entrance to the hydrophobic channel of the enzyme's active site.<sup>117</sup> The docking results suggest that this residue might also play an important role in stabilising protein-substrate complexes. Furthermore, only the extended docked conformations interacted with the Glu148 side chain, located further inside the hydrophobic channel above the heme and previously suggested to be involved in fine-tuning the active pocket to accommodate the substrate for reaction.<sup>125</sup> Earlier work on Glu148 mutation to alanine, histidine, and glutamine revealed that the glutamate residue affected the specific activity of the enzyme but showed no significant differences in biochemical and biophysical properties, as well as no change in oligo-isoprenoid product distribution.<sup>117</sup> Based on this, it is hypothesised that the extended substrate conformation is more representative of a catalytically relevant substrate pose within LcpK30. However, it cannot be excluded that the cleavage occurs with the substrate in the alternative, folded conformation, given the overall higher docking scores and flexibility of the system.

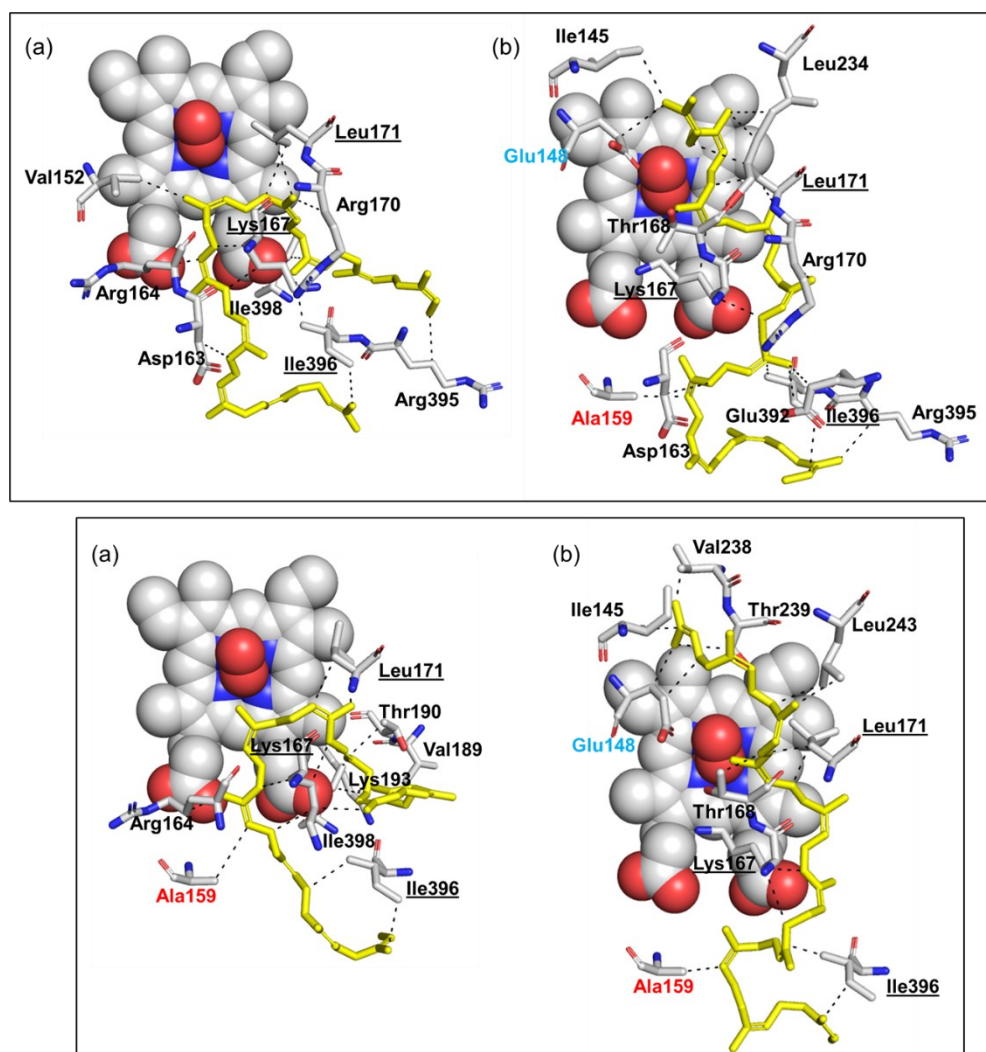


**Figure 5.6.** Protein-ligand interactions identified by PLIP analysis. The docked poses obtained with ChemPLP are shown at the top, and ChemScore is below. (a) Docked Pose 1 is representative of folded conformations, and (b) Docked Pose 3 is representative of extended conformations. The hydrophobic interactions between the ligand and interacting residues are shown by dashed lines. The three residues that appeared in all interactions are underlined. The residue that interacted only with the extended conformation is coloured in blue. The red coloured residue (Ala159) appeared in all interactions with poses obtained using ChemScore and in most interactions with poses obtained using ChemPLP.



## 5.2 Modification of LcpK30

This section outlines the work on LcpK30 modification and assessment of the variant characteristic and catalytic activity.

### 5.2.1 Mutant design

In this study, the rational design strategy was adopted, followed by introducing the mutation using site-directed mutagenesis. From the tunnel identification and molecular docking analysis, as discussed in section 5.1, four residues, namely Ala159, Lys167, Leu171, and Ile396, were discovered to be frequently involved in the protein-ligand interaction (Figure 5.7).

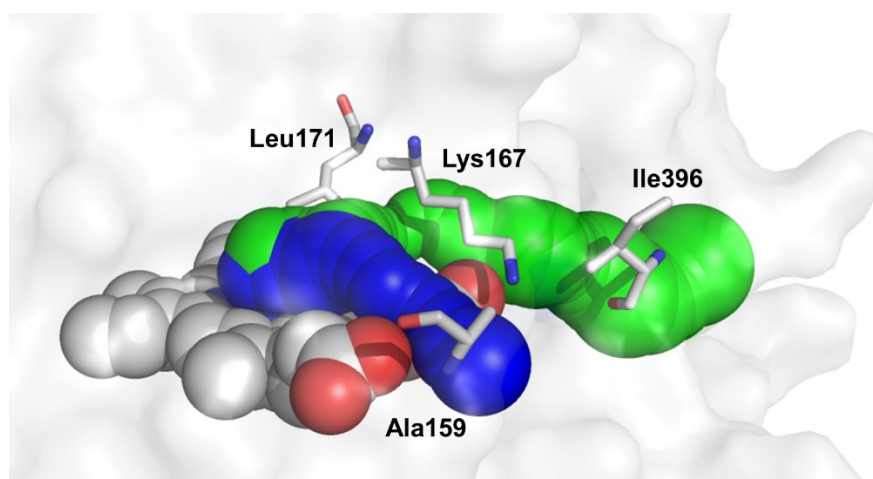


**Figure 5.7.** Position of the four residues frequently interacting with the ligand in docked poses. Tunnel 1 is coloured blue, and Tunnel 2 is green.

These residues might influence the conformational changes of LcpK30 and the ligand. These residues were found lining up the hydrophobic pocket above the heme, and Lys167 is the only residue that has been extensively discussed in several published works.<sup>117,125</sup> The hydrophobic amino acid Leu171 is located deeper into the protein buried site nearer to the central heme iron. The distance of its side chain to the central iron is 5.5 Å on average. Meanwhile, the Ala159 and Ile396 are further away from the central iron towards the outer surface of the protein. These three residues provided a potential site to be mutated.

Furthermore, mutation of Leu171 will probably provide more evidence of its involvement in LcpK30 catalytic activity. Moreover, mutation of LcpK30 at those positions has not yet been documented by any studies.

Apart from using the finding on the LcpK30 pathway and protein-ligand interaction to determine the site for mutation, further analysis was performed by comparing the protein sequences of LcpK30 with its homolog, LcpSH22a. LcpSH22a is the only Lcp protein that can degrade *cis*- and *trans*-1,4-polyisoprene.<sup>108,268</sup> The protein sequences of LcpK30 (Genbank AAR25849.1) and LcpSH22a (GenBank AHH18878.1) were aligned using protein-protein Basic Local Alignment Search Tool (blastp) (Appendix C5.3). An amino acid change at position 171 was observed between LcpK30 and LcpSH22a, where phenylalanine (Phe) replaced leucine (Leu). In addition, the position of Leu171 is near the central iron of heme (Figure 5.7). Therefore, it was hypothesised that a single point mutation at that site with similar residues as in LcpSH22a (Phe) will probably modulate LcpK30 substrate scope towards both isoprene isomers (*cis*-isoprene and *trans*-isoprene). Besides Phe, the exchange of Leu by another two non-polar residues (alanine (Ala) and tryptophan (Trp)) was chosen to observe the effect of increasing or reducing steric bulk on LcpK30 activity and structure. Thus, three LcpK30 mutants (Leu171Ala, Leu171Phe and Leu171Trp) were designed.

### **5.2.2 Tunnel identification in LcpK30 mutants**

Before introducing the mutation, mutagenesis via computational models was employed to get an early understanding of any variations between the mutant and wild-type LcpK30. The initial overview of the structural changes was based on tunnel identification. Mutagenesis on LcpK30 crystal structure in the open state (PDB:5O1L) was carried out using PyMol to obtain the protein structure of the variants. In the previous finding, identifying the tunnel in the static X-ray

structure of LcpK30 confirmed the presence of two dominant tunnels (Figure 5.1a). The result was further supported by pocket detection using fpocket and MD simulation.<sup>269</sup> By using similar software and parameters of CAVER-Pymol plug-in 3.0.3, the pathway mapping on the LcpK30 mutants was predicted.

Identification of tunnels in Leu171Ala mutant revealed two dominant tunnels pointing in the same direction as those found in wild-type LcpK30 (Figure 5.8b). The tunnel length, average tunnel radius, and bottleneck radius of the dominant tunnel (tunnel 1) identified in the Leu171Ala mutant were quite similar to those of the wild type.

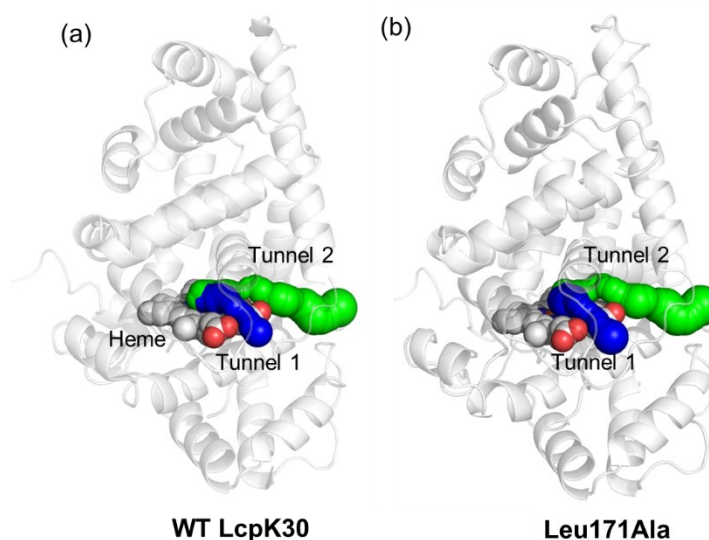


**Figure 5. 8.** Identified tunnels in LcpK30 and its mutants. (a) Dominant tunnels in the X-ray structure of wild type LcpK30 and (b) Leu171Ala mutant. The figure shows only two pathways with the highest possibility.

However, the second highest probability identified tunnel (tunnel 2) in the Leu171Ala mutant has a narrower pathway beginning near the heme (1.3 Å distance from central heme iron) up to 4 Å in length followed by a broader average radius compared to the wild type at certain length (Figure 5.9). These findings may suggest that substitution with smaller residues at position 171 does not essentially influence the putative ligand pathways.

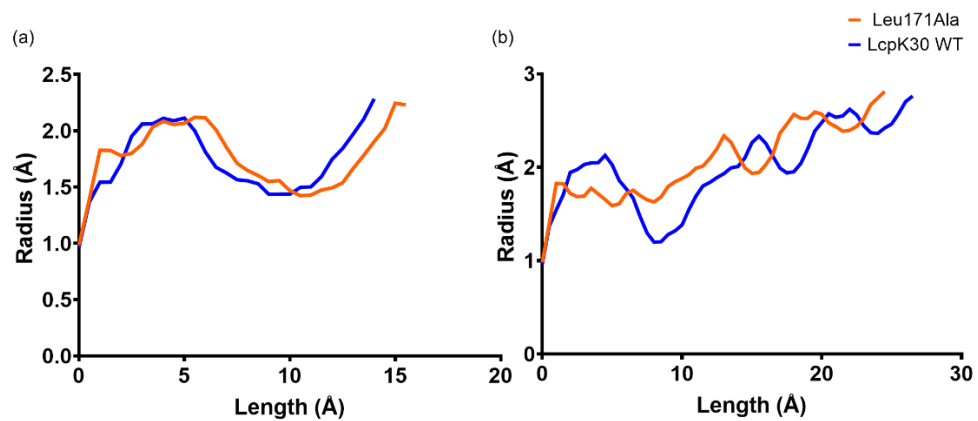


**Figure 5. 9.** Tunnel radius and length of the two tunnels identified in Leu171Ala mutant and LcpK30 wild type (WT) with the highest probability (a) Tunnel 1 (b) Tunnel 2.

On the other hand, tunnels in Leu171Phe and Leu171Trp mutants showed different tunnel mapping. There were only two tunnels identified in those mutants. Tunnel 1 was found at a position similar to the Leu171Ala mutant and the wild type. However, tunnel 2 of Leu171Phe and Leu171Trp mutants were completely diverted from tunnel 2 found in the wild type. Its position was similar to tunnel 4, which was identified in the wild type (Figure 5.10a). It was assumed that the presence of bulk amino acid at position 171 might be blocking the pathway leading to tunnel 2 as in the wild type. This result may suggest that a single point mutation near the active site with bulkier residue could affect the pathway mapping.

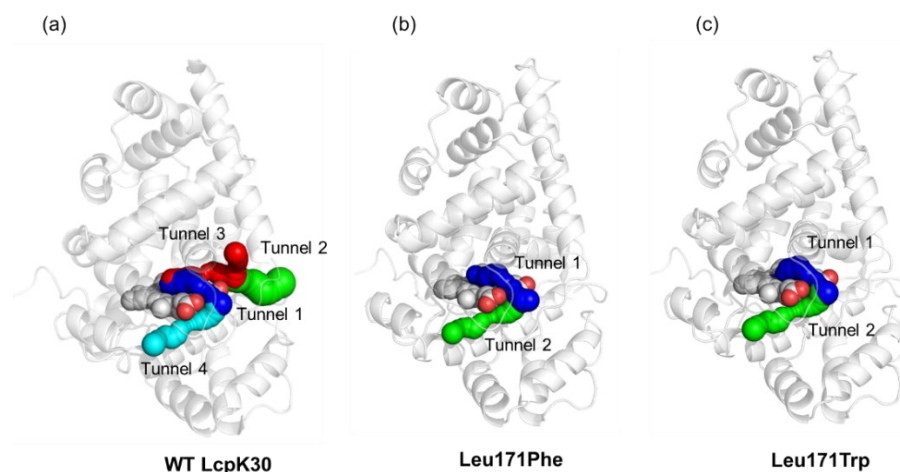


**Figure 5. 10.** Identified tunnels in LcpK30 and its mutants. (a) All tunnels in the X-ray structure of wild type LcpK30, (b) Leu171Phe mutant and (c) Leu171Trp mutant. The figure shows all identified pathways.

### 5.2.3 Molecular docking of *cis*- and *trans*- 1,4-polyisoprene ligands to wild-type LcpK30 and the mutants

This section interpreted *cis*- and *trans*- 1,4-polyisoprene interaction with LcpK30 mutants based on the earlier finding on the molecular docking of *cis*-1,4-polyisoprene with ten C=C onto wild-type LcpK30. Firstly, the protein-ligand conformers were identified as extended or folded conformations. Secondly, the distance between the C=C bond and the distal oxygen atom of the Fe-O<sub>2</sub> complex less than 5 Å was used to determine a potential pre-activation/reactivation state. Besides using *cis*-1,4-polyisoprene with ten C=C bonds as the ligand model, another ligand model of *trans*-1,4-polyisoprene with a similar number of C=C bonds was also used to evaluate any changes in substrate specificity of the mutants.

Molecular docking was performed using ChemPLP scoring functions in the GOLD software with flexible docking. A similar ten amino acid sidechains in the active site of LcpK30 were allowed for full torsional flexibility (Chapter 2.2.12.3). Both ligands were docked onto the wild-type LcpK30 and the three mutants. Overall, eight sets of molecular docking were performed. From the docking, ten protein-ligand conformations with varying fitness scores from each set of docking were obtained. Increased fitness score resulted from reduced steric clashes between atoms of neighbouring residues in the protein structure during the computational docking process. Thus, the fitness score was qualitatively used as an indicator to determine the higher accessibility of ligands into the protein active site.

Figure 5.11 shows the highest fitness score for the protein-ligand complexes in all LcpK30 variants. Compared to the wild-type, the fitness score for the conformation complex of *cis*-1,4-polyisoprene was lower in Leu171Trp and Leu171Phe mutants. This might be due to the bulkier residues that could

increase the steric clashes, thus lowering the fitness score. In contrast, substituting Leu171 with a smaller residue (alanine) reduced the protein steric clashes, thus increasing the fitness score. In addition, out of four LcpK30 variants, only the Leu171Phe mutant shows preferential interaction with *trans*-1,4-polyisoprene against the *cis*- configured.

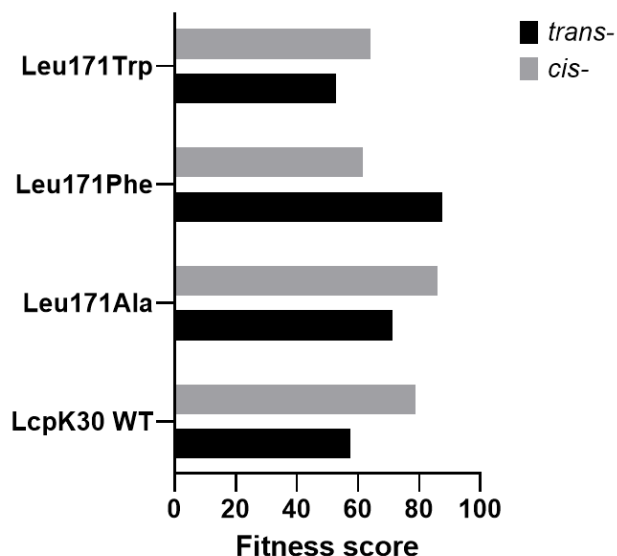


**Figure 5. 11.** Fitness score of the first rank docking solution. The bar represents the highest fitness score from eight sets of *cis*- and *trans*-1,4-polyisoprene ligand docking on wild-type LcpK30 and the mutants.

The ten docking solutions of protein-ligand complexes obtained from the ChemPLP molecular docking exhibited structures according to the two major conformations: extended and folded. The example of extended and folded conformation poses of *trans*-1,4-polyisoprene on Leu171Phe mutant is shown in Figure 5.12 (all ten docking conformations for each set of molecular docking performed are included in Appendices C5.4-C5.7). Protein-ligand conformations with a greater possibility of initiating the enzymatic reaction have a positive fitness score and a distance lower than 5 Å between the C=C bond and the distal oxygen atom of the Fe-O<sub>2</sub> (Appendices C5.8 and C5.9). A very low or even negative fitness score was obtained in several conformations,

prominently when the ligands were docked on the Leu171Trp mutant. Although fitness score is not always an absolute indicator of an active protein-ligand interaction<sup>267</sup> these results may suggest that some of the mutants could improve the catalytic activity of LcpK30 and alter substrate scope towards *trans*-isoprene.

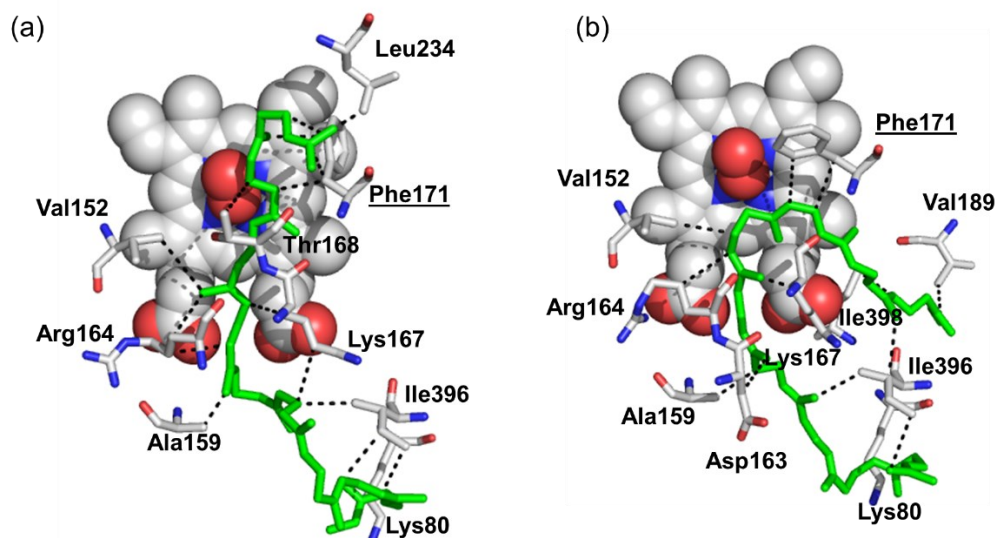


**Figure 5.12.** Example of *trans*-1,4-polyisoprene docking poses. (a) Extended docked pose of *trans*-1,4-polyisoprene on Leu171Phe mutant with the highest fitness score. (b) The folded docked pose of *trans*-1,4-polyisoprene on the Leu171Phe mutant has the second-highest fitness score. Protein-ligand interactions were extracted from PLIP analysis. The hydrophobic interactions between the ligand and interacting residues are shown by dashed lines. The mutated residue is underlined.

#### 5.2.4 Expression and purification of LcpK30 mutants

The mutation was introduced *via* site-directed mutagenesis. The primers used for the mutations were included in Appendix C5.10. After the polymerase chain reaction (PCR) was completed, the undigested PCR products were checked using agarose gel electrophoresis. The desired PCR products were not observed for Leu171Trp (Figure 5.13). Nevertheless, all of the reactions proceeded with the DpnI digestion and transformation of the final reaction into competent cells (XL10-Gold ultracompetent cells). A fair number of colonies were obtained from cells transformed with Leu171Ala and Leu171Phe mutation,

whereas fewer colonies were observed from the cells transformed with the reaction of Leu171Trp mutation.

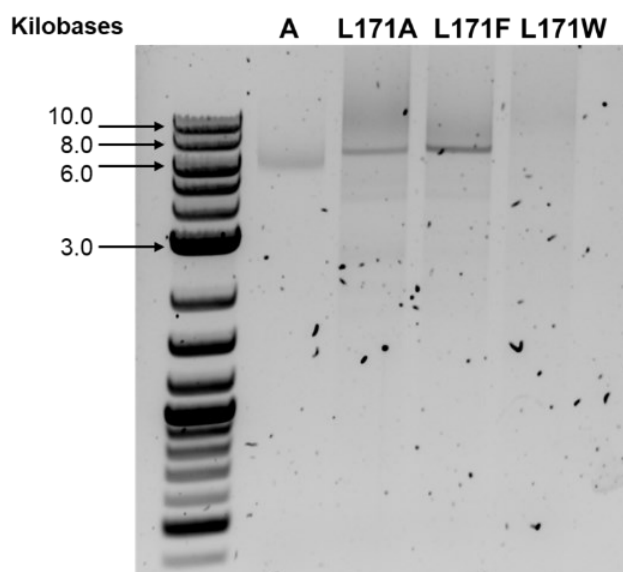


**Figure 5.13.** The products after PCR reactions. Lane A is the parent plasmid of pET21a(+) (5443 bp) with the LcpK30 (1194 bp, GenBank Accession Number: AAR25849.1) gene (1194 bp). The label L171A, L171F and L171W represented Leu171Ala, Leu171Phe and Leu171Trp mutant, respectively.

Plasmid sequencing confirmed the success of the Leu171Ala and Leu171Phe mutations (Appendices C2.3 and C2.4). However, the desired mutation is not present in the plasmid produced from the Leu171Trp reaction, which still had the wild-type sequence. Therefore, only two mutants of LcpK30 (Leu171Ala and Leu171Phe) proceeded with expression and purification.

The mutants were expressed and purified using the previously developed procedure for preparing wild-type LcpK30. However, the induction was carried out using 1 mM IPTG after a few unsuccessful trials to induce the expression using 3 mM lactose and at other IPTG concentrations. The induction was performed at a higher cell density ( $OD_{600} = 0.8 - 1$ ), and the agitation after induction was reduced from 200 rpm to 100 rpm. SDS-PAGE analysis of the cell extract from the expression of wild-type LcpK30, Leu171Ala and Leu171Phe mutants are shown in Figure 5.14.



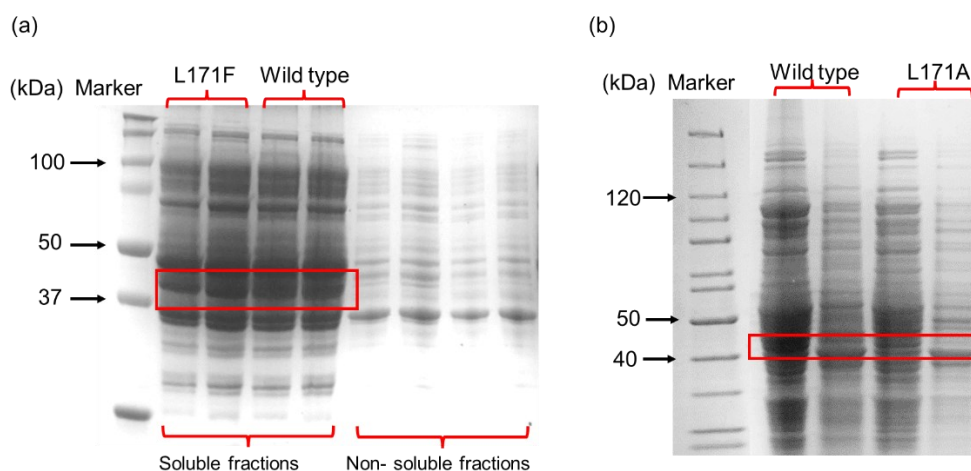


**Figure 5. 14.** SDS-PAGE analysis of LcpK30 wild type and the mutants (40.6 kDa estimated using ExPASy ProtParam; <https://web.expasy.org/protparam/>) expression by *Escherichia coli* strain C41(DE3) harbouring plasmid pET21a(+):*strep-lcpK30*, pET21a(+):*strep-lcpK30(L171A)* and pET21a(+):*strep-lcpK30(L171F)* in Lysogeny Broth medium with the presence of yeast and hemin. Overexpression was induced by 1mM IPTG. (a) Leu171Phe expression (b) Leu171Ala expression (left-soluble fraction; right- non-soluble fraction). The red box indicates the position of the LcpK30 protein band.

Purification of the mutant proteins was performed by affinity chromatography and was eluted at a maximum of 70 % concentration of 2.5 mM desthiobiotin buffer, similar to the purification of the wild-type. The SDS-PAGE of purified wild-type LcpK30, Leu171Ala and LeuPhe proteins are shown in Appendix C5.11. The incorporation of the heme cofactor at the active site was detected by strong absorption at 412 nm, indicating iron in a ferric resting stage ( $\text{Fe}^{+3}$ ). Accordingly, the absorbance spectrum of purified proteins at  $1 \text{ mg mL}^{-1}$  of all variants showed absorption peaks at 412 nm (Figure 5.15). This indicates that the exchange of Leu did not alter the heme surroundings.

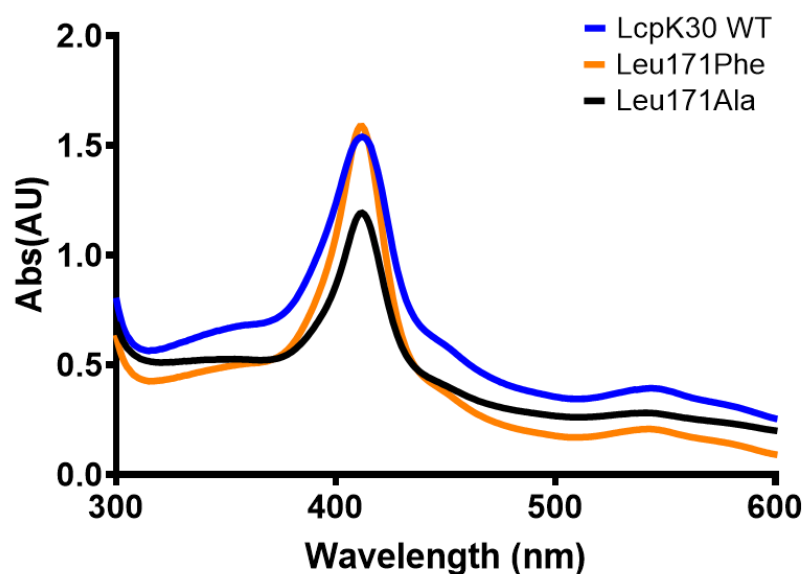


**Figure 5. 15.** Heme absorption at 412 nm of purified protein at 1 mg mL<sup>-1</sup> indicates the presence of heme in the protein scaffold.

Heme occupancy of a purified protein was quantified using the  $R_z$  value representing the ratio between the Soret band ( $A_{412}$ ) over  $A_{280}$  (indicating protein concentration).<sup>199,200</sup> The  $R_z$  value of the purified Leu171Phe was higher than the wild-type LcpK30 and Leu171Ala mutant, suggesting that the point mutation of Leu to Phe might influence the heme binding (Table 5.5). Although a higher  $R_z$  value was obtained from the Leu171Phe mutant protein, there was no significant difference in its specific activity compared to the wild-type (Table 5.5). Higher  $R_z$  value was commonly directly correlated with increasing specific activity when heme was introduced. The heme can be introduced during the expression of heme-containing protein either by adding into the culture medium, by co-expression of a gene encoding for heme, or by using a recombinant host of higher intracellular heme protein producers.<sup>200,219</sup> However, this is not always applicable as the  $R_z$  value measures the heme content but not the enzyme activity. Even with the same  $R_z$  value, enzymes can exhibit varying measurements of specific activity.<sup>270</sup>

**Table 5. 5.** Purification yield and specific activity following expression and purification of WT LcpK30 and the mutants.

Protein variant	Total protein concentration (mg mL <sup>-1</sup> )	<sup>a</sup> Enzyme concentration (mg mL <sup>-1</sup> )	<sup>b</sup> Volume (mL)	<sup>c</sup> Purification yield (mg)	<sup>d</sup> A <sub>412</sub> /A <sub>280</sub>	<sup>e</sup> Specific activity (U mg <sup>-1</sup> )
WT	39	10	3	30	2.6	1.43±0.44
L171A	23	10	0.6	6	2.3	0.73±0.21
L171F	33	10	1	10	3.4	1.34±0.34

<sup>a</sup> Protein concentration was quantified after purification and concentrated using a 10 kDa cutoff value concentrator tube

<sup>b</sup> Volume of the concentrated protein

<sup>c</sup> Purification yield was calculated from 800 mL culture

<sup>d</sup> The absorbance was measured on 1 mg mL<sup>-1</sup> of purified protein

<sup>e</sup> Specific activity was measured using a dissolved oxygen assay of 4 µg purified protein. The measurement was performed in triplicates to determine the standard deviation

The colourimetric assay indicated a low catalytic activity from the reaction in the presence of purified Leu171Ala mutant (Figure 5.16). This observation was further supported by the dissolved oxygen assay that quantifies the specific activity of the proteins. The specific activity of the Leu171Ala mutant was reduced by 50% compared to the wild type. In the next section, further investigation of the catalytic activity of the mutants is discussed.

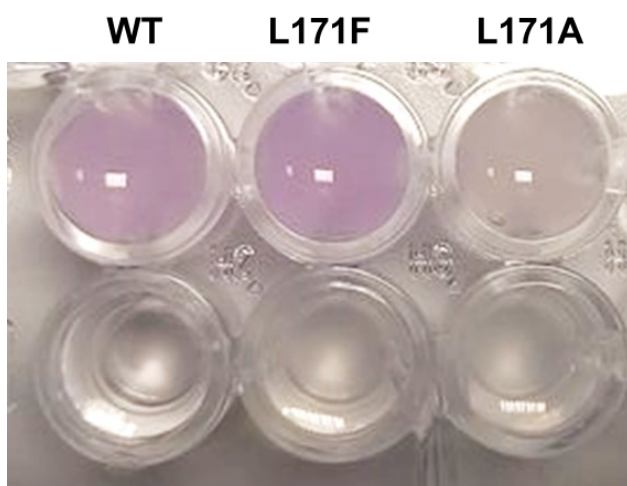


**Figure 5. 16.** Colorimetric assay by staining the enzymatic reaction solution with Schiff's Reagent. Aldehyde compound existence was qualitatively indicated by colour shifts from colourless to pink or purple.

### 5.2.5 Degradation of *cis*-1,4-polyisoprene catalysed with LcpK30 wild type and mutants

NR latex was incubated with purified enzymes of each variant (wild-type LcpK30, Leu171Ala and Leu171Phe mutants). Both mutants catalysed the cleavage of the *cis*-1,4-polyisoprene chain, resulting in a similar size distribution of oligomers based on the HPLC chromatogram (Figure 5.17).

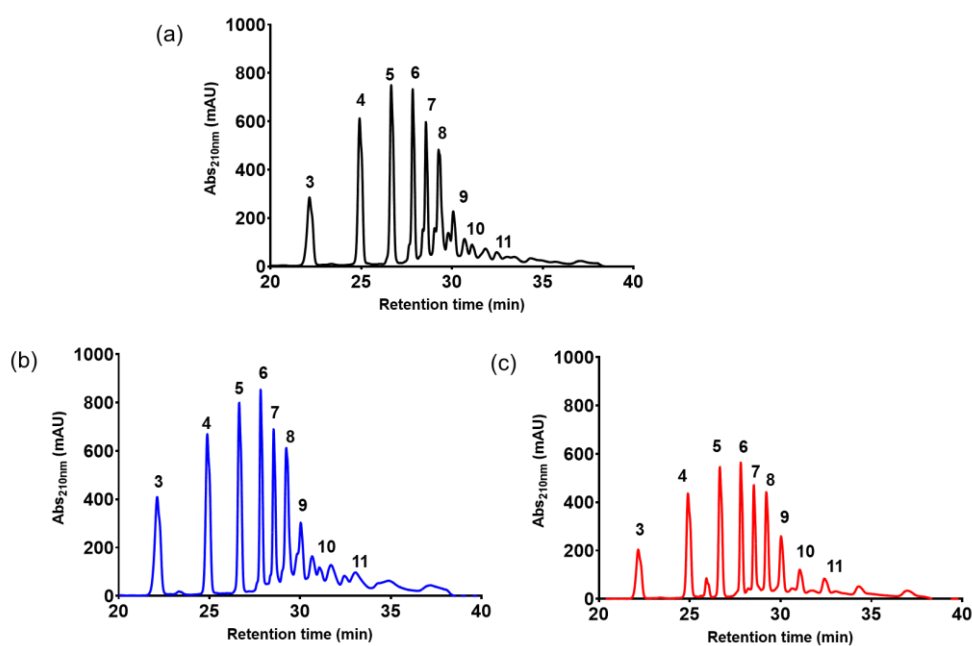


**Figure 5.17.** HPLC chromatogram of oligomers derived from natural *cis*-1,4-polyisoprene rubber enzymatically cleaved by LcpK30 variants; (a) wild-type LcpK30; (b) Leu171Phe and (c) Leu171Ala. The number on top of the peak represents the repetitive number of isoprene units.

Different patterns of the most prevalent oligomers were identified by estimating the quantity of each oligomeric compound based on a relative comparison with the peak area (%) of 1 mM linalool (Appendix C5.12). Table 5.6 outlines the relatively abundant oligomer in products derived from NR degradation catalysed by wild-type LcpK30, Leu171Ala and Leu171Phe mutants.

**Table 5.6.** The relatively abundant oligomers in the NR degradation products catalysed by the LcpK30 variants, as observed by the HPLC chromatogram.

<b>LcpK30 variants</b>	<b>Isoprene unit (n)</b>	<b><math>A_{(\text{oligomer})}/A_{(\text{linalool})} * 100</math></b>
<b>Wild type</b>	4	50
	5	50
<b>Leu171Ala</b>	5	37
<b>Leu171Phe</b>	4	67

The percentage of peak area for the oligomers was calculated relative to the peak area (%) of 1 mM linalool. The oligomers with the stated isoprene unit number are the most abundant compared to the other sizes of oligomers.

Based on the information in Appendix C5.12, the overall amount of oligomers produced after NR degradation catalysed with the enzyme was followed in this enzyme order: Leu171Phe > wild-type Lcp > Leu171Ala. This finding is consistent with the lower oligomer mass extracted from degradation catalysed with Leu171Ala. On the contrary, the oligomer yield from the reaction with the Leu171Phe mutant is less than the NR degradation catalysed by the wild type (Table 5.7). The accessibility of the polyisoprene chains into the enzyme active site may be affected by changes in the protein cavity, which may thus have an impact on the rate at which the substrate is converted into products.

**Table 5.7.** Mass balance of oligomers and retrieved rubber after solvent extraction and drying.

<b>LcpK30 variants</b>	<b>Recovered rubber mass (mg)</b>	<b>*Recovered oligomer mass (mg)</b>
Wild type	46.7	65.0
Leu171Ala	84.6	21.2
Leu171Phe	48.4	33.2

Reaction condition: NR loading was 20 mg mL<sup>-1</sup> in a 5 mL volume reaction. Purified LcpK30 was added three times (6 μM per addition) to a final concentration of 18 μM. The reaction was performed for 24 hours at 30 °C and 450 rpm stirring. The initial mass of NR was theoretically at 100 mg. \* Recovered oligomer mass is equal to the oligomer yield.

Furthermore, the presence of aldehyde was confirmed by <sup>1</sup>H NMR in the oligomers extracted from all reactions. Based on the <sup>1</sup>H NMR spectra of the products (Appendix C5.13), an average number of repeating isoprene units of oligomers was determined by integrating the prominent peaks for olefinic proton

(-C=CH-CH<sub>2</sub>-; 2), and aldehyde proton (-CH=O; 7). The integration number obtained from the <sup>1</sup>H NMR and the results on the estimated repeating isoprene unit are tabulated in Table 5.8. The number of repeating units was calculated using the equation that has been described in Chapter 3, Section 3.2.6.

**Table 5. 8.** The integration number of proton in the oligomer's environment

Moiety	Chemical shift ( $\delta$ ) ppm	Peak Area			No. of protons
		WT	Leu171Ala	Leu171Phe	
Olefinic	5.12	1	1	1	1
Aldehyde	9.8	0.1	0.05	0.1	1
<b>*No. of repeating units</b>		<b>10</b>	<b>20</b>	<b>10</b>	

The estimated average length of oligomers produced after oxidative cleavage catalysed by the Leu171Ala mutant was longer by ten isoprene units (20 isoprene units) compared to the oligomers produced in the reaction catalysed by the wild-type and the Leu171Phe mutant. This average length of oligomers from the reaction with Leu171Ala estimated by <sup>1</sup>H NMR spectroscopy was similar to the number average molecular weight ( $M_n$ ) of 1395 g mol<sup>-1</sup> determined by the GPC (Table 5.9). The population of the oligomers was also highly variable in length, indicated by a higher polydispersity index ( $\mathcal{D} = 4.28$ ). These results might demonstrate that more extended oligomers are dominating the oligomers population derived from NR degradation catalysed by the Leu171Ala mutant. However, the presence of these longer oligomeric species might be too diluted to be visualised in the HPLC chromatogram.

**Table 5. 9.** Characteristic of oligomers derived from degradation catalysed by LcpK30 variants

<b>LcpK30 variants</b>	<b>M<sub>n</sub> (g mol<sup>-1</sup>)</b>	<b>M<sub>w</sub> (g mol<sup>-1</sup>)</b>	<b>Đ</b>
Wild type	1239	2285	1.84
Leu171Ala	1395	5968	4.28
Leu171Phe	1017	2346	2.31

Interestingly, there was an improvement in the polydispersity of the oligomers except for those derived from the reaction catalysed by Leu171Ala. However, the polydispersity of oligomers produced from NR degradation catalysed by the mutants was still higher than the oligomers produced from reaction with the wild type, which indicates that none of the mutants could regulate the cleavage mechanisms to produce oligomers which is less heterogeneous.

The M<sub>n</sub> determined by GPC for oligomers derived from NR degradation catalysed with Leu171Phe reflected the maximum length observed from the HPLC chromatogram. However, in this experiment, analysis from the peak integration of <sup>1</sup>H NMR results in a lower average length for oligomers produced from the reaction with the wild-type and Leu171Phe. Table 5.10 summarises the findings on the estimation of the molecular weight of the oligomeric products based on the isoprene unit number extracted from HPLC, GPC and <sup>1</sup>H NMR. These results might suggest that a single mutation of Leu might cause subtle conformational changes. Hence, it impacted how the polyisoprene chain threaded through the hydrophobic channel into the active site for C=C bond cleavage.

**Table 5.10.** Molecular weight determination reflected the repeating isoprene unit number as extracted with different analytical approaches.

<b>LcpK30 variants</b>	<b><sup>a</sup>HPLC</b>	<b><sup>b</sup>GPC</b>	<b><sup>1</sup>H NMR</b>
Wild-type	13	17	10
Leu171Ala	12	19	20
Leu171Phe	14	13	10

<sup>a</sup> isoprene unit number was extracted from the peak represent the largest oligomers

<sup>b</sup> isoprene unit number was calculated by subtracting the  $M_n$  with  $M_w$  of carbonyl end-group ( $102.1 \text{ g mol}^{-1}$ ) and dividing the results with  $M_w$  of an isoprene ( $68.1 \text{ g mol}^{-1}$ )

Information on the molecular characteristics of the oligomers, such as molecular weight or size, could be important in determining its potential application and as an approach to scrutinise the catalysing pattern of LcpK30 and its variants for protein engineering.

### 5.2.6 Degradations of *trans*-1,4-polyisoprene catalysed with LcpK30 wild type and the mutants

To further investigate the changes in substrate scope of LcpK30 due to the mutation, degradation on *trans*-1,4-polyisoprene in the presence of wild-type LcpK30 and Leu171Phe mutant was performed. The *trans*-1,4-polyisoprene used in this experiment was a commercially available polymer with  $M_w$  of  $\sim 10^6 \text{ g mol}^{-1}$  and was synthetically synthesised into a hard pellet. After grinding the pellet under liquid nitrogen, the particles were sieved and separated according to size (Figure 5.18). The smallest particle size obtained ( $250 \mu\text{m}$ ) was used as the substrate for the degradation reaction.

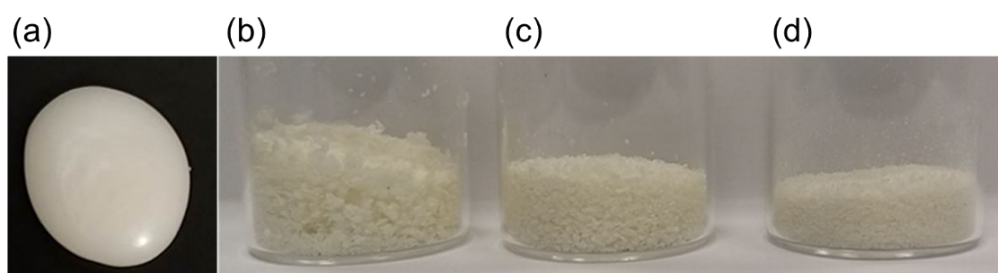


**Figure 5.18.** The physical appearance of synthetic *trans*-1,4-polyisoprene. (a) before and (b) after grinding in liquid nitrogen, and the particles were separated into (c)  $600 \mu\text{m}$  and (d)  $250 \mu\text{m}$  particle size.



Degradation of *trans*-1,4-polyisoprene was performed with an initial amount of rubber at 10 mg mL<sup>-1</sup>. Once the reaction was completed, the rubber mass (mg) that was retrieved after solvent extraction was relatively similar to the initial rubber mass, thus indicating that the *trans*-polyisoprene rubber was not being degraded. Slight physical differences between the samples retrieved from the reaction with and without enzyme (negative control) were detected when observing the *trans*-1,4-polyisoprene particles under the microscope. The edge of *trans*-1,4 polyisoprene particles from the negative control reaction can be seen under the microscope without colouration (Figure 5.19). In contrast, the particles recovered from the other two reactions with wild-type LcpK30 and Leu171Phe mutant seem to be clumping together with evidence of colouration due to the red pigment of heme from the enzyme.

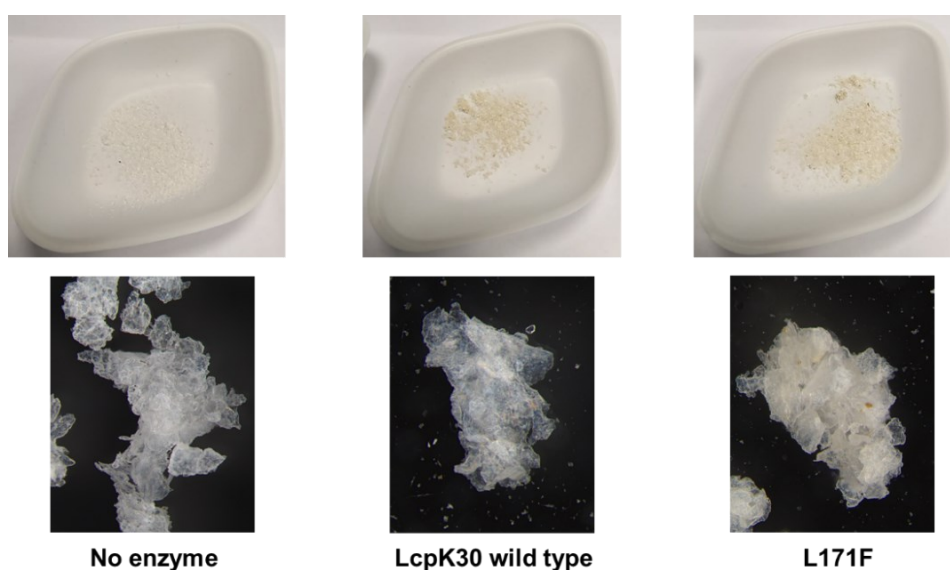


**Figure 5. 19.** Physical appearance of *trans*-1,4 polyisoprene particles after washing with ethyl acetate and drying under the fume hood.

HPLC analysis on the dried residual after solvent extraction from all reactions revealed three consistent peaks at 24.3, 25.6, and 26.6 minutes of retention time (Figure 5.20). These peaks were assumed to represent small oligomers present in the material from the polymerisation process. Nevertheless, it is worth

noting that in samples obtained from the reaction conducted in the enzyme's presence, minor peaks emerged beyond a retention time of 30 minutes. This observation suggests the possibility of the enzyme catalysing the cleavage of the polyisoprene chain in a *trans*-configuration.

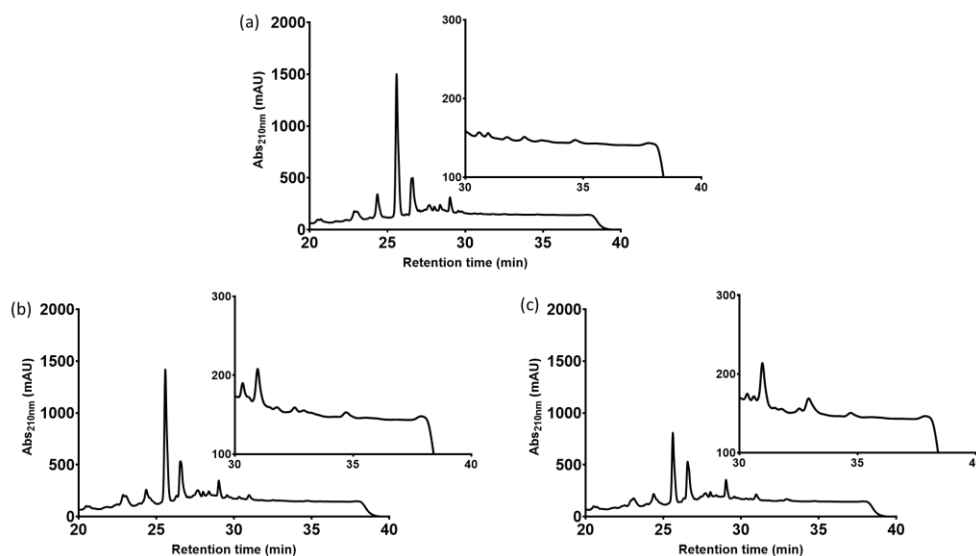


**Figure 5. 20.** HPLC chromatogram of dried products recovered after ethyl acetate extraction from a reaction of 10 mg mL<sup>-1</sup> *trans*-1,4 polyisoprene in 5 mM KPi buffer. (a) in the absence of enzyme, (b) in the presence of 750 µg mL<sup>-1</sup> Leu171Phe mutant enzyme and (c) in the presence of 750 µg mL<sup>-1</sup> LcpK30 wild type.

Unfortunately, <sup>1</sup>H NMR spectra showed no evidence of the presence of an aldehyde proton. Moreover, there were no other compound peaks to justify the appearance of peaks in the HPLC chromatogram after 30 min of retention time (Figure 5.22). Nevertheless, the inability of <sup>1</sup>H NMR analysis to acquire any compound signals could be due to a very low concentration of the compounds. Based on the result, it showed that the LcpK30 variants could not catalyse the degradation of *trans*-1,4-polyisoprene.

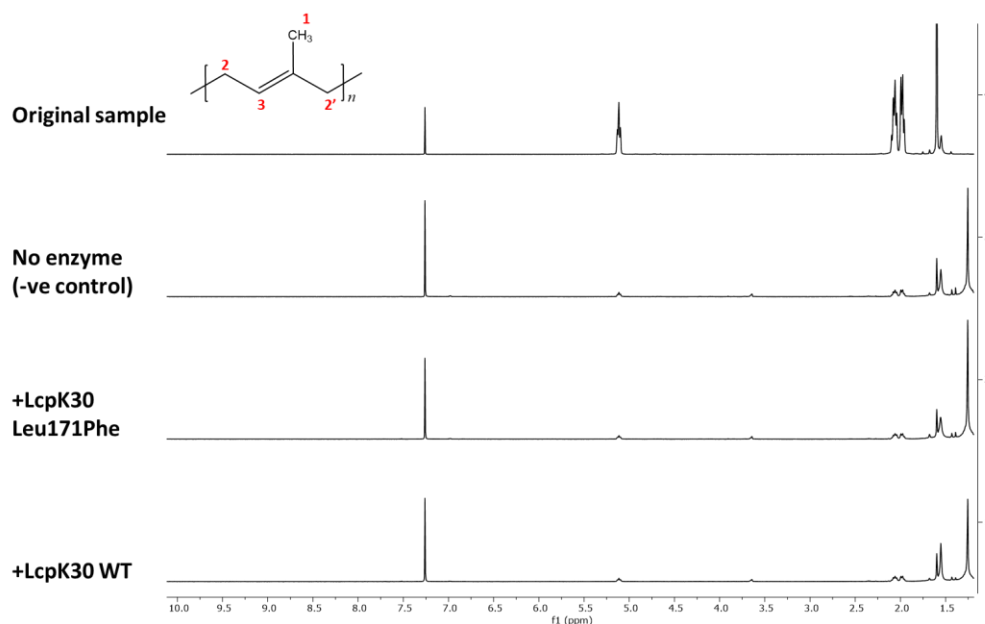


**Figure 5. 21.**  $^1\text{H}$  NMR spectrum spectra of dried samples extracted from degradation reactions of *trans*-1,4-polyisoprene. The degradation reaction consists of  $18\ \mu\text{M}$  purified LcpK30 variants as the catalyst. The  $^1\text{H}$  NMR spectra from the samples were compared to the original polymer sample (5 mg of *trans*-1,4 polyisoprene 250  $\mu\text{m}$  particles were directly dissolved in deuterated chloroform). Reaction with no enzyme was prepared as a negative control and treated similarly to the reactions with the enzyme.

### 5.3 Discussion

The natural substrate of LcpK30 is a long polymer consisting of more than 10,000 repeating isoprene units, which would be too complex for standard docking into protein.<sup>24</sup> Modelling of the interaction between a polyisoprene-type substrate and LcpK30 has been previously reported in a study by Zhang and Liu, in which they carried out docking of a short oligomer with four repeating units into the binding site near the heme cofactor containing bound dioxygen.<sup>125</sup> In their work, the authors primarily focused on the QM/MM calculations of the LcpK30 catalytic mechanism featuring the oxidative cleavage of the C=C double bond. Interestingly, in this study, insight into the interactions occurring further away from the active site that may also affect the substrate binding and the outcome of the catalysis, which cannot be fully described by a short substrate model, were obtained. Computational docking of a large substrate model with

ten repeating isoprene units ( $C_{50}H_{82}$ ), using two different scoring functions within the GOLD program, revealed two main bound conformations: extended and folded.

Residues Lys167, Leu171, Ile396 and Ala159 were involved in the protein-substrate interactions in most of the docking solutions. Therefore, it was suggested that those residues play an important role in stabilising protein-substrate complexes. The residue Glu148 was previously shown to affect enzyme activity. Investigation of several mutants substituting Glu148 revealed that this residue is important for fine-tuning the active pocket to accommodate the substrate for reaction.<sup>125</sup> Interestingly, Glu148 was found only to interact when the substrate is in an extended conformation. Thus, the result justified that the extended conformation is the most reactive state of protein-ligand complexes that will trigger the oxidative cleavage of the C=C double bond. However, it is possible that the catalytic activity also occurs when the substrate appears in folded conformation.

It is important to note that the docking study's observation may not reflect the actual reaction inside the active pocket.<sup>271</sup> The interaction of the substrate and product with the protein can be influenced by several factors, such as protein dynamic, conformational changes in protein structure, energy profiles and other physio-chemical conditions. Thus, a more specific computational aiding method should be applied. Nevertheless, results obtained in this study provide a better picture of protein-substrate interaction within LcpK30, and the information was used for further scrutinising the molecular dynamics of this protein, which was explained thoroughly in an article by Hassan *et al.* (2023).<sup>269</sup>

According to the results in section 5.2.4, the Leu171Phe mutant might bind heme better than the wild type. The main difference between Leu and Phe is the presence of an aromatic side chain in Phe. Aromatic side chains exhibited an important role in heme binding and structure stability.<sup>272</sup> The binding of heme in the heme proteins scaffold involved considerably variable interaction, including non-polar interactions, van der Waals contacts, stacking interactions and electrostatic bridges.<sup>273,274</sup> Heme binding pocket has been reported to be dominantly associated with hydrophobic interaction that consists of non-polar and aromatic binding residues.<sup>275</sup> The non-polar residues create a hydrophobic environment suitable for the heme ring structure to maintain the oxidation level of iron and expose them for participation in the catalytic reaction.<sup>272,276</sup> The aromatic residues (phenylalanine, tyrosine, and tryptophan) form contacts with the heme through stacking interaction that significantly stabilises heme binding.<sup>277,278</sup> Due to this, there might be a possibility that substituting Leu171 with Phe improves the heme binding by forming a stacking interaction with the neighbouring aromatic residue, for example, tyrosine (Tyr173).

The experimental results exhibited a lack of coherence with the previous findings obtained using computational molecular docking. Specifically, the Leu171Ala variant, which had demonstrated a favourable interaction with *cis*-1,4-polyisoprene by attaining the highest fitness score among the several LcpK30 variants, did not align with the experimental outcomes. The reduced size of alanine may potentially lead to a decrease in the affinity of the polyisoprene chain binding to the active site through the hydrophobic channel. Consequently, this reduction in affinity may decrease the likelihood of oxidative cleavage of the C=C bonds. These results show that a single point mutation of Leu171 near the central iron of the LcpK30 heme group could create changes in the protein cavity, thus affecting the catalytic activity of LcpK30.

The computational docking results indicated potential interaction between the Leu171Phe mutant and polyisoprene with a *trans*-configuration. However, the experimental findings contradicted the outcomes of the computational simulations. Limitations on cleaving *trans*-1,4-polyisoprene enzymatically could be due to the polymer morphology and higher molecular weight. The high molecular weight of *trans*-1,4-polyisoprene contributes to its low ability to be solubilised in solvents. The solubility of *trans*-1,4-polyisoprene in several solvents, including hexadecane, tetradecane, hexane, tetrahydrofuran (THF) and its derivative (2-methylTHF and 2,5-dimethylTHF) was tested. However, this polymer cannot be dissolved. Thus, the degradation of *trans*-1,4-polyisoprene was prepared in a solid-based system, which eventually limits the enzyme's ability to reach the C=C bonds of the polymer chains. A previous study has shown a polymer consisting of a mixture of *cis*- and *trans*- structures prepared in a co-solvent stabilised emulsion can be enzymatically degraded by LcpK30.<sup>111</sup> However, it could potentially be that only the C=C bonds in the *cis* configuration were being cleaved and still, so far only LcpSH22a that can catalyse the degradation of polyisoprene with 99% *trans*-1,4 isomerisms.<sup>108</sup>

#### **5.4 Summary and Conclusions**

The finding discussed in this chapter, is the first work on the identification of LcpK30 tunnels and molecular docking of longer polyisoprene ligand with ten C=C. The results offer a valuable understanding of the distant interactions that take place beyond the active site, which can influence both substrate binding and the catalytic outcome. These interactions cannot be adequately explained by a simple substrate model. In the initial finding of this study, two tunnels were discovered that mapped around the LcpK30 active site close to the heme. The tunnels identified in this study serve as potential pathways for transporting the substrate and product to and from the active site. These tunnels are

characterised by residues previously established as crucial for LcpK30 activity, namely Glu148, Arg164, Lys167, and Thr168. The flexibility of the protein structure and the ligands makes it challenging to understand substrate binding and transportation just from mapping the tunnels. Therefore, more information on the protein-substrate interactions was obtained with molecular docking.

Computational docking of a large substrate model with ten repeating isoprene units ( $C_{50}H_{82}$ ), using two different scoring functions within the GOLD program, revealed the existence of two main bound conformations: extended and folded. Residues Lys167, Leu171, Ile396 and Ala159 were involved in the protein-substrate interactions in most of the docking structures, which suggested they might play an important role in stabilising protein-substrate complexes. Interestingly, only the extended substrate conformations interacted with residue Glu148. The proposition of the extended conformation provides a better representation of a substrate pose that is relevant to the catalytic activity of the enzyme.

The following findings discussed the introduction of mutation in LcpK30 based on single-point mutation. Among the four residues (Lys167, Leu171, Ile396, and Ala159) identified as frequently interacting with the ligand in the docking conformation, Leu171 emerges as a potentially favourable candidate for mutation to investigate its impact on catalytic activity and substrate preferences. This is due to its proximity to the heme and its position where an amino acid change occurred compared to the LcpSH22a sequences. The exchange of Leu171 with a smaller non-polar residue (alanine) and two aromatic residues with different steric bulk (phenylalanine and tryptophan) was analysed using computational techniques.

Based on the computational analysis, the Leu171Phe mutant showed a different tunnel mapping than the wild-type LcpK30. Molecular docking of *cis*- and *trans*-

1,4-polyisoprene in Leu171Phe mutant revealed a preference towards *trans*-substrate and similar potential as the wild-type to interact with *cis*- substrate. Meanwhile, the Leu171Ala mutant showed a higher fitness score for *cis*-1,4-polyisoprene binding than the wild-type and other mutants. Identifying high-probability tunnels in Leu171Ala mutant resulted in similar tunnel orientation with wild-type LcpK30 but with increasing tunnel radius on average. For the Leu171Trp mutant, a tunnel mapping similar to Leu171Phe was observed but had a lower fitness score for both ligands.

Experimentally, a single point mutation at position 171 with a smaller or aromatic non-polar residue affected the heme association and catalytic activity. The enzymatic cleavage of the C=C bond catalysed by Leu171Phe was comparable with the wild type. In contrast, Leu171Ala was shown to have reduced catalytic activity. Interestingly, the oligo-isoprenoid produced from NR degradation catalysed by the Leu171Ala mutant was more variable and dominated by more extended oligomers. Modifying Leu171 to Ala and Phe does not affect the LcpK30 substrate preference because none of the mutants could catalyse the degradation of *trans*-1,4-polyisoprene.

In conclusion, the work discussed in this chapter further explains the relationship between LcpK30 structure, catalytic activity and the interaction with its substrate (*cis*-1,4-polyisoprene). This study confirmed the involvement of other residues (Ala159, Leu171, and Ile396) that are important for ligand interaction when a more extended ligand model is employed for molecular docking. Eventually, the effect of a single point mutation at the Leu171 position provides evidence of subtle changes in the protein structure conformation and heme association. Subsequently, it influences the protein-ligand interaction that results in different degradation products. However, it is important to note that this mutation cannot modify the substrate scope of LcpK30. Further



investigation is required to understand this aspect fully. Nevertheless, the findings obtained in this study are useful to advance the research on LcpK30 mutations, such as developing a mutant library.

## CHAPTER 6

### OVERALL DISCUSSION, CONCLUSION AND FUTURE WORKS

#### 6.1 Overall discussion

The highlights of the findings from this thesis are:-

1. LcpK30 is able to catalyse the degradation of high molecular weight synthetic *cis*-1,4-polyisoprene, similar to Lcp1VH2. It can also react on other C=C bond rubbers such as ENR25 as well as co-solvent emulsified low molecular weight synthetic *cis*-1,4-polyisoprene synthesised from natural or synthetic monomer and produced oligomers with three to five and seven isoprene units.
2. An initial understanding of the pathway mapping in LcpK30 was acquired by the identification of two major tunnels. Further analysis of LcpK30 and polyisoprene interaction was conducted using molecular docking, employing a more comprehensive ligand model with ten C=C bonds. This research unveiled two primary conformations of the ligand: extended and folded. Three residues (Ala159, Leu171, and Ile396) that have not been mentioned in other studies showed the potential to be mutated for protein engineering.

The work described in this thesis represented the three main objectives of this research, which include obtaining pure LcpK30, investigating the potential of LcpK30 to degrade other rubbers containing C=C bond and an attempt to create LcpK30 mutants, based on the understanding of its structure and catalytic mechanisms obtained from computational analysis.

This research is the first work investigating the potential of LcpK30 conducted in the laboratory of Sustainable Process Technology, University of Nottingham. The first part of this research focused on the expression and purification of

active and pure LcpK30. The works include a comprehensive analysis of the production of LcpK30, characterisation of its properties, determining the enzyme degradability limiting factors (substrate concentration, temperature, and enzyme concentration) and optimising the production of bifunctional oligomeric products from natural rubber (NR) degradation catalysed by LcpK30. The expression approach of the Strep-tagged LcpK30 version in this study was developed based on thorough work by previous researchers.<sup>113,118,120,130</sup>

In the initial part of LcpK30 production, as described in Chapter 3, it was concluded that 11.1 mg protein yield per 800 mL expression culture was the optimum that could be produced. The heterologous expression in *E. coli* C41(DE3) was induced using 3 mM lactose after the cell reached an optical density of OD<sub>600</sub> 0.6. The value was less by ~3.9 mg compared to the previous study on upscaling LcpK30 production by Rother *et al.* (2017).<sup>119</sup> Several adjustments were made throughout this research, especially involving the work to optimise the production of an enzyme from the mutants of LcpK30 created in this study. The mutants express the protein better when induced with isopropyl β-D-1-thiogalactopyranoside (IPTG) after the *E. coli* C41(DE3) host cell reached a higher density. Therefore, the same approach was used to express the wild-type LcpK30. Interestingly, the production of wild-type LcpK30 was improved at about three times higher than the initial production by inducing the cell with 1 mM IPTG at a higher cell density (OD<sub>600</sub> = 0.8 - 1) with slower agitation (100 rpm) after induction. The stability of pure LcpK30 on storage was better in the presence of glycerol, as described in previous literature.<sup>130</sup> Therefore, LcpK30 at a concentration of 10 mg mL<sup>-1</sup> was stored with 50 % glycerol at - 80 °C was adapted as routine storage up until one month, while for short-term storage, the enzyme was kept at - 20 °C. The stability of LcpK30 on several hydrocarbon solvents showed a maximum of 70 % activity reduction in the

presence of 1 % (vol/vol) solvents. Although reductions in LcpK30 activity were observed, *n*-hexadecane, *n*-tetradecane and *n*-hexane can potentially be used for pretreatments of rubber before proceeding with biodegradation.

The following experiment to achieve the first objective of this thesis, as discussed in Chapter 3, was the investigation of the reaction system for NR degradation catalysed by LcpK30. The enzyme concentration was linearly correlated with the produced oligomers. It was concluded that the reaction performed better at 30 °C. The main limiting factor of the reaction system was the concentration of substrates, which probably influenced substrate supply to the enzyme active site (mass transfer limitation).<sup>279</sup> The theories on accessible surface area (ASA) and specific surface area (SSA) could be applied to enzymatic catalyse reactions of all hydrophobic substrates.<sup>222</sup> These theories, which have been thoroughly discussed in Chapter 3, gave an insightful view that help envisage the work described in Chapter 4.

In the biodegradation of polymers, pretreatment of these materials has become crucial to increase the biodegradation rate by enhancing the accessible and specific surface area between the polymer and the enzyme.<sup>280,281</sup> In order to adhere to a sustainable framework, it is preferable to utilise a pretreatment technique that does not necessitate excessive energy consumption or additional chemical usage and can be easily implemented on a large scale. This study demonstrated three pretreatment techniques: transforming solid elastic rubber into films and particles and turning viscous liquid rubber into a solvent-stabilized emulsion, effectively increasing the rubber's surface area, and making it more accessible to LcpK30.

LcpK30 has shown its ability to degrade other C=C bond polymers. As discussed in Chapter 4, LcpK30 can catalyse the degradation of ENR with 25 % epoxide content and synthetic *cis*-IR of high (*h*-IR-100K) and low (*l*-IR-

35K and *I*-IR-38K) molecular weight in different substrate morphology. The enzyme's ability to interact with the film-prepared substrate implied that other rubber products that were already in film form might react with LcpK30 for biodegradation provided the rubber has gone through the appropriate pretreatment, such as solvent precipitation to get thinner film or solvent extraction to eliminate the additives. Another promising approach is by dissolving the rubber in hydrocarbon solvents (e.g., *n*-tetradecane, *n*-hexadecane) and emulsifying it as oil-in-water droplets. The presence of small droplets in the aqueous medium will result in an increase in the surface area available for the enzyme. An essential factor in ensuring a stable emulsion is the correct balance between the hydrophobic and hydrophilic moieties that can be governed by adding surfactant.<sup>282</sup> However, the presence of surfactant might cause a detrimental effect on the enzyme activity. Thus, the stability of the co-solvent emulsion is maintained by steric repulsion, which can be improved by using longer hydrocarbon chains and polymers with higher hydrophobicity.<sup>246</sup> The higher molecular weight *cis*-1,4-polyisoprene was also pretreated by physical grinding into  $\pm 2$  mm and 600  $\mu\text{m}$  particles. The conversion of the polymer into bifunctional oligomers was better when the degradation was performed with the smaller particles coherent with results reported in previous literature.<sup>137,203,283</sup> Presence of an epoxide group in epoxidised NR (ENR) or vinyl branching group in polybutadiene rubber (PBR) and stereochemistry of the C=C bond have proven that the variation of the chemical structures results in different enzymatic degradability.

The findings for the third objective of this research have provided a more valuable understanding through computational analysis of the complex interaction between two flexible macromolecules of LcpK30 and its substrate (*cis*-1,4- polyisoprene). Based on the finding of LcpK30 tunnels mapping and a

more directive molecular docking of a longer *cis*-1,4-polyisoprene with ten repetitive isoprene units, four residues (Ala159, Lys167, Leu171 and Ile396) were found to have mostly and frequently interacted with the substrate. Considering the proximity of the Leu171 residue to the heme, which serves as the active site of LcpK30, the study proceeded by introducing a single point mutation at Leu171, substituting it with Ala, Phe, and Trp. The objective was to assess if this mutation may potentially modify the substrate specificity of LcpK30 towards *trans*-1,4-polyisoprene or enhance the enzyme's catalytic activity. Although none of the enzymes could catalyse the degradation of *trans*-1,4-polyisoprene, there is an improvement in heme occupancy in the Leu171Phe mutant with comparable specific activity between the mutant and the wild type.

## **6.2 Conclusions and future work**

The primary aim of this study is to utilise an enzyme that catalyses the oxidative cleavage of C=C bonds in NR, known as LcpK30, as a biocatalyst to introduce a sustainable biotechnology-based approach for rubber waste treatment. Therefore, the early focus was to produce pure and active LcpK30. Variable approaches have been taken to ensure higher production of LcpK30 compared to previous literature could be obtained. Optimum LcpK30 expression required mild conditions (20 °C, 100 rpm) with a more stable inducing agent (1 mM IPTG) and a suitable high cell density for starting the induction process. The performance of LcpK30 produced in this lab was consistent with previous literature. Nevertheless, improvements in LcpK30 specific activity and the quantity of oligomers produced still need to be achieved. Therefore, future work on LcpK30 could focus on improving its characteristics (heme occupancy), activity, and stability.

The ability of LcpK30 to degrade hydrophobic rubber was highly reflected in the substrate loading, chemical structure, and physical morphology. In this study,

LcpK30 is able to catalyse the enzymatic degradation of high and low molecular weight IR and ENR25. The oligomer yield from high molecular weight IR and ENR25 biodegradation was 66 % or 33 mg from 50 mg initial mass and 5 % or 25 mg from 500 mg initial mass. However, the presence of other chemical groups, such as ENR50 with higher epoxidation levels of 50 % and vinyl group in PBR, might hinder the ability of LcpK30 to access the C=C bond. It is suggested that another strategy for synthetic rubber biodegradation can be carried out by performing a synergistic enzymatic catalyse biodegradation using multiple types of Lcps such as Lcp1VH2, LcpSH22a and LcpK30. Rother *et al.* (2017) showed an example of this reaction system, which used rubber oxygenases (RoxA and RoxB) and LcpK30 to degrade NR and produce more oligomers with smaller sizes.<sup>119</sup>

LcpK30 catalyses the degradation of NR through the endo-cleavage of the C=C bond, which results in a mixture of oligomers with different lengths. Thus, additional steps such as FPLC would be required to separate and purify the oligomers to be suitable for other applications. However, this step could be evaded by using rubber oxygenase such as RoxA that degrades the *cis*-1,4-polyisoprene chain into a single oligo-isoprenoid (C<sub>15</sub>) identified as 2-oxo-4,8-dimethyl-trideca-4,8-diene-1-al (ODTD).<sup>284</sup> Nevertheless, mixtures of oligomers with a low polydispersity could be used as valuable materials, for example, as replacements of squalene in emulsion for vaccine adjuvant formulation.

The site for single point mutation of LcpK30 was determined based on several aspects that include identification of residues lining up the main pathway in LpK30, molecular docking of *cis*-1,4-polyisoprene with ten isoprene unit on LcpK30, and sequence comparison with LcpSH22a. One of the mutants (Leu171Phe) showed better heme occupancy but with no increment of specific

activity. Additionally, the mutant could not catalyse the C=C bonds in *trans*-1,4-polyisoprene, indicating that substituting Leu171 with Phe could not alter the LcpK30 substrate scope. Besides Leu171, another two residues (Ala159 and Ile396) would allow more options to introduce mutation in LcpK30. Given that the position of Ala159 and Ile396 are near the bulk solvent, there is a potential to mutate these residues with aromatic non-polar residues, for example, to observe its effect on solvent resistance.

Another approach to creating supreme LcpK30 variants is by directed evolution. To materialise this method, rapid screening for active variants is essential. Developing a quantitative Schiff's reagent colourimetric assay based on spectrophotometry is promising. The work described in Chapter 4, Section 4.4 provides insightful information on the reaction between the analyte (the degraded NR reaction mixture and the ethyl-acetate solubilised fraction) and Schiff's reagent. Extensive validation would be required to improve this assay because achieving a good standard of an analytical assay supported with solid validations would be crucial.

The work described here has opened more possibilities for conducting more research related to LcpK30 and perhaps other Lcps to boost its potential as a biocatalyst for sustainable rubber waste treatment. From the perspective of the rubber industry, it is envisioned that the use of LcpK30 can be materialised not only as a biocatalyst for rubber biodegradation but also as a tool for NR modification to develop new speciality rubber.



## **APPENDICES**

### **Appendix 1: COVID-19 Impact statement**

I started my PhD in April 2019. During my first six months, the time was mostly spent on training, literature review and designing the experimental work. My first objective for my PhD project was to obtain pure and active LcpK30. Laboratory work started in the second six months of my first year. The work focused more on hands-on training to acquire protein expression and purification skills. The gene sequence for LcpK30 expression has been designed and sent for synthesis. While waiting for the gene that was constructed into a plasmid to arrive, I performed protein expression and purification work using the P450BM3 enzyme to familiarise myself with the lab work and the usage of the instruments, especially the Fast Protein Liquid Chromatography for protein purification. By January 2020, the first attempt to produce LcpK30 was carried out, but an active enzyme was not obtained due to several challenges. A new strategy to improve the LcpK30 production was to use different *E. coli* strains for the protein expression host. I ordered the cells, but then the pandemic started.

Starting on March 18th, 2020, the University must be closed due to government instruction for a national lockdown to control the COVID-19 pandemic. Thus, all activities in the laboratory must be halted and will only be resumed until further notice. Students must adopt a new working culture from home and conduct meetings/seminars via online mediums. During the national lockdown, all other businesses and services, including the school, were forced to close and work from home. As I just entered my 2<sup>nd</sup> (second) year on April 1st, 2020, I am supposed to focus more on experimental work and gain more data for analysis. However, due to the lockdown, I could not perform any experimental work and, therefore, couldn't reach my research objective planned for 2020 according to the timeline.

As a parent of five (5) children aged from 2 to 12 years old, four of them were in primary school. Due to the national lockdown, they have to stay at home and adapt to online learning at home. No childminder or nursery is available at this moment. Therefore, my husband and I have to provide 100% caring responsibility. The situation became more challenging as my husband was also doing his doctoral study (PhD) at King's College University of London and was allowed to work remotely from Nottingham. In the middle of June 2020, the schools started to re-open with strict regulations due to COVID-19 prevention measures. The schools were open only two weeks before the end-of-term school holiday, which started in July and went on until September. At the end of August (August 24th, 2020), research laboratories were resumed for re-opening. Overall, the laboratory works were halted for 6 (six) months.

Below is the list of limitations and challenges during the six months of national lockdown and university closure that impacted my routine and PhD work progress: -

1. Reduced working hours by 50% compared to regular working hours
2. Alternately, I schedule my working hours with my husband, who is also a postgraduate student
3. Shared caring responsibility for the children, especially the youngest (2-year-old daughter)
4. Have to supervise the children during their home online learning session
5. Responsible for doing the house chores/ household management
6. Time balancing between PhD and household management is challenging

Despite reducing working hours during the lockdown, frequent supervision with my supervisor via online meetings helped divert the plan of my research work. Besides my principal supervisor, I also have regular conversations through

emails with my co-supervisor and other experts related to my work. During the lockdown, I improved my writing and critical analysis skills by summarising my results and discussing the experimental data I obtained before the lockdown. I've also investigated some computational approaches to my project, but progress has been slow since this is an entirely new skill to learn. Nevertheless, I learned some computational tools, including Autodock Vina, Caver, PyMol, and docking analysis (LigPlot, Protein.plus and Protein-Ligand Interaction Profiler). My limited knowledge and experience in bioinformatics require me to continuously learn to improve my understanding and to use all the tools effectively. At the beginning of this work, the software installation was a hurdle due to the unfamiliarity of the process and limited support from the technical team and experts.

In early September 2020, all the children could return to school, and the laboratory's re-opening came with new challenges. The post-COVID-19 lockdown period has caused the working hours to be reduced to 7 hours (9 am- 4 pm) and on a rotation basis (one week on and one week off). Priority was given to all final-year PhD students and industrial researchers. Some of the challenges and limitations that I faced during the new working culture are listed below: -

1. Risk of being unable to perform everyday activities due to self-isolation requirement - Due to the COVID crisis, the school and university standard procedure for illness has changed. Every student showing any of three major Covid symptoms will be prohibited from schooling and must take the Covid screening test to confirm whether their symptoms are related to Covid or not. While waiting for the test, the student and everyone in the household must self-isolate. If the result is negative, students will be advised to seek a GP consultation to get treatment and

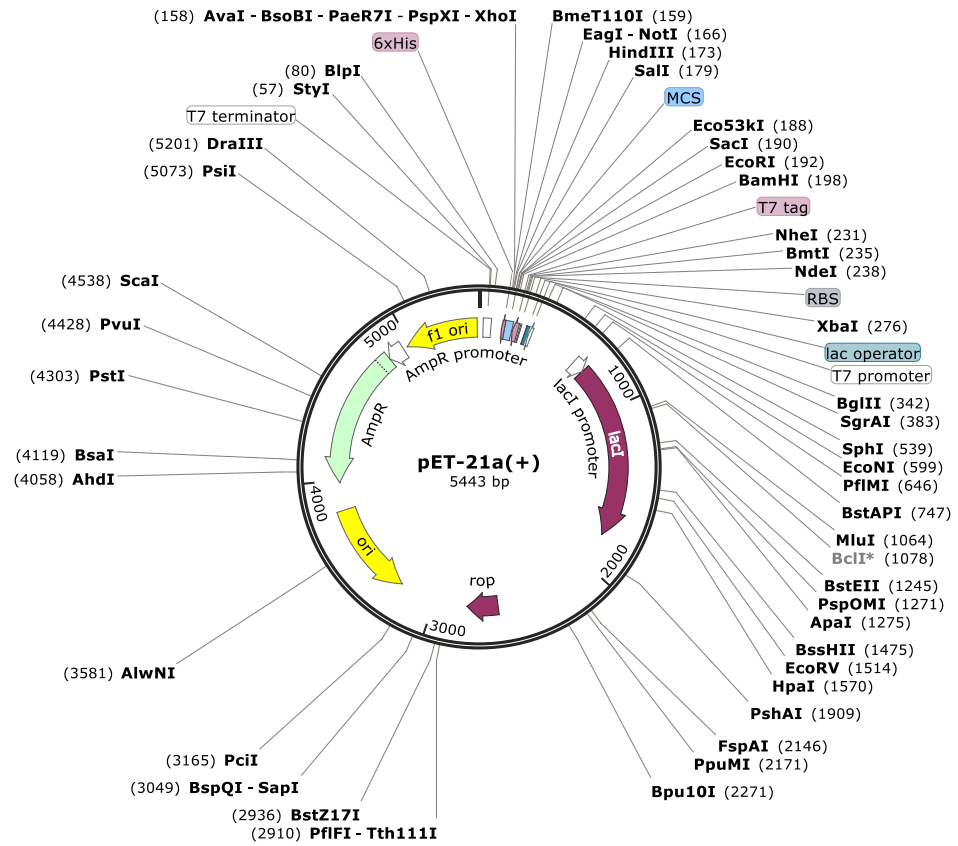
return to the school once they completely recover. If they are unable to take the Covid test, the student and everyone in the household must self-isolate for at least 14 days.

2. During self-isolation, the children will continue with home online learning that needs to be supervised by the parents.
3. Difficulty in finding a childminder for the youngest daughter; therefore, my husband and I need to share care responsibility.
4. Working at the laboratory on a weekly basis for one week (~ 6 h), and one week off (working at home with 50% capability, similar to during the lockdown) has caused the work progress to be very slow.

Since then, there have been a few occasions when my children needed to quarantine at home because of new COVID-19 infections at school. Ultimately, three (3) of my children were infected in February 2022. The second wave of COVID-19 that struck my family was in July 2022. My husband and our two younger children were having mild symptoms. Unfortunately for me, the symptoms were quite severe. It took about one month to fully recover, which caused another delay in my PhD work.

Overall, delays have accumulated in the project, which is very likely to need an extension to the thesis period to get experimental data and results of PhD quality. Due to that, MRB has granted me a one-year extension with a stipend to complete my experimental work. Another six months were given, but without a stipend, to complete my thesis writing.

## Appendix C2.1: Plasmid map of pET-21a(+)



## Appendix C2.2: Gene and amino acid sequences of the wild-type LcpK30

### Gene sequences (1194 bp, GenBank Accession Number: AAR25849.1)

CGGCCTCTGTGGACGTGGTCACCCAGCGCGTCCGGTGGCGGGCACGGG  
CGTGGGCGTCGATCCGGAGTACGTCTGGGACGAGGAGGCCGACCCGGT  
ACTCGCCGCAGTCATCGACCGCGGGGAGGTGCCCGCGGTCAACGCGCT  
GCTGAAACAGTGGACGCGGAACGACCAAGCGCTGCCCGGCGGACTCCC  
GGGAGACCTGCGGGAGTTCATGGAGCATGCGCGCAGGATGCCGTCTTG  
GGCGGACAAGGCAGCACTCGACCGCGGTGCCAGTTCAGCAAGACCAA  
GGGGATCTACGTCCGAGCCCTGTACGGCCTCGGCAGTGGACTGATGAG  
CACCGCCATACCAGGGAGTCGCGCGCCGTCTACTACTCCAAGGGCGG  
CGCGGACATGAAGGACCGCATCGCCAAGACCGCACGGCTCGGGTACGA  
CATCGGAGACCTGGACGCCTATCTGCCGCACGGTTCGATGATCGTGACC  
GCCGTCAAGACACGGATGGTGCACGCGGCGGTGCGCCACCTGCTGCCG  
CAGTCCCCGGCCTGGTCGCAGACCAGCGGCGGCCAGAAGATCCCGATC  
AGCCAGGCCGACATCATGGTCACTGGCACAGCCTGGCCACTTTCGTCA  
TGCGCAAGATGAAGCAGTGGGGCGTCCGGGTCAACACCGCCGACGCGG  
AGGCGTACCTTCACGTGTGGCAGGTCAGTGCGCACATGCTCGGGCGTCAG  
CGACGAGTACATCCCCGCGACCTGGGACGCGGCCAACGCGCAGTCGAA  
GCAGGTCTCGACCCGATCCTCGCCACACGCCCGAGGGGGAGGCGCT  
GACAGAGGTCTCTCGGCATCGTGGCCGAGCTCGACGCCGGCCTCAC  
CCGCCCCCTGATCGGCGGTTCTCCAGGTACACACTCGGCGGGCAGGT  
CGGCGACATGATCGGACTGGCCAAGCAGCCGGTCTGGAACGGCTGAT  
CGCGACGGCCTGGCCCCTGCTCGTGGCCTTCCGTGAAGGTCTGATACCT  
CTTCCCGCCGTCCCGGCGGTCTCTGGACACTCGAGGAAGCGCTCCGT  
AAGTTCGTCTGCTCTTCTCTCCGAGGGCCGGCGCATCGCCATCGACA  
TCCCGGACGTCAACCGCCCGTCC

Codon optimised gene sequence (The gene sequence used was codon optimised for expression in *E. coli* by the synthesising company, Biomatik. Underline is the added start codon)

atgtggagccatccgcagttgaaaaaagcagcggcgaaaatctgtatttcagggcggcagccgcccgt  
gtggacctggagccctagtgcaagtgtggcaggcaccggcgtggcgtggatccggaatatgttgggatg  
aagaagcagatccggttctggcagcagttattgatcgtggtgaagtccggcagtgaaatgactgctgaaac  
agtggaccgtaatgatcaggcactgcccggcgccctgcccgggtgacttacgtgaattcatggaacatgcc  
cgccgatgccgagctgggcagataaagcagccctggatcgtggtgacagtttagcaaaaccaaaggt  
atctatgtgggtgccctgtatggtctgggtagcggctctgatgagtaccgcaattccgctgaaagccgtgcagt  
gtattatagtaaaggcgtgacagatatgaaagatcgtattgcaaaaaccgcccgcctgggctatgatattggt  
gacctggatgatatctgccgatggtagcatgatttgaccgcccgtgaaaccctatggtgatgccgca  
gtcgtcatctgctgccgacagctccggcatggagtcagaccagtggtggccagaaaattccgattagcca  
ggcagatattatggtgacctggcatagcctggcaacctttgttatgctgaaaatgaaacagtggggtgtgctg  
gtgaataccgccgatgccgaagcatalctgcatgttggcaggttagcggccacatgctgggtgtgagtgatg  
aatatattccggcaacctgggatgcagcaaatgccagagtaaacaggttctggatccgattctggcacata  
ccccggaaggtgaagcactgaccgaagttctgctgggtattgttcagaaactggatgcaggtctgaccgca  
ccgctgattggtgcatttcacgttataacctggcggtgaagtgggtgacatgattggtctggccaaacagcc  
ggtgctggaacgcctgattgccaccgatggcgcgtgctggttcatttcgcaaggcctgattccgctgccg  
gcagttccggccgtgctgtggacctggaagaagccctgctgaaattgtgctgctgtttctgagtgaaagcc  
gtcgtattgcaattgatattccggatgtaaatcgtccgagc

**Amino acid sequence (397 aa, NCBI accession number: AAR25849)**

MWSHPQFEKSSGENLYFQGGSRPLWTWSPSASVAGTGVGVDPPEYVWDEE  
ADPVLAVIDRGEVPAVNALLKQWTRNDQALPGGLPGDLREFMEHARRMPS  
WADKAALDRGAQFSKTKGIYVGALYGLGSGLMSTAI PRESRAVYYSKGGAD  
MKDRIAKTARLG YDIGDL DAYLPHGSMIVTAVKTRMVHAAVRHLLPQSPAWS  
QTSGGQKIPISQADIMVTWHSLATFVMRKMKQWGV RVNTADAEAYLHVWQ  
VSAHMLGV SDEYIPATWDAANAQSKQVLDPI LAHTPEGEALTEVLLGIVAELD  
AGLTRPLIGAFSRYTLGGEV GDMIGLAKQPVLERLIATAWPLL VAFREGLIPLP  
AVPAVLWTL EEALRKFVLLFLSEGRRIAIDIPDVNRPS

**Appendix C2.3: Gene and amino acid sequences of the mutated LcpK30**

**(Leu171Ala)**

**Gene sequences were obtained from sequencing analysis performed by Source BioScience**

ATGTGGAGCCATCCGCAGTTTGAAAAAGCAGCGGGCGAAAATCTGTATTT  
TCAGGGCGGCAGCCGCCCGCTGTGGACCTGGAGCCCTAGTGCAAGTGT  
GGCAGGCACCGGCGTTGGCGTGGATCCGGAATATGTTTGGGATGAAGAA  
GCAGATCCGGTTCTGGCAGCAGTTATTGATCGTGGTGAAGTTCCGGCAG  
TGAATGCACTGCTGAAACAGTGGACCCGTAATGATCAGGCACTGCCGGG  
CGGCCTGCCGGGTGACTTACGTGAATTCATGGAACATGCCCGCCGCATG  
CCGAGCTGGGCAGATAAAGCAGCCCTGGATCGTGGTGCACAGTTTAGCA  
AAACCAAAGGTATCTATGTGGGTGCCCTGTATGGTCTGGGTAGCGGTCT  
GATGAGTACCGCAATTCCGCGTGAAAGCCGTGCAGTGTATTATAGTAAAG  
GCGGTGCAGATATGAAAGATCGTATTGCAAAAACCGCCCGCGGGGCTA  
TGATATTGGTGACCTGGATGCATATCTGCCGCATGGTAGCATGATTGTGA  
CCGCCGTGAAAACCCGTATGGTGCATGCCGCAGTGCGTGCATCTGCTGCC  
GCAGAGTCCGGCATGGAGTCAGACCAAGTGGTGGCCAGAAAATTCCGATT  
AGCCAGGCAGATATTATGGTGACCTGGCATAGCCTGGCAACCTTTGTTAT  
GCGTAAAATGAAACAGTGGGGTGTGCGTGTGAATACCGCCGATGCCGAA  
GCATATCTGCATGTTTGGCAGGTTAGCGCCACATGCTGGGTGTGAGTG  
ATGAATATATTCCGGCAACCTGGGATGCAGCAAATGCCAGAGTAAACAG  
GTTCTGGATCCGATTCTGGCACATAACCCGGAAGGTGAAGCACTGACCG  
AAGTTCTGCTGGGTATTGTTGCAGAACTGGATGCAGGTCTGACCCGCCC  
GCTGATTGGTGCATTTTCACGTTATACCCTGGGCGGTGAAGTGGGTGAC  
ATGATTGGTCTGGCCAAACAGCCGGTGCTGGAACGCCTGATTGCCACCG  
CATGGCCGCTGCTGGTTGCATTTCCGGAAGGCCTGATTCCGCTGCCGGC  
AGTTCCGGCCGTGCTGTGGACCCTGGAAGAAGCCCTGCGTAAATTTGTG  
CTGCTGTTTCTGAGTGAAGGCCGTGCTATTGCAATTGATATTCCGGATGT  
TAATCGTCCGAGCTAAAAGCTT

**Protein translation: Bold and underlined in red is the single-point mutation of Leu171Ala (L171A)**

MWSHPQFEKSSGENLYFQGGSRPLWTWSPSASVAGTGVGVDPPEYVWDEE  
ADPVLAVIDRGEVPAVNALLKQWTRNDQALPGGLPGDLREFMEHARRMPS  
WADKAALDRGAQFSKTKGIYVGALYGLGSGLMSTAIPRESRAVYYSKGGAD  
MKDRIAKTAR**A**GYDIGDLDAYLPHGSMIVTAVKTRMVHAAVRHLLPQSPAWS  
QTSGGQKIPISQADIMVTWHSLATFVMRKMKQWGVVNTADAEAYLHVWQ  
VSAHMLGVSDYIPATWDAANAQSKQVLDPIAHTPEGEALTEVLLGIVAELD  
AGLTRPLIGAFSRYTLGGEVGMIGLAKQPVLERLIATAWPLLVAFREGLIPLP  
AVPAVLWTLEEALRKFVLLFLSEGRRIAIDIPDVRPS-KL

**Appendix C2.4: Gene and amino acid sequences of the mutated LcpK30 (Leu171Phe)**

**Gene sequences were obtained from sequencing analysis performed by Source BioScience**

ATGTGGAGCCATCCGCAGTTTGAAAAAGCAGCGGCGAAAATCTGTATTT  
TCAGGGCGGCAGCCGCCCGCTGTGGACCTGGAGCCCTAGTGCAAGTGT  
GGCAGGCACCGGCGTTGGCGTGGATCCGGAATATGTTTGGGATGAAGAA  
GCAGATCCGTTTCTGGCAGCAGTTATTGATCGTGGTGAAGTTCCGGCAG  
TGAATGCACTGCTGAAACAGTGGACCCGTAATGATCAGGCACTGCCGGG  
CGGCCTGCCGGGTGACTTACGTGAATTCATGGAACATGCCCGCCGCATG  
CCGAGCTGGGCAGATAAAGCAGCCCTGGATCGTGGTGCACAGTTTAGCA  
AAACCAAAGGTATCTATGTGGGTGCCCTGTATGGTCTGGGTAGCGGTCT  
GATGAGTACCGCAATTCCGCGTGAAAGCCGTGCAGTGTATTATAGTAAAG  
GCGGTGCAGATATGAAAGATCGTATTGCAAAAACCGCCCGCTTCGGCTA  
TGATATTGGTGACCTGGATGCATATCTGCCGCATGGTAGCATGATTGTGA  
CCGCCGTGAAAACCCGTATGGTGCATGCCGCAGTGCGTGATCTGCTGCC  
GCAGAGTCCGGCATGGAGTCAGACCAGTGGTGGCCAGAAAATTCCGATT  
AGCCAGGCAGATATTATGGTGACCTGGCATAGCCTGGCAACCTTTGTTAT  
GCGTAAAATGAAACAGTGGGGTGTGCGTGTGAATACCGCCGATGCCGAA  
GCATATCTGCATGTTTGGCAGGTTAGCGCCACATGCTGGGTGTGAGTG  
ATGAATATATTCCGGCAACCTGGGATGCAGCAAATGCCAGAGTAAACAG  
GTTCTGGATCCGATTCTGGCACATACCCCGGAAGGTGAAGCACTGACCG  
AAGTTCTGCTGGGTATTGTTGCAGAACTGGATGCAGGTCTGACCCGCC  
GCTGATTGGTGCATTTTACGTTATACCCTGGGCGGTGAAGTGGGTGAC  
ATGATTGGTCTGGCCAAACAGCCGGTGTGGAACGCCTGATTGCCACCG  
CATGGCCGCTGCTGGTTGCATTTTCGCGAAGGCCTGATTCCGCTGCCGGC  
AGTTCCGGCCGTGCTGTGGACCCTGGAAGAAGCCCTGCGTAAATTTGTG  
CTGCTGTTTCTGAGTGAAGGCCGTCGATTGCAATTGATATTCCGGATGT  
TAATCGTCCGAGCTAAAAGCTT

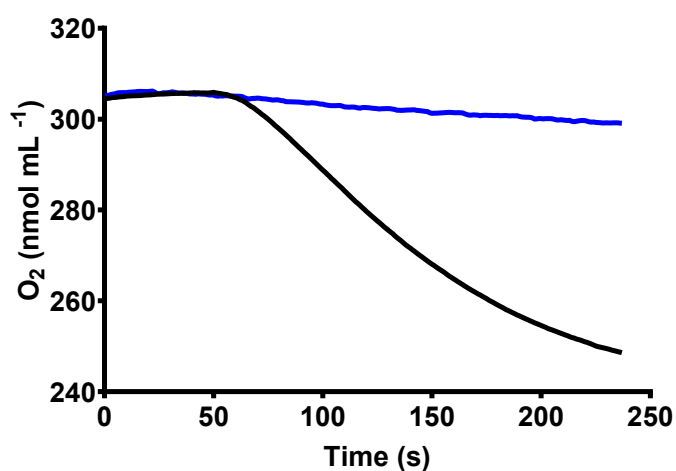


**Protein translation: Bold and underlined in red is the single-point mutation of Leu171Phe (L171F)**

HMWSHPQFEKSSGENLYFQGGSRPLWTWSPSASVAGTGVGVDPEYVWDE  
EADPVLAVIDRGEVPAVNALLKQWTRNDQALPGGLPGDLREFMEHARRMP  
SWADKAALDRGAQFSKTKGIYVGALYGLGSGLMSTAIPRESRAVYYSKGGA  
DMKDRIAKTARFGYDIGDLDAYLPHGSMIVTAVKTRMVHAAVRHLLPQSPAW  
SQTSGGQKIPISQADIMVTWHSLATFVMRKMKQWGV RVNTADAEAYLHVW  
QVSAHMLGVSDEYIPATWDAANAQSKQVLDPILAHTPEGEALTEVLLGIVAEL  
DAGLTRPLIGAFSRYTLGGEVGD MIGLAKQPVLERLIATAWPLLVAFREGLIPL  
PAVPAVLWTL EEALRKFVLLFLSEGRRIAIDIPDVNRPS-KL

### Appendix C3.1: Oxygen consumption assay of purified LcpK30

Example of graph for oxygen consumption assay of purified LcpK30 in the presence of natural rubber latex. Blue line: Control, Black line: 4  $\mu\text{g mL}^{-1}$  purified LcpK30 expressed in *E.coli* C41(DE3).



**Appendix C3.2: Sum of HPLC chromatogram peak area of oligomer derived from reactions with different enzyme concentration**

<b>LcpK30 concentrations (μM)</b>	<b>6</b>			<b>12</b>		<b>18</b>		<b>24</b>	
<i>Isoprene number (n)</i>	<i>Retention time (min)</i>	<i>Area</i>	<i>Retention time (min)</i>	<i>Area</i>	<i>Retention time (min)</i>	<i>Area</i>	<i>Retention time (min)</i>	<i>Area</i>	
<b>3</b>	22.599	1794.5	22.619	3304.2	22.669	5497.3	22.677	5112.5	
<b>4</b>	25.244	3750.5	25.264	6588.1	25.306	11000.7	25.317	10015	
<b>5</b>	26.911	4283.8	26.934	6910.4	26.988	11440.2	26.99	10625.5	
<b>6</b>	27.976	3756	27.995	6226.8	28.03	10086.8	28.042	9844.9	
<b>7</b>	28.681	3569.8	28.695	5048.7	28.716	8226.5	28.74	10035.2	
<b>8</b>	29.404	3772.1	29.422	5295.9	29.442	8461.6	29.473	9809.6	
<b>9</b>	30.268	2181.1	30.292	3625.1	30.317	5847.5	30.355	6930.2	
<b>10</b>	31.367	1337.9	31.399	2273.2	31.432	3598.6	31.48	4909.9	
<b>11</b>	32.829	1106.9	32.87	2129.3	32.914	3562.3	32.978	5377.5	
<b>12</b>	34.84	1157.9	34.896	1694.9	34.952	2691.8	35.044	3879.8	
<b>Sum of peak area</b>	<b>26710.5</b>		<b>43096.6</b>		<b>70413.3</b>		<b>76540.1</b>		
<i>Isoprene number (n)</i>	<i>Retention time (min)</i>	<i>Area(%)</i>	<i>Retention time (min)</i>	<i>Area(%)</i>	<i>Retention time (min)</i>	<i>Area(%)</i>	<i>Retention time (min)</i>	<i>Area(%)</i>	
<b>3</b>	22.599	6.718	22.619	7.667	22.669	7.807	22.677	6.679	
<b>4</b>	25.244	14.041	25.264	15.287	25.306	15.623	25.317	13.085	
<b>5</b>	26.911	16.038	26.934	16.035	26.988	16.247	26.99	13.882	
<b>6</b>	27.976	14.062	27.995	14.448	28.03	14.325	28.042	12.862	
<b>7</b>	28.681	13.365	28.695	11.715	28.716	11.683	28.74	13.111	
<b>8</b>	29.404	14.122	29.422	12.289	29.442	12.017	29.473	12.816	
<b>9</b>	30.268	8.166	30.292	8.412	30.317	8.305	30.355	9.054	
<b>10</b>	31.367	5.009	31.399	5.275	31.432	5.111	31.48	6.415	
<b>11</b>	32.829	4.144	32.87	4.941	32.914	5.059	32.978	7.026	
<b>12</b>	34.84	4.335	34.896	3.933	34.952	3.823	35.044	5.069	
<b>Sum of peak area (%)</b>	<b>100</b>		<b>100</b>		<b>100</b>		<b>100</b>		

**Appendix C3.3: Sum of HPLC chromatogram peak area of oligomer derived from reactions with different temperature**

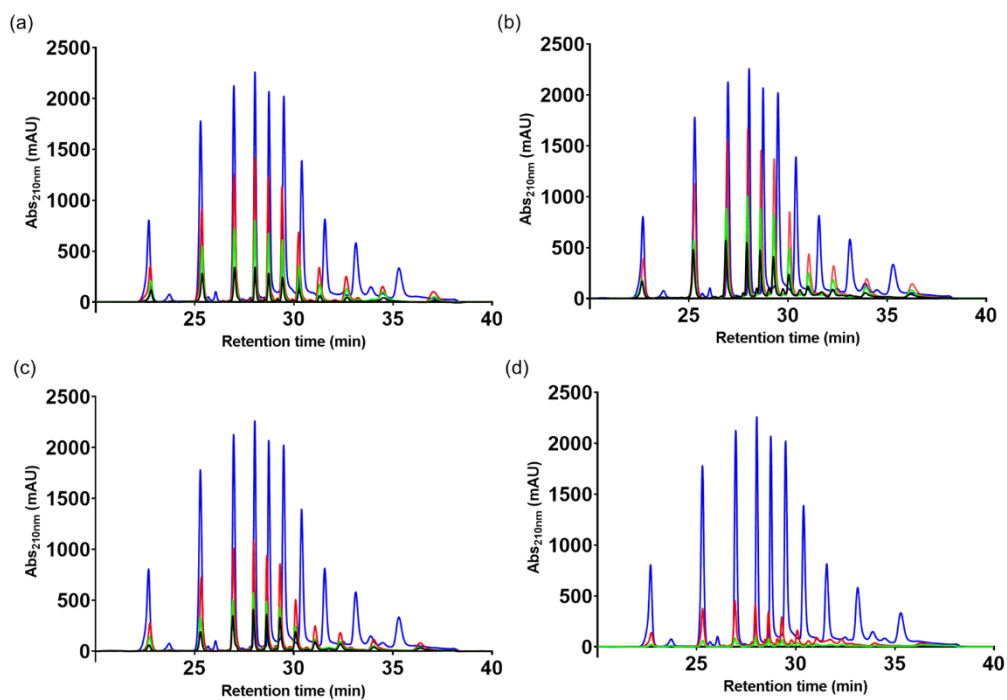
Reaction temperature (°C)		23		30	
<i>Isoprene number (n)</i>	<i>Retention time</i>	<i>Area</i>	<i>Retention time</i>	<i>Area</i>	
3	21.984	2094.4	22.022	2999.6	
4	24.73	3333.1	24.768	7642	
5	26.462	4410	26.501	8417.3	
6	27.619	4481.2	27.666	8447.6	
7	28.394	4233.2	28.446	7655.4	
8	29.185	5150.2	29.241	8844.5	
9	30.14	4729.1	30.202	7602.5	
10	31.361	3711.2	31.432	5930.6	
11	32.994	3293.1	33.071	5318.8	
11'	33.998	1936.5	not detected		
12	35.23	2523.8	35.319	3987.9	
<b>Sum of peak area</b>		<b>39895.8</b>	<b>66846.2</b>		
<i>Isoprene number (n)</i>	<i>Retention time</i>	<i>Area(%)</i>	<i>Retention time</i>	<i>Area(%)</i>	
3	21.984	5.25	22.022	4.487	
4	24.73	8.355	24.768	11.432	
5	26.462	11.054	26.501	12.592	
6	27.619	11.232	27.666	12.637	
7	28.394	10.611	28.446	11.452	
8	29.185	12.909	29.241	13.231	
9	30.14	11.854	30.202	11.373	
10	31.361	9.302	31.432	8.872	
11	32.994	8.254	33.071	7.957	
11'	33.998	4.854	not detected		
12	35.23	6.326	35.319	5.966	
<b>Sum of peak area</b>		<b>100</b>	<b>100</b>		

### Appendix C3.4: Sum of HPLC chromatogram peak area of oligomer derived from reactions with different substrate loading

Substrate loading per volume reation (mg mL <sup>-1</sup> )		10		40		60		100	
<i>Isoprene number (n)</i>	<i>Retention time (min)</i>	<i>Area</i>	<i>Retention time (min)</i>	<i>Area</i>	<i>Retention time (min)</i>	<i>Area</i>	<i>Retention time (min)</i>	<i>Area</i>	
3	22.921	2095.7	22.928	2337.7	22.892	1194.3	22.926	1948.8	
3'	-	-	23.948	1931	23.934	1352.9	-	-	
4	25.528	4401.8	25.563	4989.6	25.514	2458.9	25.557	4036.8	
5	27.156	4876.4	27.213	5353.6	27.155	3014.4	27.198	4913.9	
6	28.143	4613.2	28.188	5327.7	28.152	2841.5	28.186	4669.2	
7	28.876	4391.4	28.908	4877.9	28.885	2688.6	28.91	4262.6	
8	29.683	5363.7	29.713	5634.1	29.691	3019.7	29.718	4559	
9	30.673	3339.3	30.705	4467.6	30.679	2376.9	30.709	3355.9	
10	31.963	2950.3	32	3480.4	31.966	1940.6	32	3599.9	
11	33.707	2288.1	33.761	3811.3	33.715	1999.1	33.745	2562	
<b>Sum of peak area</b>		<b>34319.9</b>		<b>42210.9</b>		<b>22886.9</b>		<b>33908.1</b>	
<i>Isoprene number (n)</i>	<i>Retention time (min)</i>	<i>Area(%)</i>	<i>Retention time (min)</i>	<i>Area(%)</i>	<i>Retention time (min)</i>	<i>Area(%)</i>	<i>Retention time (min)</i>	<i>Area(%)</i>	
3	22.921	6.106	22.928	5.538	22.892	5.218	22.926	5.747	
3'	-	-	23.948	4.575	23.934	5.911	-	-	
4	25.528	12.826	25.563	11.821	25.514	10.744	25.557	11.905	
5	27.156	14.209	27.213	12.683	27.155	13.171	27.198	14.492	
6	28.143	13.442	28.188	12.622	28.152	12.416	28.186	13.77	
7	28.876	12.796	28.908	11.556	28.885	11.747	28.91	12.571	
8	29.683	15.629	29.713	13.348	29.691	13.194	29.718	13.445	
9	30.673	9.73	30.705	10.584	30.679	10.385	30.709	9.897	
10	31.963	8.596	32	8.245	31.966	8.479	32	10.617	
11	33.707	6.667	33.761	9.029	33.715	8.735	33.745	7.556	
<b>Sum of peak area (%)</b>		<b>100</b>		<b>100</b>		<b>100</b>		<b>100</b>	

### Appendix C3.5: HPLC chromatogram of oligomer peaks from reaction in the presence of solvents

HPLC chromatogram that shows the peaks for oligo-isoprenoids derived from natural rubber degradation catalysed by LcpK30 in the presence of solvent (a)Hexane (b)*n*-hexadecane (c)*n*-tetradecane (d)*n*-dodecane at different concentration. Blue - no solvent; Red - 0.2 % (v/v) solvent; Green - 0.5 % (v/v) solvent and Black 1.0 % (v/v) solvent.



**Appendix C3.6: HPLC chromatogram of oligomers from Reaction A and Reaction B: Calculation of the peak area percentage difference**

Reaction A (R <sub>A</sub> )			Reaction B (R <sub>B</sub> )		
Isoprene number (n)	Retention time (min)	Area	Isoprene number (n)	Retention time (min)	Area
3	22.169	21315.5	3	22.714	11180.9
4	24.827	28395.6	4	25.345	22769.8
5	26.518	23562	5	27.012	22636.8
6	27.668	16792.3	6	28.053	19969.2
7	28.395	14676.1	7	28.76	19562.5
8	29.037	13402.4	8	29.498	21514.4
9	29.762	8387.2	9	30.392	17420.5
10	30.657	3539.7	10	31.542	11809.1
11	31.808	3452.8	11	33.08	14201.7
12	33.352	4837.1			
Sum of peak area		138360.7	Sum of peak area		161064.9

$$\text{Percentage difference (\%)} = \frac{R_B - R_A}{\left(\frac{R_B + R_A}{2}\right)} \times 100$$

$$\text{Percentage difference (\%)} = \frac{161064.9 - 138360.7}{\left(\frac{161064.9 + 138360.7}{2}\right)} \times 100 = 15.2 \%$$

**Appendix C3.7: HPLC chromatogram of oligomers from Reaction A and Reaction B: Calculation of the molecular weight based on area (%)**

**Reaction A**

Isoprene number (n)	Retention time (min)	Molecular mass of the oligomer (g mol <sup>-1</sup> )	Area (%)	Mole fraction
3	22.17	306.49	12.82	39.28
4	24.83	374.61	15.48	58.00
5	26.52	442.73	13.66	60.49
6	27.67	510.85	11.11	56.77
7	28.40	578.97	10.32	59.73
8	29.04	647.09	9.84	63.65
9	29.76	715.21	7.95	56.85
10	30.66	783.33	6.12	47.96
11	31.81	851.45	6.09	51.85
12	33.35	919.57	6.61	60.80
<b>Estimated average molecular weight (g mol<sup>-1</sup>)</b>				<b>555.38</b>

**Reaction B**

Isoprene number (n)	Retention time (min)	Molecular mass of the oligomer (g mol <sup>-1</sup> )	Area (%)	Mole fraction
3	22.71	306.49	6.94	21.28
4	25.35	374.61	14.14	52.96
5	27.01	442.73	14.05	62.22
6	28.05	510.85	12.40	63.34
7	28.76	578.97	12.15	70.32
8	29.50	647.09	13.36	86.44
9	30.39	715.21	10.82	77.36
10	31.54	783.33	7.33	57.43
11	33.08	851.45	8.82	75.07
<b>Estimated average molecular weight (g mol<sup>-1</sup>)</b>				<b>566.41</b>

1 isoprene unit the Mw is 68.12 (g mol<sup>-1</sup>)

1 aldehyde unit 44.05 (g mol<sup>-1</sup>)

1 ketone unit 58.08 (g mol<sup>-1</sup>)

Molecular mass of the oligomer (g mol<sup>-1</sup>) = (n × 68.1) + 102.1

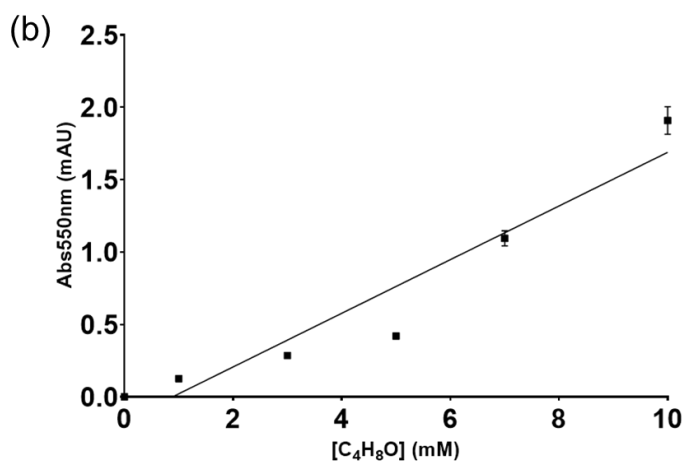
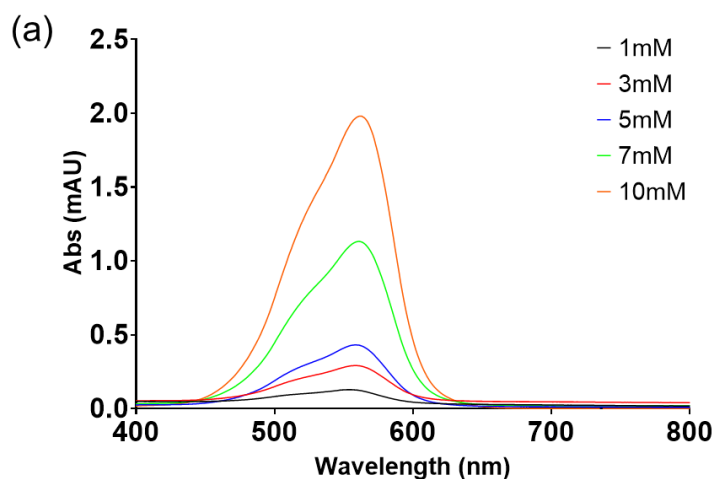
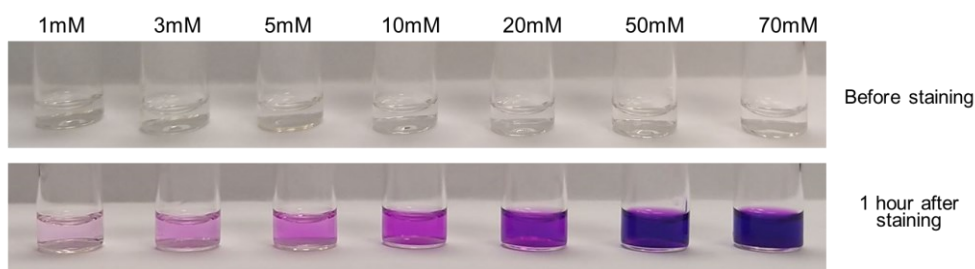
Average molecular weight

$$\begin{aligned} &= [(Area(\%)) \\ &\quad \times \text{Molecular mass of the oligomer } (g \text{ mol}^{-1})]_{n=3} \\ &\quad + \dots [(Area(\%)) \\ &\quad \times \text{Molecular mass of the oligomer } (g \text{ mol}^{-1})]_{n=11} \\ &= \left[ \left( \frac{6.94}{100} \right) \times 306.49 \right]_{n=3} + \dots \left[ \left( \frac{8.82}{100} \right) \times 851.45 \right]_{n=11} \\ &= \mathbf{566.41 \text{ g mol}^{-1}} \end{aligned}$$



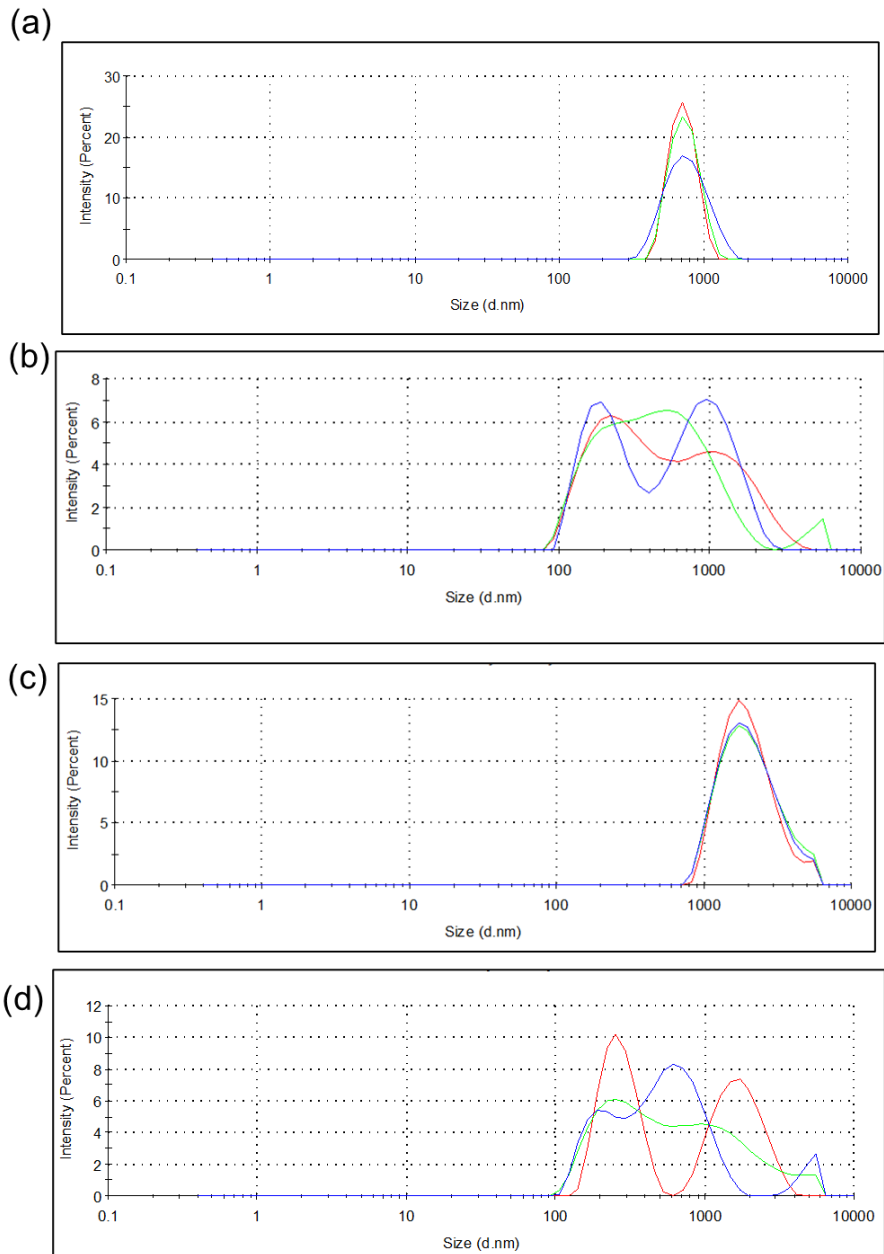
### Appendix C3.8: Schiff's reagent reaction on butyraldehyde

Colour development of butyraldehyde in different concentration staining with Schiff's reagent (top figure). (a) In the absorption spectrum from 350 to 800 nm, the  $C_4H_8O$  – Schiff reagent complex showed optimal absorbance at 560 nm. (b) A linear relationship between the absorbance measurement and aldehyde concentration was possible only over a small range of concentration (1 to 10 mM)

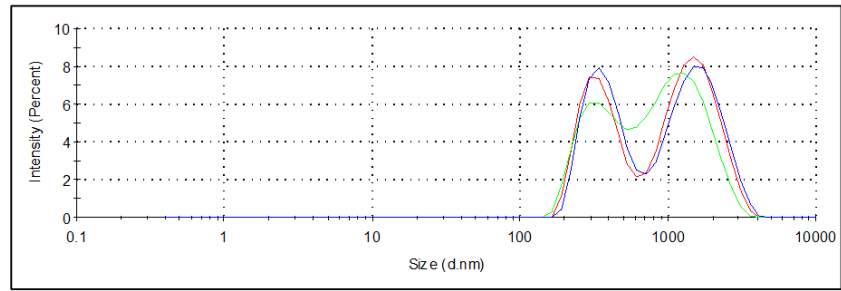


### Appendix C4.1: Size distribution intensity of emulsion droplets in the co-solvent emulsion

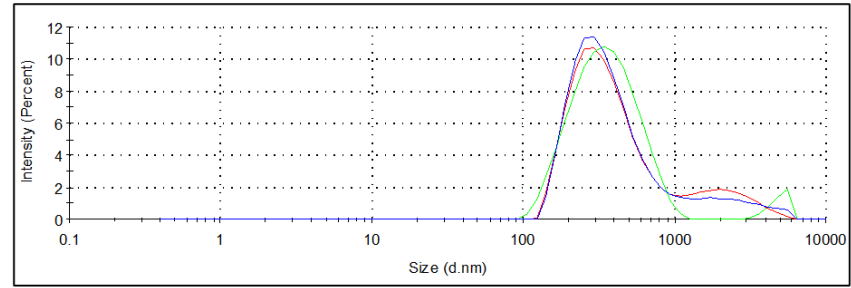
(a) Natural rubber (control) (b) *I*-IR-38K (c) *I*-IR-35K (d) PB-5000 (e) PB-2200 (f) PB-1300 (g) PB-1500 and (h) PB-5000S. The graph represents the size distribution intensity from three replicates of measurements.



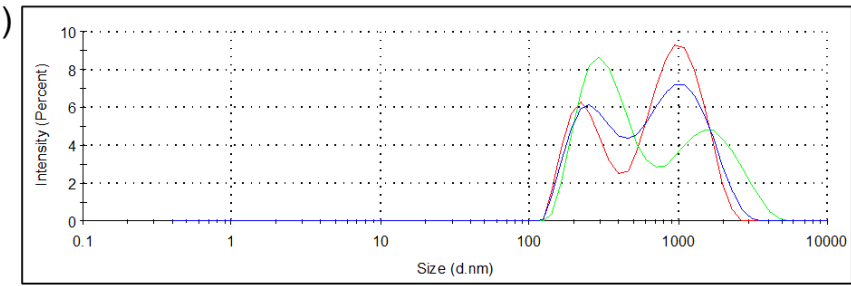
(e)



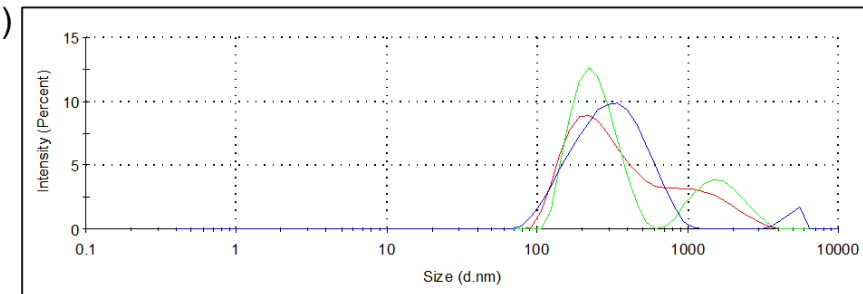
(f)



(g)

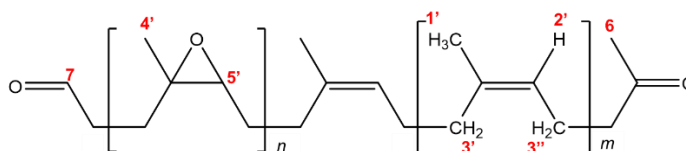


(h)



## Appendix C4.2: Estimation of the number of repeating units based on <sup>1</sup>H NMR spectrum of products from enzymatic degradation of ENR

Extracted values of the salient peak areas from the <sup>1</sup>H NMR spectrum. The number of repeating isoprene is represented by the olefinic moiety, and epoxy-isoprene units are represented by the epoxy methine moiety.



Moiety	Chemical shift (δ) ppm	Peak Area	No. of protons	<sup>a</sup> No. of repeating units when aldehyde is the moiety y
Olefinic (2')	5.12	1	1	200
Epoxy methine (5')	2.72	0.36	1	72
Aldehyde (7)	9.77	0.004	1	1
Aldehyde'	9.82	0.001	1	1

The calculation for the average length of the oligomer

$$n_{olefin} = \frac{1}{(0.004 + 0.001)} = 200$$

$$n_{epoxy\ methine} = \frac{0.36}{0.004 + 0.001} = 72$$

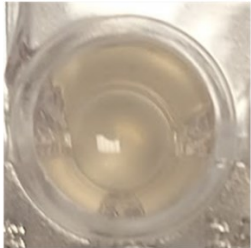

1 isoprene unit the Mw is 68.12 (g mol<sup>-1</sup>)

1 aldehyde unit 44.05 (g mol<sup>-1</sup>)

1 ketone unit 58.08 (g mol<sup>-1</sup>)

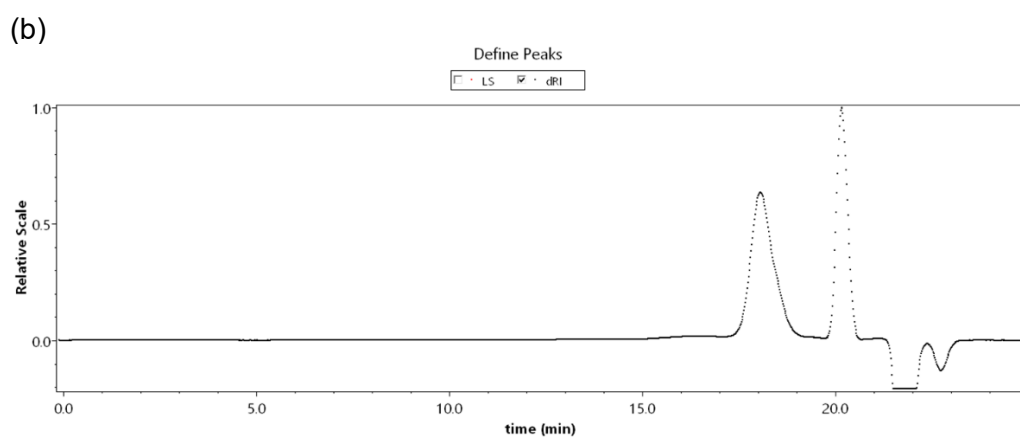
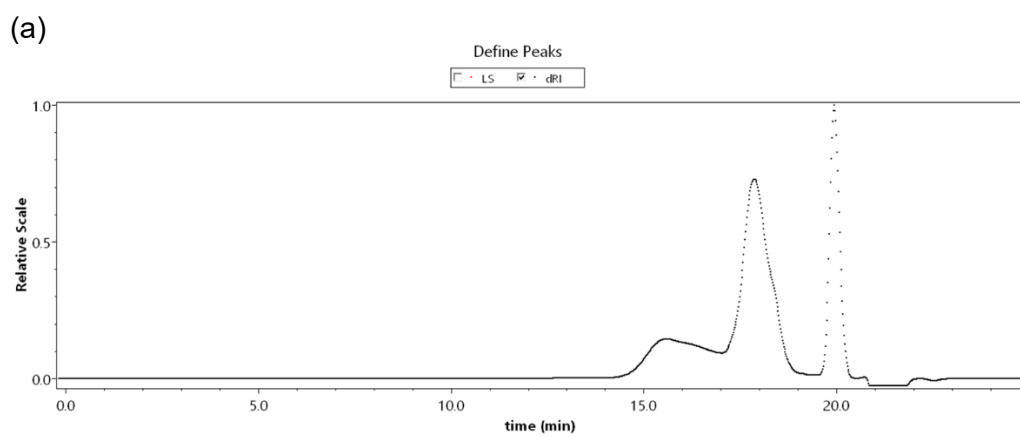
$$\text{Molecular mass of the oligomer (g mol}^{-1}\text{)} = (n \times 68.1) + 102.1$$

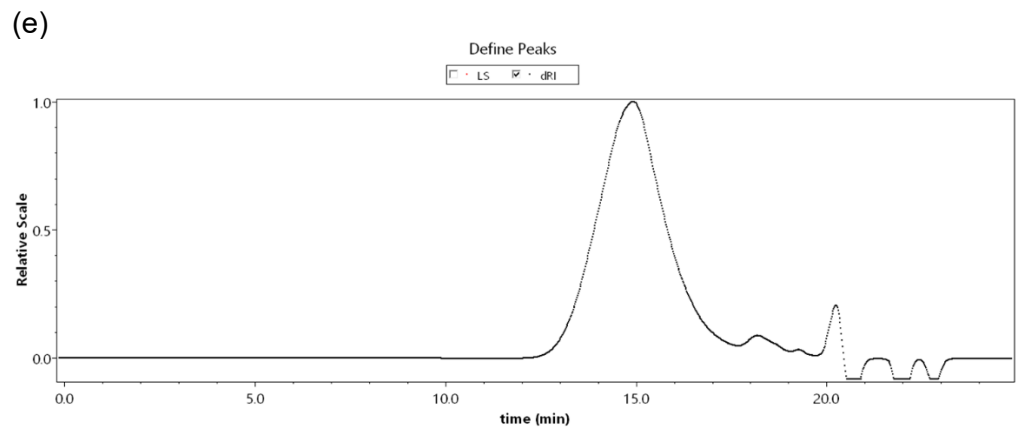
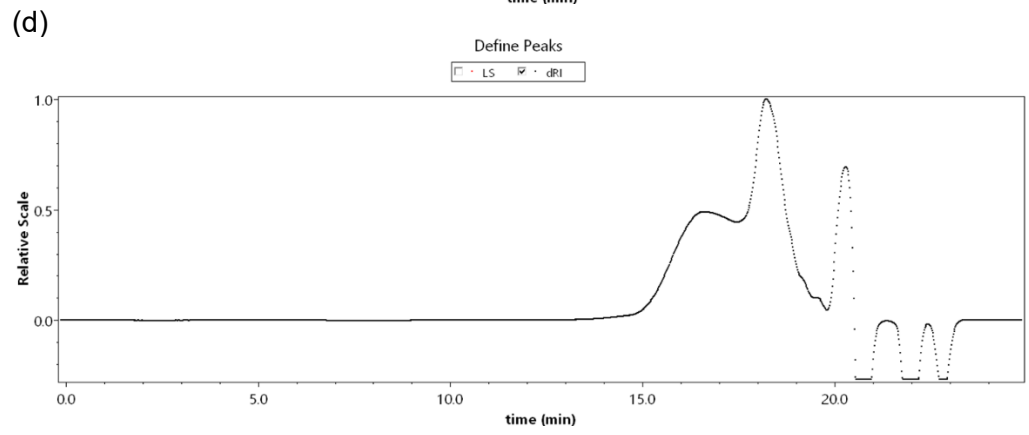
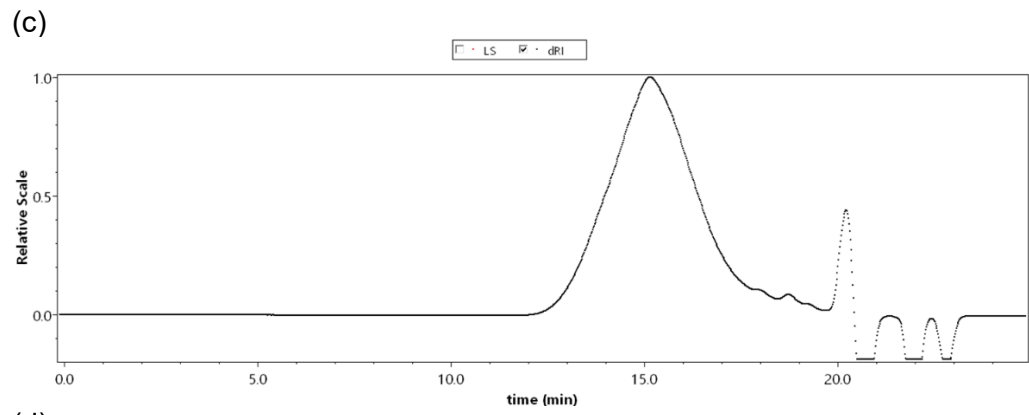
### Appendix C4.3: Colourimetric assay of the reaction suspension of NR degradation in solid-film form.

Polymer (substrate)	Colourimetric assay	
	+ LcpK30	- LcpK30
Natural rubber		

### Appendix C4.4: Molecular weight size distribution of oligo-isoprenoids

Molecular weight size distribution of oligo-isoprenoids derived from (a) Natural rubber (b) ENR25 (c) *l*-IR-38K (d) *h*-IR-100K and (e) *l*-IR-35K measured by Gel Permeation Chromatography (GPC).





**Appendix C4.5: HPLC chromatogram and <sup>1</sup>H NMR spectra of oligomers from the degradation of *h*-IR-100K in 600 μM particles**

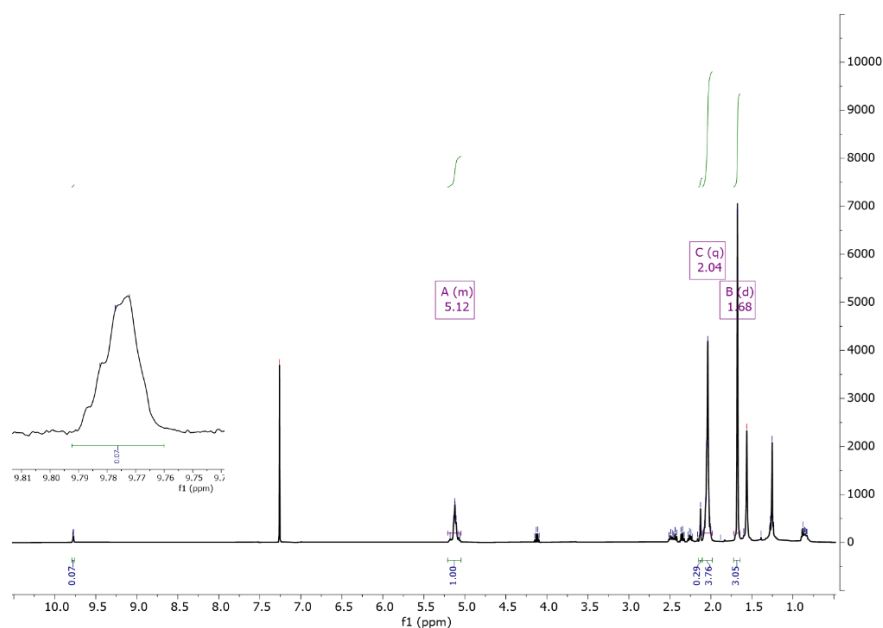
The calculation of the average molecular weight was based on area (%).

Isoprene number (n)	Retention time (min)	Molecular mass of the oligomers (g mol <sup>-1</sup> )	Area (%)	Area fractions
3	22.15	306.49	11.22	34.38
4	24.82	374.61	12.11	45.35
5	26.50	442.73	12.10	53.58
6	27.65	510.85	12.69	64.85
7	28.40	578.97	10.87	62.95
8	29.10	647.09	11.80	76.34
9	29.92	715.21	9.13	65.30
10	30.96	783.33	7.54	59.05
11	32.33	851.45	6.65	56.63
12	34.20	919.57	5.89	54.16
<b>Estimated average molecular weight (g mol<sup>-1</sup>)</b>				<b>572.59</b>

The average length of the oligomer was calculated based on <sup>1</sup>H NMR spectra.

Moiety	Chemical shift (δ) ppm	Peak Area	No. of protons	<sup>a</sup> No. of repeating units when aldehyde is the moiety y
Olefinic (2')	5.12	1	1	14
Aldehyde (7)	9.77	0.07	1	1

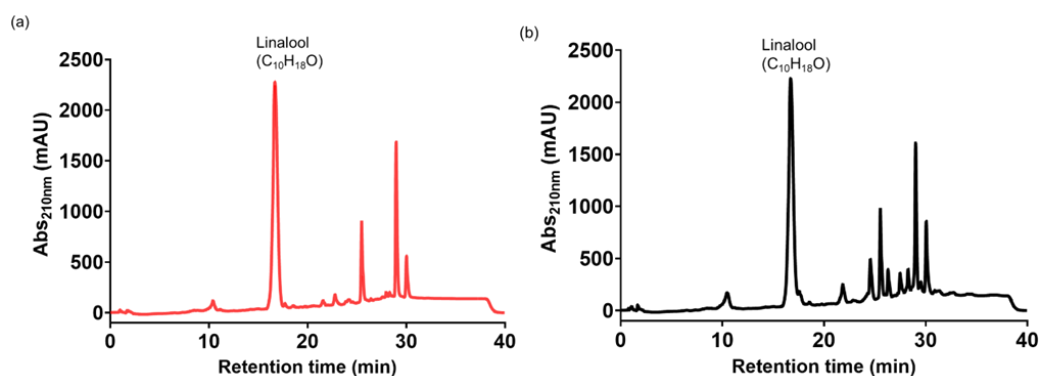
$$n_{olefin} = \frac{1}{(0.07)} = 14.28$$



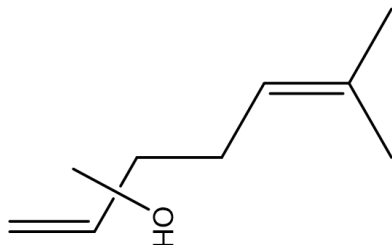
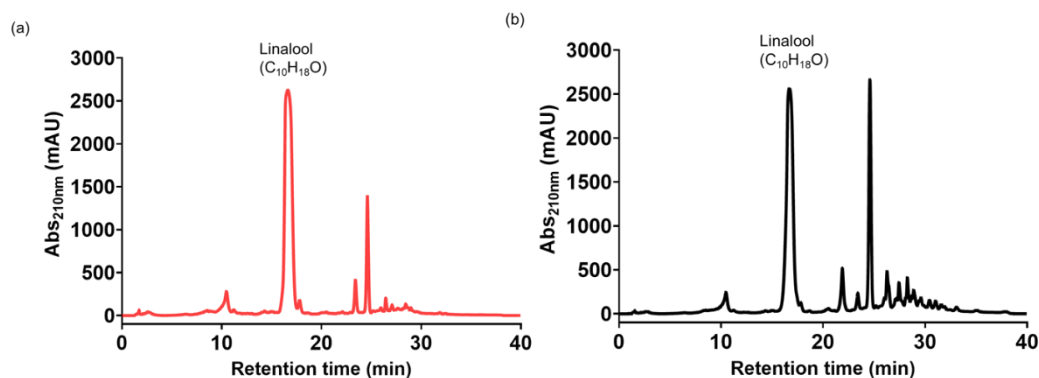
**Appendix C4.6: HPLC Chromatogram of dried residual extract from *I*-IR-35K and *I*-IR-38K degradation with and without LcpK30.**

(a) The dried residual extract from the reaction without LcpK30 was resuspended in 200  $\mu$ L methanol and added with 1 mM linalool (b) Similarly, 1 mM linalool was added into the HPLC vial containing 1 mg mL<sup>-1</sup> of oligomers obtained from the degradation.

*I*-IR-35K



*I*-IR-38K

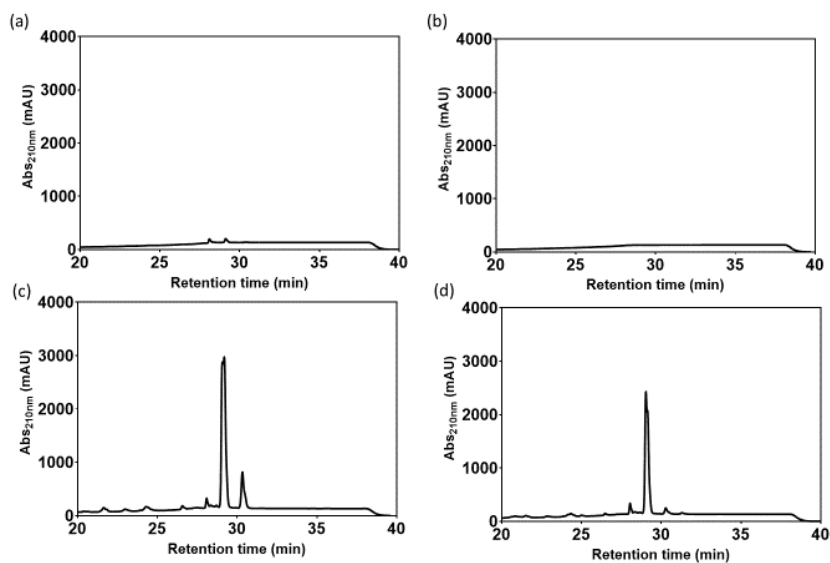


The chemical structure of linalool .



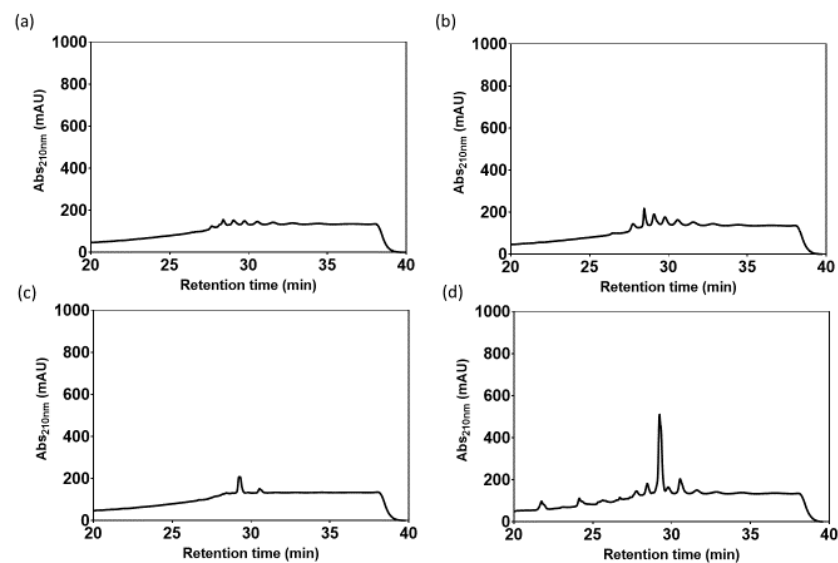
**Appendix C4.7: HPLC chromatogram of dried residual extract from a reaction with PB-5000**

(a) untreated PB-5000, (b) 100 mg mL<sup>-1</sup> PB-5000 dissolved in *n*-tetradecane, (c) dried residual extracted from the reaction on PB-5000 without LcpK30 and (d) dried residual extracted from the reaction on PB-5000 with LcpK30.



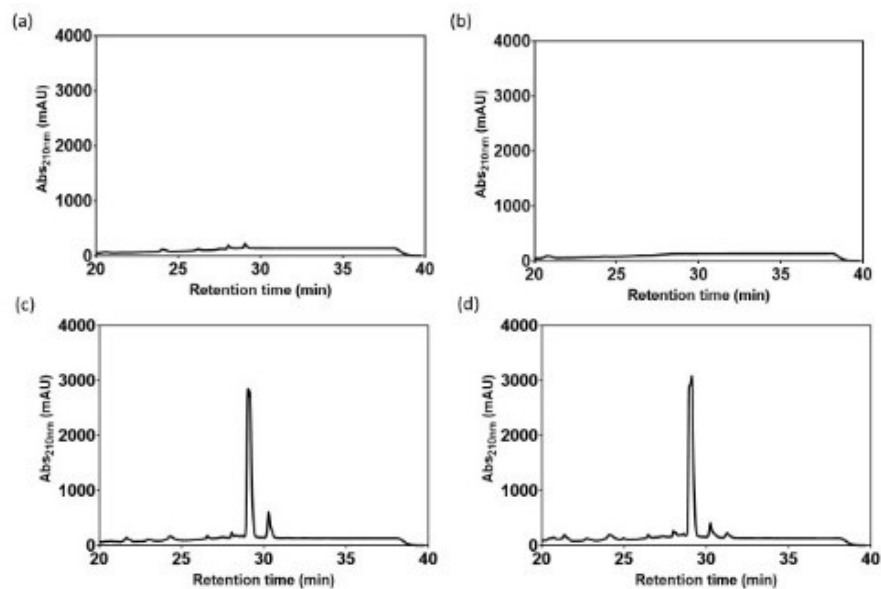
**Appendix C4.8: HPLC chromatogram of dried residual extract from a reaction with PB-2200**

(a) untreated PB-2200, (b) 100 mg mL<sup>-1</sup> PB-2200 dissolved in *n*-tetradecane, (c) dried residual extracted from the reaction on PB-2200 without LcpK30 and (d) dried residual extracted from the reaction on PB-2200 with LcpK30.



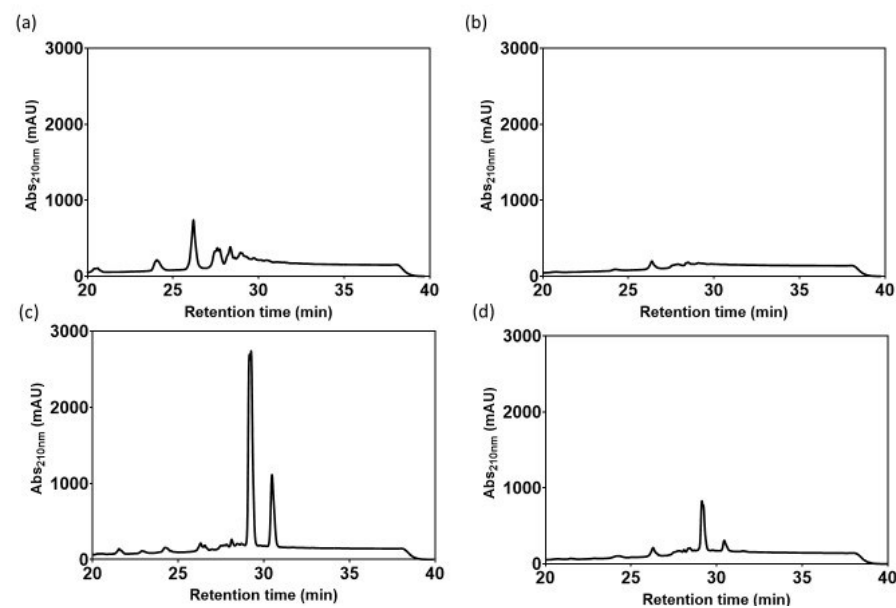
#### Appendix C4.9: HPLC chromatogram of dried residual extract from a reaction with PB-5000S

HPLC chromatogram of (a) untreated PB-5000S, (b) 100 mg mL<sup>-1</sup> PB-5000S dissolved in *n*-tetradecane, (c) dried residual extracted from the reaction on PB-5000S without LcpK30 and (d) dried residual extracted from the reaction on PB-5000S with LcpK30.



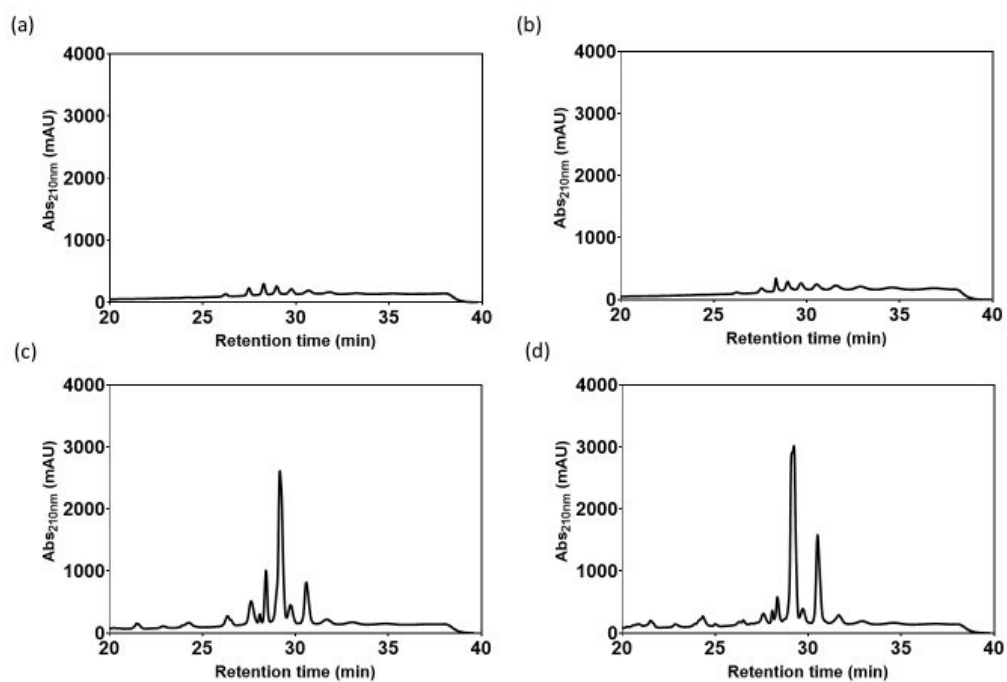
#### Appendix C4.10: HPLC chromatogram of dried residual extract from a reaction with PB-1300

(a) untreated PB-1300, (b) 100 mg mL<sup>-1</sup> PB-1300 dissolved in *n*-tetradecane, (c) dried residual extracted from the reaction on PB-1300 without LcpK30 and (d) dried residual extracted from the reaction on PB-1300 with LcpK30.



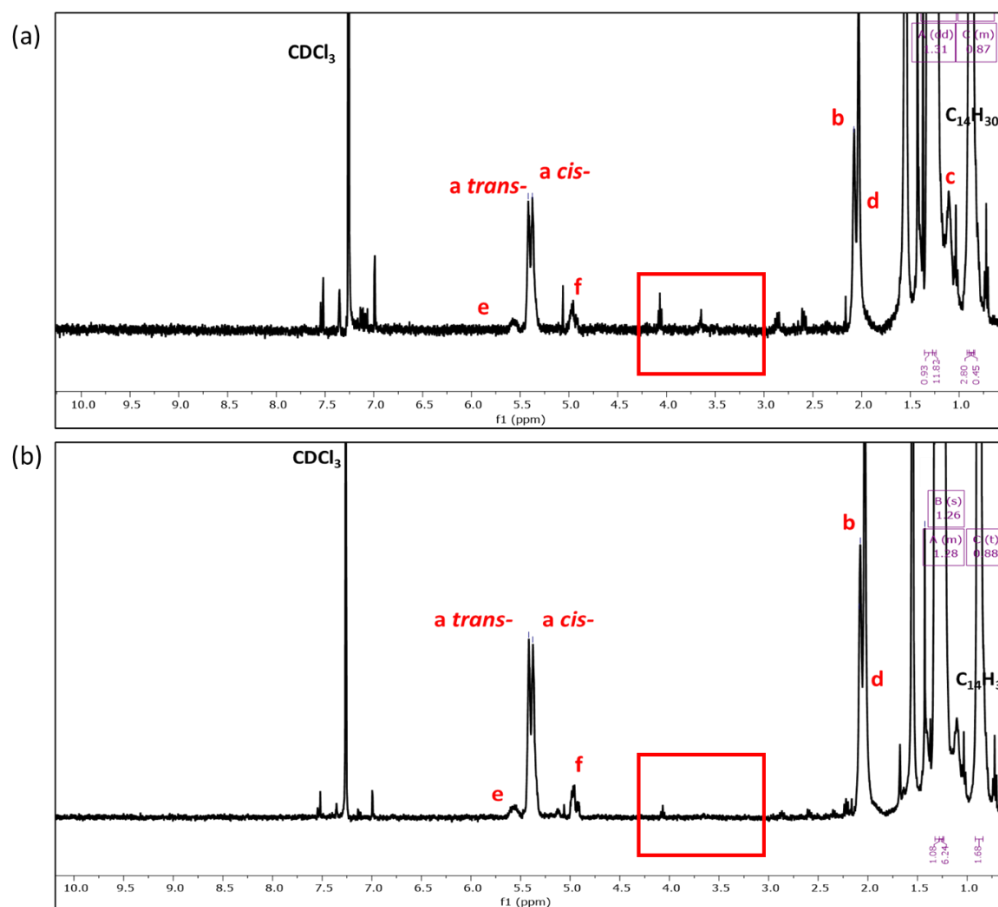
### Appendix C4.11: HPLC chromatogram of dried residual extract from a reaction with PB-1500

(a) untreated PB-1500, (b) 100 mg mL<sup>-1</sup> PB-1500 dissolved in *n*-tetradecane, (c) dried residual extracted from the reaction on PB-1500 without LcpK30 and (d) dried residual extracted from the reaction on PB-1500 with LcpK30.



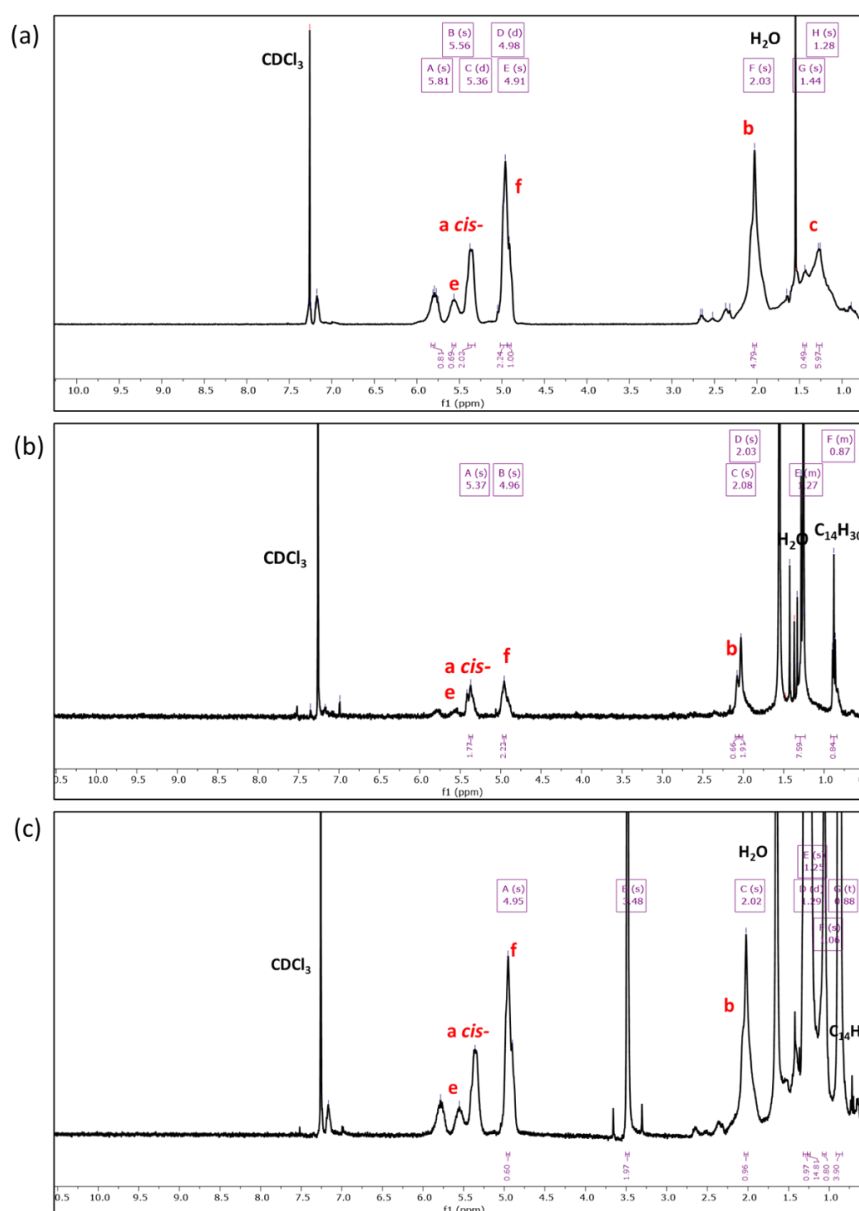
**Appendix C4.12:  $^1\text{H}$  NMR spectrum of dried residual extract from a reaction with PB-5000**

(a) Control setup of PB-5000 emulsion stabilised with n-tetradecane incubated without LcpK30 (b) PB-5000 emulsion stabilised with n-tetradecane incubated with LcpK30 analysed in  $\text{CDCl}_3$ . The box outlined in red shows the difference in chemical peaks between both reaction setups.



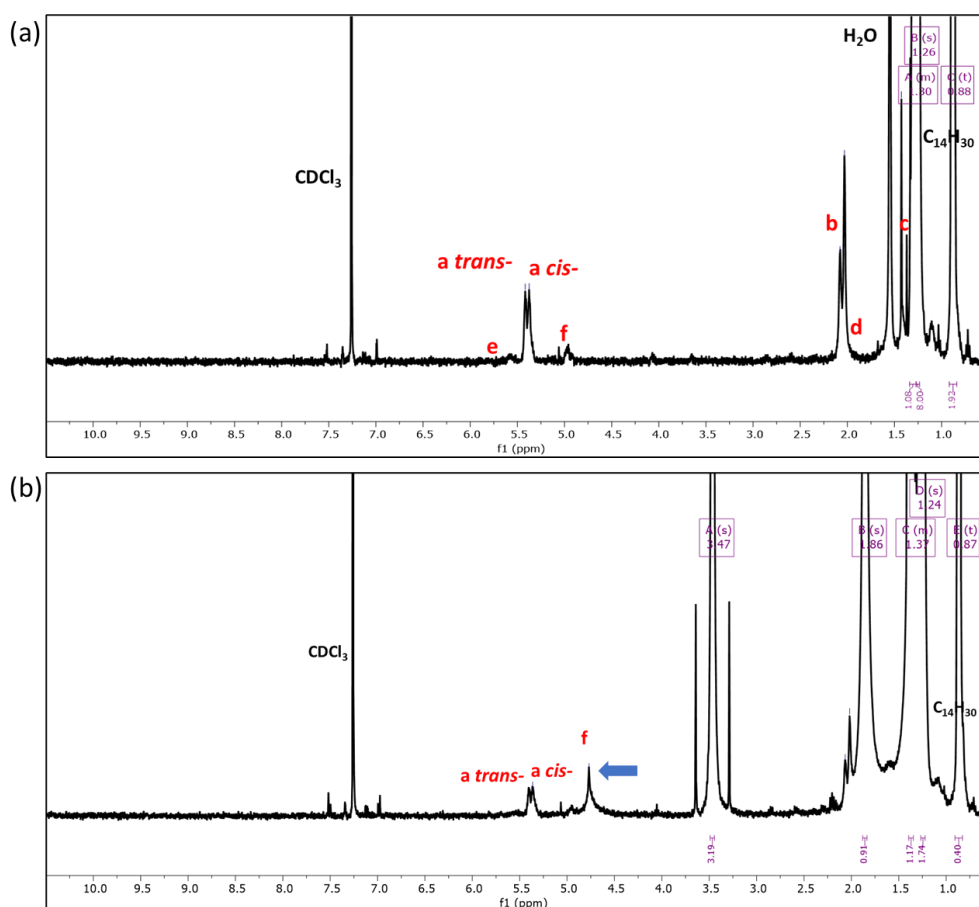
**Appendix C4.13:  $^1\text{H}$  NMR spectrum of dried residual extract from a reaction with PB-1300**

(a) PB-1300 before solubilised in *n*-tetradecane, dried residues extracted using ethyl acetate from (b) Control setup of PB-1300 emulsion stabilised with *n*-tetradecane incubated without LcpK30 (c) PB-1300 emulsion stabilised with *n*-tetradecane incubated with LcpK30 analysed in  $\text{CDCl}_3$ . Traces of methanol were detected in samples derived from emulsified PB-1300 incubated with LcpK30 with no significant differences with other chemical peaks compared to the spectrum in Figure (a).



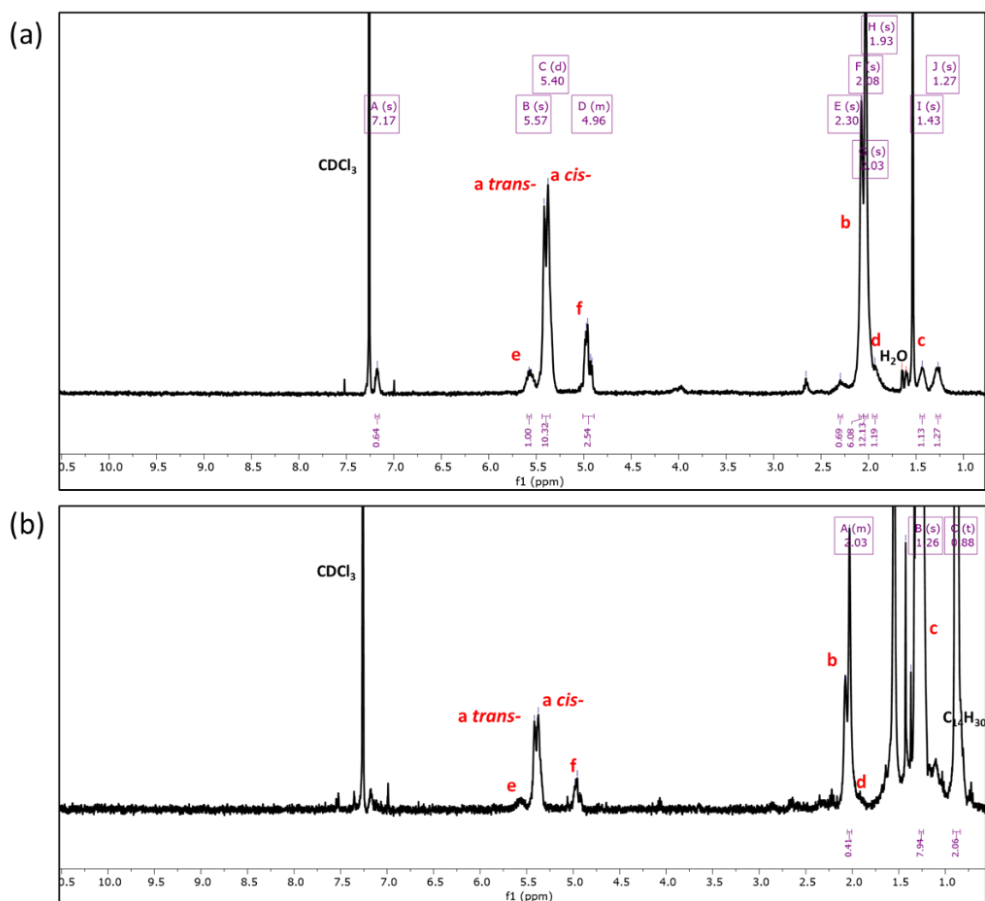
**Appendix C4.14:  $^1\text{H}$  NMR spectrum of dried residual extract from a reaction with PB-5000S**

(a) Control setup of PB-5000S emulsion stabilised with *n*-tetradecane incubated without LcpK30 (c) PB-5000S emulsion stabilised with *n*-tetradecane incubated with LcpK30 analysed in  $\text{CDCl}_3$ . A chemical peak representing the proton at methylene of the vinyl group from emulsified PB-5000S incubated with LcpK30 shifted from 4.98 ppm to 4.77 ppm, pointed by the blue arrow.



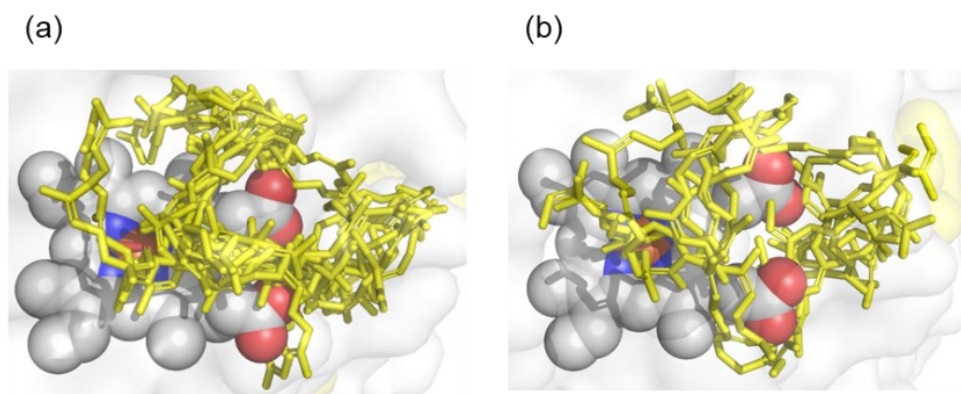
**Appendix C4.15:  $^1\text{H}$  NMR spectrum of dried residual extract from a reaction with PB-1500**

(a) Control setup of emulsified PB-1500 without LcpK30 and (b) emulsified PB-1500 with LcpK30 analysed in  $\text{CDCl}_3$  showing no significant difference in the chemical environment of samples retrieved from both reaction condition.



**Appendix C5.1a: Superimposed of ten docking poses result from rigid docking of *cis*-1,4-polyisoprene C<sub>50</sub>H<sub>82</sub> within LcpK30**

(a) Protein-ligand conformations obtained using the Goldscore/default scoring function; (b) Protein-ligand conformations obtained using Goldscore/p450\_pdb scoring function.



**Appendix C5.1b: Docking solutions obtained from rigid docking within GOLD software**

The docking solutions were ranked based on the fitness score from highest to lowest.

Rank	Fitness Score	C=C closest to Fe-O <sub>2</sub> complex <sup>a</sup>	Distance of C=C to the oxygen atom (Å) <sup>b</sup>		Ligand conformation
			-H <sub>2</sub> C-C=	=C-CH <sub>3</sub>	
<b>Goldscore/default docking protocol</b>					
1	-387	8	4.2	3	Folded
2	-415	9	3.1	4.5	Folded
3	-526	5	5.1	3.9	Folded
4	-537	6	3	4.3	Folded
5	-547	7	5	4.1	Folded
6	-551	5	3.2	3	Folded
7	-631	4	3.8	3.1	Extended
8	-687	5	4.8	5.3	Folded
9	-711	8	4.7	4.3	Folded
10	-839	2	2.7	2.6	Folded



---

**Goldscore/p450\_pdb docking protocol**

<b>1</b>	0	6	2.3	3.4	Folded
<b>2</b>	0	-	-	-	Folded
<b>3</b>	0	8	2.8	3.5	Folded
<b>4</b>	-374	9	2.5	2	Extended
<b>5</b>	-489	9	2.5	1.5	Extended
<b>6</b>	-562	4	3.8	3.8	Folded
<b>7</b>	-665	4	4.3	5.1	Folded
<b>8</b>	-759	2	1.8	1.2	Extended
<b>9</b>	-794	9	1.6	1.3	Extended
<b>10</b>	-863	8	1.6	2.9	Extended

<sup>a</sup> the first C=C unit number was counted from the end terminal with two methyl group R-C=C-(CH<sub>3</sub>)<sub>2</sub> – see scheme

<sup>b</sup> the distance was measured from each C atom in the double bond to the distal O atom of the Fe-O<sub>2</sub> complex

### Appendix C5.2a: List of residues interacting with the docked *cis*-1,4-polyisoprene

The residues were extracted from PLIP analysis of 10 docking poses obtained using ChemPLP. Docking solutions were ranked based on the fitness score from highest to lowest. Residues that interact with all / most poses are highlighted in grey and light grey, respectively.

Residue number	No of poses interacting with residue	Pose rank									
		1	2	3	4	5	6	7	8	9	10
LYS80	2						/		/		
TYR134	1								/		
MET141	1										/
ILE145	3			/					/		/
GLU148	4			/			/		/		/
VAL152	5	/	/			/	/			/	
ALA159	7			/	/		/	/	/	/	/
ASP163	7	/		/	/	/		/		/	/
ARG164	5	/	/		/		/			/	
<b>LYS167</b>	<b>10</b>	<b>/</b>	<b>/</b>	<b>/</b>	<b>/</b>	<b>/</b>	<b>/</b>	<b>/</b>	<b>/</b>	<b>/</b>	<b>/</b>
THR168	6		/	/		/	/		/		/
ARG170	8	/		/	/	/		/	/	/	/
<b>LEU171</b>	<b>10</b>	<b>/</b>	<b>/</b>	<b>/</b>	<b>/</b>	<b>/</b>	<b>/</b>	<b>/</b>	<b>/</b>	<b>/</b>	<b>/</b>
TYR173	0										

ASP174	1					/					
ILE175	2					/		/			
VAL189	0										
THR190	2							/	/		
LYS193	0										
THR194	0										
VAL197	0										
ILE227	0										
VAL229	1										/
THR230	3							/	/		/
TRP231	0										
LEU234	6			/		/	/	/	/		/
TRP261	1							/			
ALA265	0										
LEU268	1							/			
LEU290	1										/
LEU294	1										/
GLU392	1			/							
ARG395	2	/		/							
<b>ILE396</b>	<b>10</b>	<b>/</b>	<b>/</b>	<b>/</b>	<b>/</b>	<b>/</b>	<b>/</b>	<b>/</b>	<b>/</b>	<b>/</b>	<b>/</b>
ALA397	4					/	/		/	/	
ILE398	4	/	/			/			/		
ASP399	1							/			

### Appendix C5.2b: List of residues interacting with the docked *cis*-1,4-polyisoprene

The residues were extracted from PLIP analysis of 10 docking poses obtained using ChemScore. Docking solutions were ranked based on the fitness score from highest to lowest. Residues that interact with all / most poses are highlighted in grey and light grey, respectively.

Residue number	No of poses interacting with residue	Pose rank									
		1	2	3	4	5	6	7	8	9	10
LYS80	1									/	
ILE145	5			/	/	/		/			/
GLU148	6		/	/	/	/		/			/
VAL152	4		/					/		/	/
<b>ALA159</b>	<b>10</b>	<b>/</b>	<b>/</b>	<b>/</b>	<b>/</b>	<b>/</b>	<b>/</b>	<b>/</b>	<b>/</b>	<b>/</b>	<b>/</b>
ASP163	4		/				/	/	/		
ARG164	4	/	/							/	/
<b>LYS167</b>	<b>10</b>	<b>/</b>	<b>/</b>	<b>/</b>	<b>/</b>	<b>/</b>	<b>/</b>	<b>/</b>	<b>/</b>	<b>/</b>	<b>/</b>

THR168	5		/	/	/	/				/	
ARG170	3								/	/	/
<b>LEU171</b>	<b>10</b>		/	/	/	/	/	/	/	/	/
TYR173	2						/				/
ASP174	3						/		/	/	
ILE175	2						/		/		
VAL189	1	/									
THR190	5	/					/		/	/	/
LYS193	1	/									
THR194	1						/				
VAL197	1					/					
ILE227	1						/				
VAL229	1			/							
THR230	5		/	/		/		/			/
TRP231	1						/				
LEU234	7		/	/	/	/		/	/		/
TRP261	2						/		/		
ALA265	1						/				
LEU268	1						/				
<b>ILE396</b>	<b>10</b>		/	/	/	/	/	/	/	/	/
ALA397	5		/		/	/		/		/	
ILE398	4	/							/	/	/
ASP399	1								/		

### Appendix C5.3: Protein sequences alignment of LcpK30 and LcpSH22a

LcpK30 (Genbank AAR25849.1) was assigned as the subject sequence, and LcpSH22a (GenBank AHH18878.1) was assigned as the query sequence. The alignment was performed using the online protein-protein Basic Local Alignment Search Tool (blastp) at <https://blast.ncbi.nlm.nih.gov/Blast.cgi>.

#### latex clearing protein [Streptomyces sp. K30]

Sequence ID: [AAR25849.1](#) Length: 397 Number of Matches: 1

Range 1: 4 to 395 [GenPept](#) [Graphics](#)

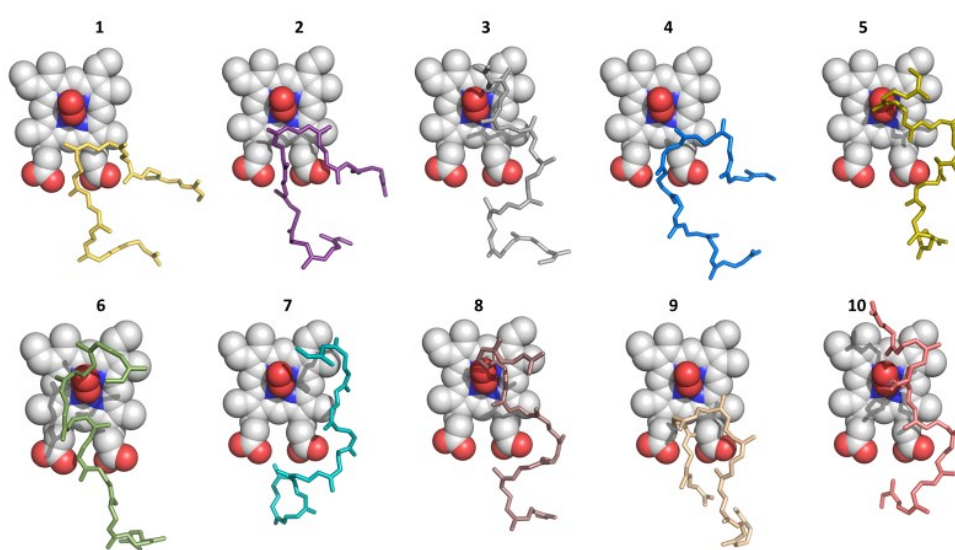
[▼ Next Match](#) [▲ Pre](#)

Score	Expect	Method	Identities	Positives	Gaps
411 bits(1056)	6e-147	Compositional matrix adjust.	205/395(52%)	272/395(68%)	7/395(1%)
Query 15	GLVGAVGALALGARTARAEPWTWSPSGSVLGSGGGADPLTVWDPEADPVLADVMDHADVP				74
Sbjct 4	.AL.....GAAT.ALARPL.....A..A.T.V.V..EY...E.....A.I.RGE..				63
Query 75	AINRLLATWVFNDQPIPAGLPKNLRFMEYARQLPSWTDQNKLAASFENKKRGTYLGVL				134
Sbjct 64	.V.A..KQ.TR...AL.G...GD..E...H..RM...A.KAA.DRGAQ.S.TK.I.V.A..				123
Query 135	YAFASGMMSTVIPHEARAVYYSRGGSHMKERIAKTAKFGYDIGTVNAYGPGGEMVTVCK				194
Sbjct 124	.GLG..L...A..R.S.....K..AD..D.....RL.....DLD..L.H.S.I..A..				183
Query 195	TRIIHAAVRHLLPRSPHPNGI----TPISQDDLMTWHSLATTIMRTFRTWNVIIPPGE				250
Sbjct 184	..MV.....Q..A.SQTSGGQKI...A.I.....FV..KMKQ.G.RVNTAD				243
Query 251	SDGYLHSWQLAGHLLGIRDEYIPATWQQADDQAKQVLDPIIAPTAEGVDLAHKLLDLGFD				310
Sbjct 244	AEA...V..VSA.M..VS.....DA.NA.S.....L.H.P..EA.TEV..GIVAE				303
Query 311	IDLTLLSKPILSAFTRFILGDKVADWLQLAREPVWSPLLEVAWGPFVAVREGVMGVIPPT				370
Sbjct 304	L.AG-.TR.LIG..S.YT..GE.G.MIG..KQ..LER.IAT..PLL..F...LI-PL.AV				361
Query 371	ADATWMFDEFRLRQFVLWYMAELRMPLSIEIPQTNR		405		
Sbjct 362	PAVL.TLE.A..K...LFLS.G.R-IA.D..DV..		395		

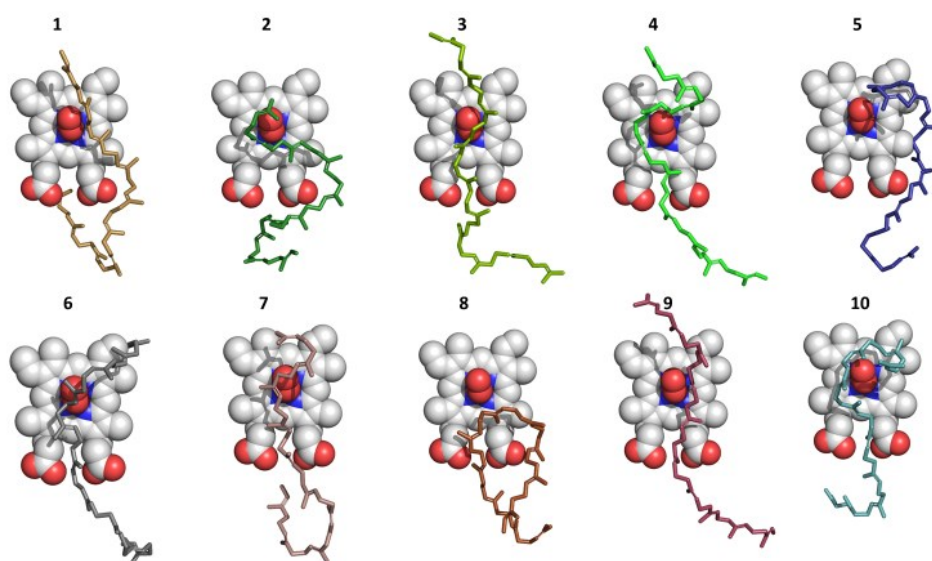
**Appendix C5.4: Docking conformation of (a) *cis*-1,4-polyisoprene and (b) *trans*-1,4-polyisoprene on wild-type LcpK30**

The docking conformations were obtained with ChemPLP fitness function ranked by the fitness score from highest to lowest. Docking solutions were calculated with induced fit docking using 10 Å binding site. Enzymes and hydrogens were omitted for the sake of clarity

(a)



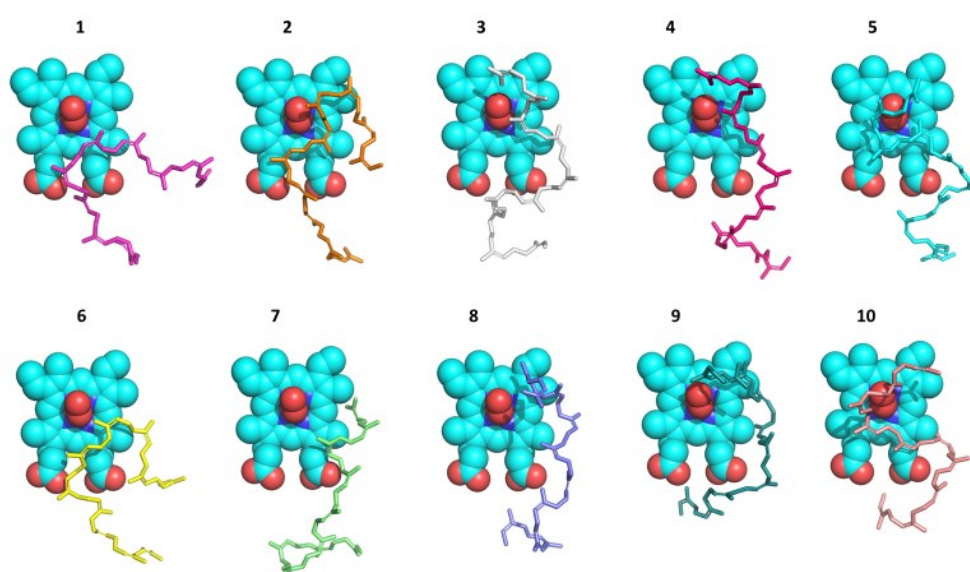
(b)



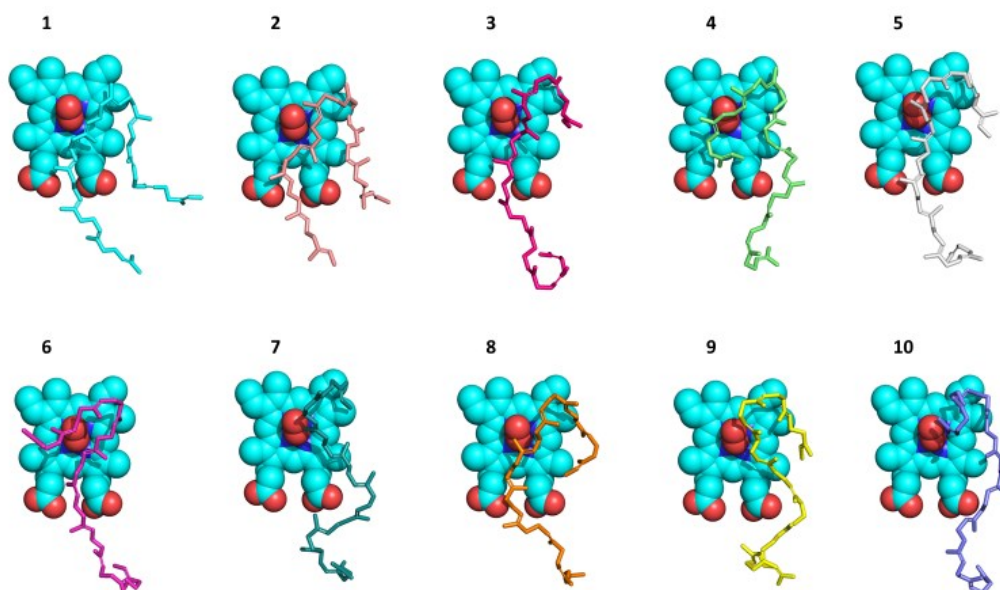
**Appendix C5.5: Docking conformation of (a) *cis*-1,4-polyisoprene and (b) *trans*-1,4-polyisoprene on Leu143Ala mutant**

The docking conformations were obtained with ChemPLP fitness function ranked by the fitness score from highest to lowest. Docking solutions were calculated with induced fit docking using 10 Å binding site. Enzymes and hydrogens were omitted for the sake of clarity.

(a)



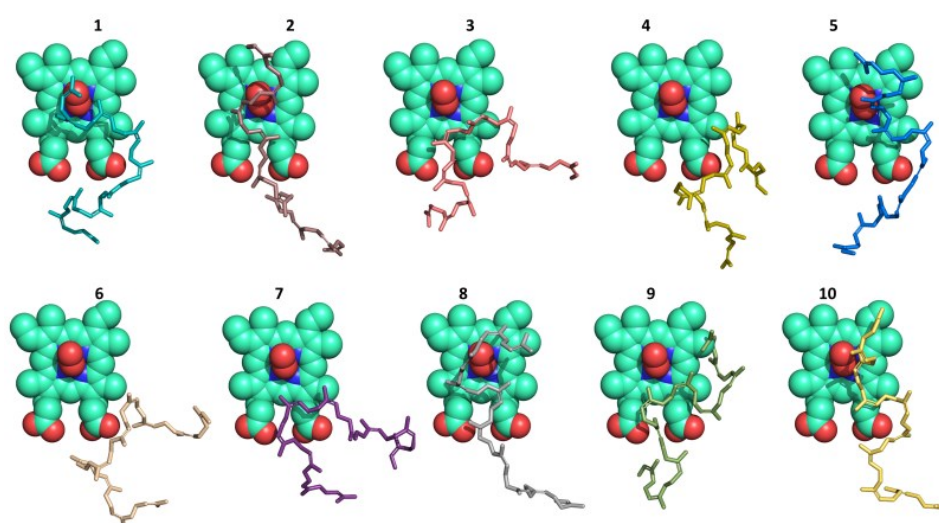
(b)



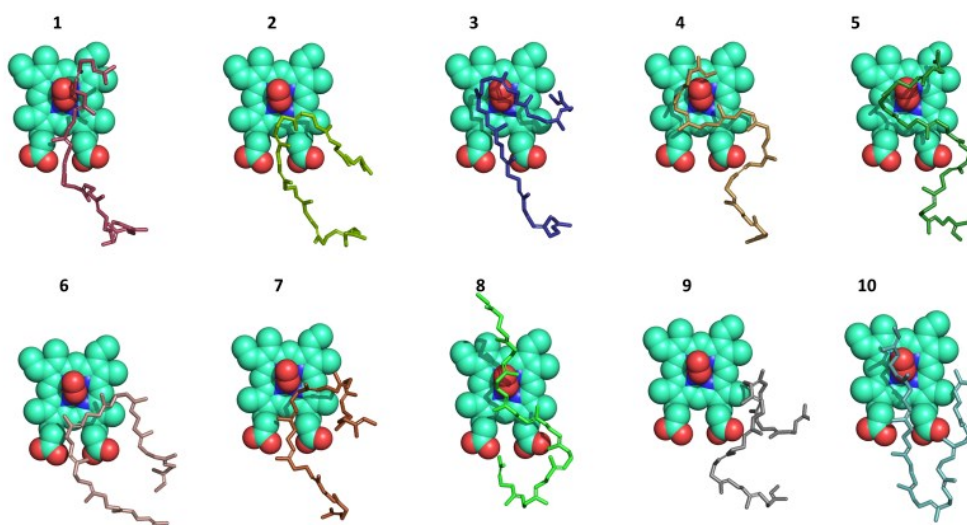
**Appendix C5.6: Docking conformation of (a) *cis*-1,4-polyisoprene and (b) *trans*-1,4-polyisoprene on Leu143Phe mutant**

The docking conformations were obtained with ChemPLP fitness function ranked by the fitness score from highest to lowest. Docking solutions were calculated with induced fit docking using 10 Å binding site. Enzymes and hydrogens were omitted for the sake of clarity.

(a)



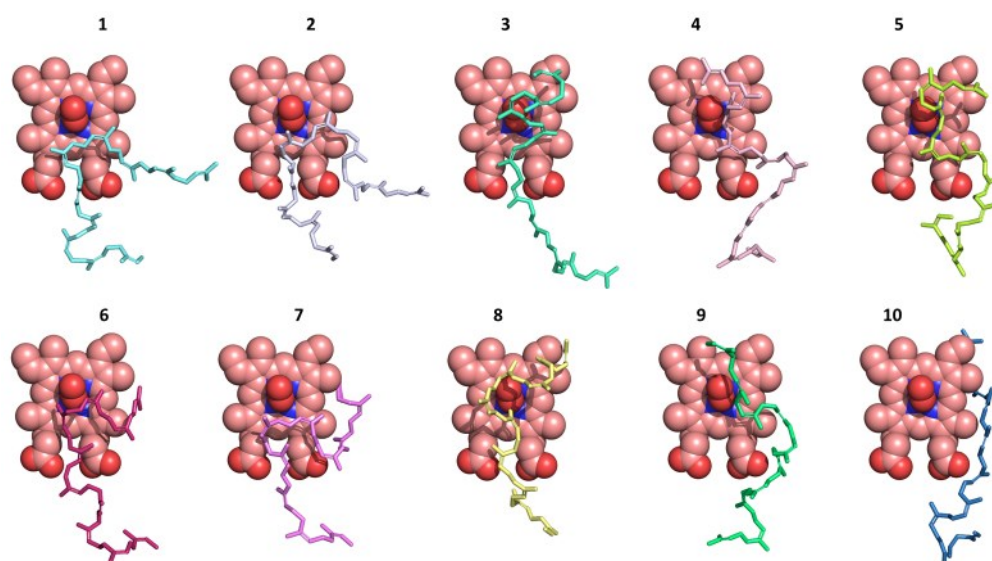
(b)



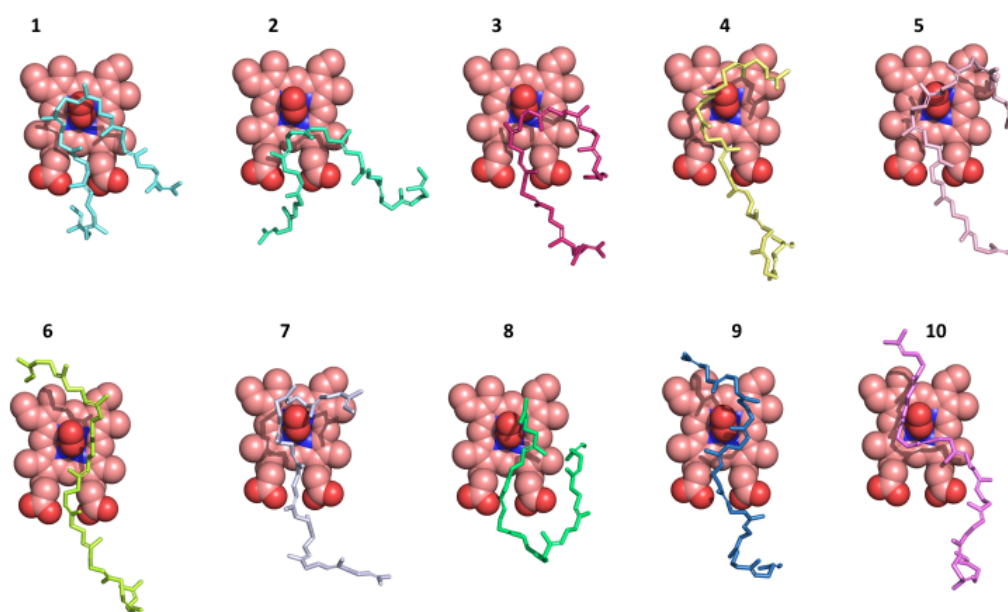
**Appendix C5.7: Docking conformation of (a) *cis*-1,4-polyisoprene and (b) *trans*-1,4-polyisoprene on Leu143Trp mutant**

The docking conformations were obtained with ChemPLP fitness function ranked by the fitness score from highest to lowest. Docking solutions were calculated with induced fit docking using 10 Å binding site. Enzyme and hydrogens were omitted for the sake of clarity.

(a)



(b)





**Appendix C5.8: Structural features of the *cis*-1,4-polyisoprene docking poses**

Docking conformation of *cis*-1,4-polyisoprene on (a) LcpK30 wild type, (b) Leu171Ala mutant, (c) Leu171Phe mutant and (d) Leu171Trp mutant obtained from induced fit docking using ChemPLP scoring function in GOLD program. Additional structural features of the docking poses are also shown. The distance was measured from each C atom to the distal O atom of the Fe-O<sub>2</sub> complex.

(a)

Rank	Fitness Score	Distance of C=C to the oxygen atom (Å)		Ligand conformation
		-H <sub>2</sub> C-C=	=C-CH <sub>3</sub>	
1	78.94	5	5.3	Folded
2	67.25	5.2	4	Folded
3	64.8	4.3	3.5	Extended
4	40.51	5.9	5.1	Folded
5	29.74	3.8	2.5	Extended
6	21.37	2.2	2.6	Extended
7	19.99	5.9	7	Extended
8	-13.14	2.6	2.4	Extended
9	-42.16	5	5.4	Folded
10	-60.12	3.2	2.9	Extended

(b)

Rank	Fitness Score	Distance of C=C to the oxygen atom (Å)		Ligand conformation
		-H <sub>2</sub> C-C=	=C-CH <sub>3</sub>	
1	86.12	4.3	4.6	Folded
2	81.64	3.5	3.3	Folded
3	58.25	4.2	3.2	Extended
4	58.25	4.2	3.5	Extended
5	56.80	3.5	3.1	Extended
6	44.79	4.8	4.2	Folded
7	32.86	7.5	6.4	Extended
8	2.13	4.4	4.7	Folded

<b>9</b>	-1.65	2.7	3.5	Folded
<b>10</b>	-50.71	3.5	3.5	Folded

(c)

Rank	Fitness Score	Distance of C=C to the oxygen atom (Å)		Ligand conformation
		-H <sub>2</sub> C-C=	=C-CH <sub>3</sub>	
<b>1</b>	61.57	3.6	3.3	Extended
<b>2</b>	44.94	2.9	3.4	Extended
<b>3</b>	39.29	5.2	5	Folded
<b>4</b>	32.92	7.7	7.5	Folded
<b>5</b>	20.16	2	2.7	Extended
<b>6</b>	13.75	9.6	8.8	Folded
<b>7</b>	11.37	5.6	5.7	Folded
<b>8</b>	-2.72	3.4	3.8	Extended
<b>9</b>	-21.49	4.3	5	Folded
<b>10</b>	-71.15	2.4	2.6	Extended

(d)

Rank	Fitness Score	Distance of C=C to the oxygen atom (Å)		Ligand conformation
		-H <sub>2</sub> C-C=	=C-CH <sub>3</sub>	
<b>1</b>	64.11	3.8	4.8	Folded
<b>2</b>	17.48	3.5	4.4	Folded
<b>3</b>	11.87	3.3	2.5	Extended
<b>4</b>	10.57	2.2	2.9	Extended
<b>5</b>	-7.95	2.4	2.4	Extended
<b>6</b>	-15.01	2.7	3.2	Folded
<b>7</b>	-38.21	4	5.3	Folded
<b>8</b>	-56.99	2.3	3	Folded
<b>9</b>	-71.78	4	3.7	Extended
<b>10</b>	-75.56	7.6	7.9	Extended

**Appendix C5.9: Structural features of the *trans*-1,4-polyisoprene docking poses**

Docking conformation of *trans*-1,4-polyisoprene in (a) LcpK30 wild type, (b) Leu171Ala mutant, (c) Leu171Phe mutant and (d) Leu171Trp mutant obtained from induced fit docking using ChemPLP scoring function in GOLD program and are ranked based on the fitness score from highest to lowest. Additional structural features of the docking poses are also shown. The distance was measured from each C atom to the distal O atom of the Fe-O<sub>2</sub> complex.

(a)

Rank	Fitness Score	Distance of C=C to the oxygen atom (Å)		Ligand conformation
		-H <sub>2</sub> C-C=	=C-CH <sub>3</sub>	
1	57.41	4.3	3.5	Extended
2	52.42	3.5	3.8	Folded
3	23.64	3.7	3.7	Extended
4	14.75	2.2	2.9	Extended
5	13.53	4.4	3.8	Folded
6	13.25	2.8	3.2	Extended
7	11.67	3.3	2.9	Extended
8	-5.99	4.4	4.3	Folded
9	-10.92	3.3	2.5	Extended
10	-33.74	2.7	2.9	Extended

(b)

Rank	Fitness Score	Distance of C=C to the oxygen atom (Å)		Ligand conformation
		-H <sub>2</sub> C-C=	=C-CH <sub>3</sub>	
1	71.13	3	3.6	Folded
2	70.49	3.5	3.3	Folded
3	60.16	3.1	3.7	Folded
4	30.07	3.3	3	Folded
5	12.04	4.2	3.1	Folded
6	11.71	3.9	4.3	Folded
7	10.80	3.6	3	Folded
8	10.57	3.6	3.1	Folded
9	7.50	2.6	3.3	Folded

<b>10</b>	-57.00	5.1	3.9	Folded
-----------	--------	-----	-----	--------

(c)

Rank	Fitness Score	Distance of C=C to the oxygen atom (Å)		Ligand conformation
		-H <sub>2</sub> C-C=	=C-CH <sub>3</sub>	
<b>1</b>	87.54	3.6	3.8	Extended
<b>2</b>	68.70	4.2	4.2	Folded
<b>3</b>	64.33	3.7	3.5	Folded
<b>4</b>	39.51	3.1	3.5	Folded
<b>5</b>	26.40	3.1	3.9	Folded
<b>6</b>	18.87	5.6	4.9	Folded
<b>7</b>	2.70	4.6	3.6	Folded
<b>8</b>	-16.72	2.8	3	Extended
<b>9</b>	-41.17	7.6	8.4	Folded
<b>10</b>	-88.37	2.3	3.1	Extended

(d)

Rank	Fitness Score	Distance of C=C to the oxygen atom (Å)		Ligand conformation
		-H <sub>2</sub> C-C=	=C-CH <sub>3</sub>	
<b>1</b>	52.78	2.4	3.1	Folded
<b>2</b>	51.37	3.9	4.3	Folded
<b>3</b>	49.14	3.4	4	Folded
<b>4</b>	13.38	2.1	3.1	Extended
<b>5</b>	9.69	3.2	2.9	Folded
<b>6</b>	-6.00	2.7	3.3	Extended
<b>7</b>	-13.82	2.6	3.8	Extended
<b>8</b>	-15.27	3.4	3.9	Folded
<b>9</b>	-26.47	3.7	3.1	Extended
<b>10</b>	-33.84	2.4	2.4	Extended

**Appendix C5.10: Primers used for site-directed mutagenesis**

Primer Sequence (5' to 3') for Leu171Phe mutant

5'-GTCACCAATATCATAGCCGAAGCGGGCGGTTTTTGCAt-3'  
5'-ATTGCAAAAACCGCCCGCTTCGGCTATGATATTGGTGAC-3'

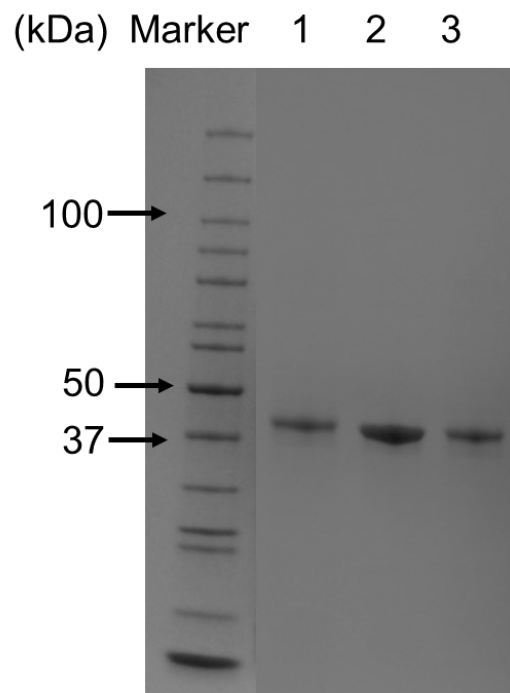
Primer Sequence (5' to 3') for Leu171Ala mutant

5'-CACCAATATCATAGCCCGCGCGGGCGGTTTTTGCAA-3'  
5'-TTGCAAAAACCGCCCGCGCGGGCTATGATATTGGTG-3'

Primer Sequence (5' to 3') for Leu171Trp mutant

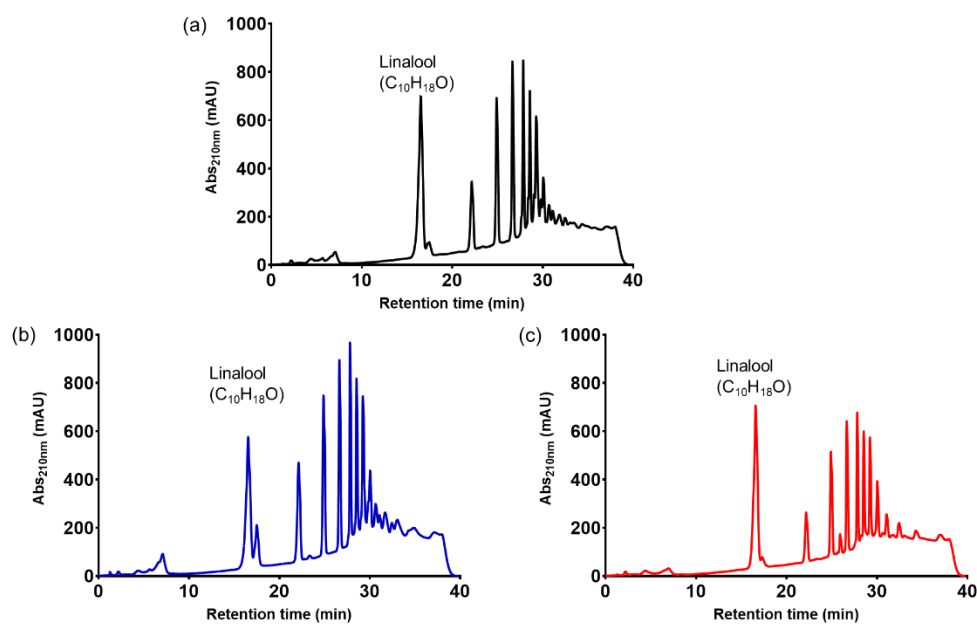
5'-GTCACCAATATCATAGCCCCAGCGGGCGGTTTTTGCATA-3'  
5'-TATTGCAAAAACCGCCCGCTGGGGCTATGATATTGGTGAC-3'

**Appendix C5.11: SDS-PAGE analysis of purified proteins (1) wild-type LcpK30 (2) Leu171Phe mutant and (c) Leu171Ala mutant**



**Appendix C5.12: HPLC Chromatogram of oligomers from NR degradation catalysed by LcpK30 variants.**

HPLC chromatogram of oligomers derived from natural *cis*-1,4-polyisoprene rubber enzymatically cleaved by LcpK30 variants; (a) wild-type LcpK30; (b) Leu171Phe and (c) Leu171Ala. Before analysis 1 mM linalool was added into the HPLC sample.



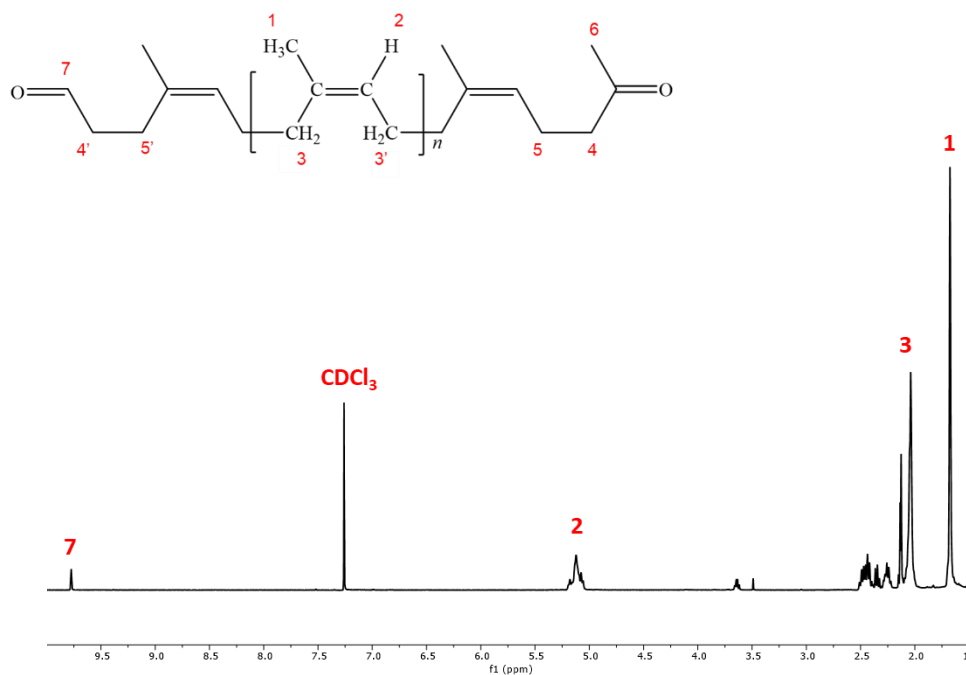
Oligo-isoprenoids produced by enzymatic cleavage of NR catalysed by purified wild type LcpK30 and mutated proteins of Leu171Ala and Leu171Phe. The percentage of relative comparison was calculated by comparing the peak area (%) of 1 mM linalool.

Isoprene number (n)	Retention time	Area	Area (%)	$A_{(Oligomer)}/A_{(Linalool)}*100$
<b>Leu171Ala</b>				
Linalool	16.58	18816.2	31.38	100
3	22.16	4027.4	6.72	21.40
4	24.90	6756.3	11.27	35.91
4'	25.92	1067.4	1.78	5.67
5	26.66	6914.9	11.53	36.75
6	27.81	5473.2	9.13	29.09
7	28.53	4862.4	8.11	25.84
8	29.22	4781.2	7.97	25.41
9	30.03	3117.3	5.20	16.57
10	31.05	1743.9	2.91	9.27
11	32.42	1416.8	2.36	7.53
12	34.29	991.6	1.65	5.27
				218.71%
<b>Leu171Phe</b>				
Linalool	16.54	16402.90	19.42	100
3	22.12	8756.00	10.37	53.38
4	24.88	10908.30	12.92	66.50
5	26.64	10550.50	12.49	64.32
6	27.82	9120.30	10.80	55.60
7	28.54	7940.20	9.40	48.41
8	29.23	9209.40	10.90	56.14
9	30.03	4600.40	5.45	28.05
10	30.66	1705.20	2.02	10.40
11	31.06	807.60	0.96	4.92
12	31.70	1743.90	2.07	10.63
13	32.44	731.00	0.87	4.46
14	33.05	1981.30	2.35	12.08
				414.89%
<b>Wild type</b>				
Linalool	16.51	20004.9	27.949	100
3	22.146	6333.5	8.849	31.66
4	24.904	9955.7	13.909	49.77
5	26.647	10067.9	14.066	50.33
6	27.832	7819.2	10.924	39.09
7	28.561	5600.2	7.824	27.99
8	29.26	6305.8	8.81	31.52
9	30.064	2174.2	3.038	10.87
10	30.681	1127.7	1.576	5.64
11	31.094	778.5	1.088	3.89
12	31.836	929.5	1.299	4.65
13	32.458	479.7	0.67	2.40
				257.80%

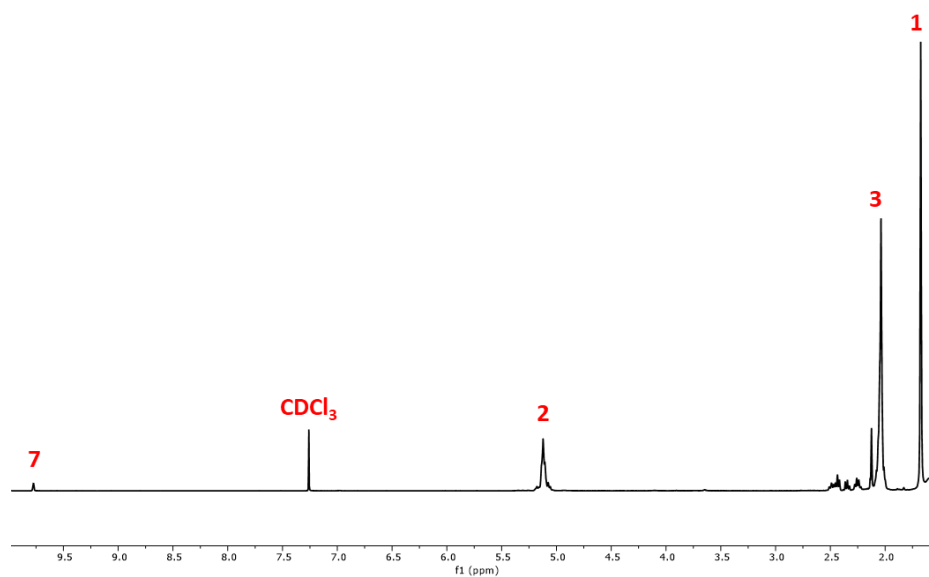
**Appendix C5.13:  $^1\text{H}$  NMR spectra of oligomers from NR degradation catalysed by (a) LcpK30 wild type (b) LcpK30 Leu171Ala and (c) LcpK30 Leu171Phe**

Schematic structure of an oligomer produced after enzymatic degradation of natural *cis*-1,4-polyisoprene rubber (top left)

(a)

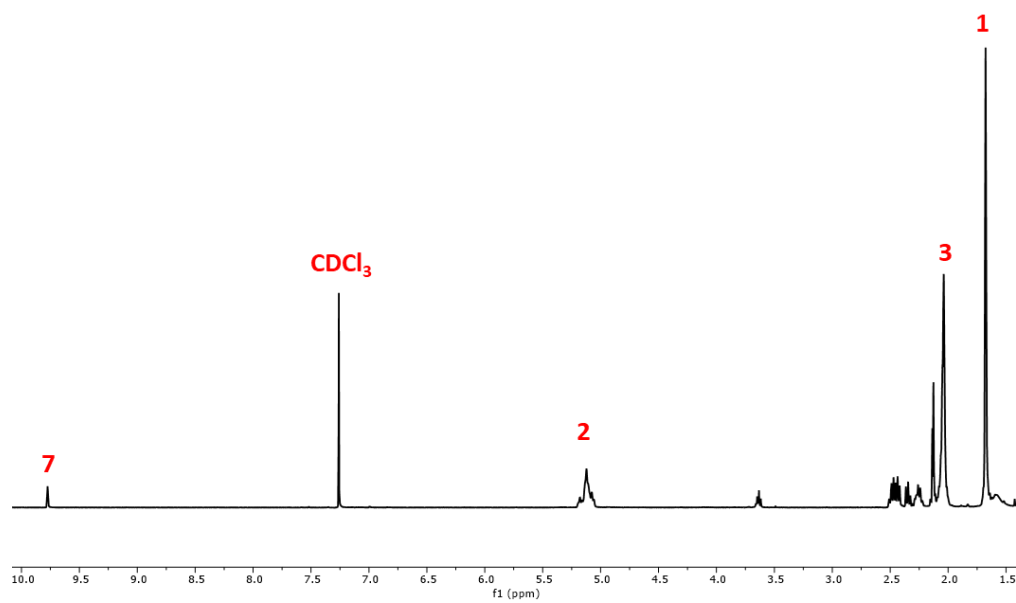


(b)





(c)



## REFERENCES

- (1) Lambert, S.; Sinclair, C. J.; Bradley, E. L.; Boxall, A. B. A. Effects of Environmental Conditions on Latex Degradation in Aquatic Systems. *Science of the Total Environment* **2013**, *447*, 225–234. <https://doi.org/10.1016/j.scitotenv.2012.12.067>.
- (2) Thomas, J.; Patil, R. The Road to Sustainable Tire Materials: Current State-of-the-Art and Future Perspectives. *Environ Sci Technol* **2023**, *57* (6), 2209–2216. <https://doi.org/10.1021/acs.est.2c07642>.
- (3) Chittella, H.; Yoon, L. W.; Ramarad, S.; Lai, Z. W. Rubber Waste Management: A Review on Methods, Mechanism, and Prospects. *Polym Degrad Stab* **2021**, *194*, 109761. <https://doi.org/10.1016/j.polymdegradstab.2021.109761>.
- (4) Dobrota, D. Experimental Research Regarding Processing Rubber Waste with Metallic Insertions. *Materiale Plastice* **2006**, *43* (1), 65–67.
- (5) Torretta, V.; Rada, E. C.; Ragazzi, M.; Trulli, E.; Istrate, I. A.; Cioca, L. I. Treatment and Disposal of Tyres: Two EU Approaches. A Review. *Waste Management* **2015**, *45*, 152–160. <https://doi.org/10.1016/j.wasman.2015.04.018>.
- (6) Miranda, M.; Pinto, F.; Gulyurtlu, I.; Cabrita, I. Pyrolysis of Rubber Tyre Wastes: A Kinetic Study. *Fuel* **2013**, *103*, 542–552. <https://doi.org/10.1016/j.fuel.2012.06.114>.
- (7) Scott, E. Malaysian Dump Linked to Pyrolysis. *Tyre and Rubber Recycling*. Malaysia March 2019, p 2. <https://www.tyreandrubberrecycling.com/latest-news/posts/2019/march/malaysian-dump-linked-to-pyrolysis/>.
- (8) Wu, B.; Zhou, M. H. Recycling of Waste Tyre Rubber into Oil Absorbent. *Waste Management* **2009**, *29* (1), 355–359. <https://doi.org/10.1016/j.wasman.2008.03.002>.
- (9) Markl, E.; Lackner, M. Devulcanization Technologies for Recycling of Tire-Derived Rubber: A Review. *Materials* **2020**, *13* (5). <https://doi.org/10.3390/ma13051246>.
- (10) Ibrahim, S.; Daik, R.; Abdullah, I. Functionalization of Liquid Natural Rubber via Oxidative Degradation of Natural Rubber. *Polymers (Basel)* **2014**, *6* (12), 2928–2941. <https://doi.org/10.3390/polym6122928>.
- (11) Silpa Kaza; Lisa Yao; Perinaz Bhada-Tata; Woerden, F. Van. *A Global Snapshot of Solid Waste Management to 2050*, 2nd ed.; World Bank Publications: Washington DC, 2018.
- (12) Tangpakdee, J.; Tanaka, Y. Characterization of Sol and Gel in Hevea Natural Rubber. *Rubber Chemistry and Technology* **1997**, *70* (5), 707–713. <https://doi.org/10.5254/1.3538454>.
- (13) Nawamawat, Kanjane.; Sakdapipanich, J. T.; Ho, C. C.; Ma, Yujie.; Song, Jing.; Vancso, J. G. Surface Nanostructure of Hevea Brasiliensis Natural Rubber Latex Particles. *Colloids Surf A Physicochem Eng Asp* **2011**, *390* (1–3), 157–166. <https://doi.org/10.1016/j.colsurfa.2011.09.021>.

- (14) Wei, Y. C.; Zhu, D.; Xie, W. Y.; Xia, J. H.; He, M. F.; Liao, S. In-Situ Observation of Spatial Organization of Natural Rubber Latex Particles and Exploring the Relationship between Particle Size and Mechanical Properties of Natural Rubber. *Ind Crops Prod* **2022**, *180* (September 2021), 114737. <https://doi.org/10.1016/j.indcrop.2022.114737>.
- (15) Rochette, C. N.; Crassous, J. J.; Drechsler, M.; Gaboriaud, F.; Eloy, M.; De Gaudemaris, B.; Duval, J. F. L. Shell Structure of Natural Rubber Particles: Evidence of Chemical Stratification by Electrokinetics and Cryo-TEM. *Langmuir* **2013**, *29* (47), 14655–14665. <https://doi.org/10.1021/la4036858>.
- (16) Cornish, K.; Wood, D. F.; Windle, J. J. Rubber Particles from Four Different Species, Examined by Transmission Electron Microscopy and Electron-Paramagnetic-Resonance Spin Labeling, Are Found to Consist of a Homogeneous Rubber Core Enclosed by a Contiguous, Monolayer Biomembrane. *Planta* **1999**, *210* (1), 85–96. <https://doi.org/10.1007/s004250050657>.
- (17) Tarachiwin, L.; Sakdapipanich, J.; Ute, K.; Kitayama, T.; Tanaka, Y. Structural Characterization of  $\alpha$ -Terminal Group of Natural Rubber. 2. Decomposition of Branch-Points by Phospholipase and Chemical Treatments. *Biomacromolecules* **2005**, *6* (4), 1858–1863. <https://doi.org/10.1021/bm058004p>.
- (18) Sakdapipanich, J. T. Structural Characterization of Natural Rubber Based on Recent Evidence from Selective Enzymatic Treatments. *J Biosci Bioeng* **2007**, *103* (4), 287–292. <https://doi.org/10.1263/jbb.103.287>.
- (19) Tanaka, Y. Structural Characterization of Natural Polyisoprenes: Solve the Mystery of Natural Rubber Based on Structural Study. *Rubber Chemistry and Technology* **2001**, *74* (3), 355–375. <https://doi.org/10.5254/1.3547643>.
- (20) Amerik, A. Y.; Martirosyan, Y. T.; Gachok, I. V. Regulation of Natural Rubber Biosynthesis by Proteins Associated with Rubber Particles. *Russ J Bioorg Chem* **2018**, *44* (2), 140–149. <https://doi.org/10.1134/S106816201801003X>.
- (21) Salomez, M.; Subileau, M.; Intapun, J.; Bonfils, F.; Sainte-Beuve, J.; Vaysse, L.; Dubreucq, E. Micro-Organisms in Latex and Natural Rubber Coagula of *Hevea Brasiliensis* and Their Impact on Rubber Composition, Structure and Properties. *J Appl Microbiol* **2014**, *117* (4), 921–929. <https://doi.org/10.1111/jam.12556>.
- (22) Payungwong, N.; Inoue, T.; Sakdapipanich, J. A Model Study of the Influence of the Natural Rubber (NR)- Endogenous Gel Fraction on the Rheological Performance of NR Using Synthetic Polyisoprene Rubber (IR) Blends with Different Ratios of Gel. *ACS Appl Polym Mater* **2022**, *4* (10), 7061–7069. <https://doi.org/10.1021/acsapm.2c00979>.
- (23) Varyan, I.; Kolesnikova, N.; Xu, H.; Tyubaeva, P.; Popov, A. Biodegradability of Polyolefin-Based Compositions: Effect of Natural Rubber. *Polymers (Basel)* **2022**, *14* (3), 1–19. <https://doi.org/10.3390/polym14030530>.
- (24) Tarachiwin, L.; Sakdapipanich, J. T.; Tanaka, Y. Relationship between Particle Size and Molecular Weight of Rubber from *Hevea Brasiliensis*.

*Rubber Chemistry and Technology* **2005**, 78 (4), 694–704.  
<https://doi.org/10.5254/1.3547907>.

- (25) Kovuttikulrangsie, S.; Sakdapipanich, J. T. The Molecular Weight ( MW ) and Molecular Weight Distribution ( MWD ) of NR from Different Age and Clone Hevea Trees. *Songklanakarin Journal of Science and Technology* **2005**, 27 (2), 338–342.
- (26) Subramaniam, A. Gel Permeation Chromatography of Natural Rubber. *Rubber Chemistry and Technology* **1972**, 45 (1), 346–358.
- (27) Dinsmore, R. P. Rubber Chemistry. In *Industrial & Engineering Chemistry*; 2007; Vol. 43, pp 795–803.  
<https://doi.org/10.1021/ie50496a014>.
- (28) Boonying, P.; Boonpavanitchakul, K.; Kangwansupamonkon, W. Green Bio-Composite Coating Film from Lignin/Pre-Vulcanized Natural Rubber Latex for Controlled-Release Urea Fertilizer. *J Polym Environ* **2022**, 31 (4), 1642–1655. <https://doi.org/10.1007/s10924-022-02706-9>.
- (29) Pichaiyut, S.; Wisunthorn, S.; Thongpet, C.; Nakason, C. Novel Ternary Blends of Natural Rubber/Linear Low-Density Polyethylene/Thermoplastic Starch: Influence of Epoxide Level of Epoxidized Natural Rubber on Blend Properties. *Iranian Polymer Journal* **2016**, 25, 711–723. <https://doi.org/10.1007/s13726-016-0459-z>.
- (30) *Global natural rubber forecast with a CAGR of 4.8 percent through 2028*. Rubber World Magazine. <https://rubberworld.com/global-natural-rubber-forecast-with-a-cagr-of-4-8-percent-through-2028/>.
- (31) Aguilar-Bolados, H.; Bascuñan-Heredia, A.; Alvarez, G. Sustainable Approach of the Natural Rubber. In *Green-Based Nanocomposite Materials and Applications*; Springer International Publishing, 2023; pp 279–294. [https://doi.org/10.1007/978-3-031-18428-4\\_14](https://doi.org/10.1007/978-3-031-18428-4_14).
- (32) Ciullo, P. A.; Hewitt, N. Compounding Materials. In *The Rubber Formulary*; Noyes Publication: Norwich, New York, USA, 1999; pp 4–49. <https://doi.org/10.1016/B978-081551434-3.50003-8>.
- (33) Ngamchokwathana, C.; Chaiear, N. Latex Anaphylaxis in Healthcare Worker and the Occupational Health Management Perspective: A Case Report. *SAGE Open Med Case Rep* **2023**, 11, 0–3. <https://doi.org/10.1177/2050313X231179303>.
- (34) Critchley, E.; Pemberton, M. N. Latex and Synthetic Rubber Glove Usage in UK General Dental Practice: Changing Trends. *Heliyon* **2020**, 6 (5), e03889. <https://doi.org/10.1016/j.heliyon.2020.e03889>.
- (35) Chandrasekaran, C. Raw Materials for Rubber Lining Compounds. In *Anticorrosive Rubber Lining*; 2017; pp 77–86. <https://doi.org/10.1016/b978-0-323-44371-5.00011-6>.
- (36) Liu, B.; Wang, S.; Liu, J.; Tang, Z.; Guo, B. Promoted Strain-Induced Crystallization of Cis-1, 4-Polyisoprene with Functional Carbon Nanodots. *Advanced Industrial and Engineering Polymer Research* **2019**, 2 (1), 25–31. <https://doi.org/10.1016/j.aiepr.2019.01.002>.
- (37) K.S. Sisanth; Thomas, M. G.; Abraham, J.; Thomas, S. General Introduction to Rubber Compounding. In *Progress in Rubber Nanocomposites*; 2017; pp 1–39.

- (38) Chaikumpollert, O.; Yamamoto, Y.; Suchiva, K.; Kawahara, S. Mechanical Properties and Cross-Linking Structure of Cross-Linked Natural Rubber. *Polym J* **2012**, *44* (8), 772–777. <https://doi.org/10.1038/pj.2012.112>.
- (39) Sethulekshmi, A. S.; Saritha, A.; Joseph, K. A Comprehensive Review on the Recent Advancements in Natural Rubber Nanocomposites. *Int J Biol Macromol* **2022**, *194* (September 2021), 819–842. <https://doi.org/10.1016/j.ijbiomac.2021.11.134>.
- (40) Chauhan, N. P. S.; Jangid, N. K.; Punjabi, P. B.; Kalal, S.; Ameta, R. Crosslinkers: Functionalized Polymeric. *Encyclopedia of Biomedical Polymers and Polymeric Biomaterials*; Taylor and Francis Group, 2015; pp 2230–2242. <https://doi.org/10.1081/e-ebpp-120050695>.
- (41) Gelling, I. R. Epoxidized Natural Rubber. *Journal of Rubber Research* **1991**, *6* (3), 184–205.
- (42) Phinyocheep, P. Chemical Modification of Natural Rubber (NR) for Improved Performance. In *Chemistry, Manufacture and Applications of Natural Rubber*; Kohjiya, S., Ikeda, Y., Eds.; Woodhead Publishing Limited: United Kingdom, 2014; pp 68–118. <https://doi.org/10.1533/9780857096913.1.68>.
- (43) Larpkasemsuk, A.; Raksaksri, L.; Chuayjuljit, S.; Chaiwutthinan, P.; Boonmahitthisud, A. Effects of Sulfur Vulcanization System on Cure Characteristics, Physical Properties and Thermal Aging of Epoxidized Natural Rubber. *Journal of Metals, Materials and Minerals* **2019**, *29* (1), 49–57. <https://doi.org/10.14456/jmmm.2019.xx>.
- (44) Hamzah, R.; Bakar, M. A.; Dahham, O. S.; Zulkepli, N. N.; Dahham, S. S. A Structural Study of Epoxidized Natural Rubber (ENR-50) Ring Opening under Mild Acidic Condition. *J Appl Polym Sci* **2016**, *133* (43), 13. <https://doi.org/10.1002/app.44123>.
- (45) Sone, T. Industrial Synthetic Method of the Rubbers. 1. Butadiene Rubber. *International Polymer Science and Technology* **2016**, *43* (1), 49–54.
- (46) Kumar, A.; Mohanty, S.; Gupta, V. K. Butadiene Rubber: Synthesis, Microstructure, and Role of Catalysis. *Rubber Chemistry and Technology* **2021**, *94* (3), 393–409.
- (47) Marzocca, A. J.; Rodriguez Garraza, A. L.; Sorichetti, P.; Mosca, H. O. Cure Kinetics and Swelling Behaviour in Polybutadiene Rubber. *Polym Test* **2010**, *29* (4), 477–482. <https://doi.org/10.1016/j.polymertesting.2010.02.008>.
- (48) Farias, F. R. L.; Vasconcelos, M. K.; Brandão, A. L. T. Influence of Number of Catalyst Sites in 1,3-Butadiene Solution Polymerizations Catalyzed by Titanium Tetrachloride. *Engineering Reports* **2021**, *3* (5), 1–10. <https://doi.org/10.1002/eng2.12333>.
- (49) Hua, J.; Liu, K.; Wang, Z.; Geng, J.; Wang, X. Effect of Vinyl and Phenyl Group Content on the Physical and Dynamic Mechanical Properties of HVBR and SSBR. *J Appl Polym Sci* **2018**, *135* (12). <https://doi.org/10.1002/app.45975>.

- (50) Rivera, M. R.; Herrera Nájera, R.; Benvenuta Tapia, J. J.; Ríos Guerrero, L. Structure and Properties of Model Polybutadienes - Effect of Microstructure on the Dynamic Mechanical Properties of Rubber. *Journal of Elastomers and Plastics* **2005**, *37* (3), 267–278. <https://doi.org/10.1177/0095244305051505>.
- (51) Gazeley, K. F.; Gorton, A. D. T.; Pendle, T. D. Natural Rubber Science and Technology. In *Oxford science publications*; Roberts, A. D., Ed.; Oxford University Press: England, 1988; pp 63–98.
- (52) Afreen, S.; Haque, K. R.; Huda, M. K. Troubleshooting for the Observed Problems in Processing Latex Concentrate from Natural Resource. *IOP Conf Ser Earth Environ Sci* **2013**, *16* (1), 012007. <https://doi.org/10.1088/1755-1315/16/1/012007>.
- (53) Bhowmick, A. K.; Hall, M. M.; Benarey, H. A. *Rubber Products Manufacturing Technology*, 1st ed.; Routledge, 1994.
- (54) Rajan, V. V.; Dierkes, W. K.; Joseph, R.; Noordermeer, J. W. M. Science and Technology of Rubber Reclamation with Special Attention to NR-Based Waste Latex Products. *Progress in Polymer Science (Oxford)* **2006**, *31* (9), 811–834. <https://doi.org/10.1016/j.progpolymsci.2006.08.003>.
- (55) Nuzaimah, M.; Sapuan, S. M.; Nadlene, R.; Jawaid, M. Recycling of Waste Rubber as Fillers: A Review. *IOP Conf Ser Mater Sci Eng* **2018**, *368* (1). <https://doi.org/10.1088/1757-899X/368/1/012016>.
- (56) Kaewunruen, S.; Li, D.; Chen, Y.; Xiang, Z. Enhancement of Dynamic Damping in Eco-Friendly Railway Concrete Sleepers Using Waste-Tyre Crumb Rubber. *Materials* **2018**, *11* (1169), 1–20. <https://doi.org/10.3390/ma11071169>.
- (57) Chen, C. Y.; Lee, M. T. Application of Crumb Rubber in Cement-Matrix Composite. *Materials* **2019**, *12* (3), 1–11. <https://doi.org/10.3390/ma12030529>.
- (58) Miranda, M.; Pinto, F.; Gulyurtlu, I.; Cabrita, I.; Nogueira, C. A.; Matos, A. Response Surface Methodology Optimization Applied to Rubber Tyre and Plastic Wastes Thermal Conversion. *Fuel* **2010**, *89* (9), 2217–2229. <https://doi.org/10.1016/j.fuel.2010.03.009>.
- (59) Chin, K. P.; Wan, N. Y.; Saad, C. S. Mt. Microcellular Rubber: A Study on Reclaimed Natural Rubber (NR) Latex Gloves/Standard Malaysian Rubber (SMR) 20 Blends. *Pertanika J Sci Technol* **2011**, *19* (1), 171–176.
- (60) Mahamood, M. A.; Mohamad, N.; Jeeffeerie, A. R.; Mohd Zain, A. H.; Shueb, M. I.; Maulod, H. E. A. Correlation of Open Cell Structure with Properties of Green Rubber Foam from Epoxidised Natural Rubber/Reclaimed Rubber Glove. *Journal of Mechanical Engineering* **2017**, *Special Is* (1), 113–122.
- (61) Basik, A.; Sanglier, J.-J.; Yeo, C.; Sudesh, K. Microbial Degradation of Rubber: Actinobacteria. *Polymers (Basel)* **2021**, *13* (12), 1989. <https://doi.org/10.3390/polym13121989>.
- (62) Naddeo, M.; Viscusi, G.; Gorrasi, G.; Pappalardo, D. Degradable Elastomers: Is There a Future in Tyre Compound Formulation?

- (63) Swift, G. Biodegradable Polymers in the Environment: Are They Really Biodegradable? In *Biotechnology and Bioactive Polymers*; Springer US: Boston, MA, 1994; pp 161–168. [https://doi.org/10.1007/978-1-4757-9519-6\\_15](https://doi.org/10.1007/978-1-4757-9519-6_15).
- (64) Göpferich, A. Mechanisms of Polymer Degradation and Erosion. *The Biomaterials: Silver Jubilee Compendium* **1996**, *17* (2), 117–128. <https://doi.org/10.1016/B978-008045154-1.50016-2>.
- (65) Fainleib, A.; Pires, R. V.; Lucas, E. F.; Soares, B. G. Degradation of Non-Vulcanized Natural Rubber Renewable Resource for Fine Chemicals Used in Polymer Synthesis. *Polímeros Ciência e Tecnologia* **2013**, *23* (4), 441–450. <https://doi.org/10.4322/polimeros.2013.070>.
- (66) Rooshenass, P.; Yahya, R.; Gan, S. N. Comparison of Three Different Degradation Methods To Produce Liquid Epoxidized Natural Rubber. *Rubber Chemistry and Technology* **2016**, *89* (1), 177–198. <https://doi.org/10.5254/RCT.15.84878>.
- (67) Yusof, N. H.; Darji, D.; Nesan, K. V. B.; Rasdi, F. R. M. Preparation of Liquid Epoxidized Natural Rubber in Latex Stage by Chemical Degradation. *AIP Conf Proc* **2018**, *1985*, 2. <https://doi.org/10.1063/1.5047183>.
- (68) Basheer Khan, A. S.; Che Man, S. H.; Baharulrazi, N.; Othman, N. Preparation and Characterization of Hydroxyl Terminated Liquid Epoxidized Natural Rubber. *Chem Eng Trans* **2020**, *78* (2015), 157–162. <https://doi.org/10.3303/CET2078027>.
- (69) Salehuddin, S. M. F.; Baharulrazi, N.; Che Man, S. H.; Wan Ali, W. K.; Yusof, N. H. The Characterization of Hydroxyl Terminated Epoxidized Natural Rubber (HTeNR) via Oxidation Degradation Method. *Chem Eng Trans* **2020**, *78*, 151–156. <https://doi.org/10.3303/CET2078026>.
- (70) Smith, R. F.; Boothroyd, S. C.; Thompson, R. L.; Khosravi, E. A Facile Route for Rubber Breakdown via Cross Metathesis Reactions. *Green Chemistry* **2016**, *18*, 3448–3455. <https://doi.org/10.1039/c5gc03075g>.
- (71) Herman, J. A.; Seazzu, M. E.; Hughes, L. G.; Wheeler, D. R.; Washburn, C. M.; Jones, B. H. Depolymerization of Cross-Linked Polybutadiene Networks in Situ Using Latent Alkene Metathesis. *ACS Appl Polym Mater* **2019**, *1* (8), 2177–2188. <https://doi.org/10.1021/acsapm.9b00434>.
- (72) Rajagopalan, A.; Lara, M.; Kroutil, W. Oxidative Alkene Cleavage by Chemical and Enzymatic Methods. *Adv Synth Catal* **2013**, *355* (17), 3321–3335. <https://doi.org/10.1002/adsc.201300882>.
- (73) Mutti, F. G. Alkene Cleavage Catalysed by Heme and Nonheme Enzymes: Reaction Mechanisms and Biocatalytic Applications. *Bioinorg Chem Appl* **2012**, *2012*, 1–13. <https://doi.org/10.1155/2012/626909>.
- (74) Rajagopalan, A.; Lara, M.; Kroutil, W. Oxidative Alkene Cleavage by Chemical and Enzymatic Methods. *Adv Synth Catal* **2013**, *355* (17), 3321–3335. <https://doi.org/10.1002/adsc.201300882>.

- (75) Van Ornum, S. G.; Champeau, R. M.; Pariza, R. Ozonolysis Applications in Drug Synthesis. *Chemical Reviews* **2006**. <https://doi.org/10.1021/cr040682z>.
- (76) Wang, Z.; Tong, S.; Chen, M.; Jing, B.; Li, W.; Guo, Y.; Ge, M.; Wang, S. Study on Ozonolysis of Asymmetric Alkenes with Matrix Isolation and FT-IR Spectroscopy. *Chemosphere* **2020**. <https://doi.org/10.1016/j.chemosphere.2020.126413>.
- (77) Tyagi, V.; Gupta, A. K. Efficient and Convenient Method for Workup of Ozonolysis Reaction Using Sodium Hydrosulfite. *Synth Commun* **2012**. <https://doi.org/10.1080/00397911.2010.531876>.
- (78) Cochran, B. M. One-Pot Oxidative Cleavage of Olefins to Synthesize Carboxylic Acids by a Telescoped Ozonolysis-Oxidation Process. *Synlett* **2016**. <https://doi.org/10.1055/s-0035-1560659>.
- (79) Liang, Z.; Wei, T.; Xie, J.; Li, H.; Liu, H. Direct Conversion of Terminal Alkenes to Aldehydes via Ozonolysis Reaction in Rotating Zigzag Bed. *Journal of the Iranian Chemical Society* **2020**, *17* (9), 2379–2384. <https://doi.org/10.1007/s13738-020-01933-y>.
- (80) Koike, K.; Nifuku, M.; Izumi, K.; Nakamura, S.; Fujiwara, S.; Horiguchi, S. Explosion Properties of Highly Concentrated Ozone Gas. In *Journal of Loss Prevention in the Process Industries*; **2005**. <https://doi.org/10.1016/j.jlp.2005.07.020>.
- (81) Spannring, P.; Bruijninx, P. C. A.; Weckhuysen, B. M.; Gebbink, R. J. M. K. Transition Metal-Catalyzed Oxidative Double Bond Cleavage of Simple and Bio-Derived Alkenes and Unsaturated Fatty Acids. *Catal Sci Technol* **2014**, *4*, 2182–2209. <https://doi.org/10.1039/c3cy01095c>.
- (82) Ikram, A. Specific Degradation Rate of Decomposing NR Latex Films. *Malaysian Rubber Technology Development* **2006**, 14–17.
- (83) Ikram, A.; Alias, O.; Napi, D. Biodegradability of NR Gloves in Soil. *Journal of Rubber Research* **2000**, *3* (2), 104–114.
- (84) Rose, K.; Tenberge, K. B.; Steinbüchel, A. Identification and Characterization of Genes from *Streptomyces* Sp. Strain K30 Responsible for Clear Zone Formation on Natural Rubber Latex and Poly(Cis-1,4-Isoprene) Rubber Degradation. *Biomacromolecules* **2005**, *6* (1), 180–188. <https://doi.org/10.1021/bm0496110>.
- (85) Bröker, D.; Dietz, D.; Arenskötter, M.; Steinbüchel, A. The Genomes of the Non-Clearing-Zone-Forming and Natural-Rubber-Degrading Species *Gordonia Polyisoprenivorans* and *Gordonia Westfalica* Harbor Genes Expressing Lcp Activity in *Streptomyces* Strains. *Appl Environ Microbiol* **2008**, *74* (8), 2288–2297. <https://doi.org/10.1128/AEM.02145-07>.
- (86) Ali Shah, A.; Hasan, F.; Shah, Z.; Kanwal, N.; Zeb, S. Biodegradation of Natural and Synthetic Rubbers: A Review. *Int Biodeterior Biodegradation* **2013**, *83*, 145–157. <https://doi.org/10.1016/j.ibiod.2013.05.004>.
- (87) Rose, K.; Steinbüchel, A. Biodegradation of Natural Rubber and Related Compounds: Recent Insights into a Hardly Understood Catabolic Capability of Microorganisms. *Appl Environ Microbiol* **2005**, *71* (6), 2803–2812. <https://doi.org/10.1128/AEM.71.6.2803-2812.2005>.



- (88) Yikmis, M.; Arenskötter, M.; Rose, K.; Lange, N.; Wernsmann, H.; Wiefel, L.; Steinbüchel, A. Secretion and Transcriptional Regulation of the Latex-Clearing Protein, Lcp, by the Rubber-Degrading Bacterium *Streptomyces* Sp. Strain K30. *Appl Environ Microbiol* **2008**, *74* (17), 5373–5382. <https://doi.org/10.1128/AEM.01001-08>.
- (89) Inderthal, H.; Tai, S. L.; Harrison, S. T. L. Non-Hydrolyzable Plastics – An Interdisciplinary Look at Plastic Bio-Oxidation. *Trends Biotechnol* **2020**, *39* (1), 12–23. <https://doi.org/10.1016/j.tibtech.2020.05.004>.
- (90) Azevedo, H.; Reis, R. *Understanding the Enzymatic Degradation of Biodegradable Polymers and Strategies to Control Their Degradation Rate*; 2005. <https://doi.org/10.1201/9780203491232.ch12>.
- (91) Banerjee, A.; Chatterjee, K.; Madras, G. Enzymatic Degradation of Polymers: A Brief Review. *Materials Science and Technology (United Kingdom)* **2014**, *30* (5), 567–573. <https://doi.org/10.1179/1743284713Y.0000000503>.
- (92) Pérez, J.; Muñoz-Dorado, J.; de la Rubia, T.; Martínez, J. Biodegradation and Biological Treatments of Cellulose, Hemicellulose and Lignin: An Overview. *International Microbiology* **2002**, *5* (2), 53–63. <https://doi.org/10.1007/s10123-002-0062-3>.
- (93) Schmidt, J.; Wei, R.; Oeser, T.; Silva, L. A. D. e. S.; Breite, D.; Schulze, A.; Zimmermann, W. Degradation of Polyester Polyurethane by Bacterial Polyester Hydrolases. *Polymers (Basel)* **2017**, *9* (2), 65. <https://doi.org/10.3390/polym9020065>.
- (94) Biundo, A.; Reich, J.; Ribitsch, D.; Guebitz, G. M. Synergistic Effect of Mutagenesis and Truncation to Improve a Polyesterase from *Clostridium Botulinum* for Polyester Hydrolysis. *Sci Rep* **2018**, *8* (1), 1–7. <https://doi.org/10.1038/s41598-018-21825-9>.
- (95) Decker, A.; Solomon, E. I. Dioxygen Activation by Copper, Heme and Non-Heme Iron Enzymes: Comparison of Electronic Structures and Reactivities. *Curr Opin Chem Biol* **2005**, *9* (2), 152–163. <https://doi.org/10.1016/j.cbpa.2005.02.012>.
- (96) Solomon, E. I.; Decker, A.; Lehnert, N. Non-Heme Iron Enzymes: Contrasts to Heme Catalysis. *Proc Natl Acad Sci U S A* **2003**, *100* (7), 3589–3594. <https://doi.org/10.1073/pnas.0336792100>.
- (97) Dunham, N. P.; Arnold, F. H. Nature's Machinery, Repurposed: Expanding the Repertoire of Iron-Dependent Oxygenases. *ACS Catal* **2020**, *10* (20), 12239–12255. <https://doi.org/10.1021/acscatal.0c03606>.
- (98) Geng, J.; Weitz, A. C.; Dornevil, K.; Hendrich, M. P.; Liu, A. Kinetic and Spectroscopic Characterization of the Catalytic Ternary Complex of Tryptophan 2,3-Dioxygenase. *Biochemistry* **2020**. <https://doi.org/10.1021/acs.biochem.0c00179>.
- (99) Zhang, Y.; Kang, S. A.; Mukherjee, T.; Bale, S.; Crane, B. R.; Begley, T. P.; Ealick, S. E. Crystal Structure and Mechanism of Tryptophan 2,3-Dioxygenase, a Heme Enzyme Involved in Tryptophan Catabolism and in Quinolate Biosynthesis. *Biochemistry* **2007**. <https://doi.org/10.1021/bi0620095>.

- (100) Yikmis, M.; Steinbüchel, A. Historical and Recent Achievements in the Field of Microbial Degradation of Natural and Synthetic Rubber. *Appl Environ Microbiol* **2012**, *78* (13), 4543–4551. <https://doi.org/10.1128/AEM.00001-12>.
- (101) Jendrossek, D. Rubber Oxygenases. *Appl Microbiol Biotechnol* **2019**, *103*, 125–142.
- (102) Birke, J.; Röther, W.; Jendrossek, D. RoxB Is a Novel Type of Rubber Oxygenase That Combines Properties of Rubber Oxygenase RoxA and Latex Clearing Protein (Lcp). *Appl Environ Microbiol* **2017**, *83* (14), 1–13. <https://doi.org/10.1128/aem.00721-17>.
- (103) Braaz, R.; Armbruster, W.; Jendrossek, D. Heme-Dependent Rubber Oxygenase RoxA of *Xanthomonas* Sp. Cleaves the Carbon Backbone of Poly(Cis-1,4-Isoprene) by a Dioxygenase Mechanism. *Appl Environ Microbiol* **2005**, *71* (5), 2473–2478. <https://doi.org/10.1128/AEM.71.5.2473-2478.2005>.
- (104) Hiessl, S.; Schuldes, J.; Thürmer, A.; Halbsguth, T.; Bröker, D.; Angelov, A.; Liebl, W.; Daniel, R.; Steinbüchel, A. Involvement of Two Latex-Clearing Proteins during Rubber Degradation and Insights into the Subsequent Degradation Pathway Revealed by the Genome Sequence of *Gordonia polyisoprenivorans* Strain VH2. *Appl Environ Microbiol* **2012**, *78* (8), 2874–2887. <https://doi.org/10.1128/AEM.07969-11>.
- (105) Oetermann, S.; Vivod, R.; Hiessl, S.; Hogeback, J.; Holtkamp, M.; Karst, U.; Steinbüchel, A. Histidine at Position 195 Is Essential for Association of Heme-b in Lcp1VH2. *Earth Systems and Environment* **2018**, *2* (1), 5–14. <https://doi.org/10.1007/s41748-018-0041-2>.
- (106) Braga, S. P.; dos Santos, A. P.; Paganini, T.; Barbosa, D.; Epamino, G. W. C.; Morais, C.; Martins, L. F.; Silva, A. M.; Setubal, J. C.; Vallim, M. A.; Pascon, R. C. First Report of Cis-1,4-Polyisoprene Degradation by *Gordonia paraffinivorans*. *Brazilian Journal of Microbiology* **2019**, 1051–1062. <https://doi.org/10.1007/s42770-019-00143-w>.
- (107) Watcharakul, S.; Röther, W.; Birke, J.; Umsakul, K.; Hodgson, B.; Jendrossek, D. Biochemical and Spectroscopic Characterization of Purified Latex Clearing Protein (Lcp) from Newly Isolated Rubber Degrading *Rhodococcus rhodochrous* Strain RPK1 Reveals Novel Properties of Lcp. *BMC Microbiol* **2016**, *16* (1), 1–13. <https://doi.org/10.1186/s12866-016-0703-x>.
- (108) Vivod, R.; Andler, R.; Oetermann, S.; Altenhoff, A.-L.; Seipel, N.; Holtkamp, M.; Hogeback, J.; Karst, U.; Steinbüchel, A. Characterization of the Latex Clearing Protein of the Poly(Cis-1,4-Isoprene) and Poly(Trans-1,4-Isoprene) Degrading Bacterium *Nocardia nova* SH22a. *J Gen Appl Microbiol* **2019**, *65* (6), 293–300. <https://doi.org/10.2323/jgam.2019.01.003>.
- (109) Warneke, S.; Arenskötter, M.; Tenberge, K. B.; Steinbüchel, A. Bacterial Degradation of Poly(Trans-1,4-Isoprene (Gutta Percha). *Microbiology (N Y)* **2007**, *153* (2), 347–356. <https://doi.org/10.1099/mic.0.2006/000109-0>.
- (110) Birke, J.; Jendrossek, D. *Solimonas fluminis* Has an Active Latex-Clearing Protein. *Appl Microbiol Biotechnol* **2019**, *103* (19), 8229–8239. <https://doi.org/10.1007/s00253-019-10085-w>.

- (111) Adjedje, V. K. B.; Schell, E.; Wolf, Y. L.; Laub, A.; Weissenborn, M. J.; Binder, W. H. Enzymatic Degradation of Synthetic Polyisoprenes: Via Surfactant-Free Polymer Emulsification. *Green Chemistry* **2021**, *23* (23), 9433–9438. <https://doi.org/10.1039/d1gc03515k>.
- (112) Zhang, H.; Kong, D.; Wang, L.; Xia, W.; Yao, C.; Wu, J. Degradation of UV-Pretreated Polyolefins by Latex Clearing Protein from *Streptomyces* Sp. Strain K30. *Science of the Total Environment* **2022**, *806* (150779). <https://doi.org/10.1016/j.scitotenv.2021.150779>.
- (113) Altenhoff, A. L.; Thierbach, S.; Steinbüchel, A. High Yield Production of the Latex Clearing Protein from *Gordonia Polyisoprenivorans* VH2 in Fed Batch Fermentations Using a Recombinant Strain of *Escherichia Coli*. *J Biotechnol* **2020**, *309*, 92–99. <https://doi.org/10.1016/j.jbiotec.2019.12.013>.
- (114) Röther, W.; Austen, S.; Birke, J.; Jendrossek, D. Molecular Insights in the Cleavage of Rubber by the Latex-Clearing-Protein (Lcp) of *Streptomyces* Sp. Strain K30. *Appl Environ Microbiol* **2016**, *82* (22), 6593–6602. <https://doi.org/10.1128/AEM.02176-16>.
- (115) Seidel, J.; Schmitt, G.; Hoffmann, M.; Jendrossek, D.; Einsle, O. Structure of the Processive Rubber Oxygenase RoxA from *Xanthomonas* Sp. *Proc Natl Acad Sci U S A* **2013**, *110* (34), 13833–13838. <https://doi.org/10.1073/pnas.1305560110>.
- (116) Wiedemann, C.; Kumar, A.; Lang, A.; Ohlenschläger, O. Cysteines and Disulfide Bonds as Structure-Forming Units: Insights From Different Domains of Life and the Potential for Characterization by NMR. *Front Chem* **2020**, *8* (April), 1–8. <https://doi.org/10.3389/fchem.2020.00280>.
- (117) Ilcu, L.; Röther, W.; Birke, J.; Brausemann, A.; Einsle, O.; Jendrossek, D. Structural and Functional Analysis of Latex Clearing Protein (Lcp) Provides Insight into the Enzymatic Cleavage of Rubber. *Sci Rep* **2017**, *7* (1), 1–11. <https://doi.org/10.1038/s41598-017-05268-2>.
- (118) Birke, J.; Röther, W.; Jendrossek, D. Latex Clearing Protein (Lcp) of *Streptomyces* Sp. Strain K30 Is a b -Type Cytochrome and Differs from Rubber Oxygenase A (RoxA) in Its Biophysical Properties. *Appl Environ Microbiol* **2015**, *81* (11), 3793–3799. <https://doi.org/10.1128/aem.00275-15>.
- (119) Röther, W.; Birke, J.; Grond, S.; Beltran, J. M.; Jendrossek, D.; Beltran, M.; Jendrossek, D. Production of Functionalized Oligo-Isoprenoids by Enzymatic Cleavage of Rubber. *Microb Biotechnol* **2017**, *10* (6), 1426–1433. <https://doi.org/10.1111/1751-7915.12748>.
- (120) Birke, J.; Jendrossek, D. Rubber Oxygenase and Latex Clearing Protein Cleave Rubber to Different Products and Use Different Cleavage Mechanisms. *Appl Environ Microbiol* **2014**, *80* (16), 5012–5020. <https://doi.org/10.1128/AEM.01271-14>.
- (121) Basran, J.; Booth, E. S.; Lee, M.; Handa, S.; Raven, E. L. Analysis of Reaction Intermediates in Tryptophan 2,3-Dioxygenase: A Comparison with Indoleamine 2,3-Dioxygenase. *Biochemistry* **2016**, *55* (49), 6743–6750. <https://doi.org/10.1021/acs.biochem.6b01005>.
- (122) Booth, E. S.; Basran, J.; Lee, M.; Handa, S.; Raven, E. L. Substrate Oxidation by Indoleamine 2,3-Dioxygenase: Evidence for a Common

Reaction Mechanism. *Journal of Biological Chemistry* **2015**, *290* (52), 30924–30930. <https://doi.org/10.1074/jbc.M115.695684>.

- (123) Lewis-Ballester, A.; Batabyal, D.; Egawa, T.; Lu, C.; Lin, Y.; Marti, M. A.; Capece, L.; Estrin, D. A.; Yeh, S. R. Evidence for a Ferryl Intermediate in a Heme-Based Dioxygenase. *Proc Natl Acad Sci U S A* **2009**, *106* (41), 17371–17376. <https://doi.org/10.1073/pnas.0906655106>.
- (124) Lung, W. C.; Li, X.; Sugimoto, H.; Shiro, Y.; Morokuma, K. Density Functional Theory Study on a Missing Piece in Understanding of Heme Chemistry: The Reaction Mechanism for Indoleamine 2,3-Dioxygenase and Tryptophan 2,3-Dioxygenase. *J Am Chem Soc* **2008**. <https://doi.org/10.1021/ja803107w>.
- (125) Zhang, S.; Liu, Y. Mechanical Insights into the Enzymatic Cleavage of Double C-C Bond in Poly(Cis-1,4-Isoprene) by the Latex Clearing Protein. *Inorg Chem* **2020**, *59* (14), 9627–9637. <https://doi.org/10.1021/acs.inorgchem.0c00726>.
- (126) Sono, M.; Roach, M. P.; Coulter, E. D.; Dawson, J. H. Heme-Containing Oxygenases. *Chem Rev* **1996**, *96* (7), 2841–2888.
- (127) Bai, J.; Hou, Q.; Zhu, W.; Liu, Y. Mechanical Insights into the Oxidative Cleavage of Resveratrol Catalyzed by Dioxygenase NOV1 from: *Novosphingobium Aromaticivorans*: Confirmation of Dioxygenase Mechanism by QM/MM Calculations. *Catal Sci Technol* **2019**, *9* (2), 444–455. <https://doi.org/10.1039/c8cy01885e>.
- (128) Yikmis, M.; Steinbüchel, A. Importance of the Latex-Clearing Protein (Lcp) for Poly(Cis-1,4-Isoprene) Rubber Cleavage in *Streptomyces* Sp. K30. *Microbiologyopen* **2012**, *1* (1), 13–24. <https://doi.org/10.1002/mbo3.3>.
- (129) Varnado, C. L.; Goodwin, D. C. System for the Expression of Recombinant Hemoproteins in *Escherichia Coli*. *Protein Expr Purif* **2004**, *35* (1), 76–83. <https://doi.org/10.1016/j.pep.2003.12.001>.
- (130) Andler, R.; Steinbüchel, A. A Simple, Rapid and Cost-Effective Process for Production of Latex Clearing Protein to Produce Oligopolyisoprene Molecules. *J Biotechnol* **2017**, *241*, 184–192. <https://doi.org/10.1016/j.jbiotec.2016.12.008>.
- (131) Andler, R.; Heger, F.; Andreeßen, C.; Steinbüchel, A. Enhancing the Synthesis of Latex Clearing Protein by Different Cultivation Strategies. *J Biotechnol* **2019**, *297*, 32–40. <https://doi.org/10.1016/j.jbiotec.2019.03.019>.
- (132) Hiessl, S.; Böse, D.; Oetermann, S.; Eggers, J.; Pietruszka, J.; Steinbüchel, A. Latex Clearing Protein—an Oxygenase Cleaving Poly(Cis -1,4-Isoprene) Rubber at the Cis Double Bonds . *Appl Environ Microbiol* **2014**, *80* (17), 5231–5240. <https://doi.org/10.1128/aem.01502-14>.
- (133) Andler, R. Bacterial and Enzymatic Degradation of Poly(Cis-1,4-Isoprene) Rubber: Novel Biotechnological Applications. *Biotechnol Adv* **2020**, *44* (June), 107606. <https://doi.org/10.1016/j.biotechadv.2020.107606>.

- (134) Andler, R.; Valdés, C.; Díaz-Barrera, A.; Steinbüchel, A. Biotransformation of Poly(Cis-1,4-Isoprene) in a Multiphase Enzymatic Reactor for Continuous Extraction of Oligo-Isoprenoid Molecules. *N Biotechnol* **2020**, *58* (April), 10–16. <https://doi.org/10.1016/j.nbt.2020.05.001>.
- (135) Röther, W.; Austen, S.; Birke, J.; Jendrossek, D. Cleavage of Rubber by the Latex Clearing Protein (Lcp) of *Streptomyces* Sp. Strain K30: Molecular Insights. *Appl Environ Microbiol* **2016**, *82* (22), 6593–6602. <https://doi.org/10.1128/AEM.02176-16>.
- (136) Birke, J.; Jendrossek, D. Rubber Oxygenase and Latex Clearing Protein Cleave Rubber to Different Products and Use Different Cleavage Mechanisms. *Appl Environ Microbiol* **2014**, *80* (16), 5012–5020. <https://doi.org/10.1128/AEM.01271-14>.
- (137) Andler, R.; Altenhoff, A. L.; Mäsing, F.; Steinbüchel, A. In Vitro Studies on the Degradation of Poly(Cis-1,4-Isoprene). *Biotechnol Prog* **2018**, *34* (4), 890–899. <https://doi.org/10.1002/btpr.2631>.
- (138) Xin, Y.; Yuan, J. Schiff's Base as a Stimuli-Responsive Linker in Polymer Chemistry. *Polymer Chemistry*. November 2012, pp 3045–3055. <https://doi.org/10.1039/c2py20290e>.
- (139) Soares, F. A.; Steinbüchel, A. Enzymatic and Chemical Approaches for Post-Polymerization Modifications of Diene Rubbers: Current State and Perspectives. *Macromol Biosci* **2021**, *21* (12), 1–19. <https://doi.org/10.1002/mabi.202100261>.
- (140) Sheldon, R. A.; Brady, D.; Bode, M. L. The Hitchhiker's Guide to Biocatalysis: Recent Advances in the Use of Enzymes in Organic Synthesis. *Chem Sci* **2020**, *11* (10), 2587–2605. <https://doi.org/10.1039/c9sc05746c>.
- (141) Chen, K.; Arnold, F. H. Engineering New Catalytic Activities in Enzymes. *Nat Catal* **2020**, *3* (3), 203–213. <https://doi.org/10.1038/s41929-019-0385-5>.
- (142) Chen, R. Enzyme Engineering: Rational Redesign versus Directed Evolution. *Trends Biotechnol* **2001**, *19* (1), 13–14. [https://doi.org/10.1016/S0167-7799\(00\)01522-5](https://doi.org/10.1016/S0167-7799(00)01522-5).
- (143) Ali, M.; Ishqi, H. M.; Husain, Q. Enzyme Engineering: Reshaping the Biocatalytic Functions. *Biotechnol Bioeng* **2020**, *117* (6), 1877–1894. <https://doi.org/10.1002/bit.27329>.
- (144) Li, C.; Zhang, R.; Wang, J.; Wilson, L. M.; Yan, Y. Protein Engineering for Improving and Diversifying Natural Product Biosynthesis. *Trends Biotechnol* **2020**, *38* (7), 729–744. <https://doi.org/10.1016/j.tibtech.2019.12.008>.
- (145) Dinmukhamed, T.; Huang, Z.; Liu, Y.; Lv, X.; Li, J.; Du, G.; Liu, L. Current Advances in Design and Engineering Strategies of Industrial Enzymes. *Systems Microbiology and Biomanufacturing* **2020**. <https://doi.org/10.1007/s43393-020-00005-9>.
- (146) Pavelka, A.; Sebestova, E.; Kozlikova, B.; Brezovsky, J.; Sochor, J.; Damborsky, J. CAVER: Algorithms for Analyzing Dynamics of Tunnels in

Macromolecules. *IEEE/ACM Trans Comput Biol Bioinform* **2016**, *13* (3), 505–517. <https://doi.org/10.1109/TCBB.2015.2459680>.

- (147) Schmidtke, P.; Bidon-chanal, A.; Luque, F. J.; Barril, X. MDpocket: Open-Source Cavity Detection and Characterization on Molecular Dynamics Trajectories. *Bioinformatics* **2011**, *27* (23), 3276–3285. <https://doi.org/10.1093/bioinformatics/btr550>.
- (148) Mohanty, M.; Mohanty, P. S. Molecular Docking in Organic, Inorganic, and Hybrid Systems: A Tutorial Review. *Monatsh Chem* **2023**, *154* (7), 683–707. <https://doi.org/10.1007/s00706-023-03076-1>.
- (149) Schwede, T.; Kopp, J.; Guex, N.; Peitsch, M. C. SWISS-MODEL: An Automated Protein Homology-Modeling Server. *Nucleic Acids Res* **2003**, *31* (13), 3381–3385. <https://doi.org/10.1093/nar/gkg520>.
- (150) Jumper, J.; Evans, R.; Pritzel, A.; Green, T.; Figurnov, M.; Ronneberger, O.; Tunyasuvunakool, K.; Bates, R.; Žídek, A.; Potapenko, A.; Bridgland, A.; Meyer, C.; Kohl, S. A. A.; Ballard, A. J.; Cowie, A.; Romera-Paredes, B.; Nikolov, S.; Jain, R.; Adler, J.; Back, T.; Petersen, S.; Reiman, D.; Clancy, E.; Zielinski, M.; Steinegger, M.; Pacholska, M.; Berghammer, T.; Bodenstein, S.; Silver, D.; Vinyals, O.; Senior, A. W.; Kavukcuoglu, K.; Kohli, P.; Hassabis, D. Highly Accurate Protein Structure Prediction with AlphaFold. *Nature* **2021**, *596* (7873), 583–589. <https://doi.org/10.1038/s41586-021-03819-2>.
- (151) Kaufmann, K. W.; Lemmon, G. H.; Deluca, S. L.; Sheehan, J. H.; Meiler, J. Practically Useful: What the Rosetta Protein Modeling Suite Can Do for You. *Biochemistry* **2010**, *49* (14), 2987–2998. <https://doi.org/10.1021/bi902153g>.
- (152) McGuffin, L. J.; Edmunds, N. S.; Genc, A. G.; Alharbi, S. M. A.; Salehe, B. R.; Adiyaman, R. Prediction of Protein Structures, Functions and Interactions Using the IntFOLD7, MultiFOLD and ModFOLDdock Servers. *Nucleic Acids Res* **2023**, *51* (W1), W274–W280. <https://doi.org/10.1093/nar/gkad297>.
- (153) Pan, Y.; Qi, R.; Li, M.; Wang, B.; Huang, H.; Han, W. Random Acceleration and Steered Molecular Dynamics Simulations Reveal the (Un)Binding Tunnels in Adenosine Deaminase and Critical Residues in Tunnels. *RSC Adv* **2020**, *10* (72), 43994–44002. <https://doi.org/10.1039/d0ra07796h>.
- (154) Kokkonen, P.; Bednar, D.; Pinto, G.; Prokop, Z.; Damborsky, J. Engineering Enzyme Access Tunnels. *Biotechnol Adv* **2019**, *37* (6), 107386. <https://doi.org/10.1016/j.biotechadv.2019.04.008>.
- (155) Pravda, L.; Berka, K.; Vařeková, R. S.; Sehnal, D.; Banáš, P.; Laskowski, R. A.; Koča, J.; Otyepka, M. Anatomy of Enzyme Channels. *BMC Bioinformatics* **2014**, *15* (379). <https://doi.org/10.12933/therya-17-423>.
- (156) Chovancova, E.; Pavelka, A.; Benes, P.; Strnad, O.; Brezovsky, J.; Kozlikova, B.; Gora, A.; Sustr, V.; Klvana, M.; Medek, P.; Biedermannova, L.; Sochor, J.; Damborsky, J. CAVER 3.0: A Tool for the Analysis of Transport Pathways in Dynamic Protein Structures. *PLoS Comput Biol* **2012**, *8* (10). <https://doi.org/10.1371/journal.pcbi.1002708>.
- (157) Lu, Z.; Li, X.; Zhang, R.; Yi, L.; Ma, Y.; Zhang, G. Tunnel Engineering to Accelerate Product Release for Better Biomass-Degrading Abilities in

Lignocellulolytic Enzymes. *Biotechnol Biofuels* **2019**, *12* (1), 1–9. <https://doi.org/10.1186/s13068-019-1616-3>.

- (158) Kaushik, S.; Marques, S. M.; Khirsariya, P.; Paruch, K.; Libichova, L.; Brezovsky, J.; Prokop, Z.; Chaloupkova, R.; Damborsky, J. Impact of the Access Tunnel Engineering on Catalysis Is Strictly Ligand-Specific. *FEBS Journal* **2018**, *285* (8), 1456–1476. <https://doi.org/10.1111/febs.14418>.
- (159) Liu, H. T.; Weng, C. Y.; Xu, S. Y.; Li, S. F.; Wang, Y. J.; Zheng, Y. G. Directed Evolution of a Carbonyl Reductase LsCR for the Enantioselective Synthesis of (1S)-2-Chloro-1-(3,4-Difluorophenyl) Ethanol. *Bioorg Chem* **2022**, *127*. <https://doi.org/10.1016/j.bioorg.2022.105991>.
- (160) Liu, H. T.; Weng, C. Y.; Zhou, L.; Xu, H. B.; Liao, Z. Y.; Hong, H. Y.; Ye, Y. F.; Li, S. F.; Wang, Y. J.; Zheng, Y. G. Coevolving Stability and Activity of LsCR by a Single Point Mutation and Constructing Neat Substrate Bioreaction System. *Biotechnol Bioeng* **2023**, *120* (6), 1521–1530. <https://doi.org/10.1002/bit.28357>.
- (161) Abookleesh, F.; Mosa, F. E. S.; Barakat, K.; Ullah, A. Assessing Molecular Docking Tools to Guide the Design of Polymeric Materials Formulations: A Case Study of Canola and Soybean Protein. *Polymers (Basel)* **2022**, *14* (17). <https://doi.org/10.3390/polym14173690>.
- (162) Gupta, M.; Sharma, R.; Kumar, A. Docking Techniques in Pharmacology: How Much Promising? *Comput Biol Chem* **2018**, *76* (February), 210–217. <https://doi.org/10.1016/j.compbiolchem.2018.06.005>.
- (163) Rasulev, B. Recent Developments in 3D QSAR and Molecular Docking Studies of Organic and Nanostructures. In *Handbook of Computational Chemistry*; Leszczynski, J., Kaczmarek-Kedziera, A., Puzyn, T., Papadopoulos, M. G., Reis, H., Shukla, M. K., Eds.; Springer International Publishing Switzerland: Switzerland, 2017; pp 2134–2156. <https://doi.org/10.1007/978-3-319-27282-5>.
- (164) Feinstein, W. P.; Brylinski, M. Calculating an Optimal Box Size for Ligand Docking and Virtual Screening against Experimental and Predicted Binding Pockets. *J Cheminform* **2015**, *7* (1). <https://doi.org/10.1186/s13321-015-0067-5>.
- (165) Pagadala, N. S.; Syed, K.; Tuszyński, J. Software for Molecular Docking: A Review. *Biophys Rev* **2017**, *9* (2), 91–102. <https://doi.org/10.1007/s12551-016-0247-1>.
- (166) Zhou, P.; Jin, B.; Li, H.; Huang, S. Y. HPEPDOCK: A Web Server for Blind Peptide-Protein Docking Based on a Hierarchical Algorithm. *Nucleic Acids Res* **2018**, *46* (W1), W443–W450. <https://doi.org/10.1093/nar/gky357>.
- (167) Verkhivker, G. M.; Bouzida, D.; Gehlhaar, D. K.; Rejto, P. A.; Arthurs, S.; Colson, A. B.; Freer, S. T.; Larson, V.; Lutty, B. A.; Marrone, T.; Rose, P. W. Deciphering Common Failures in Molecular Docking of Ligand-Protein Complexes. *J Comput Aided Mol Des* **2000**, *14* (8), 731–751. <https://doi.org/10.1023/A:1008158231558>.
- (168) Barrozo, A.; Borstnar, R.; Marloie, G.; Kamerlin, S. C. L. Computational Protein Engineering: Bridging the Gap between Rational Design and

Laboratory Evolution. *Int J Mol Sci* **2012**, *13* (10), 12428–12460. <https://doi.org/10.3390/ijms131012428>.

- (169) Ge, B. K.; Hu, G. M.; Chen, C. M. Plastic Bioconversion: Reaction Mechanism of PETases. *Chinese Journal of Physics* **2021**, *73*, 331–339. <https://doi.org/10.1016/j.cjph.2021.07.027>.
- (170) Shrimpton-Phoenix, E.; Mitchell, J. B. O.; Bühl, M. Computational Insights into the Catalytic Mechanism of Is-PETase: An Enzyme Capable of Degrading Poly(Ethylene) Terephthalate. *Chemistry - A European Journal* **2022**, *28* (70). <https://doi.org/10.1002/chem.202201728>.
- (171) da Costa, C. H. S.; dos Santos, A. M.; Alves, C. N.; Martí, S.; Moliner, V.; Santana, K.; Lameira, J. Assessment of the PETase Conformational Changes Induced by Poly(Ethylene Terephthalate) Binding. *Proteins: Structure, Function and Bioinformatics* **2021**, *89* (10), 1340–1352. <https://doi.org/10.1002/prot.26155>.
- (172) Warneke, S.; Arenskötter, M.; Tenberge, K. B.; Steinbüchel, A. Bacterial Degradation of Poly(Trans-1,4-Isoprene (Gutta Percha)). *Microbiology (N Y)* **2007**, *153* (2), 347–356. <https://doi.org/10.1099/mic.0.2006/000109-0>.
- (173) Sato, S.; Honda, Y.; Kuwahara, M.; Watanabe, T. Degradation of Vulcanized and Nonvulcanized Polyisoprene Rubbers by Lipid Peroxidation Catalyzed by Oxidative Enzymes and Transition Metals. *Biomacromolecules* **2003**, *4* (2), 321–329. <https://doi.org/10.1021/bm025683k>.
- (174) Bradford, M. M. A Rapid and Sensitive Method for the Quantitation of Microgram Quantities of Protein Utilizing the Principle of Protein-Dye Binding. *Anal Biochem* **1976**, *72*, 248–254. [https://doi.org/10.1016/0003-2697\(76\)90527-3](https://doi.org/10.1016/0003-2697(76)90527-3).
- (175) Chovancova, E.; Pavelka, A.; Benes, P.; Strnad, O.; Brezovsky, J.; Kozlikova, B.; Gora, A.; Sustr, V.; Klvana, M.; Medek, P.; Biedermannova, L.; Sochor, J.; Damborsky, J. CAVER 3.0: A Tool for the Analysis of Transport Pathways in Dynamic Protein Structures. *PLoS Comput Biol* **2012**, *8* (10), 23–30. <https://doi.org/10.1371/journal.pcbi.1002708>.
- (176) Kutov, D. C.; Katkova, E. V.; Sulimov, A. V.; Kondakova, O. A.; Sulimov, V. B. Influence of the Method of Hydrogen Atoms Incorporation into the Target Protein on the Protein-Ligand Binding Energy. *Bulletin of the South Ural State University, Series: Mathematical Modelling, Programming and Computer Software* **2017**, *10* (3), 94–107. <https://doi.org/10.14529/mmp170308>.
- (177) Jones, G.; Willett, P.; Glen, R. C.; Leach, A. R.; Taylor, R. Development and Validation of a Genetic Algorithm for Flexible Docking. *J Mol Biol* **1997**, *267*, 727–748.
- (178) Anandakrishnan, R.; Aguilar, B.; Onufriev, A. V. H++ 3.0: Automating PK Prediction and the Preparation of Biomolecular Structures for Atomistic Molecular Modeling and Simulations. *Nucleic Acids Res* **2012**, *40* (W1), 537–541. <https://doi.org/10.1093/nar/gks375>.
- (179) Liebeschuetz, J. W.; Cole, J. C.; Korb, O. Pose Prediction and Virtual Screening Performance of GOLD Scoring Functions in a Standardized



Test. *J Comput Aided Mol Des* **2012**, 26 (6), 737–748. <https://doi.org/10.1007/s10822-012-9551-4>.

- (180) Adasme, M. F.; Linnemann, K. L.; Bolz, S. N.; Kaiser, F.; Salentin, S.; Haupt, V. J.; Schroeder, M. PLIP 2021: Expanding the Scope of the Protein-Ligand Interaction Profiler to DNA and RNA. *Nucleic Acids Res* **2021**, 49 (W1), W530–W534. <https://doi.org/10.1093/nar/gkab294>.
- (181) Fulda, S.; Gorman, A. M.; Hori, O.; Samali, A. Cellular Stress Responses: Cell Survival and Cell Death. *Int J Cell Biol* **2010**, 2010, 1–23. <https://doi.org/10.1155/2010/214074>.
- (182) Sørensen, H. P.; Mortensen, K. K. Soluble Expression of Recombinant Proteins in the Cytoplasm of Escherichia Coli. *Microb Cell Fact* **2005**, 4 (1), 1–8. <https://doi.org/10.1186/1475-2859-4-1>.
- (183) Dumon-Seignovert, L.; Cariot, G.; Vuillard, L. The Toxicity of Recombinant Proteins in Escherichia Coli: A Comparison of Overexpression in BL21(DE3), C41(DE3), and C43(DE3). *Protein Expr Purif* **2004**, 37 (1), 203–206. <https://doi.org/10.1016/j.pep.2004.04.025>.
- (184) Sørensen, H. P.; Mortensen, K. K. Advanced Genetic Strategies for Recombinant Protein Expression in Escherichia Coli. *J Biotechnol* **2005**, 115 (2), 113–128. <https://doi.org/10.1016/j.jbiotec.2004.08.004>.
- (185) Rosano, G. L.; Ceccarelli, E. A. Recombinant Protein Expression in Escherichia Coli: Advances and Challenges. *Front Microbiol* **2014**, 5 (APR), 1–17. <https://doi.org/10.3389/fmicb.2014.00172>.
- (186) Tachibana, S.; Watanabe, K.; Konishi, M. Estimating Effects of Yeast Extract Compositions on Escherichia Coli Growth by a Metabolomics Approach. *J Biosci Bioeng* **2019**, 128 (4), 468–474. <https://doi.org/10.1016/j.jbiosc.2019.03.012>.
- (187) Hakobyan, L.; Gabrielyan, L.; Trchounian, A. Yeast Extract as an Effective Nitrogen Source Stimulating Cell Growth and Enhancing Hydrogen Photoproduction by Rhodospirillum Rubrum Strains from Mineral Springs. *Int J Hydrogen Energy* **2012**, 37 (8), 6519–6526. <https://doi.org/10.1016/j.ijhydene.2012.01.077>.
- (188) Tong, W. Y.; Yao, S. J.; Zhu, Z. Q.; Yu, J. An Improved Procedure for Production of Human Epidermal Growth Factor from Recombinant E. Coli. *Appl Microbiol Biotechnol* **2001**, 57 (5–6), 674–679. <https://doi.org/10.1007/s002530100793>.
- (189) Nausch, H.; Huckauf, J.; Koslowski, R.; Meyer, U.; Broer, I.; Mikschofsky, H. Recombinant Production of Human Interleukin 6 in Escherichia Coli. *PLoS One* **2013**, 8 (1). <https://doi.org/10.1371/journal.pone.0054933>.
- (190) Dvorak, P.; Chrast, L.; Nikel, P. I.; Fedr, R.; Soucek, K.; Sedlackova, M.; Chaloupkova, R.; Lorenzo, V.; Prokop, Z.; Damborsky, J. Exacerbation of Substrate Toxicity by IPTG in Escherichia Coli BL21(DE3) Carrying a Synthetic Metabolic Pathway. *Microb Cell Fact* **2015**, 14 (1), 1–15. <https://doi.org/10.1186/s12934-015-0393-3>.
- (191) Faust, G.; Stand, A.; Weuster-Botz, D. IPTG Can Replace Lactose in Auto-Induction Media to Enhance Protein Expression in Batch-Cultured Escherichia Coli. *Eng Life Sci* **2015**, 15 (8), 824–829. <https://doi.org/10.1002/elsc.201500011>.

- (192) Muñoz-Elías, E. J.; McKinney, J. D. Carbon Metabolism of Intracellular Bacteria. *Cell Microbiol* **2006**, *8* (1), 10–22. <https://doi.org/10.1111/j.1462-5822.2005.00648.x>.
- (193) Deutscher, J. The Mechanisms of Carbon Catabolite Repression in Bacteria. *Curr Opin Microbiol* **2008**, *11* (2), 87–93. <https://doi.org/10.1016/j.mib.2008.02.007>.
- (194) Huber, R.; Scheidle, M.; Dittrich, B.; Klee, D.; Büchs, J. Equalizing Growth in High-Throughput Small Scale Cultivations via Precultures Operated in Fed-Batch Mode. *Biotechnol Bioeng* **2009**, *103* (6), 1095–1102. <https://doi.org/10.1002/bit.22349>.
- (195) Du, F.; Liu, Y. Q.; Xu, Y. S.; Li, Z. J.; Wang, Y. Z.; Zhang, Z. X.; Sun, X. M. Regulating the T7 RNA Polymerase Expression in E. Coli BL21 (DE3) to Provide More Host Options for Recombinant Protein Production. *Microb Cell Fact* **2021**, *20* (1). <https://doi.org/10.1186/s12934-021-01680-6>.
- (196) Upadhyay, A. K.; Murmu, A.; Singh, A.; Panda, A. K. Kinetics of Inclusion Body Formation and Its Correlation with the Characteristics of Protein Aggregates in Escherichia Coli. *PLoS One* **2012**, *7* (3). <https://doi.org/10.1371/journal.pone.0033951>.
- (197) Singh, S. M.; Panda, A. K. Solubilization and Refolding of Bacterial Inclusion Body Proteins. *J Biosci Bioeng* **2005**, *99* (4), 303–310. <https://doi.org/10.1263/jbb.99.303>.
- (198) Grossman, T. H.; Kawasaki, E. S.; Punreddy, S. R.; Osburne, M. S. Spontaneous CAMP-Dependent Derepression of Gene Expression in Stationary Phase Plays a Role in Recombinant Expression Instability. *Gene* **1998**, *209* (1–2), 95–103. [https://doi.org/10.1016/S0378-1119\(98\)00020-1](https://doi.org/10.1016/S0378-1119(98)00020-1).
- (199) Borzouee, F.; Mofid, M.; Varshosaz, J.; Samsam Shariat, S. A. Purification of Lactoperoxidase from Bovine Whey and Investigation of Kinetic Parameters. *Adv Biomed Res* **2016**, *5* (1), 189. <https://doi.org/10.4103/2277-9175.192738>.
- (200) Fiege, K.; Querebillo, C. J.; Hildebrandt, P.; Frankenberg-Dinkel, N. Improved Method for the Incorporation of Heme Cofactors into Recombinant Proteins Using Escherichia Coli Nissle 1917. *Biochemistry* **2018**, *57* (19), 2747–2755. <https://doi.org/10.1021/acs.biochem.8b00242>.
- (201) Cattinari, G.; Steenkeste, K.; Le Bris, C.; Canette, A.; Gallopin, M.; Couty, M.; Fontaine-Aupart, M. P. Natural Rubber-Carbon Black Coagulation: Following the Nanostructure Evolution from a Colloidal Suspension to a Composite. *J Appl Polym Sci* **2021**, *138* (8). <https://doi.org/10.1002/app.50221>.
- (202) van Schie, M. M. C. H.; Spöring, J. D.; Bocola, M.; Domínguez de María, P.; Rother, D. Applied Biocatalysis beyond Just Buffers - From Aqueous to Unconventional Media. Options and Guidelines. *Green Chemistry* **2021**, *23* (9), 3191–3206. <https://doi.org/10.1039/d1gc00561h>.
- (203) Altenhoff, A. L.; Thierbach, S.; Steinbüchel, A. In Vitro Studies on the Degradation of Common Rubber Waste Material with the Latex Clearing

Protein (Lcp1VH2) of *Gordonia Polyisoprenivorans* VH2. *Biodegradation* **2021**, *32* (2), 113–125. <https://doi.org/10.1007/s10532-020-09920-z>.

- (204) Zhao, H. What Do We Learn from Enzyme Behaviors in Organic Solvents? – Structural Functionalization of Ionic Liquids for Enzyme Activation and Stabilization. *Biotechnol Adv* **2020**, *45*, 107638. <https://doi.org/10.1016/j.biotechadv.2020.107638>.
- (205) Ogino, H.; Ishikawa, H. Enzymes Which Are Stable in the Presence of Organic Solvents. *J Biosci Bioeng* **2001**, *91* (2), 109–116. <https://doi.org/10.1103/PhysRevE.58.4141>.
- (206) Kamogawa, K.; Matsumoto, M.; Kobayashi, T.; Sakai, T.; Sakai, H.; Abe, M. Dispersion and Stabilizing Effects of N-Hexadecane on Tetralin and Benzene Metastable Droplets in Surfactant-Free Conditions. *Langmuir* **1999**, *15* (6), 1913–1917. <https://doi.org/10.1021/la9806799>.
- (207) Wia, cek, A. E.; Adryańczyk, E. Interfacial Properties of Phosphatidylcholine-Based Dispersed Systems. *Ind Eng Chem Res* **2015**, *54* (25), 6489–6496. <https://doi.org/10.1021/acs.iecr.5b01429>.
- (208) Cravotto, C.; Fabiano-Tixier, A. S.; Claux, O.; Abert-Vian, M.; Tabasso, S.; Cravotto, G.; Chemat, F. Towards Substitution of Hexane as Extraction Solvent of Food Products and Ingredients with No Regrets. *Foods* **2022**, *11* (21). <https://doi.org/10.3390/foods11213412>.
- (209) Rozsypal, T. Contaminated Disposable Rubber Gloves as Evidence Samples after a Chemical Attack with Nerve Agents. *Drug Test Anal* **2023**. <https://doi.org/10.1002/dta.3468>.
- (210) Chavhan, P.; Madre, Z.; Gaikwad, V.; Kulkarni, S. J. Recycling of Rubber Scrap Tyres and Its Processes of the Utilization. In *5th IEEE International Conference on Advances in Science and Technology, ICAST 2022*; Institute of Electrical and Electronics Engineers Inc., 2022; pp 632–636. <https://doi.org/10.1109/ICAST55766.2022.10039659>.
- (211) Izunobi, J. U.; Higginbotham, C. L. Polymer Molecular Weight Analysis by <sup>1</sup>H NMR Spectroscopy. *J Chem Educ* **2011**, *88* (8), 1098–1104. <https://doi.org/10.1021/ed100461v>.
- (212) Andler, R.; Hiessl, S.; Yücel, O.; Tesch, M.; Steinbüchel, A. Cleavage of Poly(Cis-1,4-Isoprene) Rubber as Solid Substrate by Cultures of *Gordonia Polyisoprenivorans*. *N Biotechnol* **2018**, *44*, 6–12. <https://doi.org/10.1016/j.nbt.2018.03.002>.
- (213) Röther, W.; Birke, J.; Jendrossek, D. Assays for the Detection of Rubber Oxygenase Activities. *Bio Protoc* **2017**, *7* (6), 1–14. <https://doi.org/10.21769/bioprotoc.2188>.
- (214) Robins, J. H.; Abrams, G. D.; Pincock, J. A. The Structure of Schiff Reagent Aldehyde Adducts and the Mechanism of the Schiff Reaction as Determined by Nuclear Magnetic Resonance Spectroscopy. *Can J Chem* **1980**, *58* (4), 339–347. <https://doi.org/10.1139/v80-055>.
- (215) Tibor, B.; Leonard, O. Some Observation of the Reaction of Schiff Reagent with Aldehydes. *Journal of Histochemistry & Cytochemistry* **1959**, *8* (3), 208–213.
- (216) Sharma, S.; Lee, J.; Gao, P.; Steele, V. E. Toxicity Profile of Solvents by Aspiration Approach for Topical Agent Delivery to Respiratory Tract

- Epithelium. *Int J Toxicol* **2011**, 30 (3), 358–366. <https://doi.org/10.1177/1091581810396729>.
- (217) Tong, Y.; Guo, M. Bacterial Heme-Transport Proteins and Their Heme-Coordination Modes. *Arch Biochem Biophys* **2009**, 481 (1), 1–15. <https://doi.org/10.1016/j.abb.2008.10.013>.
- (218) Villarreal, D. M.; Phillips, C. L.; Kelley, A. M.; Villarreal, S.; Villalobos, A.; Hernandez, P.; Olson, J. S.; Henderson, D. P. Enhancement of Recombinant Hemoglobin Production in Escherichia Coli BL21(DE3) Containing the Plesiomonas Shigelloides Heme Transport System. *Appl Environ Microbiol* **2008**, 74 (18), 5854–5856. <https://doi.org/10.1128/AEM.01291-08>.
- (219) Ge, J.; Wang, X.; Bai, Y.; Wang, Y.; Wang, Y.; Tu, T.; Qin, X.; Su, X.; Luo, H.; Yao, B.; Huang, H.; Zhang, J. Engineering Escherichia Coli for Efficient Assembly of Heme Proteins. *Microb Cell Fact* **2023**, 22 (1). <https://doi.org/10.1186/s12934-023-02067-5>.
- (220) Leu, S. Y.; Zhu, J. Y. Substrate-Related Factors Affecting Enzymatic Saccharification of Lignocelluloses: Our Recent Understanding. *Bioenergy Res* **2013**, 6 (2), 405–415. <https://doi.org/10.1007/s12155-012-9276-1>.
- (221) Zhao, X.; Zhang, L.; Liu, D. Biomass Recalcitrance. Part I: The Chemical Compositions and Physical Structures Affecting the Enzymatic Hydrolysis of Lignocellulose. *Biofuels, Bioproducts and Biorefining* **2011**, 6, 465–482. <https://doi.org/10.1002/BBB>.
- (222) Zhu, J. Y.; Wang, G. S.; Pan, X. J.; Gleisner, R. Specific Surface to Evaluate the Efficiencies of Milling and Pretreatment of Wood for Enzymatic Saccharification. *Chem Eng Sci* **2009**, 64 (3), 474–485. <https://doi.org/10.1016/j.ces.2008.09.026>.
- (223) Mooney, C. A.; Mansfield, S. D.; Beatson, R. P.; Saddler, J. N. The Effect of Fiber Characteristics on Hydrolysis and Cellulase Accessibility to Softwood Substrates. *Enzyme Microb Technol* **1999**, 25 (8–9), 644–650. [https://doi.org/10.1016/S0141-0229\(99\)00098-8](https://doi.org/10.1016/S0141-0229(99)00098-8).
- (224) Shanthi, K.; Balasubramanian, N. A Simple Spectrophotometric Method for the Determination of Hydrogen Sulfide Based on Schiff's Reaction. *Microchemical Journal* **1996**, No. 53, 168–174.
- (225) Hladová, M.; Martinka, J.; Rantuch, P.; Nečas, A. Review of Spectrophotometric Methods for Determination of Formaldehyde. *Research Papers Faculty of Materials Science and Technology Slovak University of Technology* **2019**, 27 (44), 105–120. <https://doi.org/10.2478/rput-2019-0012>.
- (226) Herbert Elftman. A Schiff Reagent of Calibrated Sensitivity. *Journal of Histochemistry & Cytochemistry* **1959**, 7 (2), 93–97.
- (227) Kilcoyne, M.; Gerlach, J. Q.; Farrell, M. P.; Bhavanandan, V. P.; Joshi, L. Periodic Acid-Schiff's Reagent Assay for Carbohydrates in a Microtiter Plate Format. *Anal Biochem* **2011**, 416 (1), 18–26. <https://doi.org/10.1016/j.ab.2011.05.006>.

- (228) Leimgruber, S.; Trimmel, G. Olefin Metathesis Meets Rubber Chemistry and Technology. *Monatsh Chem* **2015**, *146* (7), 1081–1097. <https://doi.org/10.1007/s00706-015-1501-0>.
- (229) Altenhoff, A. L.; de Witt, J.; Andler, R.; Steinbüchel, A. Impact of Additives of Commercial Rubber Compounds on the Microbial and Enzymatic Degradation of Poly(Cis-1,4-Isoprene). *Biodegradation* **2019**, *30* (1), 13–26. <https://doi.org/10.1007/s10532-018-9858-5>.
- (230) Ibrahim, S.; Othman, N.; Sreekantan, S.; Tan, K. S.; Nor, Z. M.; Ismail, H. Preparation and Characterization of Low-Molecular-Weight Natural Rubber Latex via Photodegradation Catalyzed by Nano TiO<sub>2</sub>. *Polymers (Basel)* **2018**, *10* (11). <https://doi.org/10.3390/polym10111216>.
- (231) Isa, S. Z.; Yahya, R.; Hassan, A.; Tahir, M. The Influence of Temperature and Reaction Time in the Degradation of Natural Rubber Latex. *The Malaysian Journal of Analytical Sciences* **2007**, *11* (1), 42–47.
- (232) Ramli, R.; Bao, C. A.; Rasdi, F. R. M.; Kamaruddin, S.; Aziz, A. A.; Song, T. K.; Lang, M. K.; Hou, H. J. Preliminary Study on Epoxidized Natural Rubber Latex Composites Intended for Shoe Soles Applic. *International Journal of Emerging Trends in Engineering Research* **2020**, *8* (1.2), 122–131. <https://doi.org/10.30534/ijeter/2020/1781.22020>.
- (233) Siti Salina Sarkawi Nurul Hayati Yusof; Roland Ngeow; Ahmad Kifli Che Aziz; Rohaidah Abdul Rahim; Rassimi Abdul Ghani; Teku Zakwan Zaeimoedin; Nurul Hayati Yusof. Epoxidised Natural Rubber in Tyre Applications. In *Epoxidised Natural Rubber*; Veronica Charlotte, Ed.; Springer: Singapore, 2023; pp 99–139.
- (234) Adibi, A.; Simon, L.; Lenges, C.; Mekonnen, T. H. Sustainable Natural Rubber Composites: Masterbatch Development of Epoxidized Natural Rubber Grafted to Designed Enzymatic Polysaccharides. *Mater Chem Front* **2023**. <https://doi.org/10.1039/d3qm00080j>.
- (235) Ou, W.; Weng, Y.; Zeng, J.; Li, Y. Fully Biobased Poly(Lactic Acid)/Lignin Composites Compatibilized by Epoxidized Natural Rubber. *Int J Biol Macromol* **2023**, *236*, 123960. <https://doi.org/10.1016/j.ijbiomac.2023.123960>.
- (236) Aziana, A. H.; Shabinah Filza, M. S.; Roslim, R.; Fatimah Rubaizah, M. R. Assessing Biodegradability of Epoxidized Natural Rubber Latex. *Journal of Rubber Research* **2021**, *24* (4), 595–605. <https://doi.org/10.1007/s42464-021-00109-4>.
- (237) Darji, D.; Mohd Rasdi, F. R.; Abdul Rahim, M. A.; Danya, M. S. Epoxidised Natural Rubber (ENR) Latex: An Alternative Raw Material for Latex Dipped Products. *Journal of Rubber Research* **2020**, *23* (4), 375–385. <https://doi.org/10.1007/s42464-020-00065-5>.
- (238) Senyek, M. L. Isoprene Polymers. In *Encyclopedia of Polymer Science and Technology*; John Wiley & Sons, Inc., 2008; p 60. <https://doi.org/10.1002/0471440264.pst175>.
- (239) Ochigbo, S. S.; Lafia-Araga, R. A.; Suleiman, M. A. T. Comparison of Two Creaming Methods for Preparation of Natural Rubber Latex Concentrates from Field Latex. *Afr J Agric Res* **2011**, *6* (12), 2916–2619. <https://doi.org/10.5897/AJAR10.1173>.

- (240) Phattarateera, S.; Pattamaprom, C. The Viscosity Effect of Masticated Natural vs. Synthetic Isoprene Rubber on Toughening of Polylactic Acid. *Int J Polym Sci* **2019**, 2019. <https://doi.org/10.1155/2019/5679871>.
- (241) M. J. Shuttleworth; A. A. Watson. Synthetic Polyisoprene Rubbers. In *Developments in Rubber Technology—2. The Developments Series*; A. Whelan, K. S. Lee, Eds.; Springer: Dordrecht, 1981; Vol. 37.
- (242) Hsu, C. S.; Robinson, P. *Springer Handbook of Petroleum Technology*, 2nd ed.; Hsu, C. S., Robinson, P., Eds.; Springer International Publishing: Germany, 2017.
- (243) White, Wm. C. Butadiene Production Process Overview. *Chem Biol Interact* **2007**, 166 (1–3), 10–14.
- (244) Liu, Z. Y.; Han, L.; Wang, R. J.; Feng, Q.; Liu, G. Y.; Yong, Z. F. Influence of Liquid Polybutadiene on Crosslinking Network and Mechanical Properties of SSBR/BR. *Polym Eng Sci* **2022**, 62 (5), 1416–1426. <https://doi.org/10.1002/pen.25931>.
- (245) Bo, H.; Gustafsson, E. M.; Setterwall, F. Tetradecane and Hexadecane Binary Mixtures as Phase Change Materials (PCMs) for Cool Storage in District Cooling Systems. *Energy* **1999**, 24, 1015–1028.
- (246) Kamogawa, K.; Kuwayama, N.; Katagiri, T.; Akatsuka, H.; Sakai, T.; Sakai, H.; Abe, M. Dispersion and Stabilization in Water of Droplets of Hydrophobic Organic Liquids with the Addition of Hydrophobic Polymers. *Langmuir* **2003**, 19 (10), 4063–4069. <https://doi.org/10.1021/la020749i>.
- (247) Lv, M.; Fang, L.; Yu, H.; Rojruthai, P.; Sakdapipanich, J. Discoloration Mechanisms of Natural Rubber and Its Control. *Polymers (Basel)* **2022**, 14 (4), 1–14. <https://doi.org/10.3390/polym14040764>.
- (248) Hamzah, R.; Bakar, M. A.; Khairuddean, M.; Mohammed, I. A.; Adnan, R. A Structural Study of Epoxidized Natural Rubber (ENR-50) and Its Cyclic Dithiocarbonate Derivative Using NMR Spectroscopy Techniques. *Molecules* **2012**, 17 (9), 10974–10993. <https://doi.org/10.3390/molecules170910974>.
- (249) Jiang, Q.; Gao, Y.; Liao, L.; Yu, R.; Liao, J. Biodegradable Natural Rubber Based on Novel Double Dynamic Covalent Cross-Linking. *Polymers (Basel)* **2022**, 14 (7). <https://doi.org/10.3390/polym14071380>.
- (250) Rooshenass, P. Investigation of Different Degradation Methods to Prepare Liquid Epoxidized Natural Rubber for Coating Applications, University of Malaya, Kuala Lumpur, 2017.
- (251) Rooshenass, P.; Yahya, R.; Gan, S. N. Preparation of Liquid Epoxidized Natural Rubber by Oxidative Degradations Using Periodic Acid, Potassium Permanganate and UV-Irradiation. *J Polym Environ* **2018**, 26 (4), 1378–1392. <https://doi.org/10.1007/s10924-017-1038-x>.
- (252) Ramli, R.; Bao, C. A.; Jee Hou, H.; Kamaruddin, S.; Rubaizah Mohd Rasdi, F.; De Focatiis, D. S. Preparation and Characterisation of Specialty Natural Rubber Latex Concentrate. *Rubber Chemistry and Technology* **2022**, 95 (1), 101–118.
- (253) Phinyocheep, P.; Phetphaisit, C. W.; Derouet, D.; Campistron, I.; Brosse, J. C. Chemical Degradation of Epoxidized Natural Rubber Using Periodic Acid: Preparation of Epoxidized Liquid Natural Rubber. In *Journal of*

*Applied Polymer Science*; 2005; Vol. 95, pp 6–15.  
<https://doi.org/10.1002/app.20812>.

- (254) Shit, S. C.; Maiti, S. Application of NMR Spectroscopy in Molecular Weight Determination of Polymers. *Eur Polym J* **1986**, *22* (12), 1001–1008. [https://doi.org/10.1016/0014-3057\(86\)90082-0](https://doi.org/10.1016/0014-3057(86)90082-0).
- (255) Ng, J. W.; Othman, N.; Yusof, N. H. Various Coagulation Techniques and Their Impacts towards the Properties of Natural Rubber Latex from *Hevea Brasiliensis* — a Comprehensive Review Related to Tyre Application. *Ind Crops Prod* **2022**, *181* (February), 114835. <https://doi.org/10.1016/j.indcrop.2022.114835>.
- (256) Lehman, N.; Tuljitrarn, A.; Songtipya, L.; Uthaipan, N.; Sengloyluan, K.; Johns, J.; Nakaramontri, Y.; Kalkornsurapranee, E. Influence of Non-Rubber Components on the Properties of Unvulcanized Natural Rubber from Different Clones. *Polymers (Basel)* **2022**, *14* (9), 1–14. <https://doi.org/10.3390/polym14091759>.
- (257) Hiessl, S.; Böse, D.; Oetermann, S.; Eggers, J.; Pietruszka, J.; Steinbüchel, A. Latex Clearing Protein-an Oxygenase Cleaving Poly(Cis-1,4-Isoprene) Rubber at the Cis Double Bonds. *Appl Environ Microbiol* **2014**, *80* (17), 5231–5240. <https://doi.org/10.1128/AEM.01502-14>.
- (258) Bradbury, J. H.; Perera, M. C. S. Epoxidation of Natural Rubber Studied by Nmr Spectroscopy. *J Appl Polym Sci* **1985**, *30* (8), 3347–3364. <https://doi.org/10.1002/app.1985.070300817>.
- (259) Enoki, M.; Doi, Y.; Iwata, T. Oxidative Degradation of Cis- and Trans-1,4-Polyisoprenes and Vulcanized Natural Rubber with Enzyme-Mediator Systems. *Biomacromolecules* **2003**, *4* (2), 314–320. <https://doi.org/10.1021/bm025678g>.
- (260) Uchida, H.; Nakajima-Kambe, T.; Shigeno-Akutsu, Y.; Nomura, N.; Tokiwa, Y.; Nakahara, T. Properties of a Bacterium Which Degrades Solid Poly(Tetramethylene Succinate)-Co-Adipate, a Biodegradable Plastic. *FEMS Microbiol Lett* **2000**, *189* (1), 25–29. <https://doi.org/10.1111/j.1574-6968.2000.tb09201.x>.
- (261) Sakai, T. Surfactant-Free Emulsions. *Curr Opin Colloid Interface Sci* **2008**, *13* (4), 228–235. <https://doi.org/10.1016/j.cocis.2007.11.013>.
- (262) Sakai, T.; Kamogawa, K.; Nishiyama, K.; Sakai, H.; Abe, M. Molecular Diffusion of Oil/Water Emulsions in Surfactant-Free Conditions. *Langmuir* **2002**, *18* (6), 1985–1990. <https://doi.org/10.1021/la0111248>.
- (263) Enoki, M.; Kaita, S.; Wakatsuki, Y.; Doi, Y.; Iwata, T. Oxidative Degradation of Cis- and Trans-1,4-Polybutadienes by Horseradish Peroxidase/1-Hydroxybenzotriazole. *Polym Degrad Stab* **2004**, *84* (2), 321–326. <https://doi.org/10.1016/j.polymdegradstab.2003.12.007>.
- (264) Tsuchii, A.; Takeda, K. Rubber-Degrading Enzyme from a Bacterial Culture. *Appl Environ Microbiol* **1990**, *56* (1), 269–274.
- (265) Tsuchii, A.; Suzuki, T.; Takeda, K. Microbial Degradation of Natural Rubber Vulcanizates. *Appl Environ Microbiol* **1985**, *50* (4), 965–970.
- (266) Gunasekaran, K.; Nussinov, R. How Different Are Structurally Flexible and Rigid Binding Sites? Sequence and Structural Features Discriminating Proteins That Do and Do Not Undergo Conformational

Change upon Ligand Binding. *J Mol Biol* **2007**, *365* (1), 257–273. <https://doi.org/10.1016/j.jmb.2006.09.062>.

- (267) Wang, R.; Lu, Y.; Fang, X.; Wang, S. An Extensive Test of 14 Scoring Functions Using the PDBbind Refined Set of 800 Protein-Ligand Complexes. *J Chem Inf Comput Sci* **2004**, *44* (6), 2114–2125. <https://doi.org/10.1021/ci049733j>.
- (268) Luo, Q.; Hiesl, S.; Poehlein, A.; Steinbüchel, A. Microbial Gutta-Percha Degradation Shares Common Steps with Rubber Degradation by *Nocardia Nova* SH22a. *Appl Environ Microbiol* **2013**, *79* (4), 1140–1149. <https://doi.org/10.1128/AEM.03016-12>.
- (269) Hassan, A. A.; Hanževački, M.; Pordea, A. *Computational investigation of cis-1,4-polyisoprene binding to the latex-clearing protein LcpK30*. <https://doi.org/10.1101/2023.06.26.546638>.
- (270) Ramirez-Ramirez, J.; Martin-Diaz, J.; Pastor, N.; Alcalde, M.; Ayala, M. Exploring the Role of Phenylalanine Residues in Modulating the Flexibility and Topography of the Active Site in the Peroxygenase Variant Pada-i. *Int J Mol Sci* **2020**, *21* (16), 1–15. <https://doi.org/10.3390/ijms21165734>.
- (271) Ciemny, M.; Kurcinski, M.; Kamel, K.; Kolinski, A.; Alam, N.; Schueler-Furman, O.; Kmiecik, S. Protein–Peptide Docking: Opportunities and Challenges. *Drug Discov Today* **2018**, *23* (8), 1530–1537. <https://doi.org/10.1016/j.drudis.2018.05.006>.
- (272) Li, T.; Bonkovsky, H. L.; Guo, J. T. Structural Analysis of Heme Proteins: Implications for Design and Prediction. *BMC Struct Biol* **2011**, *11*. <https://doi.org/10.1186/1472-6807-11-13>.
- (273) Weinert, E. E.; Phillips-Piro, C. M.; Marletta, M. A. Porphyrin  $\pi$ -Stacking in a Heme Protein Scaffold Tunes Gas Ligand Affinity. *J Inorg Biochem* **2013**, *127*, 7–12. <https://doi.org/10.1016/j.jinorgbio.2013.06.004>.
- (274) Schneider, S.; Marles-Wright, J.; Sharp, K. H.; Paoli, M. Diversity and Conservation of Interactions for Binding Heme in B-Type Heme Proteins. *Nat Prod Rep* **2007**, *24* (3), 621–630. <https://doi.org/10.1039/b604186h>.
- (275) Pu, L.; Govindaraj, R. G.; Lemoine, J. M.; Wu, H. C.; Brylinski, M. Deepdrug3D: Classification of Ligand-Binding Pockets in Proteins with a Convolutional Neural Network. *PLoS Comput Biol* **2019**, *15* (2). <https://doi.org/10.1371/journal.pcbi.1006718>.
- (276) Kalinowska, B.; Banach, M.; Wiśniowski, Z.; Konieczny, L.; Roterman, I. Is the Hydrophobic Core a Universal Structural Element in Proteins? *J Mol Model* **2017**, *23* (7). <https://doi.org/10.1007/s00894-017-3367-z>.
- (277) Weinert, E. E.; Phillips-Piro, C. M.; Marletta, M. A. Porphyrin  $\pi$ -Stacking in a Heme Protein Scaffold Tunes Gas Ligand Affinity. *J Inorg Biochem* **2013**, *127*, 7–12. <https://doi.org/10.1016/j.jinorgbio.2013.06.004>.
- (278) Liu, D.; Williamson, D. A.; Kennedy, M. L.; Williams, T. D.; Morton, M. M.; Benson, D. R. Aromatic Side Chain–Porphyrin Interactions in Designed Hemoproteins. *J Am Chem Soc* **1999**, *121* (50), 11798–11812. <https://doi.org/10.1021/ja990606r>.



- (279) Siddiqui, K. S.; Ertan, H.; Poljak, A.; Bridge, W. J. Evaluating Enzymatic Productivity—The Missing Link to Enzyme Utility. *Int J Mol Sci* **2022**, *23* (13). <https://doi.org/10.3390/ijms23136908>.
- (280) Berekaa, M. M.; Linos, A.; Reichelt, R.; Keller, U.; Steinbüchel, A. Effect of Pretreatment of Rubber Material on Its Biodegradability by Various Rubber Degrading Bacteria. *FEMS Microbiol Lett* **2000**, *184* (2), 199–206. [https://doi.org/10.1016/S0378-1097\(00\)00048-3](https://doi.org/10.1016/S0378-1097(00)00048-3).
- (281) Mat Yasin, N.; Akkermans, S.; Van Impe, J. F. M. Enhancing the Biodegradation of (Bio)Plastic through Pretreatments: A Critical Review. *Waste Management* **2022**, *150* (June 2022), 1–12. <https://doi.org/10.1016/j.wasman.2022.06.004>.
- (282) Tian, Y.; Fendler, J. H.; Hungerbühler, H.; Guldi, D. M.; Asmus, K.-D. Effects of Hydrophobic-Hydrophilic Balance and Stereochemistry on the Supramolecular Assembly of Functionalized Fullerenes. *Materials Science and Engineering* **1999**, *C7*, 67–73.
- (283) Yamada-Onodera, K.; Mukumoto, H.; Katsuyaya, Y.; Saiganji, A.; Tani, Y. Degradation of Polyethylene by a Fungus, *Penicillium Simplicissimum* YK. *Polym Degrad Stab* **2001**, *72*, 323–327.
- (284) Birke, J.; Röther, W.; Schmitt, G.; Jendrossek, D. Functional Identification of Rubber Oxygenase (RoxA) in Soil and Marine Myxobacteria. *Appl Environ Microbiol* **2013**, *79* (20), 6391–6399. <https://doi.org/10.1128/AEM.02194-13>.
- (285) Brezovsky, J.; Kozlikova, B.; Damborsky, J. Computational Analysis of Protein Tunnels and Channels. *Methods in Molecular Biology* **2018**, *1685* (2), 25–42. [https://doi.org/10.1007/978-1-4939-7366-8\\_3](https://doi.org/10.1007/978-1-4939-7366-8_3).